Structural Insights into the Extracellular Assembly of the Hematopoietic FLT3 Ligand-Receptor Complex

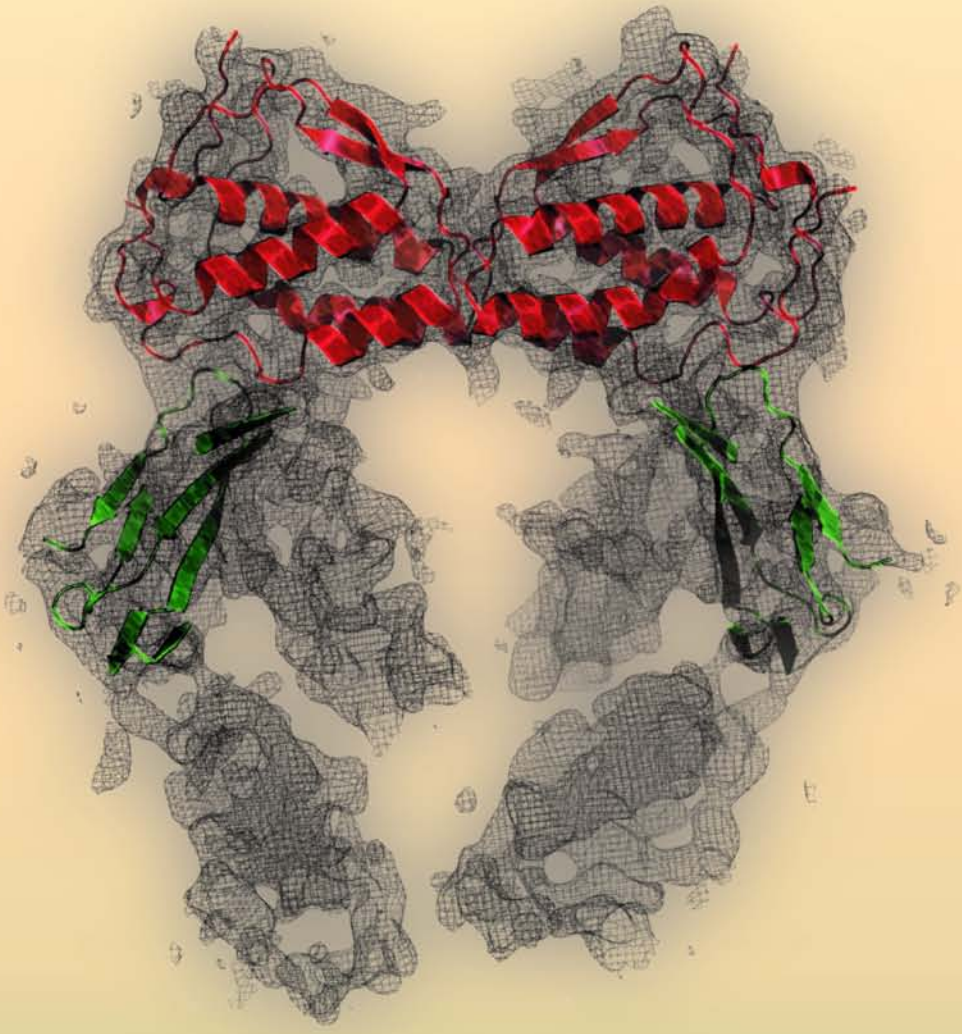

Kenneth Verstraete

UNIVERSITEIT GENT

FACULTY OF SCIENCES

Department of Biochemistry and Microbiology
Laboratory for Protein Biochemistry and Biomolecular Engineering
Unit for Structural Biology and Biophysics

STRUCTURAL INSIGHTS INTO THE EXTRACELLULAR ASSEMBLY OF THE HEMATOPOIETIC FLT3 LIGAND-RECEPTOR COMPLEX

Kenneth Verstraete

March, 2011

Dissertation presented to the Faculty of Sciences in partial fulfillment of the requirements for the degree of Doctor of Science: Biochemistry

Promotor: Prof. Dr. Savvas N. Savvides
Co-promotor: Prof. Dr. Em. Jozef Van Beeumen

Dutch translation of the title:

Structurele inzichten in de extracellulaire opbouw van het hematopoietische Flt3 ligand-receptor complex

Front Cover illustration:

The figure shows a density modified map (2mFo - DFc-like) calculated by PARROT, based on the rigid-body refined molecular replacement solutions for FL (green) and a search model for $Flt3_{D3}$ (red). The map contains contiguous density for unmodelled receptor domains $Flt3_{D2}$ and $Flt3_{D4}$, and was of crucial importance in the structure solution process of the $Flt3_{D1-D4}$:FL complex to 4.3 Å resolution.

all rights reserved.

© 2011 Verstraete Kenneth

No part of this thesis protected by this copyright notice may be reproduced or utilized
in any form of by any means, electronic or mechanical, including photocopying, recording
or by any information storage or retrieval system without the written permission of the author.

K. Verstraete - Structural insights into the extracellular assembly of the
hematopoietic Flt3 ligand-receptor complex.

Ph.D. thesis, Faculty of Sciences, Ghent University, Ghent, Belgium
Publicly defended in Ghent, March 11th, 2011.

This doctoral research was financially supported by the
Fund for Scientific Research-Flanders (FWO-Vlaanderen), Belgium.

EXAMINATION COMMITTEE

Prof. Dr. Bart Devreese (chairman)
Laboratory for Protein Biochemistry and Biomolecular Engineering (L-ProBE)
Faculty of Sciences, UGent, Ghent

Prof. Dr. Savvas N. Savvides (promotor)
Laboratory for Protein Biochemistry and Biomolecular Engineering (L-ProBE)
Faculty of Sciences, UGent, Ghent

Prof. Dr. Em. Jozef Van Beeumen (co-promotor)
Laboratory for Protein Biochemistry and Biomolecular Engineering (L-ProBE)
Faculty of Sciences, UGent, Ghent

Dr. Bjorn Vergauwen
Laboratory for Protein Biochemistry and Biomolecular Engineering (L-ProBE)
Faculty of Sciences, UGent, Ghent

Dr. Radu Aricescu
Division of Structural Biology (STRUBI)
Medical Sciences Division, University of Oxford, Oxford

Prof. Dr. Chris Ulens
Laboratory of Structural Neurobiology
Faculty of Medical Sciences, KUL, Leuven

Prof. Dr. Ir. Remy Loris
Structural Biology Brussels laboratory (SBB)
Faculty of Science and Bio-engineering Sciences, VUB-VIB, Brussels

Prof. Dr. Frank Peelman
Cytokine Receptor Lab (CRL)
Faculty of Medicine and Health Sciences, UGent-VIB, Ghent

CONTENTS

Abbreviations		i
Overview of discussed structures		iv
Scope		vi
CHAPTER 1	Literature Survey	1
CHAPTER 2	Efficient Production of Bioactive Recombinant Human Flt3 Ligand in *E. coli*	57
CHAPTER 3	Inducible Production of Recombinant Human Flt3 Ectodomain Variants in Mammalian Cells and Preliminary Crystallographic Analysis of Flt3 Ligand-Receptor Complexes.	73
CHAPTER 4	Structural Insights into the Extracellular Assembly of the Hematopoietic Flt3 Signaling Complex	89
CHAPTER 5	Summary and Perspectives	113
	Samenvatting	120
Appendices		125
References		131
Dankwoord		149
Curriculum vitae		150

ABBREVIATIONS

AML	acute myelogenous leukemia
ATP	adenosine-5'-triphosphate
BiFC	bimolecular fluorescence complementation
BS^3	bis(sulfosuccinimidyl)suberate
CD	circular dichroism
cDNA	complementary DNA
CHO	Chinese hamster ovary
CLP	common lymphoid progenitor
CMP	common myeloid progenitor
CSF	colony stimulating factor
CSF-1R	colony stimulating factor-1 receptor
DC	dendritic cell
DMEM	Dulbecco's modified Eagle medium
DMSO	dimethyl sulfoxide
Dox	doxycycline
DSS	disuccinimidyl suberate
EDAC	1-ethyl-3-(3-dimethylaminopropyl)carbodiimide hydrochloride
EGFR2	epidermal growth factor receptor-2 (a.k.a. ErbB2)
EndoH	endoglycosidase H
EPO	erythropoietin
ERK	extracellular signal-regulated kinase (a.k.a. MAPK)
ESI-MS	electrospray ionization mass spectrometry
FACS	fluorescence activated cell Sorting
FCS	fetal calf serum
FGFR	fibroblast growth factor receptor
FL	Flt3 ligand
Flk-2	fetal liver kinase 2
Flt3	fms-like tyrosine kinase 3 (a.k.a. STK-1 and Flk-2)
FMS	feline McDonough sarcoma viral oncogene homolog (a.k.a. CSF-1R)
FRET	förster resonance energy transfer
GAPDH	glyceraldehyde 3-phosphate dehydrogenase
G-CSF	granulocyte colony stimulating Factor
GISTs	gastrointestinal stromal tumors
GM-CSF	granulocyte-macrophage colony stimulating factor
GMP	granulocyte-monocyte progenitor

GNTI	N-acetylglucosaminyltransferase I
GRB2	growth factor receptor-bound protein 2
HEK	human embryonic kidney
HSC	hematopoietic stem cell
IL	interleukin
IMAC	immobilized metal ion affinity chromatography
IPTG	isopropyl β-D-1-thiogalactopyranoside
ITC	isothermal titration calorimetry
ITD	internal-tandem duplication
JM	juxtamembrane
$\mathbf{K_d}$	dissociation constant
kDa	kilodalton
$\mathbf{k_{off}}$	dissociation rate constant
$\mathbf{k_{on}}$	association rate constant
Lin	lineage-associated surface markers
LT-HSC	long-term hematopoietic stem cell
mAb	monoclonal antibody
MAPK	mitogen-activated protein kinase
M-CSF	macrophage colony-stimulating factor (a.k.a. CSF-1)
MEP	megakaryocyte-erythroid progenitor
MIR	multiple isomorphous replacement
MPP	multipotent progenitor
MR	molecular replacement
MUSK	muscle specific kinase
NCS	non-crystallographic symmetry
NGFR	nerve growth factor receptor
NK	natural killer cell
NRTK	non-receptor tyrosine kinase
PBS	phosphate buffered saline
PCR	polymerase chain reaction
PDB	Protein Data Bank
PDGF-R	platelet-derived growth factor receptor
PEI	polyethyleneimine
PI3K	phosphatidylinositol 3-kinase
PKB	protein kinase B (a.k.a. AKT)
PLCγ	phospholipase C-γ
PlGF	placental growth factor
PMF	peptide mass fingerprinting

rhFL	recombinant human FL
RMSD	root mean square deviation
RTK	receptor tyrosine kinase
RTKIII	receptor tyrosine kinase type III
Sca-1	stem cell antigen-1
SCF	stem cell factor
SDS-PAGE	sodium dodecyl sulfate polyacrylamide gel electrophoresis
SEC	size-exclusion chromatography
Sf	Spodoptera frugiperda
SH2	src homology-2 domain
SH3	src homology-3 domain
SIRAS	single isomorphous replacement with anomalous scattering
SPR	surface plasmon resonance
SRC	Rous sarcoma viral oncogene homolog
STAT5	signal transducer and activator of transcription 5
ST-HSC	short-term hematopoietic stem cell
STK-1	stem cell tyrosine kinase 1
Tc	tetracycline
Thy1	thymocyte differentiation antigen-1
TK	tyrosine kinase
TKD	tyrosine kinase Domain
TMD	transmembrane Domain
TPO	thrombopoietin
TrkA	tropomyosin-related kinase A (a.k.a. NGFR)
VEGF-R	vascular endothelial growth factor receptor

LIST OF DISCUSSED STRUCTURES

PDB code	Description	Resolution (Å)	Reference
1HMC	Human CSF-1	2.5	Pandit *et al.*, 1992
1PDG	Human PDGF-BB	3.0	Oefner *et al.*, 1992
1VPF	Human VEGF-A	2.5	Muller *et al.*, 1997
1FLT	Human VEGF-R1$_{D2}$:VEGF-A complex	1.7	Wiesmann *et al.*, 1997
1EXZ	Human SCF	2.3	Zhang *et al.*, 2000
1SCF	Human SCF	2.2	Jiang *et al.*, 2000
1ETE	Human FL	2.2	Savvides *et al.*, 2000
1RJB	TKD of human Flt3	2.1	Griffith *et al.*, 2004
1RV6	Human VEGF-R1$_{D2}$:PlGF complex	2.5	Christinger *et al.*, 2004
2O26	Murine KIT$_{D1-D3}$:SCF complex	2.5	Liu *et al.*, 2007
2O27	Murine SCF	2.2	Liu *et al.*, 2007
2EC8	Human KIT$_{D1-D5}$ ectodomain	3.0	Yuzawa *et al.*, 2007
2E9W	Human KIT$_{D1-D5}$:SCF complex	3.5	Yuzawa *et al.*, 2007
3EJJ	Murine CSF1-R$_{D1-3}$:CSF-1 complex	2.4	Chen *et al.*, 2008
3KVQ	Dimer of human VEGF-R2$_{D7}$	2.7	Yang *et al.*, 2010
3MJG	Human PDGF-Rβ_{D1-3}:PDGF-BB complex	2.3	Shim *et al.*, 2010
2X1W	Human VEGF-R2$_{D2-D3}$:VEGF-C complex	2.7	Leppänen *et al.*, 2010
3QS7	Human Flt3$_{D1-D4}$:FL complex	4.3	Verstraete *et al.*, 2011
3QS9	Human Flt3$_{D1-D5}$:FL complex	7.8	Verstraete *et al.*, 2011

SCOPE

Fms-like tyrosine kinase 3 (Flt3) is a type III receptor tyrosine kinase (RTKIII) expressed at the cell surface of hematopoietic stem cells and early hematopoietic progenitors and initiates signaling pathways crucial for the development of the pluripotent cell population that gives rise to the cellular repertoire of the human blood and immune systems.

The Flt3 receptor is activated by the dimeric four-helical bundle cytokine termed **Flt3 Ligand** (FL). The aim of the research described in this work was to obtain molecular insights into the first key step of this activation process, namely the binding of the ligand to the extracellular region of its receptor, by methods as X-ray crystallography, small-angle X-ray scattering, negative-stain electron microscopy and isothermal titration calorimetry.

In the first part of this thesis, **Chapter 1**, the existing scientific knowledge about RTKIII activation is reviewed. The chapter starts with an introductory section on the hematopoietic system and the diverse types of tyrosine kinase receptors. Next, the molecular properties of the Flt3 receptor and its ligand are discussed and the homology with the other ligands and receptors in the RTKIII and RTKV families is highlighted. Then, following a short section about the important function of the Flt3 system in hematopoiesis, a detailed overview of the landmark experiments that lead to the current understanding of ligand-induced receptor activation in the RTKIII and closely related RTKV family is presented. The chapter ends with a discussion on the activation mechanism of the intracellular tyrosine kinase domains for both wild-type and oncogenic Flt3.

Chapters 2, 3 and 4 present the results obtained during this doctoral research. In the first stage of the project, protocols for the efficient production of recombinant human FL and Flt3 ectodomains were established. As clarified in **Chapter 2**, a soluble bioactive form of FL could be obtained by refolding inclusion bodies produced in *E. coli*. **Chapter 3** describes the production of Flt3 receptor ectodomain variants as secreted proteins in inducible mammalian cell lines, and the crystallization of Flt3 ligand-receptor complexes for structural studies by X-ray crystallography. In **Chapter 4**, the acquired structural and thermodynamic insights into the molecular mechanism that underlies the human Flt3 ligand-receptor interaction are presented, with a focus on the determined X-ray structure of a ternary Flt3 ligand-receptor complex.

Finally, in **Chapter 5,** the results are discussed and suggestions for future research are presented.

Chapter 1

LITERATURE SURVEY

Introduction to the hematopoietic system

The cellular compartment of blood, which constitutes about 45% of its volume, consists of the oxygen-transporting erythrocytes ('red blood cells'), the blood platelets that mediate clotting, and the leukocytes of the immune system (**Fig. 1**). The leukocytes or 'white blood cells' are a collection of diverse cell types on which both the innate and adaptive immune responses depend. They guard the peripheral tissues by circulating in the blood and lymphatic system. Innate immunity largely involves granulocytes and macrophages. The granulocytes include the phagocytic neutrophils, the eosinophils and the basophils. Dendritic cells (DCs) are the most potent antigen presenting cells and are thus important for initiating the adaptive immune response. The effector cells of the adaptive immune response are the B and T lymphocytes, which also provide the lifelong immunity that can follow exposure to disease or vaccination. The natural killer (NK) cells are a type of cytotoxic lymphocytes that constitutes a major component of the innate immune system.

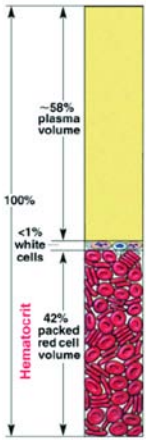

	Males	Females
Hematocrit	40–54%	37–47%
Hemoglobin (g Hb/dL* blood)	14–17	12–16
Red cell count (cells/μL)	4.5–6.5 x 10^6	3.9–5.6 x 10^6
Total white cell count (cells/μL)	4–11 x 10^3	4–11 x 10^3
Differential white cell count		
Neutrophils	50-70%	50-70%
Eosinophils	1-4%	1-4%
Basophils	<1%	<1%
Lymphocytes	20–40%	20–40%
Monocytes	2–8%	2–8%
Platelets (per μL)	200–500 x 10^3	200–500 x 10^3

* 1 deciliter (dL) = 100 mL

FIGURE 1. Cellular composition of normal peripheral blood.

The vast majority of mature blood cells only have a limited life-span. For example, granulocytes remain functionally active for a few hours and erythrocytes live for an average of 120 days before they are cleared from the blood stream. To sustain steady-state levels of all blood and immune cell types, ~ 10^{11} - 10^{12} new cells must be produced every day to replace those lost due to natural decay. This lifelong process, termed hematopoiesis, is dependent on a small population of hematopoietic stem cells (HSCs) that reside in the bone marrow and are able to self-renew, proliferate and differentiate into all mature blood cell types (**Fig. 2**). In addition to maintaining steady-state hematopoiesis, the hematopoietic system also responds to physiological stresses, such as bleeding or infection. During hematopoietic development, HSCs gradually lose self-renewal potential as they start to differentiate towards their immediate progeny, the multipotent progenitor (MPP). These MPP cells lack *in vivo* self-renewal ability but have the capacity for multilineage differentiation, giving rise to the common myeloid progenitors (CMP) and common lymphoid progenitors (CLP).

CLPs populate the lymphoid compartment, which consists of B and T lymphocytes and NK cells. CMPs can develop into the megakaryocyte-erythroid progenitor (MEP) and the granulocyte-monocyte progenitor (GMP). The MEP progenitor can differentiate in megakaryocyte cells that are responsible for platelet production or into erythrocytes. The GMP progenitor gives rise to the different types of granulocytes and to the monocytes which develop into macrophages. DCs can arise from both the CMP and CLP in response to specific stimuli (Wu and Liu, 2007).

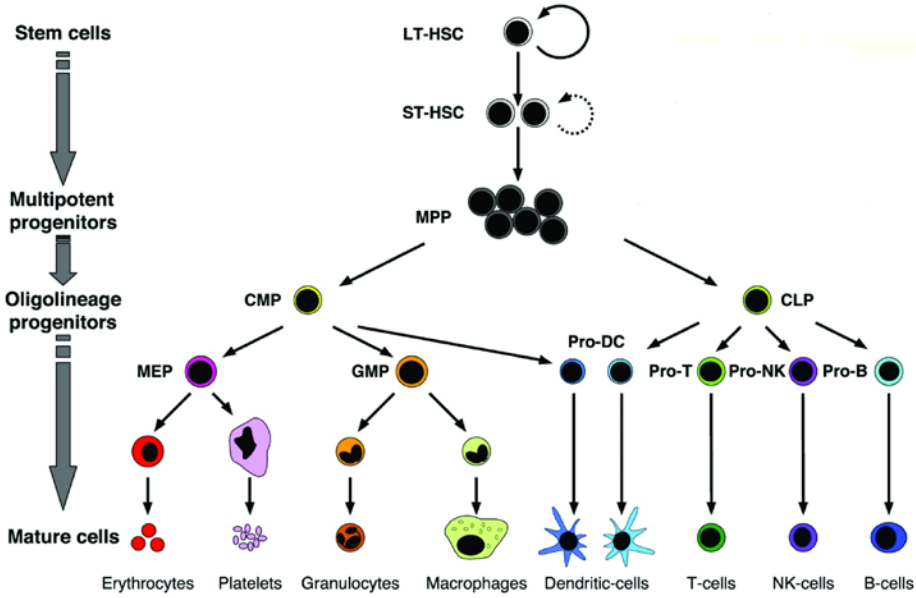

FIGURE 2. The hierarchy of hematopoietic development

HSCs can be divided into LT-HSCs, highly self-renewing cells that repopulate an animal for its entire life span, or ST-HSCs, which repopulate the animal for a limited period. ST-HSCs differentiate into MPPs, which do not or briefly self-renew, and have the ability to differentiate into oligolineage-restricted progenitors that ultimately give rise to differentiated progeny through functionally irreversible maturation steps. The CLPs give rise to T lymphocytes, B lymphocytes, and natural killer (NK) cells. The CMPs give rise to GMPs, which then differentiate into monocytes/macrophages and granulocytes, and to megakaryotic/erythroid progenitors (MEP), which produce megakaryocytes/platelets and erythrocytes. Both CMPs and CLPs can give rise to dendritic cells. All of these stem and progenitor populations are separable as pure populations by using cell surface markers.

Adopted from Passegue et al., 2003.

The earliest site of hematopoiesis during embryonic development is extra-embryonically in the yolk sac (Auerbach *et al.*, 1996). From there HSCs migrate to the fetal spleen and liver, and finally to the bone marrow which is the major site of hematopoiesis in adults (Mikkola and Orkin, 2006).

The stem cell compartment of the bone marrow includes a heterogeneous population of cells that can be divided into two subpopulations based on their ability to reconstitute the hematopoietic system of lethally irradiated mice. The most immature fraction of the HSC compartment is the long-term stem cell population (LT-HSC), which has the greatest capacity for self-renewal and the ability

to repopulate the hematopoietic system of irradiated mice for more than six months and to subsequently be serially transplanted into secondary recipients (Morrison and Weissman, 1994). LT-HSCs generate their immediate progeny, short-term stem cells (ST-HSC) which are capable of multilineage commitment but have reduced self-renewal potential, and are only able to repopulate irradiated mice for 6-8 weeks and lack the ability to be serially transplanted (Adolfsson *et al.*, 2001; Christensen and Weissman, 2001). Even though HSCs are present at a very low level in the bone marrow, it is possible to isolate them in nearly pure form based on their immunophenotypical characteristics. The finding that a single transplanted stem cell is capable of completely repopulating a host's ablated hematopoietic system demonstrates the enormous power of HSC self-renewal (Camargo *et al.*, 2006; Dykstra *et al.*, 2007; Wagers *et al.*, 2002).

The hematopoietic process is orchestrated by the concerted action of cell surface-bound and soluble cytokines that activate their cognate receptors presented at the cell surface of HSCs and their progenitors. Cytokines of the hematopoietic system include stem cell factor (SCF), FL, colony-stimulating factors (CSFs), interleukins (ILs), interferons, erythropoietin (EPO) and thrombopoietin (TPO) (**Fig. 3**). Many hematopoietic receptors belong to the type I cytokine receptor or type III tyrosine kinase receptor families.

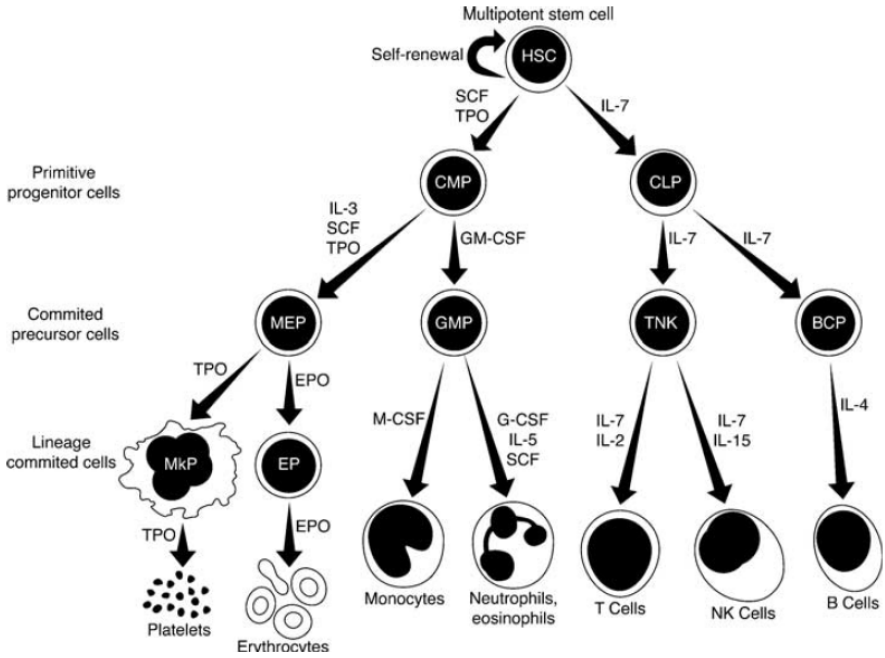

FIGURE 3. Hematopoiesis and the role of cytokines *in vivo*.

Cytokines act on both multipotential HSC/progenitor cells and their committed offspring. Major points, pinpointed by gene-targeting studies, at which cytokines act to provide survival and proliferation signals and, in some cases, differentiative signals are indicated. ***Adopted from Robb, 2007.***

Two general models for the role of cytokines and their receptors in hematopoietic differentiation have been proposed: the instructive model and the stochastic model. In the instructive model, cytokines transmit specific signals to multipotential hematopoietic cells directing their lineage commitment and differentiation. In the stochastic, or permissive, model lineage commitment and terminal differentiation are intrinsically determined by a program of transcription factors with cytokines providing permissive growth and survival signals. The instructive model recognizes the role of transcription factors but proposes that cytokine signaling also plays a fundamental role in lineage determination. Evidence is accumulating that some, but not all, cytokine receptors can transduce a genuine lineage-determining signal at some points in hematopoiesis, especially at the point of divergence of the myeloid and lymphoid lineages. Further studies are however needed to fully explore the scope of instructive signaling (Robb, 2007).

Receptor Tyrosine Kinases (RTKs)

Protein kinases constitute a large and diverse family of enzymes that catalyze the transfer of the terminal phosphoryl group from a nucleoside donor, such as ATP to the hydroxyl side chain of a specific serine, threonine or tyrosine residue in a protein substrate and thereby regulate the activity of their target protein. Unlike serine and threonine protein kinases, which constitute the large majority of protein kinases in the human genome (Manning *et al.*, 2002), and are conserved in both unicellular and multicellular eukaryotes, tyrosine protein kinases (TKs) are only found in Metazoans. In these organisms they are critical components of processes that require intercellular communication such as growth, differentiation, adhesion, motility and cell death. Many TKs are known as proto-oncogenes, which emphasizes their important role in cell signaling.

TKs can be divided into two subgroups: the single-pass transmembrane receptor tyrosine kinases (RTKs), and the intracellular non-receptor protein tyrosine kinases (NRTKs). Complete sequencing of the human genome revealed that it encodes for 90 TKs of which 58 are of the receptor type (**Fig. 4**) (Robinson *et al.*, 2000).

The NRTKs are integral components of the signaling cascades triggered by RTKs and other cell surface receptors such as G protein-coupled receptors and cytokine receptors. Some NRTKs (Janus kinases) are directly associated with the membrane-bound type I and II cytokine receptors. Some types are anchored to the membrane by N-terminal modifications such as myristoilyation or palmitoylation (e.g. Src), and others types exist as intracellular soluble proteins (e.g. BRK/PTK6). In addition to a tyrosine kinase domain, NRTKs possess other domains - such as Src homology-2 (SH2) and Src homology-3 (SH3) domains - that modulate their activity.

The 58 RTKs are embedded in the membrane and have a similar modular structure composed of an extracellular ligand binding domain, a single transmembrane spanning helix and a well conserved intracellular tyrosine kinase domain. They are divided into 20 classes according to the molecular architecture of their extracellular ligand binding domains (**Fig. 5**) (Lemmon and Schlessinger, 2010).

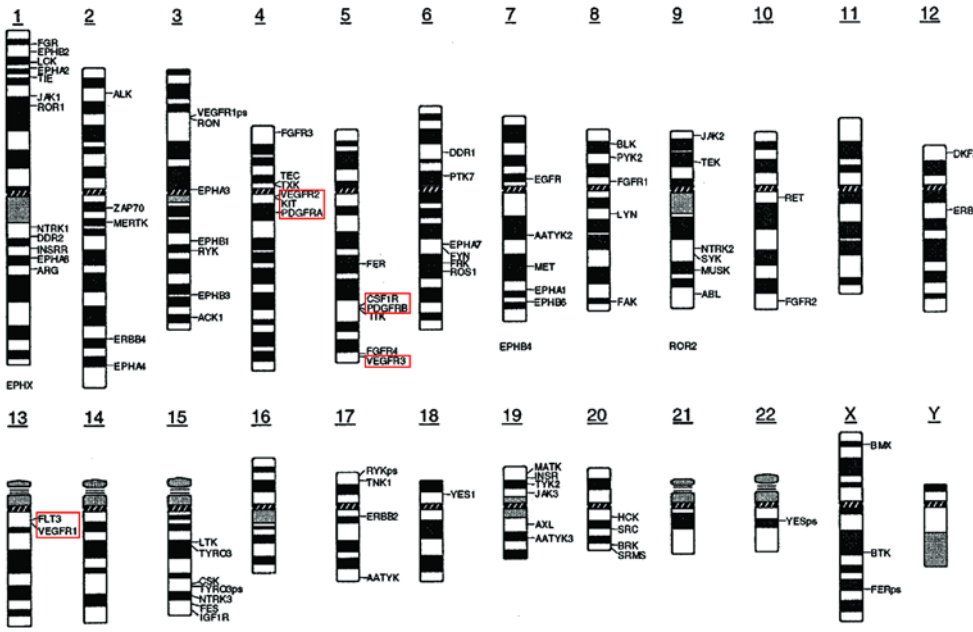

FIGURE 4. Distribution of the 90 protein tyrosine kinase genes in the human genome.

The chromosomal localization of the RTKIII genes for the KIT, CSF-1R, Flt3, PDGF-Rα and PDGF-Rβ receptors, and the RTKV genes for the VEGF-R1, VEGF-R2 and VEGF-R-3 receptors are indicated with a red box. The *Flt3* gene is located on chromosome 13. ***Adapted from Robinson et al., 2000.***

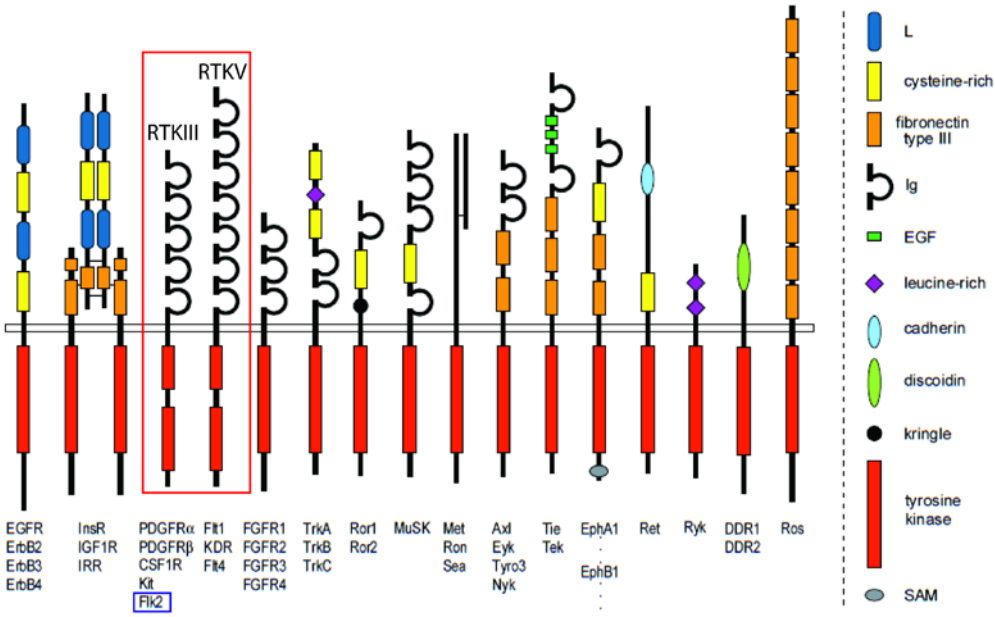

FIGURE 5. Domain organization for a variety of RTK classes.

The extracellular portion of the receptors is on top and the cytoplasmic TKD below. The receptors as shown are only approximately to scale. The different types of domains found in the extracellular regions of RTKs are shown schematically on the right. The closely related RTKIII and RTKV families with 5 and 7 Ig-like domains, respectively, are indicated with a red box. The Flt3/Flk2 receptor (blue box) is a member of the RTKIII-family. Note the presence of a kinase insert domain in the RTKIII/V family. ***Adapted from Hubbard and Till, 2000.***

With the exception of members of the insulin receptor family, which are preformed dimers linked by a disulfide bridge, it is believed that most RTKs diffuse as inactive monomers in the cell membrane. However, for a number of RTKs, including EGFR (Moriki *et al.*, 2001) and TrkA (Shen and Maruyama, 2011), it has been shown that they exist as inactive preformed dimers or in a monomer-dimer equilibrium. The techniques used to study the oligomeric state of these RTKs in the cell membrane include chemical crosslinking, FRET, bimolecular fluorescence complementation (BiFC), luciferase fragment complementation assays, fluorescence correlation spectroscopy and, more recently, quantum-dot-based optical tracking of single molecules (Chung *et al.*, 2010).

It is interesting to note that the type I cytokine receptors, EpoR and GHR also exist as preformed dimers (Constantinescu *et al.*, 2001; Brown *et al.*, 2005).

RTKs are activated by the binding of a cognate protein ligand to their extracellular region. Ligand-binding, which can be accompanied by conformational changes in the receptor ectodomain, leads to the formation of a dimeric receptor assembly in which the adjacent intracellular TKDs are orientated in a state that allows their activation by a process termed trans-autophosphorylation. Subsequently, the activated TKDs initiate a signaling cascade that may lead to a cellular response. The activation mechanism of the TKDs will be discussed further.

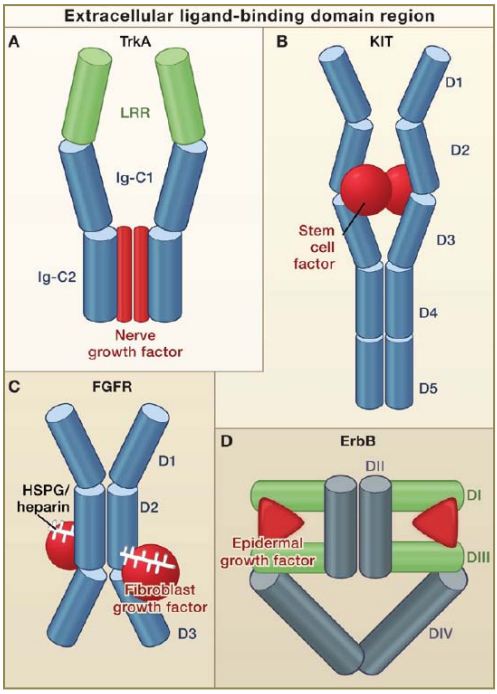

FIGURE 6. A diversity of mechanisms to dimerize RTKs.

(A) A nerve growth factor dimer (red) crosslinks two TrkA receptors molecules without any direct contact between the two receptors (Wehrman *et al.*, 2007). (**B)** A stem cell factor dimer (red) also crosslinks two KIT molecules. In addition, two Ig-like domains (D4 and D5), which reorient upon receptor activation, interact across the dimer interface (Yuzawa *et al.*, 2007). Thus, KIT combines ligand-mediated and receptor-mediated dimerization modes. (**C)** Two fibroblast growth factor receptor (FGFR) molecules contact one another through the Ig-like domain D2, and the accessory molecule heparin or heparin sulfate proteoglycans (white sticks) also contact this domain (Schlessinger *et al.*, 2000). In addition, each fibroblast growth factor molecule (red) contacts Ig-like domains D2 and D3 of both FGFR molecules. (**D)** Dimerization of ErbB receptors is mediated entirely by the receptor. Binding simultaneously to two sites (DI and DIII) within the same receptor molecule, the ligand drives conformational changes in the epidermal growth factor receptor (EGFR) that expose a previously occluded dimerization site in domain II (Garrett *et al.*, 2002; Ogiso *et al.*, 2002). ***Adopted from Lemmon and Schlessinger, 2010.***

An increasing number of high-resolution structures of ligand-receptor complexes learn that there exist many different mechanisms by which ligands induce the dimerization of their receptor (**Fig. 6**). Receptor-dimerization can be entirely ligand-mediated, without the formation of receptor-receptor contacts (e.g. TrkA, **Fig. 6A**). On the other extreme, dimerization can be entirely receptor-mediated (e.g. ErbB, **Fig. 6D**). In such a case the ligand induces a conformational change in the unbound autoinhibited receptor that exposes a dimerization motif. Also complexes where both the ligand and the receptor directly contribute to the dimerization have been observed (e.g. KIT and FGFR, **Fig. 6B, C**) (Hubbard and Miller, 2007; Lemmon and Schlessinger, 2010).

That some receptor tyrosine kinases play an important role in hematopoietic development was established by the discovery of the RTKIII receptors, FMS and KIT. FMS (a.k.a. CSF-1R) is the cellular counterpart of v-FMS encoded by the leukemia-causing Feline McDonough Sarcoma virus and was shown to be the receptor for Colony Stimulating Factor-1 (CSF-1), a growth factor required for the proliferation and differentiation of monocytes (McDonough *et al.*, 1971; Ralph *et al.*, 1986; Sacca *et al.*, 1986). KIT, the cellular counterpart of v-KIT, encoded by Hardy-Zuckerman 4 feline sarcoma virus, is the receptor for Stem Cell Factor (SCF) (a.k.a. Steel Factor). As its name implies, SCF directly acts on hematopoietic stem cells and their early progenitors. The genes for KIT and SCF were found to colocalize with the White Spotting (W) and the Steel (Sl) locus, respectively. In mice that carry mutations in these loci, hematopoiesis is severely affected (Besmer *et al.*, 1986; Chabot *et al.*, 1988; Huang *et al.*, 1990; Zsebo *et al.*, 1990).

FLT3, a type III receptor tyrosine kinase

Discovery and initial characterization of the Flt3 receptor

In search for additional hematopoietic RTKs, Matthews and colleagues performed degenerate PCR on cDNA isolated from murine fetal liver. The primers they used were mixtures of oligonucleotides directed against two invariant amino acid motifs present in tyrosine kinase domains (Wilks and Kurban, 1988). As such, a unique tyrosine kinase sequence was discovered. Subsequently, its complete cDNA was cloned and shown to encode for a receptor tyrosine kinase. The newly identified protein was designated as Fetal liver kinase - 2 (Flk-2) (Matthews *et al.*, 1991). The ligand for Flk-2 was yet unknown.

In an alternative approach, Rosnet and collaborators performed low-stringency hybridization against murine cDNA libraries with a cDNA probe that encoded the FMS kinase region. The RTK they discovered was termed FMS-like tyrosine kinase 3 (Flt3) (Rosnet *et al.*, 1991). Flt3 and Flk-2 corresponded to the same protein. Using murine probes, the human Flt3 cDNA was consequently isolated and cloned by two independent groups (Rosnet *et al.*, 1993; Small *et al.*, 1994).

The human Flt3 gene is located on chromosome 13 and contains 24 exons that span a length of about 100 kbp (Abu-Duhier *et al.*, 2001). Its cDNA encodes a 993 amino acids long protein that has an overall sequence identity of 86% with its murine ortholog. This level of identity is observed all along the molecule. Analysis of the human Flt3 protein sequence shows that it contains an N-terminal signal peptide (residues 1-26) that is followed by an extracellular region (residues 27-541) harboring 9 predicted N-linked glycosylation sites and 22 cysteines. This ectodomain is connected to a 21-residue long transmembrane helix (residues 542-562). On the intracellular site, the juxtamembrane region (residues 563-603) is followed by a tyrosine kinase domain (residues 604-950) interspersed with a kinase insert region (residues 711 - 780) and ending with a C-terminal tail (951-993). The kinase insert region, which connects the N-and C-lobe of the tyrosine kinase domain, is a typical feature for members of the RTKIII and RTKV family (**Fig. 5**).

Pulse-chase analysis of murine Flt3 in transfected COS-cells showed that it is expressed as an immature mannose-rich form of 143 kDa and a mature cell surface-expressed complex carbohydrate form of 158 kDa. Experiments with tunicamycin and enzymatic deglycosylation with various glycosidases showed that Flt3 is extensively N-glycosylated and bares little or no O-glycosylation (Lyman *et al.*, 1993b; Maroc *et al.*, 1993).

Expression analysis of the Flt3 mRNA by RT-PCR and Northern blot analysis in murine and human tissues showed that the Flt3 gene is expressed in virtually all fetal and adult lympho-hematopoietic organs, such as liver, spleen, thymus, lymph nodes, bone marrow and placenta. Flt3 was also found to be expressed in a series of immature cell lines and leukemias of lymphocytic origin (Lyman *et al.*, 1993b; Maroc *et al.*, 1993), and in primary leukemia and lymphoma samples (Birg *et al.*, 1992).

Homology with other RTKs

Sequence analysis of the extracellular region of the Flt3 protein revealed that it is a member of the RTKIII family. The members of this family have 5 immunoglobulin (Ig)-like domains in their ectodomain. The Ig-like domain is a module of about 100 residues and has a β-sandwich structure harboring 7 to 9 β-strands, labeled A to G. Typically, an intersheet disulfide bridge is formed between strands B and F. Apart from its presence in antibodies, the Ig-fold is found in many cell adhesion molecules and surface receptors. Ig-like domains can be classified according their number of strands and their topology (**Fig. 7A**) (Halaby *et al.*, 1999; Harpaz and Chothia, 1994).

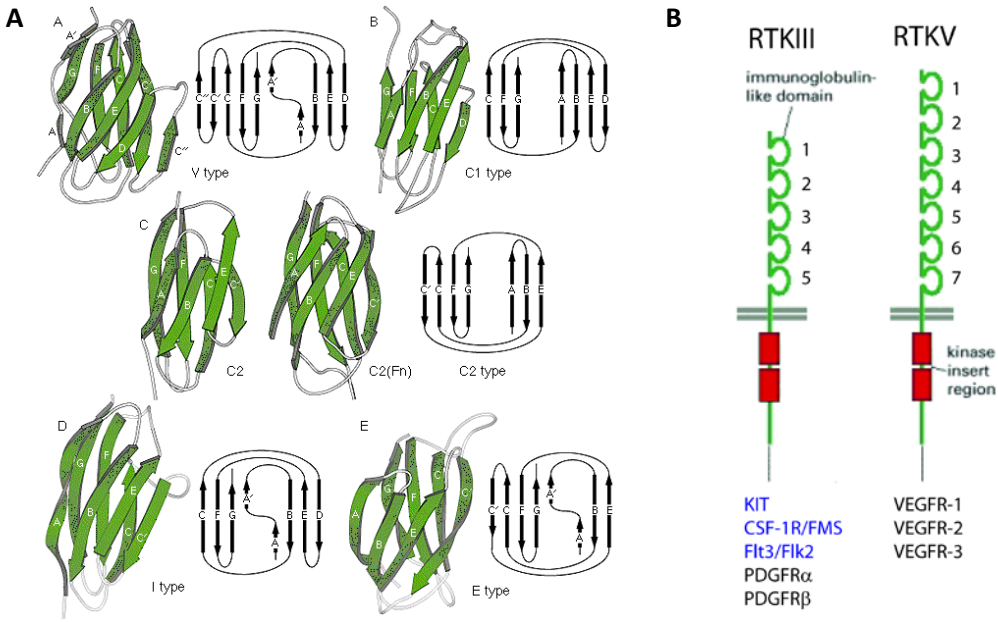

FIGURE 7

(A) Structural diversity in the immunoglobulin-like superfamily. According to the number of strands and their topology Ig-like domains can be divided into several types: the V-, C1-, C2-, I- and E-types. Flt3 domains 1, 3 and 4 belong to the I-set of Ig-like domains, while domains 2 and 5 belong to the C2-set. The characteristic disulfide bride between strands B and F is absent in Flt3 domains 1 and 4. There it is replaced by a pair of hydrophobic residues. ***Adopted from Sun et al., 2004.***

(B) Schematic representation of the structure of the RTKIII/V members. Flt3 is a member of the RTKIII-family whose members have 5 Ig-like domains (green loops) in their extracellular region. The RTKIII-family is closely related to the RTKV-family which harbors the VEGF receptors with 7 Ig-like domains.

The RTKIII family also includes the KIT, CSF-1R and the platelet-derived growth factor receptors α and β (PDGF-Rα and PDGF-Rβ), and is closely related to the RTKV family which harbors the vascular endothelial growth factor receptors (VEGF-R1, VEGF-R2 and VEGF-R3) with 7 Ig-like domains in their ectodomain (**Fig. 7B**). The overall similarity in sequence and structure between the members of these two families, together with the chromosomal localization of their genes (**Fig. 4**), suggests that these receptors evolved from a common ancestral RTKIII/V gene. Based on a molecular phylogenetic analysis and the sequence of the surrounding genomic regions Grassot *et al.* proposed that the different RTKIII/V members arose by a series of cis and trans duplications, followed by gene loss (**Fig. 8**) (Grassot *et al.*, 2006) .

Flt3 is most homologous to the hematopoietic KIT and FMS receptors. Human Flt3 shows respectively 18% and 19% identity with KIT and FMS in the extracellular region, and 63% and 64% in the tyrosine kinase domain. FMS and KIT are more closely related to each other, because they are 27% and 71% identical in their extracellular regions and kinase domains respectively.

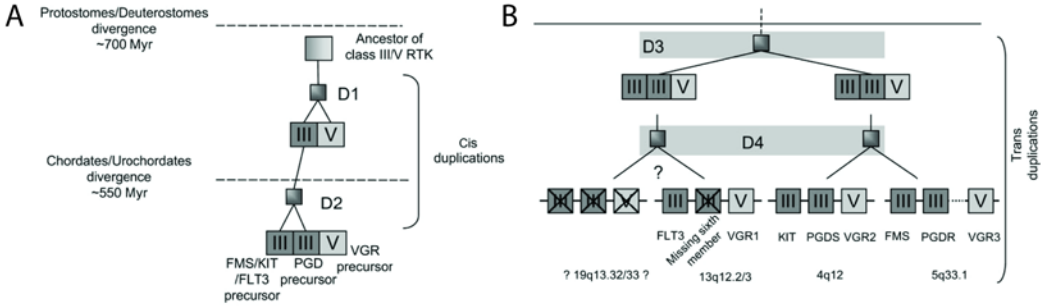

FIGURE 8. Hypothetical scenario for the origin and divergence of class III and class V RTK.

(A) Cis duplications (D1 and D2) resulted in the shared ancestor of class III and class V RTK

(B) Trans duplications resulted in class III and class V RTK diversification. Two rounds of duplication (D3 and D4) were followed by gene loss. ***Adapted from Grassot et al., 2006.***

Taken together, Flt3, KIT and CSF-1R share only 9% sequence identity in their extracellular domain (**Appendix A**). These conserved residues correspond to intramolecular disulfide bridges and other key residues that stabilize the different immunoglobulin folds in the ectodomain. The intracellular kinase domains are however strongly conserved and share an overall sequence identity of 57% (Rosnet *et al.*, 1993).

Flt3 exhibits some remarkable sequence features which are not present in the other RTKIII members. Strikingly, Flt3 contains an additional 12 cysteines which are not present in KIT or FMS. Furthermore, as characterized by a conserved spacing of cysteines, Flt3 Ig-like domains 1 and 2 share significant homology with Ig-like domains 4 and 5 (**Appendix B**). This homology suggests that the Flt3 extracellular domain has arisen by an ancient duplication event. This level of intragenic homology is not found in the other RTKIII members (Matthews *et al.*, 1991; Rosnet *et al.*, 1991).

Furthermore, in Flt3, the first Ig-like domain is preceded by an N-terminal sequence of 50 residues that shows no homology to other known proteins. Secondary structure prediction suggests that this region contains several β-strands. In this respect, it is interesting to note that the exon/intron structure of the Flt3 gene in the region which encodes the N-terminal stretch and Ig-like domains 1 and 2 is different from the one found in KIT and CSF-1R (**Fig. 9**). Further downstream the exon/intron organization between Flt3, KIT and CSF-1R is conserved (Abu-Duhier *et al.*, 2001; Agnes *et al.*, 1994) (**Appendix A**).

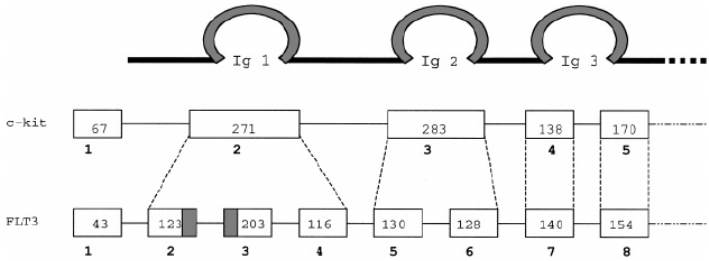

FIGURE 9. Flt3 has a unique genomic structure in the N-terminal region.
Comparison of the structural organization of the 5' end of the human Flt3 and KIT genes in relation to the first three Ig-domains. Bold numbers correspond to exon numbering while exon sizes (bp) are indicated in the corresponding boxes. The CSF-1R gene has a similar organization as the KIT gene. ***Adopted from Abu-Duhier et al., 2001.***

In 1995, the Rosnet-group identified a murine isoform of the Flt3 receptor from a placental cDNA library. This isoform lacks domain 5 and is generated by the skipping of exons 11 and 12 (**Fig. 10**). This variant was shown to be functional as Flt3 ligand induced the phosphorylation of both forms of the receptor equally well. RT-PCR analysis showed that the isoform is expressed in most tissues that were tested, together with the larger form, although at a much lower level. From this study it was concluded that the fifth Ig-like of Flt3 domain is not strictly necessary for either ligand-binding or kinase activation (Lavagna *et al.*, 1995). The biological significance of this Flt3 isoform remains however unclear and a similar human Flt3 isoform has not been reported yet.

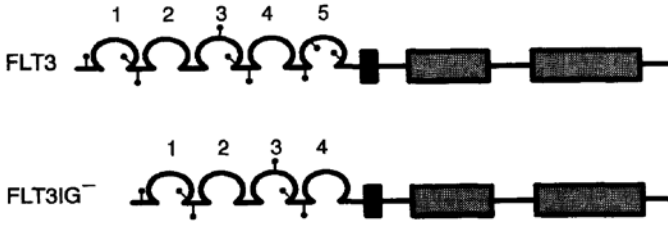

FIGURE 10. Active murine FLt3 isoform lacking the 5th domain.
Loops represent the Ig-like domains. Shade and black boxes represent the transmembrane and the split tyrosine kinase domains, respectively. Putative N-glycosylation sites are indicated by black circles. ***Adopted from Lavagna et al., 1995.***

Similar isoforms have also not been reported for the other RTKIII/V members. On the contrary, deletion of the fifth Ig-like domain of KIT results in a receptor variant that is incapable of ligand-induced phosphorylation (Broudy *et al.*, 2001).

For the KIT, PDGF-Rα and VEGF-R receptors, but not for Flt3, soluble forms of the receptor, resulting from ectodomain shedding from the cell surface or alternative splicing, have been reported and may serve as decoy receptors that modulate the function of their respective ligands (Broudy *et al.*, 2001; Rajakumar *et al.*, 2009; Tiesman and Hart, 1993; Wypych *et al.*, 1995; Philo *et al.*, 1996).

Prior to the identification of the cognate ligand for the Flt3 receptor, Maroc *et al.* showed that a CSF-1R/Flt3 chimera in which the murine CSF-1R ectodomain (residues 1 - 497) was fused to the murine Flt3 transmembrane and tyrosine kinase regions (residues 535-993) could be phosphorylated by CSF-1, and was able to transform fibroblast cells in the presence of CSF-1. Thereby it was demonstrated that the cytoplasmic Flt3 TKD can generate a strong mitogenic signal upon stimulation of a heterologous extracellular domain (Maroc *et al.*, 1993).

FL is the cognate ligand for the Flt3 receptor

Discovery and initial characterization of the Flt3 ligand

Given the homology between the Flt3 and the KIT and CSF-1R receptors, the unidentified ligand for the Flt3 receptor was expected to be a dimeric four helical bundle cytokine, like SCF and CSF-1 (Pandit *et al.*, 1992), the ligands for KIT and CSF-1R, respectively. In 1993-94, the ligand for the murine Flt3 receptor was cloned by two different groups, based on its ability to bind an Flt3-Fc fusion construct. By screening a cDNA expression library from a murine T-cell line that presented a factor at its surface that was capable of binding Flt3-Fc, Lyman and colleagues identified the Flt3 ligand (FL) (Lyman *et al.*, 1993a). In an alternative strategy, Hannum *et al.* isolated murine FL from the phytohemagglutinin-conditioned medium of a thymic stromal cell line by using an Flt3-Fc column (Hannum *et al.*, 1994). Consequently, the human FL cDNA was cloned (Lyman *et al.*, 1994; Hannum *et al.*, 1994).

The human FL gene maps to chromosome 19 and contains 8 exons. Its primary cDNA (exons 1-5 + 7 and 8) encodes for a homodimeric 235 amino acids long type I transmembrane protein consisting of four domains: 1) an N-terminal 26-residue signal peptide, 2) a 156-residue extracellular 'four-helical bundle' domain with a juxtamembrane tether region, 3) a 23-amino acid transmembrane domain and 4) a 30-residue cytoplasmic domain. Analyses of FL cDNA clones showed that alternative splicing of a putative sixth exon results in the generation of a soluble form of the FL protein (Lyman *et al.*, 1995c). A second soluble form of the ligand can be generated by proteolytic cleavage from the membrane bound form (Horiuchi *et al.*, 2009). The CSF-1 and SCF ligands have a similar genomic structure as FL and are also both active as a transmembrane or soluble form, generated by proteolytic cleavage or alternative splicing (Lyman and Jacobsen, 1998; Stein *et al.*, 1990).

In their extracellular domains, the mouse and human Flt3 ligands are 74% identical. This value is slightly below that of the extracellular domains of the mouse and human Flt3 receptor which are 83% identical. Human and murine FL appear to have a good species cross-reactivity (Lyman *et al.*, 1994). This is unlike SCF and CSF-1. Murine SCF is active on human cells but the human protein shows little or no activity towards murine cells (Martin *et al.*, 1990). On the other hand, human

CSF-1 is active on murine cells but the murine ligand does not activate the human receptor (Garceau *et al.*, 2010).

Human FL contains two potential N-linked glycosylation sites, which are conserved in murine FL. Murine FL, derived from a stromal cell line carries approximately 12 kDa of N- and O-linked carbohydrates on each chain (McClanahan *et al.*, 1996). Human FL is reported to be N-glycosylated *in vivo* (Lyman and Jacobson, 1998).

FL mRNA is found in almost every tissue that has been examined, with the highest levels in peripheral blood mononuclear cells. However, contrary to the widespread tissue expression pattern of FL mRNA, little FL is actually made, with stromal fibroblasts and T lymphocytes being the major producers (McClanahan *et al.*, 1996).

Structure and homology with SCF and CSF-1

Residues 1 to 134 of mature FL, which encompass the four helical bundle fold, were shown to be sufficient for biological activity (Escobar *et al.*, 1998). This fragment was crystallized and its structure was solved by multiple isomorphous replacement (MIR) to a resolution of 2.2 Å (**Fig.11**) (Savvides *et al.*, 2000).

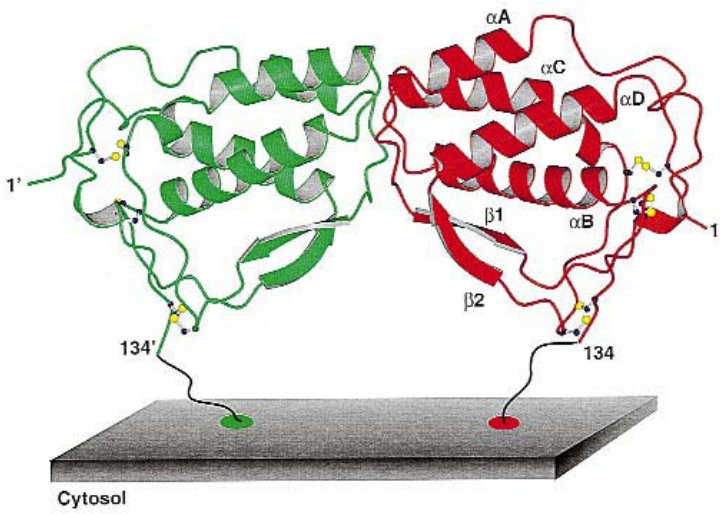

FIGURE 11. X-ray structure of human Flt3 ligand (pdb 1ETE, 2.2 Å resolution).

A cartoon representation of the FL structure (residues 1-134) in its transmembrane form is shown. The two protomers (green and red) adopt a four helical bundle fold (helices αA to αD) and interact in a 'head-to-head' arrangement through a hydrophobic dimer interface in which each subunit buries ~1,000 $Å^2$ of surface area. The three intermolecular disulfide bridges are shown as yellow 'ball-and-sticks'. FL_{1-134} was refolded from inclusion bodies.

Adopted from Savvides et al., 2000.

The structure shows that FL is a non-covalently linked homodimer with 3 intramolecular disulfide bridges. The subunits adopt a short-chain 'four helical bundle fold' with an 'up-up-down-down' topology and are arranged in a 'head-to-head' fashion. The twofold symmetry axis runs perpendicular to the bundle axis. The two FL protomers interact by a hydrophobic interface, in which each protomer buries 1000 $Å^2$ of solvent accessible area. This arrangement results in a flat elongated structure with overall dimensions of 75 Å x 35 Å x 25 Å. Although the amino acid sequence identity between FL, SCF, and M-CSF is less than 15%, these 3 cytokines have a similar structure (**Fig.12**). Four cysteine residues that form two intrachain disulfide bridges are conserved in all three proteins.

The helical bundle fold is found in many other cytokines, such as growth hormone (GH), erythropoietin (EPO), leptin, thrombopoietin and in many interleukins. These cytokines are however usually associated with type I and type II cytokine receptors that lack an intrinsic tyrosine kinase activity. As such, FL, SCF and CSF-1 constitute a small family of four helical bundle cytokines that activate type III receptor tyrosine kinases.

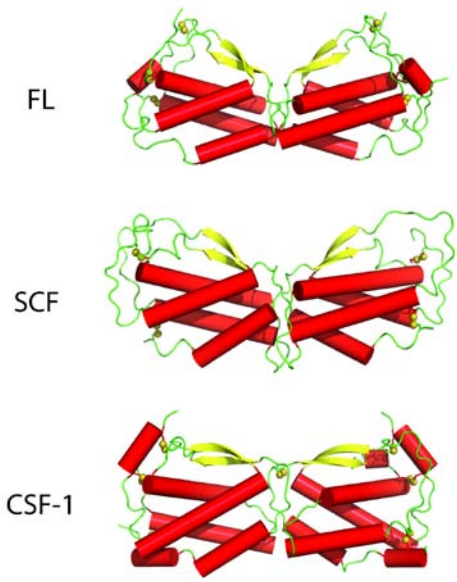

FIGURE 12. FL is structurally homologous to SCF and CSF-1.
Despite the low sequence similarity (< 15 % identity), FL (pdb 1ETE), SCF (pdb 1SCF/ pdb 1EXZ) and CSF-1 (pdb 3EJJ) adopt a similar four helical bundle fold. Four cysteine residues that form 2 disulfide bridges are conserved. FL and SCF are both non-covalently linked homodimers, while CSF-1 is a disulfide linked homodimer. The sulfur atoms involved in disulfide bridge formation are shown as yellow spheres.

The Flt3 ligand crystals contained two FL dimers in the asymmetric unit. The relative orientation of the protomers is identical in both FL dimers. On the other hand, available structures for SCF (pdb 1EXZ and 1SCF) show that the angle between the two protomers may vary by 2° to 6° (Yuzawa *et al.*, 2007). A similar variation in the angle between CSF-1 protomers has been observed (Elegheert J., personal communication).

FL and SCF are both non-covalently linked dimers while CSF-1 is a disulfide-linked dimer. By analytical gel filtration studies using radiolabeled SCF, it was shown that the majority of *E. coli* produced and refolded SCF exists as a monomer under physiological conditions (Hsu *et al.*, 1997). The dimer dissociation constant of recombinant SCF was determined by equilibrium sedimentation and size exclusion chromatography as 2.5 to 5 nM. SCF has been shown to be present at concentrations of approximately 177 pM (SCF monomer)(3 ng/mL) in human serum. Based on the determined dissociation constant, more than 90% of the circulating SCF would be in the monomeric form**.** This monomer/dimer equilibrium was found to be dependent on the pH and salt concentration, which suggested that there exist polar interactions at the dimer-interface. Recombinant SCF from CHO-cells exchanged equally well with the *E. coli*-derived non-glycosylated SCF, indicating that the attached carbohydrate moieties had no effect on monomer exchange (Lu *et al.*, 1995). Furthermore, a covalently linked form of recombinant SCF is reported to have a three times higher bioactivity then the wild-type (Lu *et al.*, 1996). Since FL is, like SCF, a non-covalently linked dimer, it is possible that it also exists as a monomeric form in human serum. This has not been investigated yet. Gel filtration studies with yeast-derived recombinant FL showed that it remains dimeric at concentrations as low as 500 nM (17 µg/mL) (Graddis *et al.*, 1998). This concentration is however much higher then the concentration of FL found in human serum (3 – 300 pM) (Chklovskaia *et al.*, 1999; Lyman *et al.*, 1995b; Wodnar-Filipowicz *et al.*, 1996). Lu and colleagues reported that a recombinant FL-FL fusion protein in which the two protomers were connected by a polyglycine linker had a ten times higher bioactivity (at a concentration of 800 pM (25 ng/mL) in their cell proliferation assay as compared to wild type FL (Lu *et al.*, 2002). This suggests that at low concentrations FL, like SCF, might dissociate into monomers.

Mutagenesis data for FL

A yeast-system based random mutagenesis screen indicated that the receptor-binding epitope of FL is located at the distal ends of the four helical bundles (Graddis *et al.*, 1998). Three hotspot regions were identified (positions 8-15, 81-87 and 116-124) (Fig. 12). The N-terminal loop (residues 8 - 15) appeared to be most crucial for binding as single point mutations in this region completely abrogated the activity of the ligand (**Fig. 13 & 14**). Mutagenesis studies for SCF and CSF-1 showed that this region is also important for their activity (reviewed in Savvides *et al.*, 2000). A mutation (Leu27Pro) that disrupts the FL dimer interface was found to decrease the bioactivity. Ensuing analytical gel filtration experiments showed that this mutant exists as a monomer at low concentrations.

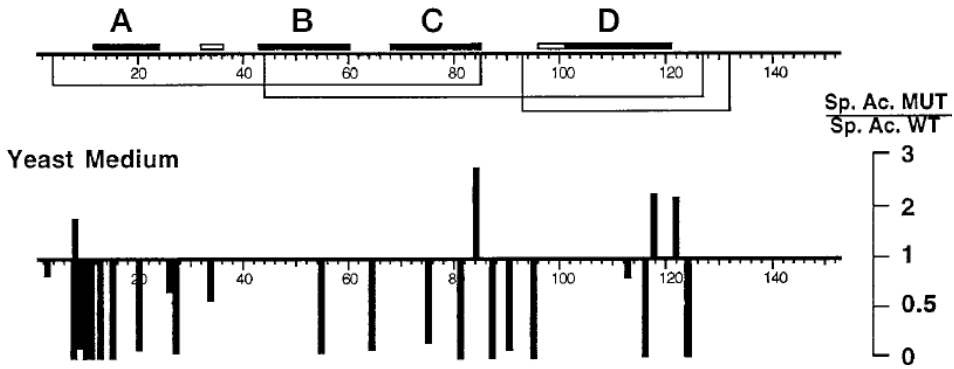

FIGURE 13. FL point-mutants that were found to have a effect on the bio-activity.

(Top) Representation of FL, including the intramolecular disulfide linkage, placement of β-sheet segments, and placement of α-helices A–D. **(Bottom)** Primary structure representation of FL with a superimposition of the relative specific activity profile of mutants with single amino acid substitutions. Their specific activity was determined by subjecting the yeast medium (in which these mutant proteins were secreted) to an ELISA and a WWF7 cell proliferation assay, which measure the levels of expression and biological activity, respectively.

Adopted from Graddis et al., 1998.

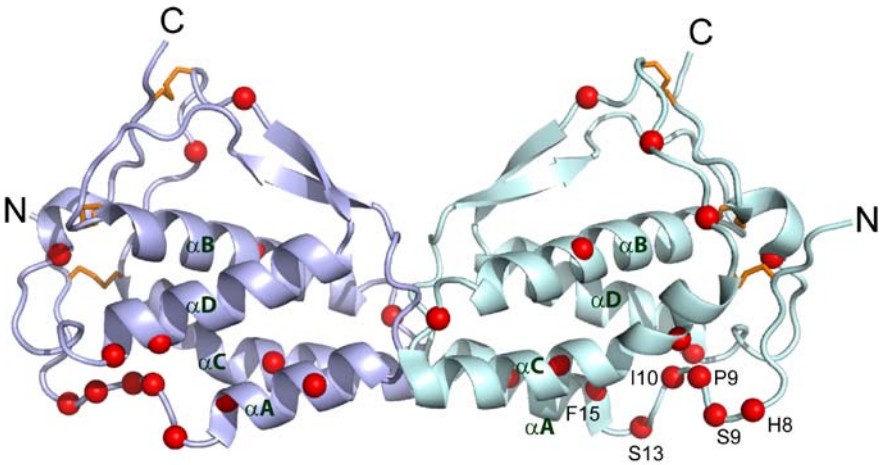

FIGURE 14. Inactivating point mutations mapped onto the FL structure.

The C-alpha atoms of residues, whose mutation resulted in reduced bio-activity are shown as red spheres. The residues in the N-terminal loop (residues 8-15) are labeled with their sequence number and one-letter amino acid code. The N- and C-terminus are indicated. The three intramolecular disulfides in each protomer are shown as orange sticks.

Role of the Flt3 ligand and receptor in hematopoiesis

FL and Flt3 knockout mice

FL$^{-/-}$ mice show a 27 to 45% decrease of the total number of complete nucleated cells in peripheral blood, bone marrow, spleen, and lymph nodes. In addition, the total number of granulocyte-monocyte progenitors (GMP) and B cell precursors is reduced. FL knockout mice also display about fivefold lower numbers of NK cells and 4 to 14 fold reduced, but functional DCs in lymphoid organs (McKenna *et al.*, 2000). By using these knock-out mice, a crucial role for FL during immune reconstitution after bone marrow transplantation and high-dose chemotherapy has been proposed (Buza-Vidas *et al.*, 2007).

Flt3$^{-/-}$ mice have a less pronounced phenotype and develop into healthy adults with normal peripheral blood counts. However, pro-B cell numbers are diminished and the bone marrow progenitors of these mice display a reduced ability to competitively repopulate lethally conditioned recipients (Mackarehtschian *et al.*, 1995).

In vitro and in vivo effects of FL

Numerous *in vitro* studies show that FL stimulates the growth of hematopoietic progenitors from the bone marrow, peripheral blood, and cord blood. FL is usually not sufficient when used as a single cytokine, but in synergy with other hematopoietic growth factors and interleukins it exerts pleiotropic effects on precursors of myeloid and lymphoid lineages. The combination of FL, SCF, TPO and IL-6 proved to be optimal for the *ex vivo* expansion of hematopoietic progenitors (Hudak *et al.*, 1995; Lyman, 1998).

When FL is administered to mice, hematopoiesis is significantly stimulated, leading to bone marrow hyperplasia, splenomegaly, and enlargement of the lymph nodes and liver (Brasel *et al.*, 1996). In combination with G-CSF, FL stimulates the mobilization of hematopoietic progenitors to the peripheral circulation in mice and primates (Molineux *et al.*, 1997; Sudo *et al.*, 1997). *In vivo* injection of FL also provides hematopoietic protection from total body irradiation (Gratwohl *et al.*, 1998).

Besides the stimulation of early hematopoiesis, FL was shown to have the remarkable activity to induce large numbers of DCs and NKs *in vivo* (Karsunky *et al.*, 2003; Maraskovsky *et al.*, 2000; McKenna *et al.*, 2000; Shaw *et al.*, 1998). For example, in healthy human volunteers, who were administrated FL for 10-14 days, a mobilization of both myeloid- and lymphoid-derived DC1 and DC2 precursors by 48- and 13-fold, respectively was observed.

In cancer immunotherapy, naive CD4+ and CD8+ T-cells must be presented with the tumor antigen and necessary co-stimulatory signals to enhance their maturation and activation. Since FL potently stimulates the expansion of dendritic cells much interest developed in its use as an antitumor agent. Studies showed that systemic administration of FL is effective in reducing tumor

growth and inducing a tumor infiltrate of DCs and cytotoxic T lymphocytes, as well as a clinically visible antitumor response (Dong *et al.*, 2002; Fong *et al.*, 2001).

In vivo FL levels reflect the state of the stem cell compartment

Under conditions of normal hematopoiesis, the FL concentration found in human serum is very low (< 3 pM) (Lyman *et al.*, 1995b). However, in hematopoietic malignancies that affect the stem cell compartment, like Fanconi anemia and acquired aplastic anemia, FL serum levels are highly elevated, up to 300 pM (Wodnar-Filipowicz, 2003). A similar 100-fold increase in FL serum levels is observed in patients that underwent chemoradiotherapy. On the other hand, FL levels do not increase in diseases affecting single blood lineages and do not normalize upon single lineage correction. This suggests that the increase in FL levels reflects a compensatory response whose aim is to restore the HSC compartment, and as such FL serum levels may serve as a surrogate maker of the HSC content in the bone marrow.

The mechanism that regulates FL serum levels is not completely understood but it is based on the release of preformed FL from intracellular stores by T lymphocytes, depending on the status of the stem cell compartment. By immunofluorescence confocal microscopy it was found that intracellular FL is stored within and close to the Golgi apparatus. The molecular mechanism that induces its release is not known (Chklovskaia *et al.*, 1999).

Flt3 expression profile in murine and human hematopoiesis

The expression profile of the Flt3 receptor in the stem cell compartment seems to be different in mice and human (**Fig. 15**) (Kikushige *et al.*, 2008). FACS-based analyses showed that in mice, the most primitive self-renewing HSC with long-term reconstituting (LT-HSC) activity are characterized by the following immunophenotype: (1) they lack the lineage-associated surface markers (Lin), they express high levels of KIT and Stem cell antigen-1 (Sca-1), (3) they show a low expression of Thymocyte differentiation antigen-1 (Thy1) and CD38 and (4) they are negative for CD34 and Flt3. Thus in mice LT-HSC are $Lin^{-}KIT^{+}Sca\text{-}1^{+}Thy1^{\mathbf{low}}CD34^{-}CD38^{\mathbf{low}}Flt3^{-}$. Human LT-HSC reside in the $Lin^{-}KIT^{+}Sca\text{-}1^{+}Thy1^{low}CD34^{+}CD38^{-}Flt3^{low}$ compartment (Ebihara *et al.*, 2002; Kikushige *et al.*, 2008; Sitnicka *et al.*, 2003). Thus contrary to mice, Flt3 seems to be expressed at low levels on LT-HSC in humans. In both species, Flt3 is upregulated in the later ST-HSC and MPP stages. In human, Flt3 is also expressed in early lymphoid and myeloid progenitors and in progenitors continuously along the granulocyte/macrophage pathway. In mouse, Flt3 is predominantly expressed in cells primed to the lymphoid pathway. Besides its role in early hematopoiesis, Flt3 expression is especially important, in both human and mice, for the development of dendritic cells, from both lymphoid and myeloid-committed progenitors. Furthermore, dendritic cells are the only mature hematopoietic cell type that express Flt3 (Karsunky *et al.*, 2003; Wu and Liu, 2007).

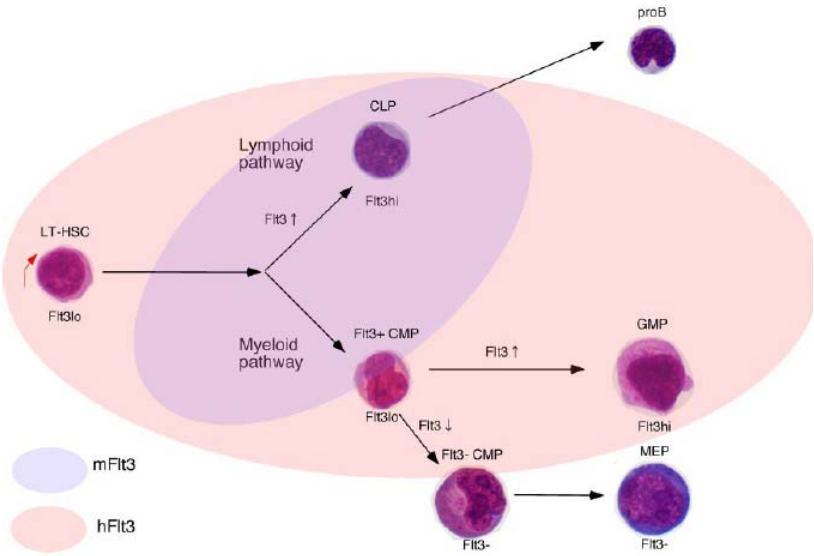

FIGURE 15. Proposed differential expression of human and mouse Flt3 in steady-state hematopoiesis.

Cellular morphology of directly sorted progenitors is shown. In human, the most primitive LT-HSC expressed hFlt3 at a low level and its expression is up-regulated at the early GM and the lymphoid progenitor stages, while it is down-regulated in MEPs. In contrast, the mouse LT-HSC lacks mFlt3 expression, and mFlt3 is expressed in cells primed to the lymphoid pathway, including CLPs and a fraction of CMPs. ***Adopted from Kikushige et al., 2008.***

RTKIII-receptors are activated by structurally diverse ligands

The cognate ligands for the Flt3, KIT and CSF-1R receptors are the hematopoietic four helical bundle cytokines FL, SCF and CSF-1. On the other hand, the ligands for the two other RTKIII receptors, PDGF-Rα and PDGF-Rβ, have a totally unrelated fold. They are 'cystine knot' cytokines and are structurally related to the ligands for the VEGF receptors of the RTKV family. These cytokines form covalently-linked dimers in which each protomer is folded into two highly twisted antiparallel pairs of β-strands. Each subunit also contains three intrachain disulfide bonds, from which two form a cystine ring through which the third bond passes. This motif is called a cystine knot. The various types of PDGF and VEGF molecules and their receptor specificity are shown in **Figures 16** and **17**, respectively. They are important regulators of lymph and blood vessel development.

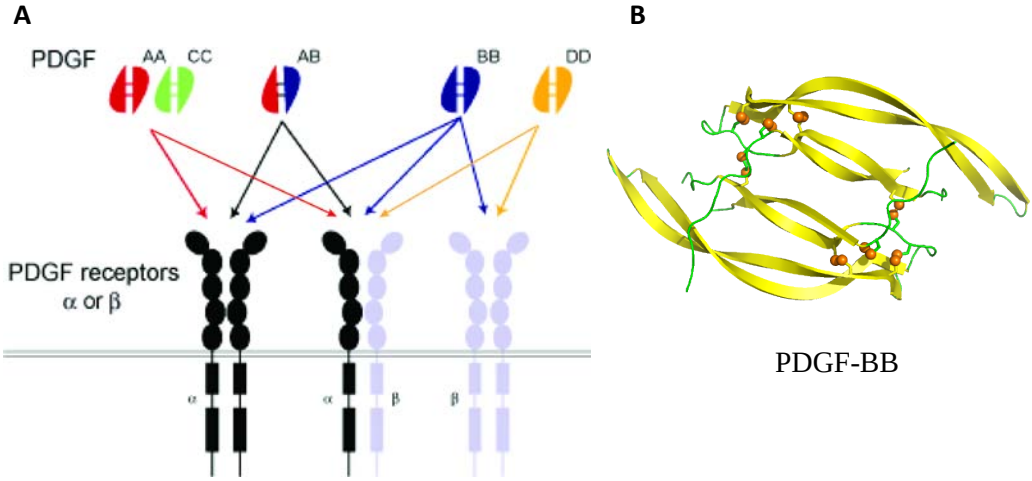

FIGURE 16. Binding specificity of various PDGF family members and their receptors.

(A) The PDGF family consists of four different PDGF chains (A–D), which assemble into functional homodimers or a PDGF-AB heterodimer, and two PDGF-R tyrosine kinases (α and β), which form a homodimer or heterodimer on ligand binding. PDGF-AA binds only PDGF-Rα, whereas PDGF-BB binds both homodimer and heterodimer PDGF-Rs. The less abundant PDGF-CC and -DD bind to PDGF-Rα and PDGF-Rβ homo-dimers, respectively, with both binding to the PDGF-Rαβ heterodimer. PDGF-C and -D are structurally more similar to the VEGF family than to the PDGFs (Ball *et al.*, 2007). **(B)** Structure of PDGF-BB (pdb 1PDG). The structure is orientated with the two-fold axis perpendicular to the plane. The three disulfide bridges that form cystine knot in each protomer and the two interchain disulfide bridges are shown as orange spheres (Oefner *et al.*, 1992).

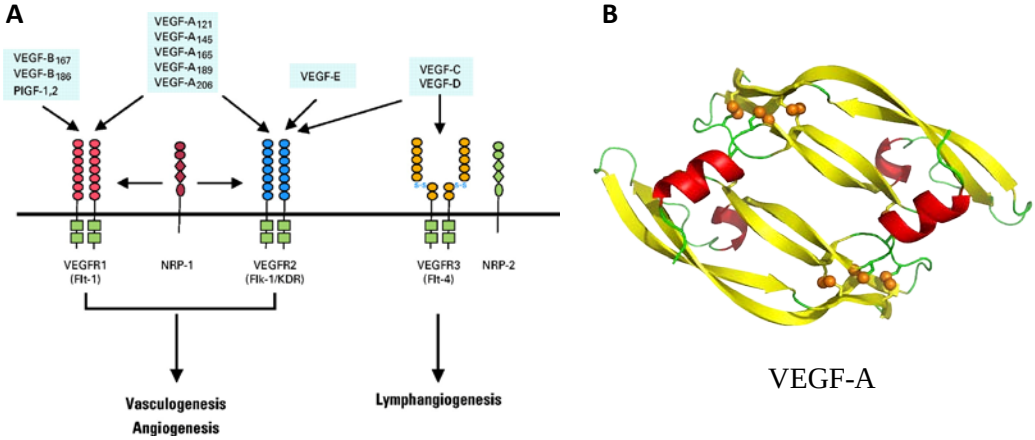

FIGURE 17. Binding specificity of various VEGF family members and their receptors.

(A) The VEGF family consists of seven ligands derived from distinct genes (VEGF-A, -B, -C, -D and -E, placenta growth factor (PlGF) -1 and -2). In addition, specific family members, such as VEGF-A, may be expressed as isoforms due to mRNA alternative splicing. VEGF family members and isoforms have specific binding affinities to VEGF-R1, VEGF-R2 and VEGF-R-3 tyrosine kinase receptors as shown. In addition, neuropilin (NRP) -1 and NRP-2 are co-receptors for specific isoforms of VEGF family members and increase binding affinity of these ligands to their respective receptors. ***Adopted from Hicklin and Ellis, 2005.*** **(B)** Structure of VEGF-A (pdb 1VPF). The VEGF-ligands are disulfide-linked cystine knot cytokines and are structurally homologous to the PDGF ligands (Muller *et al.*, 1997).

The RTKIII family of tyrosine kinase receptors thus constitutes a rare example of a receptor family that interacts with protein ligands having fundamentally different folds (**Fig. 18**). However, there exist some remarkable similarities between both types of cytokines. They all function as dimers and have two-fold axes of symmetry perpendicular to the longest dimension of the dimeric scaffolds. Furthermore, they have almost identical overall dimensions of ~70 Å x ~35 Å x ~25 Å (Savvides *et al.*, 2000). How these cytokines bind and activate their respective receptors will be the subject of the next sections.

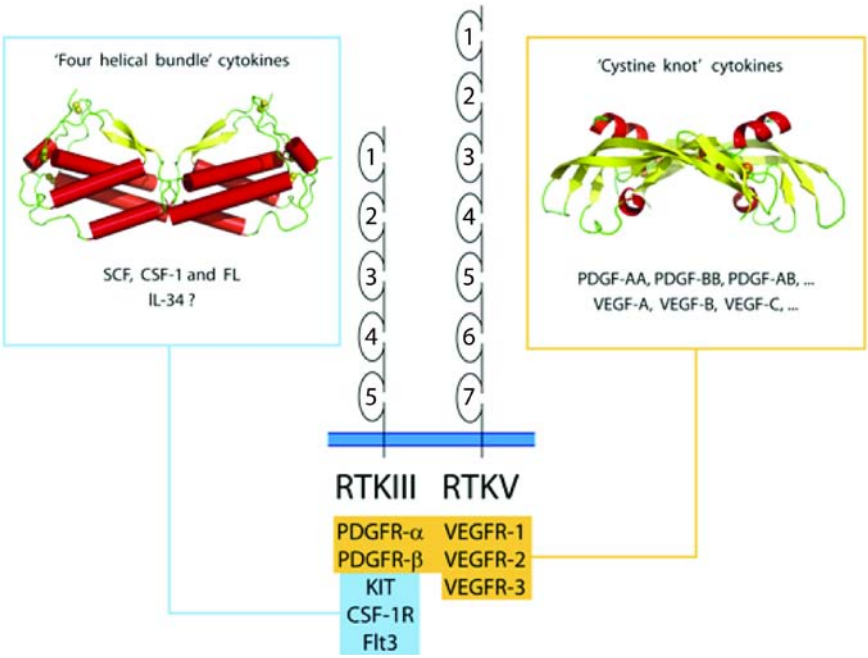

FIGURE 18. Receptors of the RTKIII family are activated by structurally unrelated cytokines. Members of the RTKIII family are activated by 'four helical bundle' cytokines (SCF, CSF-1 and FL) or by 'cystine knot' growth factors (PDGF ligands). The PDGF molecules are structurally related to the ligands for the VEGF-R receptors of the RTKV family. The structures of FL and VEGF-A are shown as a representative member for both type of cytokines. The structures are oriented with their P2-axes in the plane of the paper, and are colored according to their secondary structure (helical regions: red, β-strands: yellow).

Recently, a second ligand that can activate the CSF-1R receptor, termed interleukin-34 (IL-34) was identified (Lin *et al.*, 2008). IL-34 is a secreted homodimeric cytokine that has a monomeric length of 222 residues. Surface plasmon resonance (SPR) analysis showed that it bound to an immobilized CSF-1R$_{D1-D5}$-Fc construct with a dissociation constant of about 1 pM, while CSF-1 bound with a K_d of 34 pM. IL-34 has no significant sequence identity with CSF-1 or any other cytokine. Secondary structure predictions indicate that it is mainly α-helical but currently it is unclear if IL-34 adopts a similar fold like CSF-1.

It is also interesting to note that VEGF-A can signal through both the PDGF-Rα and PDGF-Rβ receptors. This reflects the close evolutionary and structural homologies that exist between these growth factors and their receptors (Ball *et al.*, 2007). This form of cross-talk has not been reported for the helical RTKIII cytokines.

Structure-function studies on Flt3, KIT and CSF-1R

Receptor dimerization at the cell surface

RTKs can exist in the membrane as monomers or as preformed dimers. In both cases, binding of their cognate ligand leads to the formation of active dimers. Cross-linking studies for KIT and Flt3 indicated that the unbound receptors exist as monomers in the cell membrane and that the addition of ligand induces their dimerization (**Fig. 19**) and activation (Kiyoi *et al.*, 2002; Lev *et al.*, 1992a; Turner *et al.*, 1996). For the CSF-1R receptor it was also shown that the ligand induces the formation of active dimers. One group suggested that the unbound form of CSF-1R exists, as indicated by cross-linking experiments, as an aggregate in the cell membrane (Li and Stanley, 1991). However, Carlberg and colleagues found that free CSF-1R behaves as a monomeric protein (Carlberg and Rohrschneider, 1994). For the binding of SCF to KIT, it was observed by cross-linking experiments that there occurs no dissociation of KIT dimers at high excess of SCF, in agreement with the absence a bell-shaped dose-response curve in cellular assays. This suggested that receptor dimerization is not only attributed by the bivalent nature of the ligand and that additional receptor-receptor interactions could also be involved in dimer stabilization.

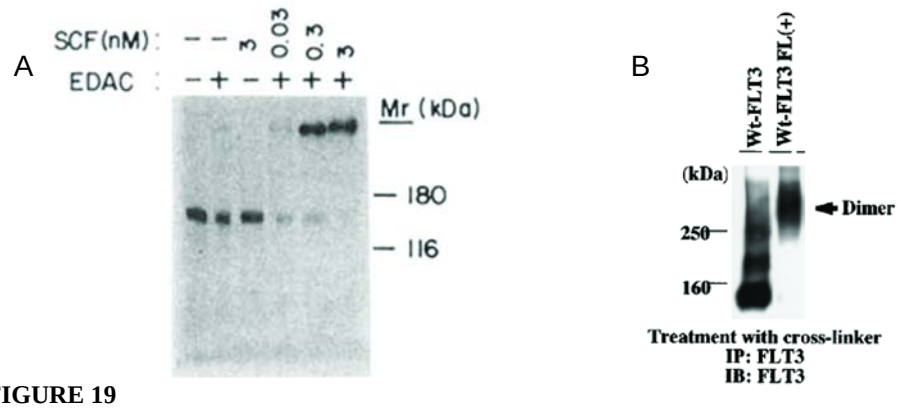

FIGURE 19

(A) Dimerization of Kit receptor in response to SCF binding.

COS-cells, expressing the KIT receptor, were incubated with increasing concentrations of recombinant SCF (as indicated). Consequently, the cells were incubated with 15 mM 1-ethyl-3-(3-dimethylaminopropyl)carbodiimide hydrochloride (EDAC). After cross-linking, the cell lysates were subjected to immunoprecipitation and Western blot analysis with anti-KIT-antibodies. A similar experiment with radiolabeled SCF indicated that SCF is contained in the cross-linked species. ***Adopted from Lev et al., 1992a.***

(B) Cross-linking of Flt3 at the cell surface.

Flt3 transfected 32D cells were incubated with 3 nM (100 ng/mL) recombinant FL and consequently incubated with 1 mM bis(sulfosuccinimidyl)suberate (BS^3). Cell lysates were subjected to immunoprecipitation and Western blot analysis with anti-Flt3-antibodies. ***Adopted from Kiyoi et al., 2002.***

SCF-induced KIT dimerization at the cell surface was also investigated by FRET. Donor and acceptor fluorochromes were coupled to a non-neutralizing KIT antibody. It was found that SCF induced a dose-dependent increase in KIT receptor dimerization that correlated well with the concentrations of SCF required to stimulate cell proliferation. Receptor dimerization was detectable within 3 minutes after the addition of SCF and was maximal 30 minutes after the addition of SCF (Broudy *et al.*, 1998).

Scatchard analysis of binding data obtained by the displacement of cell-bound radiolabeled ligand, indicated that SCF and CSF-1 bind to their receptors with an affinity of 2 nM and 35 pM, respectively (Lev *et al.*, 1992a; Wang *et al.*, 1993). Using the same approach, the affinity for the binding of FL to the full length Flt3 receptor was determined - in various cell lines - as 200 to 500 pM (Turner *et al.*, 1996).

In vitro complex formation with the soluble ectodomain

Size-exclusion chromatography (SEC) experiments with the purified soluble KIT and CSF-1R ectodomains (KIT_{D1-D5} and $CSF\text{-}1R_{D1-D5}$), produced in CHO-cells and Sf9 insect cells, respectively, showed that they were capable of forming complexes with their cognate dimeric ligands, as indicated by large shifts in the elution volume as compared to the receptor alone (**Fig. 20A,B**).

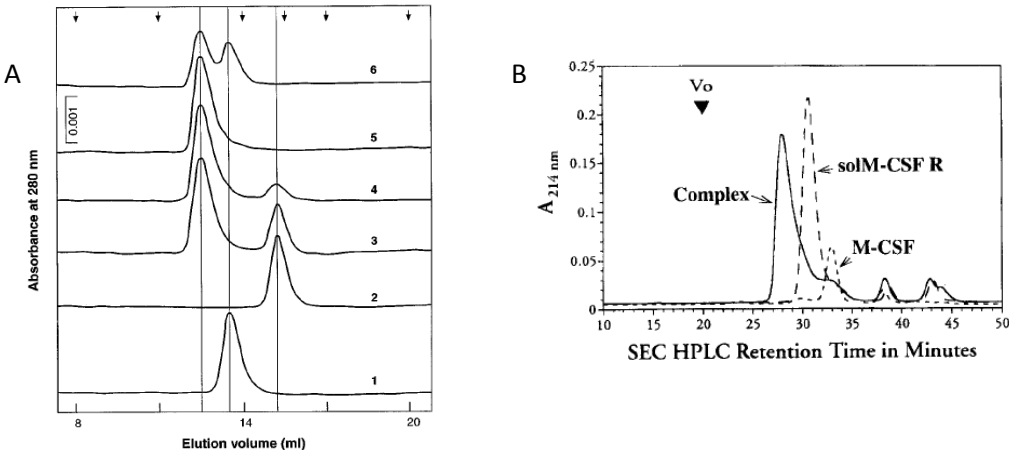

FIGURE 20. The soluble KIT and CSF-1R ectodomains form ternary complex with their ligands.
(A) KIT_{D1-D5} at 40 mg/ml (0.72 mM) was incubated with levels of *E. coli*-derived SCF ranging from 6.6 to 52.4 mg/ml (0.18–1.40 mM of SCF dimer) on a Superose 6 column. These represented molar ratios of sKit to SCF dimer of 4, 2, 1, and 0.5 (chromatograms 6, 5, 4, and 3, respectively). Chromatogram 2 represents SCF alone (in the amount used in chromatogram 3), and chromatogram 1 represents sKit alone. The MW of each component was analyzed by light scattering and equilibrium sedimentation. ***Adopted from Philo et al., 1996.***
(B) Superimposed SEC analyses (Superose 6) of the soluble extracellular domain of the CSF-1R receptor, $CSF\text{-}1R_{D1-D5}$ (solM-CSF R), a CSF-1(M-CSF) dimer, and a complex formed from a 2:1 M ratio mixture of these two molecules. The MW of each peak was confirmed on line, using light scattering. ***Adopted from Koths, 1997.***

The expected 2:1 stoichiometry for these complexes, namely, the binding of two receptors to one ligand, was confirmed by SEC combined with light scattering and later, by isothermal titration calorimetry (ITC) (Chen *et al.*, 2008; Koths, 1997; Lemmon *et al.*, 1997; Lev *et al.*, 1992b; Philo *et al.*, 1996). The dissociation constants for the full length complexes as obtained by ITC were 55 nM for the human KIT_{D1-D5}:SCF complex (at 25° C) (Lemmon *et al.*, 1997) and 9 nM for the murine CSF-$1R_{D1-D5}$:CSF-1 complex (at 30° C). The stoichiometry and the dissociation constant of the human KIT_{D1-D5}:SCF complex were also determined by equilibrium sedimentation analysis. By this method a K_d-value of 17 nM (at 25° C) was obtained (Philo *et al.*, 1996).

Native molecular weight estimations for unbound KIT_{D1-D5} and unbound CSF-$1R_{D1-D5}$, obtained by light scattering, indicated that they both are monomeric proteins in solution, and sedimentation equilibrium analysis on KIT_{D1-D5} showed that it behaved as an ideal single monomeric species, with no appreciable self-association at concentrations up to about 18 µM (1 mg/ml) (Philo *et al.*, 1996; Koths, 1997).

It was further found, by SEC and equilibrium sedimentation, that glycosylated SCF, produced in CHO-cells, has a much lower affinity for KIT_{D1-D5} then *E. coli*-derived SCF (590 nM vs 17 nM) (Philo *et al.*, 1996). This observation was consistent with its lower *in vitro* biological activity compared to non-glycosylated SCF. These differences were shown to be caused particularly by glycosylation at Asn93 and at Asn65 and presumably represent steric effects of the glycosylation (Lu *et al.*, 1992). This raises the awareness that glycosylation can strongly influence the strength of cytokine-receptor interactions.

Almost no biophysical or structural data about the Flt3 ligand-receptor interaction is available in the scientific literature. Moreover, the recombinant production of $Flt3_{D1-D5}$ or smaller ectodomain variants has never been reported. Thus, any assumptions about the molecular mechanism that underlies FL binding and receptor activation could only be made from structure-function studies on the homologous ligand-receptor complexes in the RTKIII family, and the closely related RTKV family. These studies will be discussed in the next section.

In one report however, the affinity and kinetics of binding of human FL to an $Flt3_{D1-D5}$-Fc fusion protein were analyzed by SPR. Recombinant FL from two different sources was compared: non-glycosylated *E. coli*-derived FL and glycosylated FL produced in Baby Hamster Kidney (BHK)-cells. The determined affinity for the *E. coli*-derived FL was 40 nM, with $k_{on} = 0.86 \times 10^6\ M^{-1}s^{-1}$ and $k_{off} = 34 \times 10^{-3}\ s^{-1}$. For glycosylated FL, a K_d value of 73 nM was obtained, with $k_{on} = 0.37 \times 10^6\ M^{-1}s^{-1}$ and $k_{off} = 25 \times 10^{-3}s^{-1}$ (Streeter *et al.*, 2001). Thus both forms bind Flt3-Fc with high affinity, although mammalian-derived FL binds slightly weaker. In agreement with these affinity measurements, a significant difference in the biological activity between glycosylated and non-glycosylated FL has not been reported.

Delineation of the ligand-binding epitope CSF-1R and KIT ectodomain

In order to investigate which Ig-like domains in the CSF-1R ectodomain contribute to ligand binding, a series of domain-deletion mutants (**Fig. 21**) were produced in Sf9 insect cells. Their binding affinity to CSF-1 was analyzed by competitive plate-binding immunoassays in which CSF-1R$_{D1-D5}$ was immobilized (Wang *et al.*, 1993).

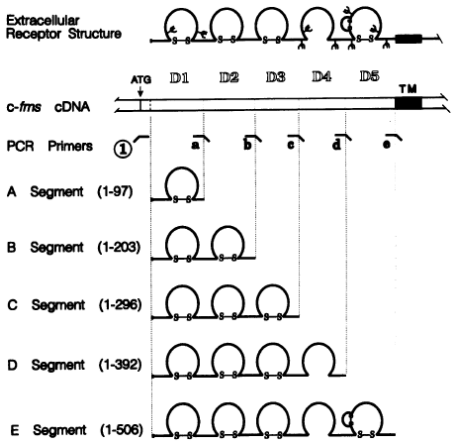

FIGURE 21. CSF-1R domain deletion mutants. CSF-1R extracellular domain segments produced as soluble proteins in Sf9 insect cells in order to delineate the ligand-binding epitope. The upper line of the diagram shows the predicted protein structural features of the murine CSF-1R extracellular domain with the cytoplasmic domain truncated just after the transmembrane (TM) region. The individual Ig-domains are designated Dl to D5, and intradomain disulfide bonds along with all nine potential sites for N-linked carbohydrate addition (small branched structures) are indicated. ***Adopted from Wang et al., 1993.***

From these experiments it was concluded that the first two N-terminal Ig-like domains do not interact with CSF-1 but, in combination with the third Ig-like domain, provide the high-affinity CSF-1 binding site. A construct that contained the fourth and fifth Ig-like domain, CSF-1R$_{D4-D5}$ did not exhibit CSF-1 binding.

Similar conclusions were drawn for the KIT:SCF interaction. By using human-mouse KIT interspecies chimera's and by mapping the binding epitope of antibodies that inhibited SCF binding, it was found that the SCF-binding site is contained in the first three N-terminal domains of KIT (Blechman *et al.*, 1993a; Lev *et al.*, 1993). Furthermore, cell-based competition binding-assays, employing recombinantly produced ectodomain variants, demonstrated that the third Ig-like domain is necessary for high-affinity binding (Blechman *et al.*, 1993b).

Probing the role of the membrane-proximal domains

In SEC experiments with the KIT ectodomain there was no evidence for the formation of ligand-receptor complexes in which only one receptor is bound to the ligand, even in the presence of a large excess of SCF. This indicated that receptor binding is positively cooperative and led to the hypothesis that the membrane-proximal domains (D4 and D5) might stabilize ligand-induced receptor dimers. By screening a series of monoclonal antibodies (mAb) directed against the KIT ectodomain that exerted little or no effect on ligand-binding, a mAb was identified that allowed SCF-binding but appeared to inhibit ligand-induced dimerization. When SCF was incubated with a KIT-expressing cell line, the presence of this antibody prevented chemical cross-linking of receptors

although SCF was able to bind (**Fig. 22A**). Moreover, this antibody was unable to recognize preformed dimeric KIT_{D1-D5}:SCF complexes (Blechman *et al.*, 1995).

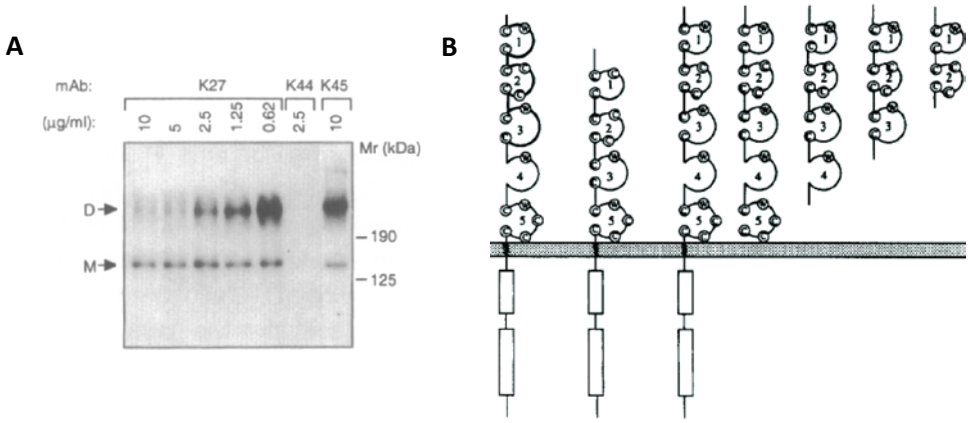

FIGURE 22

(A) mAb K27 allows SCF-binding but inhibits SCF-induced cross-linking to receptor dimers.

Monolayers of murine fibroblasts that overexpress human KIT were incubated with radiolabeled SCF in the presence of the indicated concentrations of various mAbs to Kit. Ligand-receptor complexes were covalently cross-linked with EDAC. Cell lysates were then analyzed by SDS-PAGE and the resulting autoradiograph is shown. ^{125}I-SCF, cross-linked to receptor monomers (M) and dimers (D) is indicated by arrows. It was concluded that mAb K27 allows ligand binding but inhibits cross-linking to KIT dimers in a concentration dependent manner.

(B) Epitope mapping of the mAb K27.

Schematic representation of the various recombinant soluble and membrane KIT proteins - expressed in CHO-cells - used to map the binding of epitope of mAb K7. Cysteines and conserved tryptophan residues are indicated.

Adopted from Blechman et al., 1995.

To map the binding epitope of this antibody several soluble and membrane-bound KIT mutants were generated (**Fig. 22B**). By co-immunoprecipitation experiments and cell-binding assays it was shown that the antibody bound to the fourth Ig-like domain. Further experiments showed that the antibody inhibited SCF-induced phosphorylation of KIT and a receptor mutant lacking domain 4 was unable to signal. Based on these observations, it was proposed that the fourth Ig-like domain of KIT mediates homotypic receptor-receptor contacts and as such couples ligand binding to signal transduction.

Subsequently, Lemmon and colleagues investigated the possible contribution of the membrane-proximal domains (D4 and D5) to the overall stability of KIT_{D1-D5}:SCF complex by biophysical methods. By SEC analysis, analytical ultracentrifugation, light scattering, and ITC experiments

(**Fig. 23**) it was found that KIT_{D1-D3} dimerizes upon SCF binding in a manner indistinguishable from that seen with KIT_{D1-D5}. It is interesting to note that it was not possible to chemically cross-link the receptor fragments in the $KIT_{D1-D3:}$SCF complex. Consequently, Lemmon argumented that the inhibitory antibody used by Blechman and colleagues, which was specific for D4, most likely did not prevent the ligand-induced dimerization of KIT_{D1-D5}. The absence of cross-linked receptors was most likely the result of a differential availability of reactive functional groups (Lemmon *et al.*, 1997).

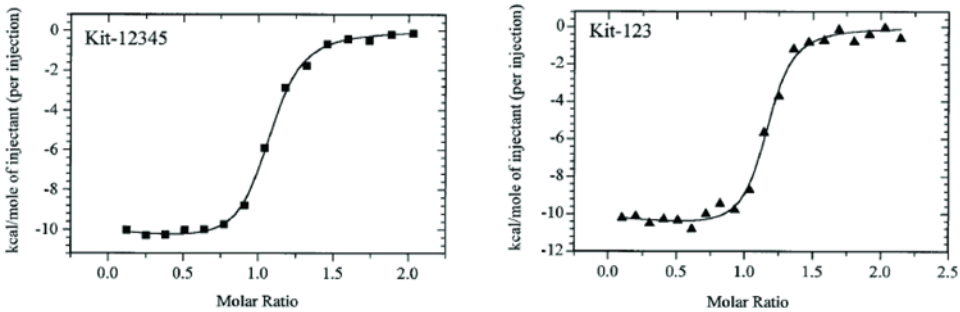

FIGURE 23. Calorimetric analysis of the binding of SCF to KIT_{D1-5} and KIT_{D1-3}.
SCF binds to KIT_{D1-D5} (left) with an affinity of 54.9 nM (with ΔH= -8.7 kcal/mol), while for KIT_{D1-D3} (right) the affinity was determined as 49.2 nM (with ΔH = -10.2 kcal/mol). The stoichiometry of both complexes is identical: one dimeric ligand binds two receptors. Binding is enthalpically driven and coupled to a small entropic penalty.
Adopted from Lemmon et al., 1997.

Since domains 4 and 5 do not contribute to the overall stability of the complex, it was concluded that KIT dimerization is primarily driven by the bivalent nature of its ligand. However, if bivalent binding of SCF were the only driving force for receptor dimerization, it should be possible to disrupt the KIT_2:SCF dimer into monomeric KIT:SCF complexes by the addition of excess SCF. In the SEC experiments for both KIT_{D1-D5} and KIT_{D1-D3} the formation of such monomeric complexes upon the addition of excess SCF could not be detected. Hence, it was suggested that the cooperativity is contained in the KIT_{D1-D3}:SCF subcomplex (Lemmon *et al.*, 1997).

Structure of the murine KIT_{D1-D3}:SCF complex

A ternary complex formed between *E. coli*-derived murine SCF and KIT_{D1-D3}, produced in Sf9 insect cells, yielded crystals that diffracted to 2.5 Å. To improve the crystal quality one of the three N-linked glycosylation sites present in KIT_{D1-D3} had been removed by mutagenesis. The structure was phased by 'single isomorphous replacement with anomalous scattering' (SIRAS) from an iodide derivative (Liu *et al.*, 2007) .

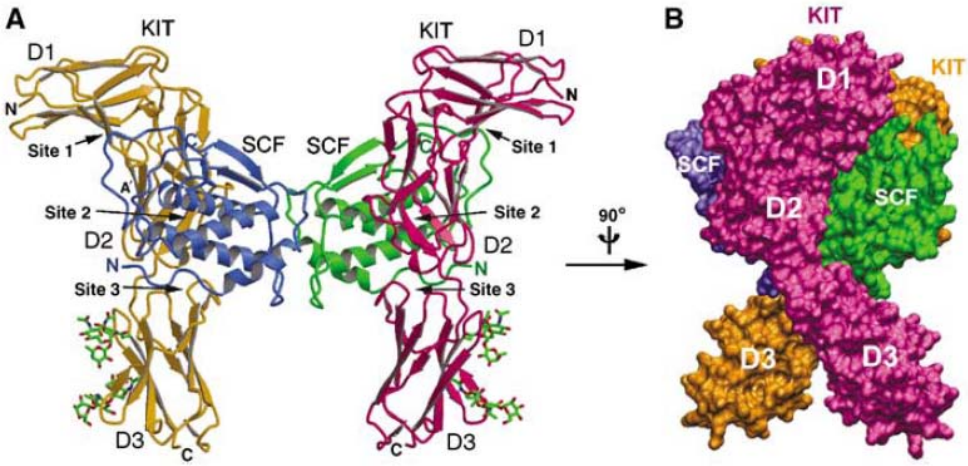

FIGURE 24. Ternary assembly of the murine KIT_{D1-D3}:SCF complex (pdb 2O26).
(A) Each KIT_{D1-D3} fragment (orange and magenta) binds one SCF protomer (blue and green) and the receptor fragments do not interact. The 3 interaction sites, one for each Ig-domain in KIT_{D1-D3} are indicated. N-linked carbohydrates are shown as green sticks. (**B)** Surface representation of the complex, showing how the KIT_{D1-D3} fragment wraps around one SCF protomer. ***Adopted from Liu et al., 2007.***

The structure shows that each KIT_{D1-D3} interacts with only one SCF, and no KIT:KIT interaction is observed (**Fig. 24**). Overall, about 2200 $Å^2$ of solvent-accessible surface is buried between each protomer of SCF and KIT_{D1-D3}, which can be subdivided into 610 $Å^2$ for site 1, the D1/SCF epitope, 760 $Å^2$ for site 2, the D2/SCF epitope, and 830 $Å^2$ for site 3, the D3/SCF epitope. Consistent with thermodynamic data which showed that KIT:SCF binding is enthalpically driven, the KIT:SCF binding interface buries large areas of hydrophilic surface, with abundant salt bridges and hydrogen bonds.

To assess any conformational changes that the ligand might undergo upon receptor binding, the X-ray structure of unbound murine SCF was determined (pdb 2O27). The unbound ligand showed a significant amount of surface regions disordered, including the N-terminal polypeptide chain (up to residue 11), the 92–104 loop and the 129–136 loop, as compared to the complexed form. The flexibility of these regions was also observed in free human SCF (pdb 1EXZ and pdb 1SCF). The disparity between the unbound and bound states suggested that the conformations of the N-terminal segment and the 92–104 loop of SCF are imposed by the receptor.

Based on the structural positions of the glycosylation sites in SCF, the authors argue that the 35-fold lower binding affinity and lower biological activity of glycosylated SCF as compared to *E. coli* derived-SCF (see higher) can be attributed to steric hindrance of the glycan chains.

Since no receptor-receptor contacts are seen for KIT_{D1-D3} it is difficult to rationalize a cooperative mode of binding as suggested by SEC experiments (Lemmon *et al.*, 1997). However, as outlined above, the ligand undergoes a series of conformational changes upon receptor binding. It cannot be excluded that the binding of the first receptor to one SCF protomer is communicated to the second protomer to form a high-affinity receptor binding site.

Structures of the human KIT_{D1-D5} ectodomain and the KIT_{D1-D5}:SCF complex

In 2007, Yuzawa and colleagues reported the crystal structures for the full length human KIT_{D1-D5} ectodomain alone, and in complex with its ligand SCF. KIT_{D1-D5} was produced in Sf9 insect cells and crystals of the partially deglycosylated protein diffracted to 3.0 Å. The dataset was phased using a combination of multi-wavelength anomalous dispersion (MAD) and multiple isomorphous replacement with anomalous scattering (MIRAS) from $K_2Pt(NO_2)_4$ and NaI derivatives. The resulting structure is shown in **Figure 25**.

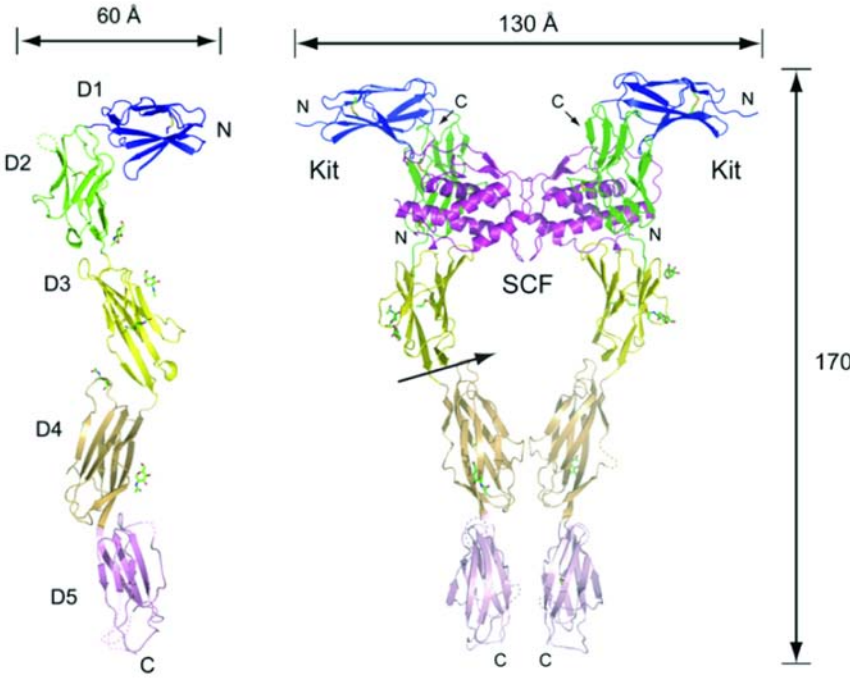

FIGURE 25. Structure of the KIT_{D1-5} ectodomain (pdb 2EC8) and SCF:KIT_{D1-5} complex.
The figure shows a comparison between the unbound KIT_{D1-D5} ectodomain (pdb 2EC8, left) and the KIT_{D1-D5}:SCF complex (pdb 2E9W, right). A SCF dimer interacts symmetrically with D1, D2, and D3 of two corresponding KIT_{D1-D5}. In addition, KIT ectodomains form homophylic interactions through lateral contacts between D4 (orange) and between D5 (pink) of two neighboring receptors. Note that D1, D2 and D3 adopt the same configuration in the unbound and SCF-bound state. N-linked carbohydrates are represented as sticks. The arrow marks the large cavity in the KIT_{D1-D5}:SCF complex. ***Adapted from Yuzawa et al., 2007.***

Crystals of the ternary KIT_{D1-D5}:SCF complex diffracted to 3.5 Å and this structure was solved by molecular replacement (MR) using the structure of the KIT ectodomain and the previously determined structure of human SCF (pdb 1EXZ). The complex structure shows that domains 1 to 3 wrap around one SCF protomer each, in a conformation similar to that seen in the murine KIT_{D1-D3}:SCF complex structure, while D4, and possibly D5, mediate homotypic receptor-receptor interactions (**Fig. 25**).

The solvent accessible surface area buried at the interface between KIT_{D1-D3} and each SCF protomer is approximately 2060 $Å^2$. A comparison of unbound KIT_{D1-D5} with SCF-bound KIT_{D1-D5} shows that domains 1 to 3 are superimposable with an RMSD of 1.1 Å for 274 aligned Cα residues of the D1-D3 region. Thus, KIT_{D1-D3} can be considered as a functional unit that is poised for SCF binding. Its conformation is maintained by the D1-D2 and D2-D3 interdomain interface regions that bury a surface area of 1240 $Å^2$ and 780 $Å^2$, respectively.

As was observed for free SCF in the murine KIT_{D1-D3}:SCF complex, several loop regions of human SCF - such as the N-terminal loop - undergo a conformational change upon receptor binding. In addition, in the full length KIT_{D1-D5}:SCF complex, an increase in the tilting angle of about 3° to 9° between both SCF-protomers is observed when compared to the structures for unbound SCF which display a variability in tilting between 2° and 6° (**Fig. 26**).

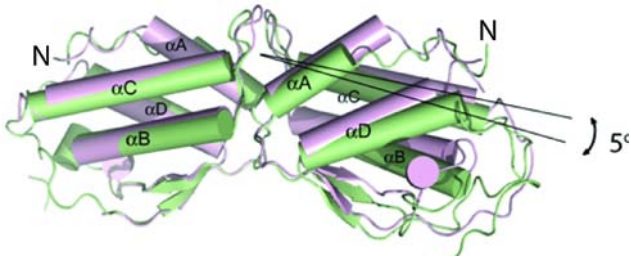

FIGURE 26. The angle between the two SCF protomers is altered upon KIT binding.
The view shows a cartoon diagram of free SCF (green) and SCF bound to KIT (magenta). Complex formation with KIT_{D1-D5} results in an increase in tilting angle of about 5°. Note the different conformation at the N-terminal loop between unbound and bound SCF. ***Adopted from Yuzawa et al., 2007.***

In the transition from the unbound to bound state, the orientations of D4 and D5 undergo a large rearrangement accompanied by the formation of D4-D4 receptor-receptor interactions (**Fig. 27A**). This occurs by a rotation along an axis in the linker connecting D3 to D4 and a rotation along an axis in the linker connecting D4 to D5, running through the D3-D4 and D4-D5 interface respectively (**Fig. 27B**).

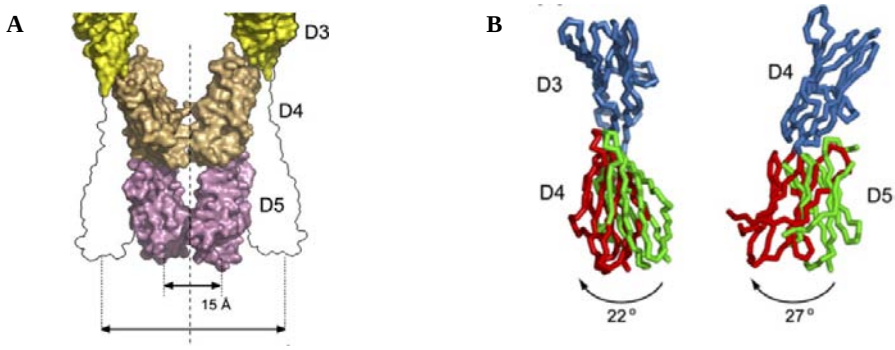

FIGURE 27. Domain 4 and 5 undergo a large conformational change upon ligand binding.

(A) The black outline shows the location of D4 and D5 in the KIT_{D1-D5} ectodomain monomers. They are bridged by SCF binding to the ligand-binding region. Reconfiguration of D4 and D5 leads to a movement of the C termini of two neighboring ectodomains from 75 Å to 15 Å from each other.

(B) Superposition of D3 from the KIT_{D1-D5} monomer with D3 of KIT_{D1-D5} bound to SCF (both colored blue) shows that D4 of the bound form (red) moves by 22° relative to the position of D4 of the free form (green). Superposition (right panel) of D4 of the two forms (both in blue) shows that D5 of the SCF-bound form (red) moves by 27° relative to the positions of D5 of the free form (green). ***Adopted from Yuzawa et al., 2007.***

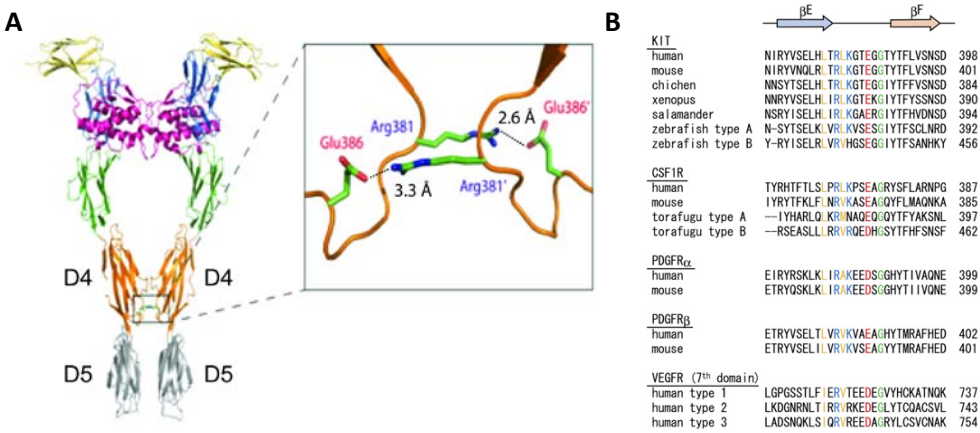

FIGURE 28. Conservation of the dimerization motif in the RTKIII and RTKV family.

(A) A zoomed view on the pair of salt bridges that mediated the D4-D4 interactions in the SCF:KIT_{D1-D5} complex. The distances between interacting atoms (dashed lines) are indicated.

(B) These salt bridges and surrounding residues in the EF-loop are conserved in D4 or D7 of the other members of the RTKIII/V family but not in Flt3. ***Adopted from Yuzawa et al., 2007.***

The KIT D4-D4 contacts are mediated by a pair of salt bridges that reside in the EF loop of D4 (**Fig. 28A**). Structure-based sequence alignments indicated that a L/IxRΦxxxD/ExG dimerization motif is present in the EF loop of D4 of most type III RTKs, including CSF-1R, PDGF-Rα and PDGF-Rβ (**Fig. 28B**). However, this fingerprint is clearly absent in Flt3 (**Appendix A**). Surprisingly, the sequence motif is also found in the membrane-proximal Ig-like domain of all members of the type V RTKs. This lead to the hypothesis that receptor-receptor interactions similar to those seen in the D4-D4 interface of KIT will also take place through a similar D7-D7 interface in the VEGF receptors.

In the KIT_{D1-D5}:SCF complex, the two copies of KIT_{D5} are arranged in a parallel fashion. The adjacent domains D5 appear however to be too far separated from each other to allow direct contacts between side-chains. The authors speculated that any specific D5-D5 interactions could be water or metal ion mediated. However no such interactions could be detected in this area of weak electron density.

The role of D4 homotypic contacts in receptor activation was investigated by site-directed mutagenesis (**Fig. 29**). It was found that SCF-induced phosphorylation of KIT was severely compromised by point mutations in the conserved residues Arg381 and Glu386 of the D4 dimerization motif. These point mutants appeared to bind the ligand with similar affinity as the wild type receptor, as shown by a cell-based radio-displacement assay. These findings now also rationalized the activation-inhibiting effect of the antibody that was employed by Blechman and colleagues (see higher).

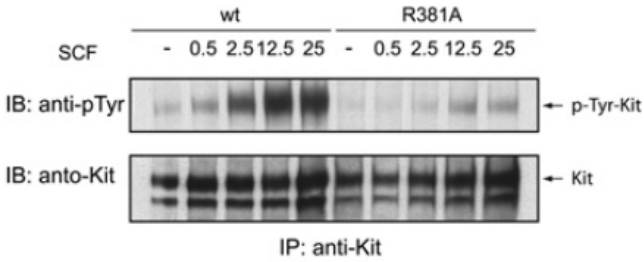

FIGURE 29. Disruption of D4-D4 contacts compromises SCF-induced phosphorylation.
3T3 cells stably expressing wild-type KIT (WT) or the R381A mutant were treated with different concentrations of SCF. Lysates from unstimulated or SCF-stimulated cells were subjected to immunoprecipitation with anti-KIT antibodies followed by SDS-PAGE and immunoblotting with anti-KIT or anti-p-Tyr antibodies. By cell-based displacement assays using ^{125}I-SCF, it was shown that the R381A mutant bound the ligand with similar affinity as the wild-type receptor. ***Adapted from Yuzawa et al., 2007.***

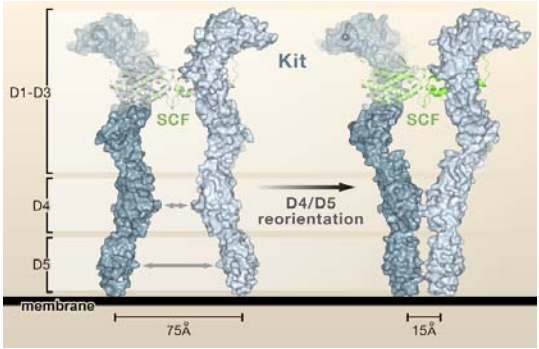

FIGURE 30. Activation mechanism of KIT. Binding of SCF to preformed binding sites on KIT contributed by Ig-domains 1 to 3, leads to KIT dimerization. This assembly facilitates the formation of homotypic receptor-receptor contacts between D4 and D5, that consequently orient the tyrosine kinase domains in a signaling competent state.
Adopted from Lemmon and Ferguson, 2007.

Earlier structure-function studies on KIT had already demonstrated that domains 4 and 5 are not necessary for ligand-induced receptor dimerization (Lemmon *et al.*, 1997). In other words, KIT dimerization is primarily driven by the bivalent nature of the ligand. Thus, rather than playing a role in receptor dimerization, homotypic D4, and possibly homotypic D5 interactions between neighboring receptors are required for the precise positioning of the membrane-proximal regions at a distance and orientation that enable interactions between their cytoplasmic domains resulting in tyrosine kinase activation. The binding affinities of D4 toward D4 and D5 toward D5 are probably too low to facilitate KIT ectodomain dimerization before the local receptor concentration on the cell surface is increased by SCF-driven dimerization and by the effect of their restricted spatial confinement (**Fig. 30**) (Yuzawa *et al.*, 2007).

Structure of the murine CSF-1R$_{D1-3}$:CSF-1 complex

Crystals of the complex formed between murine CSF-1 and CSF-1R$_{D1-D3}$ (both expressed in Sf9 insect cells) diffracted to 2.4 Å resolution. Prior the crystallization, the C-terminal His-tags were removed by carboxypeptidase A. The structure (**Fig. 31A**) was solved by MR using the previously determined structure of human CSF-1 (pdb 1HMC, Pandit *et al.*, 1992). After rebuilding and refinement of the murine CSF-1, ensuing density modification protocols, using the phases of the partial solution, revealed discernible density for domain 3 and at later stages, for domains 1 and 2 (Chen *et al.*, 2008).

Remarkably, the structure shows that only one CSF-1R$_{D1-D3}$ receptor is bound by the dimeric ligand, although the crystallization mixture contained more than a two-fold molar excess of receptor to ensure the formation of a full dimeric complex (**Fig. 31B**). This observation was however supported by ITC binding data, which showed that, in solution, the murine CSF-1R$_{D1-D3}$ fragment only forms a 1:1 complex with CSF-1 (K_d = 455 nM), whereas the full length ectodomain CSF-1R$_{D1-D5}$ forms a 2:1 complex with much higher affinity (K_d = 9.0 nM). The existence of a stable 1:1 complex suggests that the binding affinity at the second CSF-1 binding site is

significantly lower than at the first site, possibly resulting from conformational changes imposed by the binding at the first site. Although there exists a wide array of side chain conformational differences between the occupied and the unoccupied CSF-1 protomers, the main chain conformation seems rigid. Hence, the structure of the complex does not provide a clear mechanism for the apparent negative cooperativity (Chen *et al.*, 2008).

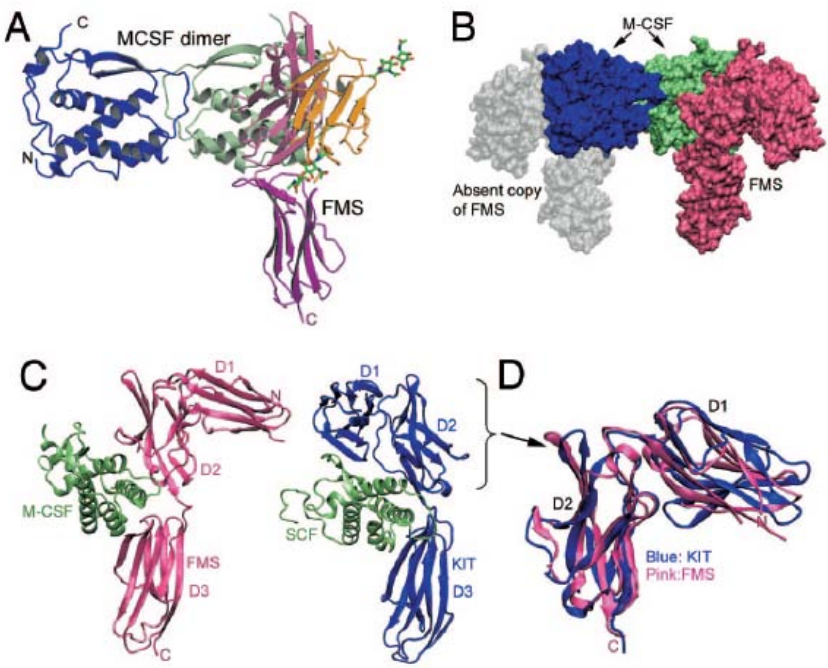

FIGURE 31. Structure of the murine CSF-1R$_{D1-3}$:CSF-1 complex (pdb 3EJJ).

(A) Ribbon representation of the complex, with the CSF-1 (a.k.a. M-CSF) protomers in green and blue, and the CSF-1R (a.k.a. FMS) D1, D2, and D3 domains in orange, pink, and purple, respectively. The two N-linked glycans attached to FMS are depicted as sticks.

(B) Surface representation of a completed, dimeric complex in which the absent copy of CSF-1R$_{D1-3}$ is modeled, based on the 2-fold symmetry between the CSF-1 protomers.

(C) The different modes of ligand recognition between CSF-1R and KIT as revealed by a comparison between the CSF-1$_{D1-D3}$:CSF-1(left) and KIT$_{D1-D3}$:SCF(right) complexes. For clarity only one pair of receptor and ligand from each complex is shown. The ligands are in the same orientation.

(D) Superposition of CSF-1R$_{D1-D2}$ and KIT$_{D1-D2}$ showing that D1 and D2 form an integral, rigid module.

Adopted from Chen et al., 2008.

The binding data reported by Chen and co-workers, are however in direct and sharp contrast with ITC data for the CSF-1R:CSF-1 complex obtained by Elegheert and colleagues (Elegheert *et al.*, *in preparation*). They showed that both murine and human CSF-1R$_{D1-D3}$ (produced in HEK293T-cells) form dimeric complexes with their *E. coli*-derived ligands, with an affinity of 348 nM and 213 nM, respectively. For the full length murine and human CSF-1R$_{D1-D5}$:CSF-1

complexes, an affinity of 22 nM and 13.6 nM, respectively, was determined. Moreover, structural models calculated from small-angle X-ray scattering (SAXS) data also indicate that both murine and human CSF-1R_{D1-D3} and CSF-1R_{D1-D5} form ternary complexes in solution. The origin of the different behavior of the CSF-1_{D1-D3} complexes in both groups is currently unknown. It seems, however, that D4 and D5 of CSF-1R play a more important role in stabilizing the complex as compared with the KIT system.

The CSF-1R_{D1-D3}:CSF-1 structure further shows that the CSF-1R:CSF-1 interaction is dramatically different from the KIT:SCF binding mode. CSF-1 is bound only by Ig-like domains 2 and 3 of the receptor, while KIT binds SCF in a wrapping fashion, with all three of the first domains interacting with SCF. Furthermore, CSF-1R_{D2} and KIT_{D2} use opposite sides of the Ig-like domain for binding.

A total surface area of 1740 $Å^2$ is buried between CSF-1 and CSF-1R_{D1-D3}, which can be divided into 900 $Å^2$ for site 1 (D2) and 840 $Å^2$ for site 2 (D3) (**Fig. 31A**). The ligand-receptor interface is mostly hydrophilic, with salt bridges and hydrogen-bounds outnumbering hydrophobic contacts. A total of surface area of 1240 $Å^2$ is buried at the CSF-1R D1-D2 interface, and D1 and D2 apparently adopt the same relative conformation as KIT D1-D2 (**Fig. 31D**). Thus D1-D2 can be considered a structural unit that is differently orientated in both complexes, mediated by a rotation around the D2-D3 linker (**Fig. 31C**). The CSF-1R D2-D3 interface itself is minimal, with few interactions between D2 and D3. Without the binding of CSF-1, the D2-D3 junction likely has hinge flexibility.

The relative orientation of D3 to the helical bundle cytokine is conserved between KIT and CSF-1R. In both complexes, the DE loops and the BC loops of D3 are used to contact the N-terminal segment of their ligand. There is, however, no similarity in the pattern of hydrogen bonds and van der Waals interactions between the two complexes.

Function of the CSF-1R membrane-proximal domains

As outlined above, the dimerization motif found in the KIT_{D4} is conserved in CSF-1R. Low-resolution structural studies for the human CSF-1R_{D1-D5}:CSF-1 complex by small-angle X-ray scattering (SAXS) and negative-stain electron microscopy showed that homotypic interactions mediated by the fourth Ig-like domain are indeed present. Furthermore, the CSF-1R-D5 domains point away from each other (Elegheert *et al.*, *in preparation*). Interestingly, mutations in the CSF-1R that lead to its ligand-independent activation are localized to fourth Ig-domain (Carlberg and Rohrschneider, 1994). It is possible that the activating effects of these mutations are caused by increasing the stability of D4 receptor-receptor interactions.

Structure-function studies on PDGF ligand-receptor complexes

Structure of the PDGF-Rβ$_{D1-3}$:PDGF-BB complex

Early binding studies, employing domain deletion mutants of the PDGF-Rα and PDGF-Rβ receptors, had shown that receptor domains 2 and 3 are sufficient for the high-affinity binding of their respective ligands (Lokker *et al.*, 1997). Recently, the crystal structure of the ternary complex between PDGF-BB and PDGF-Rβ$_{D1-D3}$ has been reported (Shim *et al.*, 2010). PDGF-BB and PDGF -Rβ$_{D1-D3}$ were co-expressed in HEK293S GnTI$^{-/-}$ cells, and following purification, the complex was glycan minimized using endoglycosidase F1 and treated with carboxypeptidase A. This protocol yielded crystals of the complex that diffracted to 2.3 Å resolution. The structure was solved by MR using the previously determined structure of PDGF-BB (pdb 1PDG, Oefner *et al.*, 1992) and D2 of VEGF-R1 (pdb 1FLT, Wiesmann *et al.*, 1997). After refinement of the partial model, NCS-averaged maps allowed the positioning of a model for D1 and, in later stages, the building of D3.

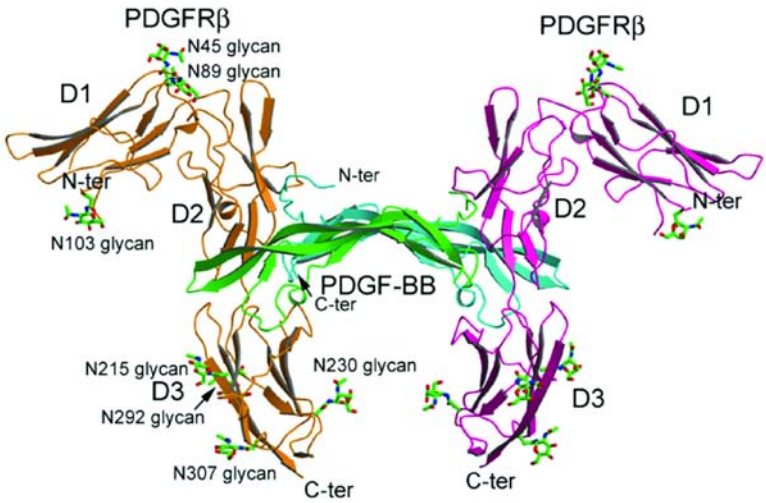

FIGURE 32. Structure of the PDGF-Rβ$_{D1-3}$:PDGF-BB complex (pdb 3MJG).
Side view of the ribbon model of the complex with the PDGF-BB protomers in green and blue, and the PDGF-Rβ receptors in pink and orange. The N-linked glycans attached to PDGF-Rβ are depicted as sticks.
Adapted from Shim et al., 2010.

The structure (**Fig. 32**) shows that each receptor molecule interacts with both ligand molecules. PDGF-BB binds in the cleft between D2 and D3 and the resulting interface buries 2870 Å^2 of solvent-accessible surface area. D1 points away from the ligand and is not involved in ligand binding. The D1-D2 interface buries 1060 Å^2 and the bent conformation between D1 and D2 is similar among PDGF-Rβ$_{D1-D2}$ and KIT$_{D1-D2}$ or CSF-1R$_{D1-D2}$. The D2–D3 junction of PDGF-Rs, with little direct interactions between D2 and D3, appears to be prone to hinge flexibility when the ligand is absent.

Function of the PDGFR membrane-proximal domains

The residues that form the pair of salt bridges that mediate homotypic contacts between the domains 4 of KIT are conserved in the PDGF-R receptors. Earlier studies had already indicated that PDGF-R_{D4} has an important role in signaling. Two groups identified a monoclonal anti-D4 antibody that allowed ligand binding but inhibited activation of the PDGF-Rβ receptor (Lokker *et al.*, 1997; Shulman *et al.*, 1997) and, studies on the activation mechanism for PDGF-Rα, which has a sequence identity of 30% with the PDGF-Rβ receptor, showed that a soluble D4-GST fusion protein acted as a receptor antagonist (Omura *et al.*, 1997).

Yang *et al.* showed that PDGF-Rβ receptors harboring point mutations in the D4 dimerization motif bound the PDGF-BB ligand with equal affinity but their ligand-induced activation was severely affected as compared to the wild-type receptor. Cross-linking studies showed that these mutant receptors are dimerized by the ligand at the cell surface, thereby proving that these point mutations do not affect the ligand-induced dimerization (Yang *et al.*, 2008). These findings indicated that the fourth Ig-like domain of the PDGF-R receptors couples ligand-binding to receptor activation in a similar way as D4 of the homologous KIT complex.

Structure-function studies on VEGF:VEGF-R ligand-receptor complexes

Structure of the VEGF-R1$_{D2}$:VEGF and VEGF-R1$_{D2}$:PlGF complexes

Similar to the findings for the PDGF-Rα/β receptors, binding studies with VEGF-R1 and domain deletion mutants showed that the second and third Ig-like domains are sufficient for high-affinity VEGF-A binding (Barleon *et al.*, 1997; Davis-Smyth *et al.*, 1996; Fuh *et al.*, 1998). Ensuing, the high-resolution X-ray structures of VEGF-$R1_{D2}$ in complex with VEGF-A (Wiesmann *et al.*, 1997) and PlGF (Christinger *et al.*, 2004) were reported. Non-glycosylated forms of VEGF-$R1_{D2}$, VEGF-A and PlGF were produced in *E. coli* as inclusion bodies and refolded *in vitro*. The structures for these minimal ligand-receptor complexes were solved by MR using the available ligand-structures and showed that two copies of VEGF-$R1_{D2}$ bind symmetrically to the distal ends of the dimeric cystine-knot ligands. Both complexes are structurally very similar, as shown in **Figure 33**.

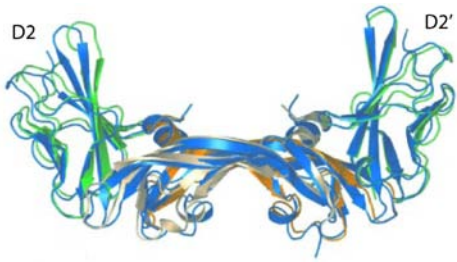

FIGURE 33. Superposition of the PlGF:VEGF-R1$_{D2}$ and VEGF-A:VEGF-R1$_{D2}$ complexes.
The PlGF homodimer (2.5 Å resolution, pdb 1RV6) is shown in *orange* and *wheat* and its bound VEGF-$R1_{D2}$ receptor domains in *green*. The VEGF-A:VEGF-$R1_{D2}$ complex (1.7 Å resolution, pdb 1FLT) is shown in *blue*. ***Adopted from Christinger et al., 2004.***

Structure of the VEGF-R2$_{D23}$:VEGF-C complex

Recently, the X-ray structure for VEGF-R2$_{D23}$ in complex with VEGF-C was reported (**Fig. 34**) (Leppänen *et al.*, 2010). VEGF-C and a VEGF-R2$_{D23}$-Fc fusion protein were both produced in Sf9 insect cells. After complex formation and purification with protein-A affinity chromatography, the Fc fragment was proteolytically removed. The resulting complex crystals yielded a dataset to 2.7 Å resolution which was phased by SIRAS from K_2PtCl_4-derivatized crystals.

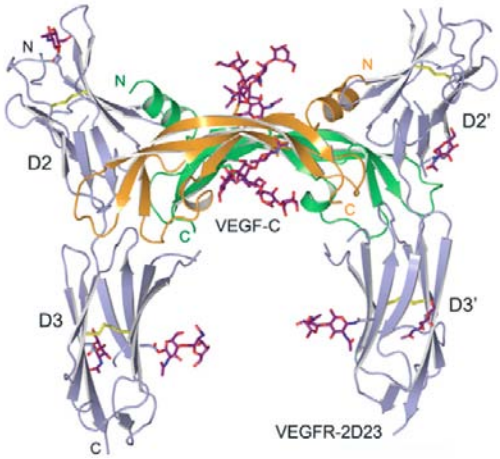

FIGURE 34. Structure of the VEGF-R2$_{D23}$:VEGF-C complex (pdb 2X1W).
The VEGF-C homodimer is shown in orange and green, and the two VEGF-R2$_{D23}$ receptor chains are colored in light blue. The sugar moieties and the disulfide bonds are shown as purple and yellow sticks, respectively.
Adopted from Leppänen et al., 2010.

A comparison of the VEGF-R2$_{D23}$:VEGF-C and the VEGF-R1$_{D2}$:VEGF-A and VEGF-R1$_{D2}$:PlGF structures shows that VEGF-R1 and VEGF-R2 utilize the same D2 interface for ligand binding. The buried surface area at the VEGF-R2$_{D23}$:VEGF-C interface is around 1300 Å^2. It is noteworthy that the conformation of VEGF-R2$_{D2-3}$ and Kit receptor domains 2 and 3 is structurally very similar despite the fact that the ligands are structurally dissimilar (Leppänen *et al.*, 2010).

Function of the membrane-proximal domains in the VEGF receptors

In RTKIII members, the evolutionarily conserved dimerization motif is present in D4. Sequence analysis showed that this sequence fingerprint is present in D7 of all three VEGF receptors of the RTKV family (Yuzawa *et al.*, 2007). A negative-stain electron microscopy study for the isolated VEGF-R2$_{D1-7}$:VEGF-A complex showed that the membrane-proximal domains D7, and possibly D4, mediate homotypic receptor-receptor interactions (**Fig. 35**). Complexes formed between VEGF-A and a mutant VEGF-R2 ectodomain in which D7 was replaced by D6, did not reveal these well defined conformations, suggesting that D7 mediates specific contacts (Ruch *et al.*, 2007).

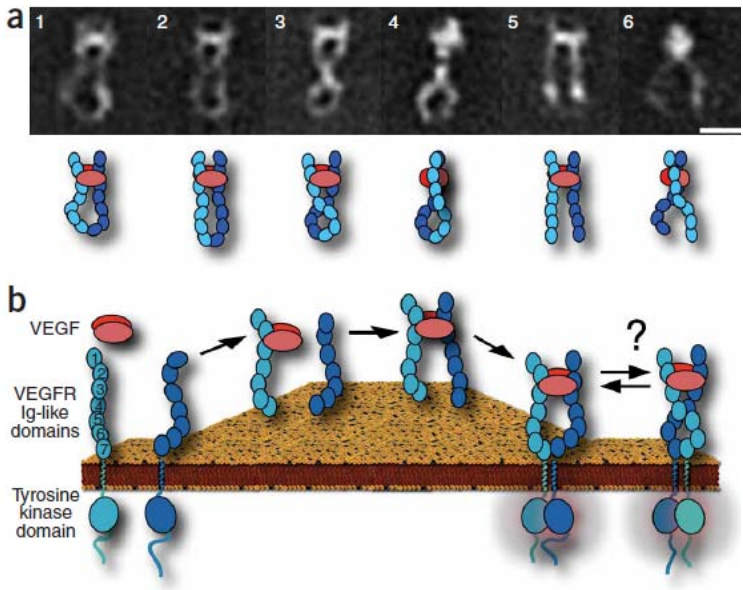

FIGURE 35. Ligand binding of VEGF-R2 promotes dimerization of membrane-proximal regions.

(A) Class averages (top) and graphic representations (bottom) of the monomeric VEGF-R2 ectodomain in complex with VEGF. Scale bar, 15 nm.

(B) Proposed model for the instigation of intracellular signaling upon VEGF binding to VEGF-R.

Adopted from Ruch et al., 2007

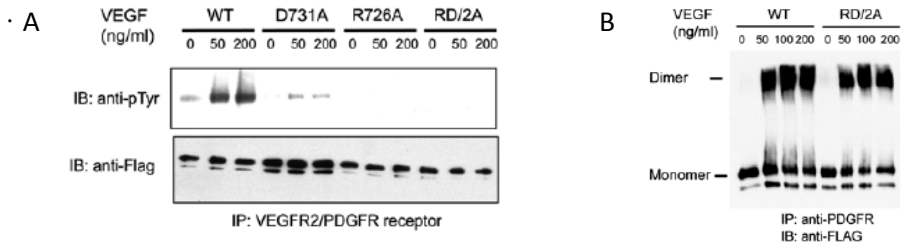

FIGURE 36. VEGF-R D7-D7 interactions are crucial for ligand-induced activation.

(A) 3T3 cells stably expressing a VEGF-R2-PDGF-Rβ chimeric receptor (composed of the ectodomain of VEGF-R2 connected to the TM and the cytoplasmic region of PDGF-R) or chimeric receptors harboring mutations in D7 region (R726A, D731A, or an R726/D731 double mutation designated RD/2A) were stimulated with VEGF-A. Lysates from unstimulated or stimulated cells were subjected to immunoprecipitation with antibodies against the cytoplasmic region of the chimeric receptor followed by immunoblotting with either anti-pTyr or anti-FLAG antibodies, respectively.

(B) Cross-linking experiments with the disuccinimidyl suberate (DSS) showed that the R726/D731 mutations do not effect VEGF-A-induced receptor dimerization at the cell surface. ***Adopted from Yang et al., 2010.***

To further investigate the role of homotypic receptor contacts in VEGF-R2 activation, a mutagenesis study was carried out. It was found that receptors with single point mutations in the

dimerization motif in D7 showed a severely compromised ligand-induced activation as compared to the wild-type receptor (**Fig. 36A**). Cross-linking studies showed that these mutations did not affect ligand-induced dimerization (**Fig. 36B**). On the other hand, mutations in the EF-loop of D4, which contains a sequence related to the dimerization motif in D7, did not affect receptor activation (Yang *et al.*, 2010). This suggests that interactions in the EF-loop of VEGF-R2$_{D4}$ are not necessary for signaling. It remains however possible that D4-D4 interactions, as suggested by the negative-stain EM class averages, are mediated by another region of D4.

Yang *et al.* also produced the isolated VEGF-R2$_{D7}$ by refolding from inclusion bodies. Crystals were formed which diffracted to 2.7 Å, and the structure was solved by MR. Surprisingly, although D7 behaved monomeric in solution, it crystallized as a dimeric assembly. The structure shows how two VEGF-R2$_{D7}$ domains interact in a way very similar as the D4 interaction in the KIT$_{D1-D5}$:SCF complex (**Fig. 37A**). The position of the EF loop in the two structures is nearly identical, and the distance between the C-termini is approximately 15 Å for both D4 and D7 dimeric structures (**Fig. 37B**) (Yang *et al.*, 2010). The high similarity between VEGF-R2$_{D7}$ and KIT$_{D4}$ in both structure and function suggests a well-conserved mechanism for RTK activation and provides further evidence for common ancestral origins of type-III and type-V RTKs.

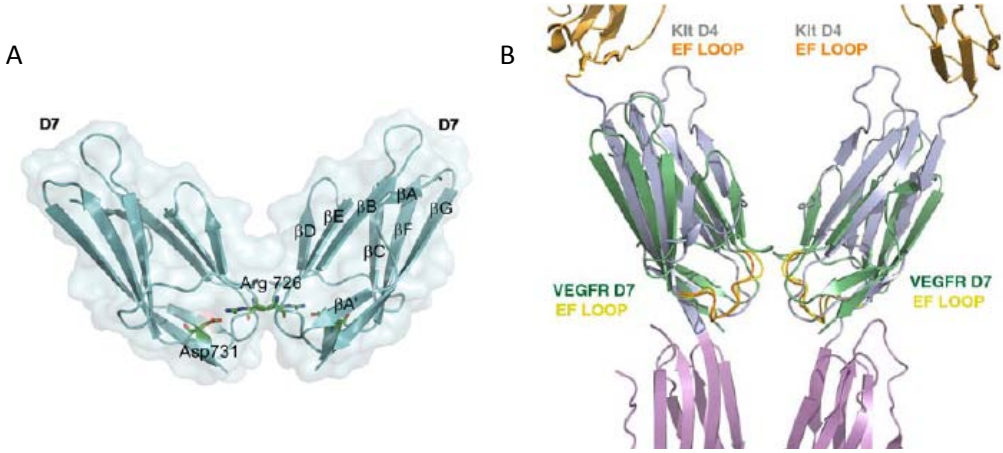

FIGURE 37. Structure of VEGF-R2$_{D7}$ homodimer (pdb 3KVQ).

(A) A ribbon diagram and a transparent molecular surface of the D7 homodimer structure. Asp731 and Arg726 are shown as sticks.

(B) View of the superimposed VEGF-R2$_{D7}$ and KIT$_{D4}$ regions reveals a high similarity in domain arrangement and homotypic contacts. D7 of VEGF-R2 is colored in green and its EF loop in yellow, while D4 of KIT is colored in gray with its EF loop is in orange. ***Adopted from Yang et al., 2010.***

Subsequently, the self-association behavior of the isolated domain D7 of VEGR-R2 was studied by equilibrium sedimentation. It was found that it remained monomeric in solution at concentrations as high as 160 µM (1.9 mg/mL). Similar experiments with isolated D4 or D5 of the KIT or PDGF-R

receptors led to the same observation. These experiments led to the conclusion that homotypic receptor-receptor interactions are inherently weak. It is hypothesized, however, that the reduced dimensionality at cell surface would enable the formation of stable homotypic contacts. Moreover, the homotypic contacts between membrane-proximal Ig-like domains in type-III and type-V RTKs are possibly supported by additional lateral interactions that take place between the TM and cytoplasmic regions of neighboring receptors (Yang *et al.*, 2010).

Role of the transmembrane helices in receptor activation

In RTKs, the extracellular ligand-binding domain is connected to the intracellular kinase domain by a single transmembrane (TM)-spanning α-helix of about 20 amino acid residues. These helices are however not just passive membrane anchors. A variety of studies on different RTKs indicate that lateral helix-helix interactions play a critical role in RTK signaling. This view is also supported by the large number of pathogenic point mutations identified in the TM-domains of many different RTKs (Li and Hristova, 2006).

Biophysical studies on isolated TM-domains by techniques as SDS-PAGE, equilibrium sedimentation and Förster resonance energy transfer (FRET) (Merzlyakov and Hristova, 2008; You *et al.*, 2005) have shown that the TM-domains of various RTKs have a weak or strong dimerization capacity, both in micelles and detergents (Oates *et al.*, 2009; Li *et al.*, 2005). Furthermore, in a recent systematic study, employing the *E. coli*-based TOXCAT-assay (Russ and Engelman, 1999), Finger and coworkers demonstrated that the TM-domains of all 58 human RTKs have an intrinsic propensity to dimerize and accordingly suggested that all RTK TM-helices encode self-interactions (Finger *et al.*, 2009).

TM-domain dimerization is believed to be mediated by specific motifs present within the helices. For example the GxxxG motif, as seen in the NMR-structure for glycophorin A (MacKenzie *et al.*, 1997), appears to frequently mediate and stabilize TM helix-helix interactions in membranes and is present in many RTKs (Sternberg and Gullick, 1990). Another dimerization motif, the leucine-zipper, is predicted to stabilize interhelical interactions in the PDGF-Rβ (Oates *et al.*, 2009) and DDR1 receptors (Noordeen *et al.*, 2006). Furthermore, motifs involving other small residues (such as Ala, Ser, or Thr) can also mediate and stabilize defined TM helix-helix interactions. Small residues are believed to allow two helices to come into close contact so that other forces, such as van der Waals interactions and hydrogen bonding, can stabilize a given TM-helix bundle (Finger *et al.*, 2009). The determination of more high-resolution NMR-structures, like those for the dimeric ErbB2, EphA1 (**Fig. 38**) and EphA2 TM-domains (Bocharov *et al.*, 2008a; Bocharov *et al.*, 2008b; Bocharov *et al.*, 2010) will provide more insights on the mechanisms and diversity of RTK TM-helix packing modes.

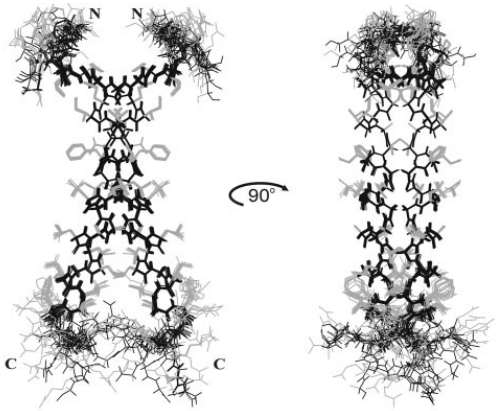

FIGURE 38. Spatial structure of the EphA1-TM dimer.

Ensemble of 12 NMR-derived structures of the EphA1-TM dimer obtained by solution NMR in lipid bicelles. Side chain and backbone heavy atom bonds are shown in *gray* and *black*, respectively. EphA1 transmembrane segments associate in a right-handed parallel-helical bundle, through the N-terminal glycine zipper motif A*X*3G*X*3G.

Adopted from Bocharov et al., 2008a.

Studies with non-native TM-helices showed that dimerization of the TM-domain (TMD) is not enough to drive the activation of the kinase domain. Bell and colleagues engineered ErbB2 receptor constructs (with or without the extracellular region) to carry artificial transmembrane domains which are dimerized by a pair of glutamic acid residues. These TMDs consisted of 23 valine and two glutamic acid residues, spaced 7 residues apart in different positions of the transmembrane helix. All of these 'TM-shift' mutants gave rise to membrane-bound protein dimers but only proteins dimerized by distinct TM-domains were active. The authors concluded that such activating TMDs must adopt a specific conformation that allows trans-activation of the kinase domains. Similar experiments for the RTKIII receptors, PDGF-Rβ and VEGF-R2, led to the same conclusion (Bell *et al.*, 2000; Dosch and Ballmer-Hofer, 2010). Furthermore, when a non-activating but dimerizing TM-variant was introduced in the full length VEGF-R2 receptor, this completely blocked ligand-induced phosphorylation. On the other hand, activating TM-peptides caused phosphorylation of the receptor, both in the presence or absence of the ligand. These experiments further highlight the need for a correct orientation of the TM-domains in order to activate the kinase domains.

In many RTKs - including the RTKIII and RTKV family members - the juxtamembrane domain has an autoinhibitory function on the kinase activity (see further). It is hypothesized that the specific orientation of the 'activating' TM-helices allows productive interactions between the opposing juxtamembrane domains that relieves this autoinhibition and consequently, the tyrosine kinase domains are activated (**Fig. 39**) (Stuttfeld and Ballmer-Hofer, 2009).

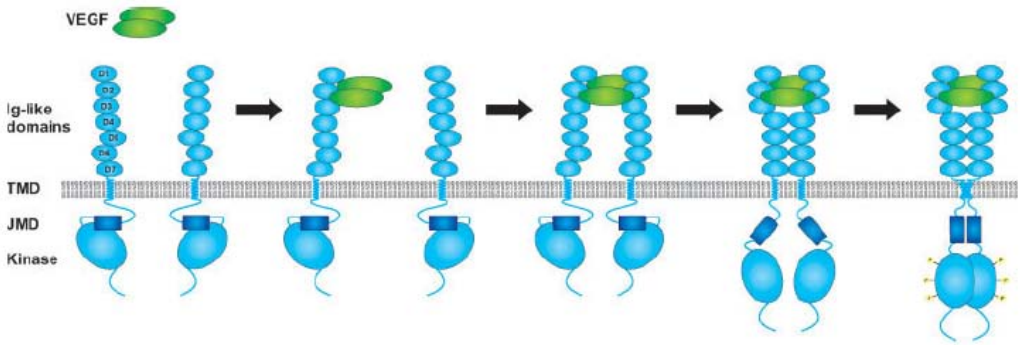

FIGURE 39. Schematic representation of the activation mechanism of VEGF-Rs.
A covalently linked VEGF dimer (green) binds to VEGF-R (blue) leading to dimerization of two receptor monomers. Additional interactions between Ig-like domains 4 and 7, the transmembrane domains, and the juxtamembrane domains (dark blue) stabilize the VEGF-VEGF-R-complex resulting in kinase activation and autophosphorylation of tyrosine residues required for downstream signaling. ***Adopted from Stuttfeld and Ballmer-Hofer, 2009.***

For RTKs that exist as dimers in the absence of ligand, ligand-binding may initiate TM-domain interactions or a rearrangement of a preformed TM dimer - which may have multiple dimerization motifs - that finally results in the active conformation of the intracellular domains (Fleishman *et al.*, 2002).

For the VEGF-R2 receptor it was also shown that the full length membrane-bound wild-type receptor is monomeric, while constructs that lack the ectodomain have a tendency to dimerize. This effect is possibly mediated by repulsive interactions between the ectodomains (Dosch and Ballmer-Hofer, 2010). Remarkably, Tao and colleagues found that VEGF-R2 mutants in which the membrane proximal domains are deleted are constitutively phosphorylated (Tao *et al.*, 2001). Repulsive interactions between receptor ectodomains in the absence of the ligand have also been proposed for the FGF-R3 receptor (Chen *et al.*, 2010).

It is believed that oncogenic mutations in the TM-region stabilize the active conformation of the TM-helices by the formation of specific, mutant amino-acid mediated contacts such a as hydrogen bonds, cation-Π interactions or disulfide bonds. For example, it was shown by FRET that the pathogenic mutation Ala391Glu found in the TM-domain of the FGF-R3 stabilizes the formation of dimers with a change in free energy of dimerization of 1,3 kcal/mol, in agreement with the hypothesis of the formation of a hydrogen bond (**Fig. 40**) (Li *et al.*, 2006). This seemingly modest value was calculated to have a significant effect on the monomer-dimer equilibrium. It should be noted that it is very difficult to observe these interactions directly since high-resolution NMR-structures of TM-domains are very demanding to determine.

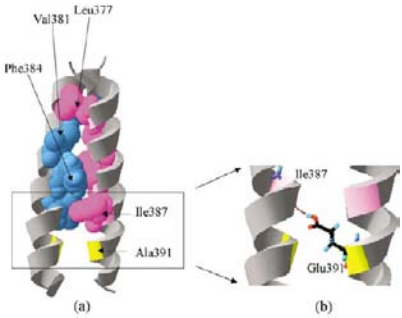

FIGURE 40. Molecular model of the wild-type and mutant TM domain dimer of FGFR3.
Contacts between the two helices are mediated by residues Leu377, Val381, Phe384, and Ile387. The side-chains of one helix (blue) pack against the side-chains of the other helix (purple). Ala391 (shown in yellow), which is mutated to Glu in Crouzon syndrome with acanthosis nigricans and cancer, faces the dimer interface. A model for the putative hydrogen bond between Glu391 (yellow) and Ile387 (pink) in the mutant dimer is shown on the right.
Adopted from Li et al., 2006.

From a variety of studies it has become clear that in many RTKs lateral interactions between TM-helices are required to activate the tyrosine kinase domains. The necessity for these interactions could be exploited to develop peptide-based therapeutics that mimic the TM-helix and interfere with its self-association. A proof-of-concept study in human cell lines on the EGF and ErbB2 receptors showed that peptides encompassing the native TM-helix can indeed specifically inhibit the signaling of their cognate receptor (Bennasroune *et al.*, 2004).

Tyrosine kinase activation

Activation by trans-autophosphorylation

Binding of the cognate ligand to the extracellular domains of RTKs induces the formation of a dimeric assembly in which the adjacent intracellular kinase domains become activated in a process termed trans-autophosphorylation (**Fig. 41**). The first step in this process is the trans-phosphorylation of key tyrosine residues located in regulatory regions of the kinase domain. Once these are phosphorylated the TKD adopts its fully active form and can phosphorylate additional tyrosine residues in its sequence. These phosphotyrosine residues act then as 'beacons' which attract signaling proteins that contain Src homology-2 (SH2) or phosphotyrosine-binding (PTB) domains (Hubbard, 2004; Schlessinger and Lemmon, 2003).

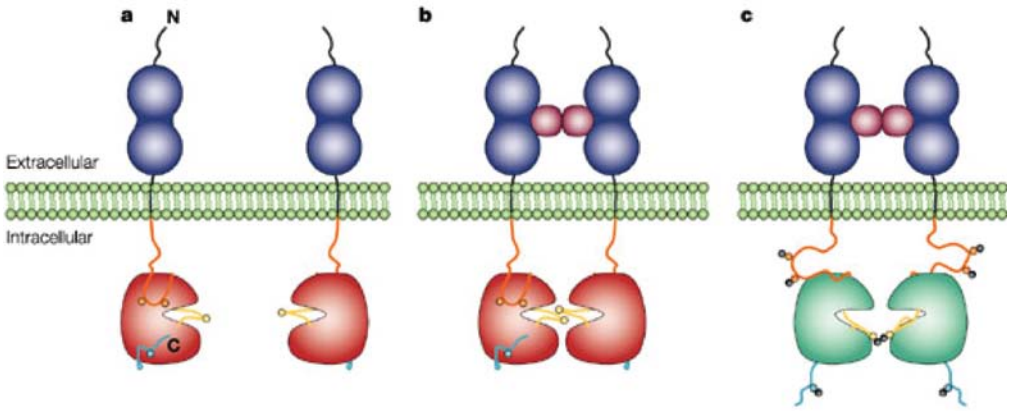

FIGURE 41. General mechanism of RTK activation.

(A) In the absence of ligand, the tyrosine kinase domain is inactive through the inhibitory interactions of the juxtamembrane region (orange) and/or the carboxy-terminal tail (blue) with the kinase domain. In addition, the activation segment (yellow) is not optimally positioned for catalysis.

(B) After ligand (pink)-mediated dimerization of the extracellular domain (blue), the cytoplasmic domains are juxtaposed, which facilitates the trans phosphorylation of tyrosine residues (shown as circles) in the juxtamembrane region, activation segment and carboxy-terminal tail.

(C) After phosphorylation and reconfiguration of the inhibitory segments, the kinase domains become fully active (green) and a subset of phosphotyrosines (black spheres) are available as recruitment sites for proteins that contain SH2- or PTB-domains.

Adopted from Hubbard, 2004.

The so-called activation loop is a key structural element in the regulation of catalytic activity. This polypeptide segment, which is approximately 20–25 residues long, usually contains 1 to 3 tyrosine phosphorylation sites. This segment contributes residues both for catalysis and for substrate-peptide binding and exists in two conformational states. When the activation loop is not phosphorylated, it is not positioned optimally for phosphoryl transfer. It is believed that

phosphorylation of the activation segment in trans, by the other receptor in the ligand-stabilized dimer, is accompanied by a conformational change that secures the segment in a catalytically competent configuration. The precise mechanism by which a productive receptor dimer results in the stimulation of tyrosine kinase activity is however not completely understood and could differ among receptor subclasses. One possibility is that the ligand-stabilized dimer merely results in an increase in the substrate concentration (that is, the other receptor) for efficient trans-phosphorylation within the dimer. In addition to facilitating transphosphorylation, dimerization might also stabilize a direct physical interaction between the two cytoplasmic domains, which is stimulatory for catalytic activity. Recent structural studies suggest that asymmetric TKD dimer formation is a common phenomenon, critical for the activation and autophosphorylation of RTKs (Bae and Schlessinger, 2010).

In many RTKs, regions other than the activation loop also contribute to autoinhibition and activation, namely the juxtamembrane (JM) region and the carboxy-terminal tail. These regions often contain tyrosine residues and they can both function as recruitment sites for downstream signaling proteins and, in some receptors, as a means of regulating catalytic activity. Many oncogenic mutations in RTKs disrupt these autoinhibitory mechanisms and cause constitutive signaling of the receptor.

Autoinhibition and activation of the Flt3 tyrosine kinase domain

In 2004, Griffith and colleagues determined the X-ray structure of the Flt3 TKD in its inactive, unphosphorylated state. The structure provided the molecular basis for the mechanism of Flt3 autoinhibition by the JM-domain and explains the activating effect of oncogenic mutations found in this region (Griffith *et al.*, 2004).

The authors crystallized a recombinant form of the cytoplasmic region of Flt3 (residues 564-993), expressed in High-5 insect cells, that lacked the kinase insert domain. The resulting crystals diffracted to a resolution of 2.1 Å and the structure (pdb 1RJB) was solved by MR using the previously determined structure of the VEGF-R2 TKD. A small region of the JM-domain that forms the linker with the TM-helix (residues 564-571), the linker between the tyrosine kinase lobes and the C-terminal tail of the TKD (residues 948-993) were not visible in the electron density.

Autoinhibited Flt3 adopts the typical kinase fold with an N- and C-terminal lobe (**Fig. 42**). The activation loop is located near the active site between the two kinase lobes and is folded in a conformation that is commonly found in inactive tyrosine kinases.

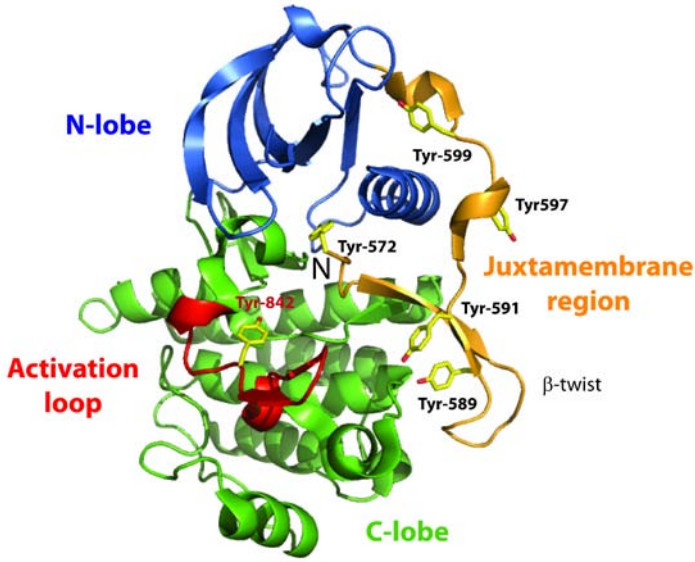

FIGURE 42. Structure of the autoinhibited Flt3 tyrosine kinase domain (pdb 1RJB).
Cartoon representation of the Flt3 TKD in its autoinhibited state. The N-terminal region of the JM-region (orange) occupies the active site, formed between the N- (blue) and C-lobes (green) of the TKD. The activation loop (red) adopts its inactive conformation. Regulatory tyrosine residues are labeled and shown as sticks. The N-terminus (N) corresponds to the first residue of the JM-region that was visible in the electron density (Tyr-572).
Adapted from Griffith et al., 2004.

The structure further shows that the first residues of the JM-domain which are visible in the electron density (residues 572 to 578) are buried in the TKD and directly interact with some of the active site residues. Extending from this region, the JM-domain folds into a two-stranded β-twist (residues 579 to 592) and then continues to connect with the N-lobe of the TKD (residues 593 to 603).

A comparison with the structures of activated tyrosine kinases showed that when the activation loop would adopt its active conformation it would structurally coincide with the N-terminal region of the juxtamembrane domain. Thus, this conformation of the JM-domain autoinhibits the tyrosine kinase by sterically hindering the activation loop from adopting is active conformation. Note, that the inactive conformation of the activation loop is stabilized by tyrosine 842 (**Fig. 42**).

The JM-domain contains several structurally important tyrosine residues (Tyr-572, Tyr-589, Tyr-591 and Tyr-599) which are hydrogen bonded to the kinase domain, and are thought to stabilize its observed autoinhibitory conformation. It is believed that once these tyrosine residues are phosphorylated, the JM-region would no longer be able to fold properly and position itself next to the C-lobe, and as a consequence the activation loop would be able to adopt its active conformation. The sequence and the structurally important tyrosine residues of the Flt3 JM-region are well conserved throughout the RTKIII family (**Fig. 43**), indicating that the mechanism of autoinhibition is conserved as well. The later determined crystal structures of the autoinhibited KIT and CSF-1R TKDs showed that their JM-regions essentially adopt the same conformation as seen in the Flt3 structure (Mol *et al.*, 2004; Walter *et al.*, 2007). Although autoinhibition by the JM-region is not a general mechanism, the JM-region plays a key role in the inhibition and activation process of various other RTKs, including the Eph, Musk and insulin receptors (Hubbard, 2004).

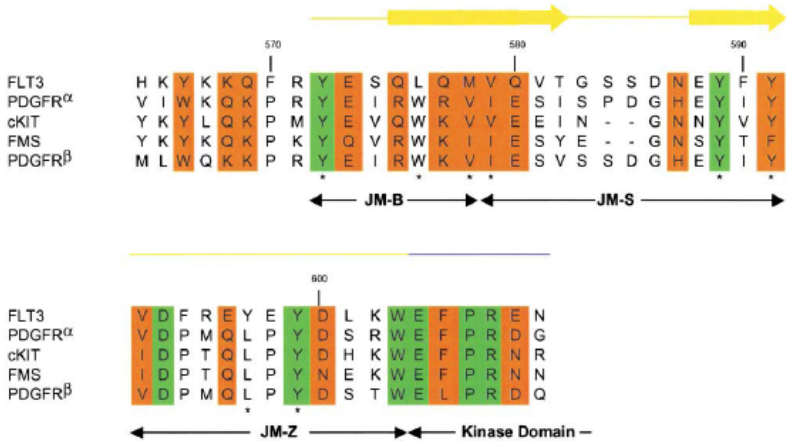

FIGURE 43. Conservation of the juxtamembrane region in the RTKIII family.
Sequence alignment of the JM-domain for FLT3, PDGF-Rα, PDGF-Rβ, KIT, and CSF-1R. Identical (green) and homologous (orange) residues are highlighted. In the Flt3 structure, the JM-Binding region (JM-B, residues 572-578) occupies that active site, the JM-switch region (JM-S, residues 579-592) forms the β-twist motif and the JM-zipper region (JM-Z) links the JM-domain with the N-lobe of the TK domain. The asterisks below PDGF-R indicate the positions of mutants that caused constitutive activation (Irusta *et al.* 2002). ***Adopted from Griffith et al., 2004.***

Although these structural studies provided valuable insights into autoinhibitory mechanism, they do not explain the precise process of trans-autophosphorylation and the order in which tyrosine residues need to be phosphorylated to transform the inactive kinase into its fully active form. Activation loop tyrosine trans-phosphorylation is generally thought to regulate kinase activation of RTKs but may play different roles in different RTKs (Huse and Kuriyan, 2002). Phosphopeptide mapping of KIT revealed that only the tyrosine residues in the JM-region contribute to kinase activation. It was found that the single tyrosine residue in the activation loop of KIT is not phosphorylated until very late in the activation process (DiNitto *et al.*, 2010). Similar to the findings

for the KIT receptor, Razumovskaya and colleagues reported that phosphorylation of tyrosine 842 in the activation loop of Flt3 is not required for activation (Razumovskaya *et al.*, 2009). The fact that phosphorylation of the Flt3 JM-region is critical for activation is also supported by the observation that a Tyr589Phe-mutant cannot be activated (Kiyoi *et al.*, 1998).

Oncogenic mutations in Flt3

Oncogenic mutations in the Flt3 gene have been found to be the most common genetic abnormality in acute myelogenous leukemia (AML) (Stirewalt and Radich, 2003). AML is one of the most common leukemias in adults, and its incidence increases with age. Although AML is a relatively rare disease, it accounts for approximately 10.000 cancer deaths per year in the United States alone (Jemal *et al.*, 2010). AML is characterized by a rapid expansion of myeloid white blood cancer cells, which compete against and block the function of normal bone marrow cells. The standard treatment regimen is conventional chemotherapy combined with, depending on the subtype diagnosis, hematopoietic stem cell transplantation (Chan, 2011).

Several types of oncogenic Flt3 mutations can be discerned. Internal-tandem duplications (ITD) in the JM-region (residues 563-603) are present in 25% to 30% of adult AML patients. These duplications range from 4 to about 68 amino acid residues, are always in frame and limited to the JM-region (Nakao *et al.*, 1996; Thiede *et al.*, 2002). The DNA sequence that encodes residues 593 to 602 is partially palindromic and it is believed that when a hairpin structure would be formed in the lagging strand during DNA replication an FLT3/ITD would be generated by replication slippage (**Fig. 44**) (Kiyoi *et al.*, 1998). Additionally, activating point mutations in the Flt3 JM-domain have been described in approximately 1% of AML cases (Reindl *et al.*, 2006).

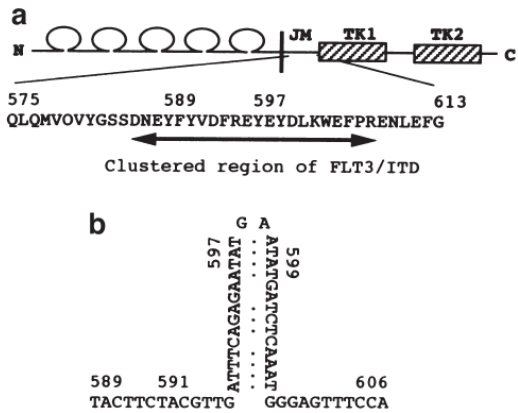

FIGURE 44. Internal tandem duplications in Flt3

(a) ITDs in Flt3 cluster around residues Y597-Y599.

(b) Proposed mechanism for the generation of FLT3-ITD. Single-strand DNA corresponding to D593 to K602 potentially forms a palindromic intermediate. If this occurs in the lagging strand during DNA replication, FLT3-ITD would be generated by replication slippage.

Adopted from Kiyoi et al., 1998.

It is hypothesized that these mutations in the JM-region make the autoinhibition mechanism leaky by disturbing the inhibitory conformation of the JM-domain. Numerous naturally occurring mutations (typically deletions) also exist in the JM-regions of the KIT and PDGF-Rα receptor and give rise to gastrointestinal stromal tumors (GISTs) (Heinrich *et al.*, 2003; Hirota *et al.*, 1998). However, ITDs in the JM-domain of KIT and CSF-1R are not found (Zheng *et al.*, 2004a).

In vitro transduction studies showed that Flt3-ITDs promote ligand-independent dimerization, auto-phosphorylation and constitutive activation of the receptor (Kiyoi *et al.*, 1998). Kiyoi and colleagues further investigated the mechanism of these activating ITDs. When wild-type (WT) Flt3 and a construct containing an ITD but lacking the complete TKD were co-expressed in IL3-dependent 32D cells, this resulted in factor-independent proliferation (**Fig. 45**). It was further shown that WT-Flt3 and ITD-5'/JM-myc formed a heterocomplex and that WT-Flt3 was constitutively phosphorylated. When WT-Flt3 was co-expressed with a similar variant that contained the wild-type JM-domain, WT-Flt3 was not activated and no heterocomplex was formed. These experiments elucidated that ITD are trans-activating (Kiyoi *et al.*, 2002).

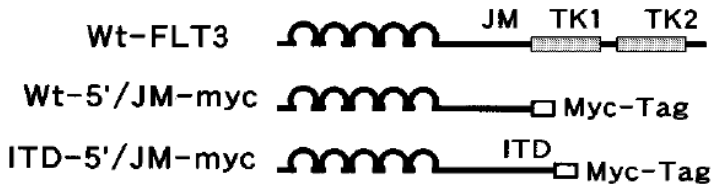

FIGURE 45. ITD-JM mutation are transactivating.
When Wt-Flt3 and ITD-5'/JM-myc were co-transfected in IL3-dependent 32D cells this resulted in constitutive receptor activation and factor-independent proliferation. By co-immunoprecipitation it was show that both constructs physically interact. On the other hand, co-transfection of Wt-Flt3 with Wt/JM-myc did not result in receptor activation and proliferation. ***Adapted from Kiyoi et al., 2002.***

A second class of activating mutations found in Flt3 are point mutations in the activation loop. These account for about 7% of AML cases. The most common nucleotide substitution (GAT→TAT) changes an aspartic acid to tyrosine (D835Y). Other mutations in codon 835, such as deletions, have also been described, but these are far less common. These mutations likely promote the active conformation of the activation loop (Stirewalt and Radich, 2003).

Recently, a high-throughput screening study, in which the entire Flt3 coding sequence in AML patients was sequenced, led to the discovery of a novel oncogenic mutation in the extracellular region (S451F). This mutation is located in the membrane-proximal domain 5 and causes constitutive signaling in the absence of FL. It probably accounts for < 1% of AML cases (Fröhling *et al.*, 2007).

Activation of wild-type Flt3 is also believed to be involved in the process of leukemogenesis since Flt3 is expressed at high levels in 70 - 100 % of AML blasts cells (Carow *et al.*, 1995; Peng *et al.*, 2008). Zheng and colleagues proposed that the activation of wild-type receptor is caused by autocrine signaling loops, since FL was found to be co-expressed with its receptor in the large majority of primary AML samples that were analyzed (Zheng *et al.*, 2004b). Another possible mechanism is that an increase in Flt3 expression levels raises the basal signaling rate.

Aberrant Flt3 signaling usually confers a poor prognosis (Chillon *et al.*, 2004; Pemmaraju *et al.*, 2011). Several small molecule FLT3-tyrosine kinase inhibitors have been developed and examined in AML patients as single agents or in combination with chemotherapy. These clinical trials gave promising results but are however variable due to the occurrence of primary and secondary resistance (Kancha *et al.*, 2007; Kindler *et al.*, 2010; Parcells *et al.*, 2006).

Recently, it was found that FL serum levels dramatically increase in AML patients that are treated with chemotherapy in combination with the FLT3 inhibitor lestaurtinib. Subsequent *in vitro* studies showed that the FL concentrations found in these patients mitigate the inhibition and cytotoxicity of various Flt3 inhibitors. These findings could have important implications regarding the design and outcome of trials of FLT3 inhibitors, and furthermore suggest a rationale for targeting FL as a therapeutic strategy (Sato *et al.*, 2011).

An alternative approach, which employs a monoclonal antibody (IMC-EB10) directed against the Flt3 ectodomain, is currently being investigated in a phase 1 clinical trial (Youssoufian *et al.*, 2010). This antibody inhibits FL-stimulated proliferation of the WT-Flt3 expressing leukemic cell line, EOL-1 and, the ligand-independent proliferation of BaF3-Flt3/ITD cells. In both EOL-1 xenograft and BaF3-Flt3/ITD leukemia models, treatment with IMC-EB10 significantly prolongs the survival of leukemia-bearing mice. IMC-EB10 binds to Flt3 with an affinity of 158 pM and blocks the binding of FL. Besides preventing FL binding, the antibody possibly mediates the internalization and degradation of cell-surface Flt3 (Li *et al.*, 2004).

Phosphorylation sites in wild-type and oncogenic Flt3

In total, the intracellular region of Flt3 contains 23 tyrosine residues. Six are located in the JM-region, one in the activation loop, two in the kinase insert domain, two in the C-terminal tail and the remaining twelve are located in the N- and C-lobes of the tyrosine kinase domain. It is instructive to note that most of the known tyrosine phosphorylation sites in RTKs reside outside the kinase domains (with exception of the activation loop tyrosines and some other rare cases) (Heldin *et al.*, 1998; Ronnstrand, 2004).

The phosphorylation sites in wild-type Flt3 and in the oncogenic Flt3-ITD and Flt3-D835Y mutants were identified by Razumovskaya and colleagues. They employed a panel of specific anti-phosphotyrosine antibodies that were raised against a set of synthetic phosphotyrosine-peptides (Razumovskaya *et al.*, 2009).

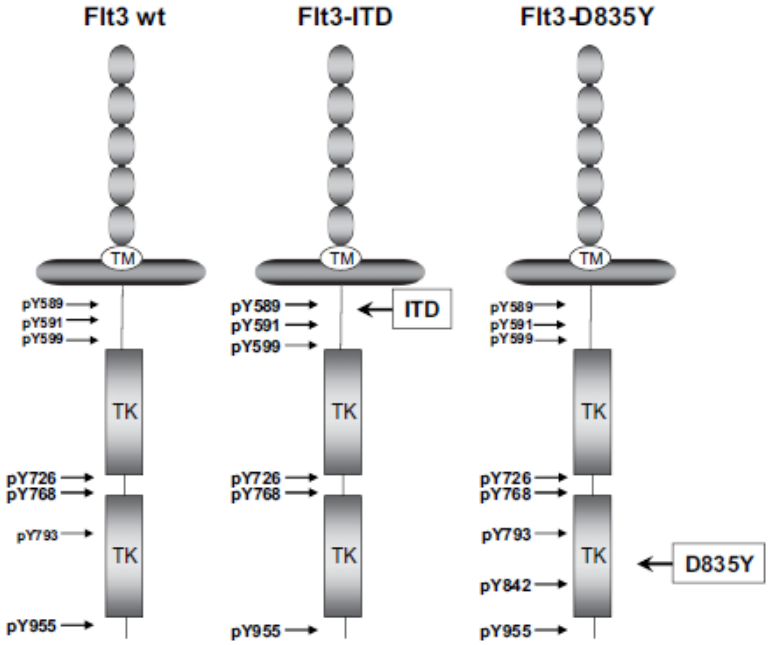

FIGURE 46. **Phosphorylation sites in wild-type and oncogenic Flt3.**
Schematic picture of the wild-type Flt3, Flt3-ITD, and FLT3-D835Y and their phosphorylation sites. The size indicates the phosphorylation ability. ***Adopted from Razumovskaya et al., 2009.***

The sites of autophosphorylation in the wild-type receptor are: Tyr589, Tyr591 and Tyr599 in the JM-region, Tyr726 and Tyr768 in the kinase insert region, Tyr793 in the C-lobe, and Tyr955 in the C-terminal tail (**Fig. 46**). The phosphorylation of Tyr842 in the activation loop is apparently not required for the activation of the kinase.

Some sites were found to be activated in a similar fashion, whereas other sites were activated selectively either by the Flt3-ITD or the Flt3-D835Y mutant. For example only in the activation loop mutant, D835Y, tyrosine residue 842 becomes phosphorylated. The use of different phosphorylation sites may result in the differential recruitment and activation of downstream signaling proteins.

Flt3 signal transduction pathway

FL-mediated activation of the Flt3 receptor induces the autophosphorylation of specific tyrosine residues which act then as recruitment sites for various signal transducing proteins that contain Src Homology-2 (SH2) domains (**Fig. 47**). Subsequently, these signaling proteins themselves become activated - by a conformational change upon binding or by tyrosine phosphorylation by Flt3 - and activate other downstream proteins or molecules that are involved in pathways connected with apoptosis, proliferation and differentiation.

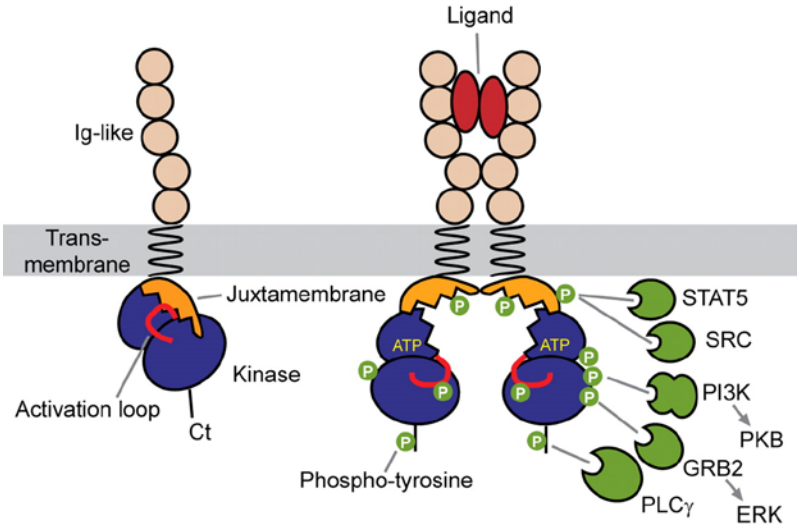

FIGURE 47. Activated Flt3 recruits various SH2-containing signal transducing molecules. Ligand binding causes receptor dimerization and phosphorylation of regulatory tyrosine residues. Phospho-tyrosines then act as docking sites for SH2 domains of a variety of signal transduction proteins. STAT5: signal transducer and activator of transcription 5 SRC: Src-family tyrosine kinase; PI3K: phosphatidylinositol 3-kinase; PKB: protein kinase B (AKT); GRB2: Growth factor receptor-bound protein 2; ERK: extracellular signal-regulated kinase (MAPK); PLCγ: phospholipase C-γ. ***Adapted from Toffalini and Demoulin, 2010.***

The two main Flt3 signaling routes are the PI3K–PKB/Akt and the Ras–Raf–MAPK/ERK pathways. Flt3-mediated PI3K activation induces the transcription of crucial regulatory genes and blocks apoptosis by phosphorylation of the Bcl-2 family protein Bad. Unlike the murine Flt3 receptor, human Flt3 does not have a PI3K binding site but activates the PI3K indirectly (Zhang and Broxmeyer, 1999). The stimulation of the Ras–Raf–MAPK/ERK pathway results in the transcription of genes involved in cell proliferation (Zhang and Broxmeyer, 2000; Stirewalt *et al.*, 2003a; Parcells *et al.*, 2006). Signaling is down-regulated by the rapid internalization and degradation of ligand-receptor complexes (Turner *et al.*, 1996).

Different groups have observed that FLT3-ITD activates STAT5 and its downstream effectors, whereas ligand-stimulated wild-type FLT3 does not. It was shown that phospho-Tyr-589 and phospho-Tyr-591, both located in the JM-domain are the docking sites for STAT5. Thus, the disruption of the JM-region by ITDs allows the binding and ensuing phosphorylation of the STAT5 transcription factor (Choudhary *et al.*, 2007; Rocnik *et al.*, 2006). That wild-type and mutant receptors can trigger different signaling pathways has also been observed for other receptors (Toffalini and Demoulin, 2010).

Chapter 2

Efficient Production of Bioactive Recombinant Human Flt3 Ligand in *E. coli*

Kenneth Verstraete[1], Sina Koch[2], Sevgi Ertugrul[1,4], Isabel Vandenberghe[3], Maarten Aerts[3], Gonzalez Vandriessche[3], Christian Thiede[2] and Savvas N. Savvides[1]

[1]Unit for Structural Biology, Laboratory for Protein Biochemistry and Biomolecular Engineering (L-ProBE), Ghent University, Belgium

[2]Medizinische Klinik und Poliklinik I, Universitätsklinikum Carl Gustav Carus der Technischen Universität Dresden, Germany

[3]Unit for Mass Spectrometry and Proteomics, Laboratory for Protein Biochemistry and Biomolecular Engineering (L-ProBE), Ghent University, Belgium

[4]Present Address:
Department of Biology, Faculty of Science,
Ankara University, Turkey

Redrafted from: The Protein Journal (2009) **28**: 57 – 65

ABSTRACT

Flt3 ligand (FL) is an early-acting hematopoietic cytokine that stimulates the proliferation and differentiation of hematopoietic progenitor cells by activating its cognate receptor, Flt3. Recently, FL was shown to potently contribute to the development and expansion of antigen-presenting dendritic cells and $CD34^+$ natural killer cell progenitors *in vivo*. Here, we report a comprehensive method for the production of bioactive recombinant human FL (rhFL) in *E. coli*, suitable for structural, biophysical and physiological studies. A soluble form of human FL capable of binding to the Flt3 receptor could be overexpressed in the *E. coli* strain Rosetta-gami(DE3) as inclusion bodies. We have established protocols for the efficient *in vitro* refolding and ensuing purification of rhFL to homogeneity (>95%), with yields approaching 5 mg of pure rhFL per liter of culture. The ability of rhFL to adopt a bioactive conformation was confirmed via a cell-proliferation assay and the activation of the Flt3 receptor in the human leukemic cell line, OCI-AML3.

INTRODUCTION

Hematopoiesis, the making of blood cells, is an exquisitely regulated process in which progenitor cells originating from a self-renewing population of hematopoietic stem cells (HSC) are directed to proliferate and differentiate. The development of HSCs and subsequent cell progenies is largely orchestrated by the synergistic activity of soluble and cell-bound hematopoietic growth factors which bind to the extracellular domains of their cognate receptors at the cell surface to initiate appropriate intracellular signaling pathways (Bryder *et al.*, 2006; Li and Li, 2006; Metcalf, 2007; Ross and Li, 2006).

Flt3 ligand (FL) stimulates early hematopoiesis by activating the Fms-like tyrosine kinase 3 (Flt3) receptor, which is expressed on a variety of early hematopoietic precursors in the bone marrow (Lyman and Jacobsen, 1998; Matthews *et al.*, 1991). As is the case for many cytokines, the hematopoietic effects of FL are most pronounced when acting in synergy with other growth factors such as interleukin 3 (IL-3), stem cell factor (SCF), granulocyte colony-stimulating factor (G-CSF), granulocyte-macrophage colony-stimulating factor (GM-CSF) and macrophage colony-stimulating factor (M-CSF) (Chklovskaia *et al.*, 2004; Hudak *et al.*, 1995; Shah *et al.*, 1996; Wodnar-Filipowicz, 2003). In recent years an ever growing body of evidence has linked FL to the development, expansion and mobilization of antigen-presenting dendritic cells, thus prompting the emergence of recombinant FL as a promising player in cancer immunotherapy (Antonysamy and Thomson, 2000; Dong *et al.*, 2002; Fong *et al.*, 2001; Karsunky *et al.*, 2003; Wu and Liu, 2007). Other *in vivo* effects of recombinant FL include the mobilization of hematopoietic progenitors to the peripheral circulation (Papayannopoulou *et al.*, 1997), and the protection and increased recovery of the hematopoietic system following irradiation (Gratwohl *et al.*, 1998).

The search for the ligand of the Flt3 receptor led to the cloning of FL cDNA which was shown to code for a type I membrane protein consisting of 235 amino acid residues (Lyman *et al.*, 1993a; Lyman *et al.*, 1993b; Hannum *et al.*, 1994) . In contrast to the limited tissue distribution of the Flt3 receptor, FL is ubiquitously expressed both in hematopoietic and non-hematopoietic tissues. Yet the presentation of FL protein at the cell surface is rather limited due to a cytokine-specific, regulatory retention mechanism (Chklovskaia *et al.*, 1999). Mature human FL lacks the first 26 amino acid residues which constitute the signal peptide. The extracellular domain is therefore defined by 156 amino acid residues harboring the receptor-binding epitope, and is followed by a 23 amino acid transmembrane helix and a 30 amino acid cytoplasmic tail.

The biologically active extracellular domain of FL exhibits a non-covalently linked homodimeric structure in which two short-chain four-helical bundles, each with three intramolecular disulfide bridges, interact head-to-head (Graddis *et al.*, 1998; Savvides *et al.*, 2000). In mice and humans soluble, bioactive forms of FL can be generated by proteolytic cleavage of the transmembrane ligands and/or alternative splicing (Lyman, 1995). FL is structurally homologous to

two other hematopoietic cytokines: SCF and M-CSF. Together, these three growth factors constitute a unique subset of helical-bundle cytokines that activate receptor tyrosine kinase type III receptors from the platelet-derived growth factor receptor (PDGF-R) family, which groups receptors targeted by cystine-knot growth factors such as PDGF and vascular endothelial growth factor (VEGF) (Savvides *et al.*, 2000).

Constitutive Flt3 signaling, caused by the overexpression of the wild type receptor or the expression of oncogenic forms of the Flt3 receptor has been linked to a number of hematopoietic malignancies. In fact, Flt3 mutations are the most frequent genetic alterations in acute myelogenous leukemia (AML) and indicate a poor prognosis (Gilliland and Griffin, 2002; Kiyoi *et al.*, 2005; Stirewalt *et al.*, 2003b). Furthermore, FL has been suggested to play a role in leukemogenesis by an autocrine signaling loop mechanism (Zheng *et al.*, 2004b). Strategies aimed to tackle constitutive Flt3 signaling include the development of specific small molecule tyrosine kinase inhibitors (Kancha *et al.*, 2007; Schmidt-Arras *et al.*, 2004) and more recently, therapeutic monoclonal antibodies (Sternberg and Licht, 2005). Gaining insights into how FL triggers Flt3 activation could lead to novel strategies to treat leukemias such as AML, and to the design of agonist molecules that could facilitate the ex vivo and *in vivo* expansion of hematopoietic progenitors.

We have launched an interdisciplinary research initiative aiming to elucidate the kinetic, thermodynamic and structural determinants of Flt3 activation by FL. To meet the high demands of the underlying experimental methods for the individual proteins, we have developed a cost-effective and efficient method for the production of milligram quantities of bioactive recombinant human FL (rhFL) in *E. coli*. To our knowledge, our work constitutes the first comprehensive protocol for the production of rhFL in a prokaryotic host, and complements the previously reported production of glycosylated rhFL in the methylotrophic yeast *Pichia pastoris* (Zhang *et al.*, 2005).

MATERIALS AND METHODS

Plasmid Construction and Expression of Recombinant Human FL in E. coli

A cDNA clone containing the full-length human Flt3 ligand cDNA (Clone ID IRALp962K2428Q) was obtained from IMAGENES (Berlin, Germany). The fragment encoding residues 1-134 was PCR amplified with Easy-A HiFi Polymerase (Stratagene, La Jolla, CA, USA). The forward primer (5’ cgatgacatatgacccaggactgctccttc 3’) carried the NdeI restriction site (underlined) and the reverse primer (5’ caggatccttagggctgacactgcagctc 3’) contained a stop codon, immediately followed by the BamHI restriction site (underlined). The PCR was performed using the following conditions: denaturation for 1 min at 95° C, annealing for 1 min at 55° C and extension for 2 min at 72° C for 30 cycles and a final extension step for 10 min at 72° C. The resulting PCR product was purified using the Qiaquick Gel Extraction KIT (Qiagen, Hilden, Germany) and ligated into the pCR2.1-TOPO vector (Invitrogen, Carlsbad, CA, USA), creating pCR2.1-rhFL.

Subsequently, pCR2.1-rhFL was digested with NdeI/BamHI and the gel-purified rhFL fragment was ligated into NdeI/BamHI cut pET15b vector (Novagen, Madison, WI, USA), using T4 DNA ligase (Promega, Madison, WI, USA). The resulting expression construct was verified by sequencing (Genome Express, Meylan, France), and designated pET15b-rhFL (**Fig. 1**).

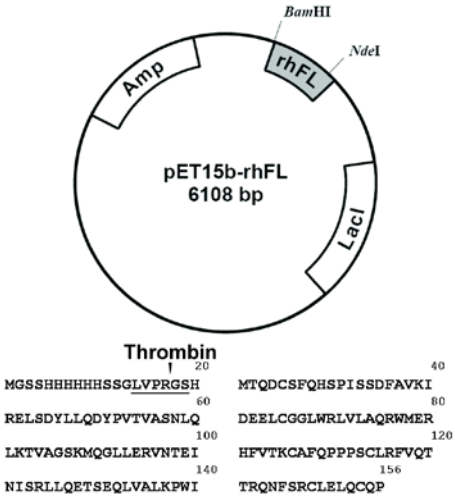

FIGURE 1. rhFL expression-plasmid and protein sequence.

The human FL cDNA, encoding residues 1–134 of the mature human FL protein was cloned between the NdeI and BamHI sites of the pET15b vector. This cloning strategy allows the expression of rhFL as a fusion protein with a cleavable N-terminal hexahistidine tag. The thrombin recognition sequence is underlined and the thrombin cleavage site is indicated with an arrow. Amp: ampicillin resistance gene. LacI: LacI coding region.

pET15b-rhFL was used to transform the Rosetta-gami(DE3) strain (Novagen) which carries the chloramphenicol-selectable pRARE plasmid. Expression cultures were grown at 37° C in Luria-Bertani medium, containing 100 µg mL^{-1} carbenicillin and 34 µg mL^{-1} chloramphenicol. Expression of rhFL was induced at a culture OD_{600} of 0.6, by the addition of isopropyl-β-D-thiogalactopyranoside (ITPG) to a final concentration of 1 mM, after which the culture was allowed to grow for an additional 4 h. The levels of recombinant protein expression were markedly lower when the culture was allowed to grow for longer periods of time. The bacteria were harvested by centrifugation (6,000 g for 20 min at 4° C) and the cellular paste was stored at -80° C.

Isolation of rhFL Inclusion Bodies and Purification of rhFL Under Denaturing Conditions

The bacterial pellet was thawed and resuspended in lysis buffer: 50 mM Tris pH 8.0, 100 mM NaCl, 1% Triton X-100, 1 mM EDTA, 0.2 mM PMSF and 1x Complete protease inhibitor mix (Roche Diagnostics, Mannheim, Germany). The cells were lysed by sonication on a 250-D Branson sonifier (total run time of 4 min with 30 s pulses at 30% output interspersed with 30 s of down time). Cell debris and inclusion bodies were isolated by centrifugation at 4° C (20,000g for 30 min). The inclusion bodies were subsequently washed twice based on the following protocol: the pellet containing the inclusion bodies was solubilized in lysis buffer and sonicated for 30 s at 30% output.

The suspension was incubated on a 'head-over-head' shaker for 30 min followed by centrifugation at 4° C (20,000g for 30 min) to harvest the pellet containing the inclusion bodies.

The washed inclusion bodies were solubilized in urea buffer (8 M urea, 100 mM $NaPO_4$, 10 mM Tris, 10 mM β-mercaptoethanol, pH 8.0) by gentle rotation in a 'head-over-head' shaker at room temperature for 2 h. Insoluble material was removed by high speed centrifugation at 4° C (100,000g for 30 min). The clarified supernatant was loaded onto a Ni-Sepharose 6 FF (GE Healthcare) column, equilibrated with urea buffer, pH 8.0. Next, the column was washed with five column volumes (CV) of urea buffer at pH 6.3 and pH 5.8. Denatured rhFL was eluted with five CV urea buffer at pH 4.5 and neutralized with Tris pH 8.0. The total amount of rhFL was estimated based on the absorbance of the sample at 280 nm and a calculated extinction coefficient of 19,855 M^{-1} cm^{-1}.

In vitro Refolding of rhFL and Purification of Refolded rhFL

Denatured rhFL was added drop wise to refolding buffer (100 mM Tris, pH 8.5, 1 M L-arginine, 5 mM GSH, 0.5 mM GSSG and 0.2 mM PMSF) at 4° C under rapid mixing, to a final protein concentration of 0.1 mg mL^{-1}. The refolding mixture was gently stirred overnight and was subsequently dialyzed against 20 mM Tris pH 8.0, 300 mM NaCl, 0.2 mM PMSF. Aggregates were removed by high speed centrifugation and the clarified refolding mixture was loaded onto a Ni Sepharose 6 FF column, equilibrated with 50 mM $NaPO_4$, 300 mM NaCl, pH 8.0. Refolded rhFL was eluted with equilibration buffer containing 500 mM imidazole.

To remove the N-terminal His-tag, the protein solution was desalted into phosphate-buffered saline (PBS) (10 mM $NaPO_4$, 150 mM NaCl, pH 7.0) and consequently incubated overnight at room temperature with one unit of biotinylated thrombin (Novagen) per milligram rhFL. The progress of proteolytic cleavage was monitored by SDS–PAGE. Biotinylated thrombin was removed using streptavidin-agarose (Novagen), following the manufacturer's recommendations. Thrombin-treated rhFL was subsequently injected onto a Prep-Grade HiLoad 16/60 Superdex 75 column (GE Healthcare, Buckinghamshire, UK) connected to an ÄKTAPurifier system (GE Healthcare), equilibrated with PBS. The fractions corresponding to rhFL were pooled and diluted into cation-exchange running buffer (20 mM MES pH 6.0), to give a final NaCl concentration of 25 mM. The protein sample was loaded onto a MonoS HR 5/5 column (GE Healthcare) connected to an ÄKTA explorer system. rhFL was eluted using a linear gradient from 0 to 1 M NaCl. Finally, to assess the correct removal of the His-tag, the digested protein was subjected to N-terminal sequence analysis by automated Edman degradation performed on a model 476A pulsed liquid protein sequencer (Applied Biosystems, Foster City, CA, USA).

To confirm the quaternary structure of refolded, purified rhFL analytical gel filtration was carried out on a Superdex-200 PC3.2 column, connected to an Ettan LC system (GE Healthcare) with PBS as running buffer. The gel filtration columns were calibrated with an equimolar mixture of ferritin (440 kDa), aldolase (158 kDa), conalbumin (75 kDa), ovalbumin (43 kDa), carbonic anhydrase (29 kDa), ribonuclease (13.7 kDa) and aprotinin (6.5 kDa).

Far-UV Circular Dichroism (CD)

Analysis CD spectra were recorded at 25° C on a Jasco J-600 spectropolarimeter (Jasco, Tokyo, Japan). Samples containing 0.3 mg mL^{-1} of rhFL in PBS buffer were analyzed using a 1 mm path length quartz cell. Spectra were recorded from 195 to 250 nm with 0.5 nm resolution, at 20 nm min^{-1}, with a response time of 4 s and a bandwidth of 1 nm. Data analysis was based on five averaged measurements after subtracting the buffer contribution.

ESI-MS

Purified, refolded rhFL was desalted using ZipTip pipette tips (Millipore). Trifluoroacetic acid (TFA) was added to the sample to a final concentration of 0.1%. A 10 µL ZipTip was wetted with 100% acetonitrile and equilibrated with 0.1% TFA. After binding the sample, the tip was washed with 0.1% TFA. The protein was eluted with 1% formic acid/50% acetonitrile. ESI-MS spectra were measured on a Q-TOF instrument (Waters), equipped with a Nanomate ionization source (Advion).

Cell Lines

OCI-AML3 and THP-1 cells are monocytic human leukemic cell lines and were purchased from the German Collection of Microorganisms and Cell Cultures (DSMZ) (Braunschweig, Germany). OCI-AML3 cells were cultured in alpha-MEM with nucleosides (Gibco, Karlsruhe, Germany) and THP-1 cells were cultured in RPMI-1640 (Gibco, Karlsruhe, Germany), with both media supplemented with 10% (v/v) heat-inactivated fetal calf serum (FCS) (Gibco, Karlsruhe, Germany) and 1% (v/v) Penicillin/Streptomycin (PAA Laboratories, Pasching, Austria) at 37° C and 5% CO_2, in a humidified atmosphere. As a positive control, rhFL produced in insect cells was purchased from R&D Systems (Minneapolis, MN, USA).

Cell Proliferation Assay

The proliferation behavior of cells was assessed using the CellTiter 96® Aqueous One Solution Cell Proliferation Assay kit from Promega (Madison, WI, USA) according to manufacturer‘s recommendations. In brief, 5,000 cells were seeded per well of a 96-well-plate in medium with 1% FCS (starvation medium) with or without the addition of rhFL and cultured for 70 h at 37° C and 5% CO_2, in a humidified atmosphere. After adding the CellTiter 96® aqueous one solution reagent, cells were incubated for further 2 h at 37° C and 5% CO2. Absorbance was recorded at 450 nm in an Anthos htll spectrometer (Anthos Labtec Instruments, Wals, Austria). Each experiment was performed in triplicate and three independent experiments were done.

Antibodies

Mouse monoclonal anti-phosphoFLT3 antibody, rabbit polyclonal anti phospho-MEK1/2 antibody, and mouse monoclonal anti-MEK1/2 antibody were purchased from Cell Signaling Technology (Danvers, MA, USA). Mouse monoclonal anti-human FLT3 antibody was purchased from R&D Systems. A mouse monoclonal anti-GAPDH antibody was purchased from Abcam (Cambridge, UK).

Protein Extraction and Western Blot Analysis

Cells were lysed in lysis buffer (10 mM Tris/HCl pH 7.5, 130 mM sodium chloride, 5 mM EDTA pH 8.0, 1% Triton-X 100, 50 mM sodium fluoride, 10 mM sodium pyrophosphate, 20 mM disodium hydrogenphosphate, 20 mM sodium dihydrogen phosphate, 1 mM sodium orthovanadate, 1 mM glycerol phosphate) supplemented with protease inhibitor cocktail from Roche Diagnostics (Mannheim, Germany) and 10 mM AEBSF-Hydrochloride (AppliChem, Darmstadt, Germany). 30 µg of total protein in 2X sample buffer (100 mM Tris pH 6.8, 200 mM DTT, 4% SDS, 0,05% bromophenol blue, 20% glycerol) were separated on reducing SDS–PAGE (8%) gels and transferred to PVDF membranes. Western blot analysis was performed with indicated antibodies followed by horse raddish peroxidase-conjugated anti-mouse IgG antibody or horse raddish peroxidase-conjugated anti-rabbit IgG antibody, and detection was performed with enhanced chemiluminescence using an ECL Plus Western Blotting Detection System (GE Healthcare, Buckinghamshire, UK).

Gel Electrophoresis

SDS–PAGE analysis was performed according to Laemmli (Laemmli, 1970) using 15% polyacrylamide gels. Samples were mixed with an equal amount of 2X sample buffer (125 mM Tris–HCl, pH 6.8, 20% glycerol, 4% SDS, 0.005% bromophenol blue, and 10% of 2-mercaptoethanol). Gels were stained with Coomassie brilliant blue R-250.

RESULTS

Overexpression of rhFL in *E. coli*

The human Flt3 ligand (hFL) cDNA, encoding residues 1–134 of the hFL ectodomain was cloned between the NdeI and BamHI sites of the pET15b vector. This vector allows high-level expression of recombinant proteins under control of the inducible T7 promoter (**Fig. 1**). Our cloning strategy focused on expressing rhFL as a fusion protein with a cleavable hexahistidine tag at the N-terminus, to facilitate purification (Fig. 1). Expression of rhFL in the Rosetta-gami(DE3) strain (**Fig. 2, Lanes 2, 3**) resulted in clear production of rhFL after induction with IPTG, which was

further confirmed by peptide mass fingerprinting (PMF) (results not shown). The Rosetta-gami(DE3) strain carries the chloramphenicol-selectable pRARE plasmid that encodes for five extra tRNAs which correct for eukaryotic codon bias. Interestingly, expression of rhFL could not be obtained in the BL21-CodonPlus(DE3)-RIL and BL21-CodonPlus(DE3)-RP strains, which also contain plasmids that encode for extra tRNAs. As is often the case for eukaryotic proteins expressed in *E. coli*, rhFL was produced as inclusion bodies. An exploration of a variety of culture growth parameters such as growth temperature and the inducer (IPTG) concentration failed to result in the expression of the target protein in the soluble fraction.

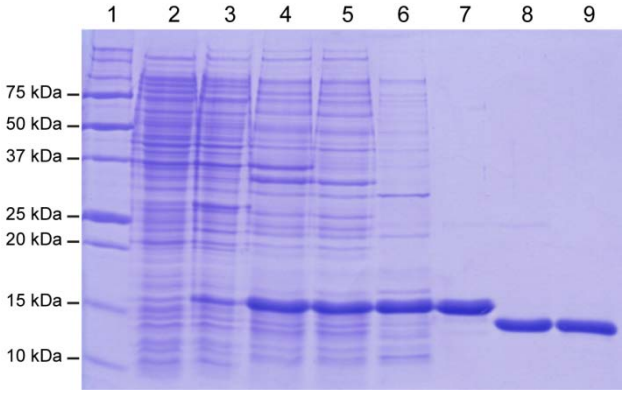

FIGURE 2. SDS–PAGE analysis of expression and purification of rhFL.
The predicted molecular weights for reduced His-tagged and thrombin-treated rhFL are 17.738 and 15.856 kDa, respectively. Lane 1: protein standards; Lane 2: bacterial cell lysate before induction; Lane 3: bacterial lysate at 4 h post-induction; Lane 4: washed IB; Lane 5: solubilized IB; Lane 6: Eluate from Ni-sepharose column at pH 4.5 under denaturing conditions; Lane 7: Capture of refolded rhFL on Ni-sepharose column; Lane 8: rhFL after removal of the His-tag by thrombin-digestion; Lane 9: Eluate from MonoS ion-exchange column.

In vitro Refolding and Purification of rhFL

The cells were lysed by sonication and cell debris and inclusion bodies (IB) were separated from the soluble fraction by centrifugation. To remove hydrophobically associated proteins, the IB were washed with buffer containing Triton X-100. Subsequently, the IB were solubilized under reducing conditions in 8 M urea. Material that could not be solubilized was removed by high speed centrifugation and the supernatant was loaded onto a Ni-Sepharose column. rhFL was eluted using a stepwise pH gradient (**Fig. 2, Lanes 4–6**). The cytokine was refolded overnight, at 4° C by the drop-wise addition of denatured rhFL to a refolding buffer containing a GSH:GSSG redox couple. The inclusion of 1 M arginine in the refolding buffer greatly improved the refolding efficiency (data not shown). Prior to the His-tag capture step of the refolded protein, arginine was removed by dialysis because it is not compatible with IMAC (immobilized metal affinity chromatography) matrices. Following concentration of the refolded product by IMAC, the N-terminal His-tag was removed

using biotinylated thrombin. Complete digestion was confirmed by SDS–PAGE (**Fig. 2, Lane 7, 8**). Thrombin was efficiently removed using streptavidine-agarose beads.

N-terminal sequence analysis identified the first seven residues as GSHMTQD which demonstrates that the fusion protein was correctly processed by thrombin (Fig. 1). rhFL was further purified using gel filtration and cation exchange chromatography (**Fig. 3**). The final purity of rhFL was estimated to be 99% on basis of Coomassie stained SDS–PAGE gel (**Fig. 2, Lane 9**). The protein yield across the different stages of the purification process is summarized in **Table I**.

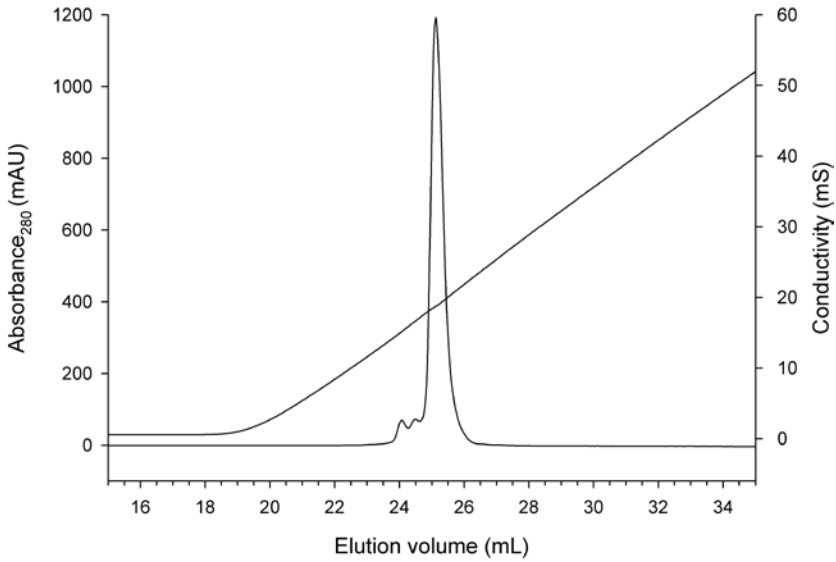

FIGURE 3. Cation exchange purification of refolded rhFL.
rhFL was eluted from a MonoS column using a linear gradient from 0 to 1 M NaCl.

Step	Total protein	Step yield (%)	Overall yield (%)
Wet cell-pellet from 1 L culture	5.3 g	–	–
Inclusion bodies (IB)	1.6 g	100	100
Washed IB	440 mg	28	28
IMAC-purification of denatured rhFL	15 mg	3.4	0.94
Gel-filtration chromatography on refolded rhFL	5.3 mg	35	0.33
Mono-S ion-exchange chromatography on refolded rhFL	4.6 mg	87	0.29

Table I. Efficiency of purification of rhFL from inclusion bodies

Protein Characterization and Bioactivity Assays

The homogeneity of purified, refolded rhFL was demonstrated by ESI-MS (**Fig. 4**). The determined molecular weight was 15,849.92 ± 0.51 kDa, which is very close to the theoretical molecular weight of rhFL (15,850.2 kDa). Far-UV CD spectra showed that the refolded cytokine had a high α-helical content (**Fig. 5**), and analytical gel filtration experiments on a calibrated column using proteins of known molecular weight demonstrated that the refolded protein possessed the expected dimeric structure (**Fig. 6**).

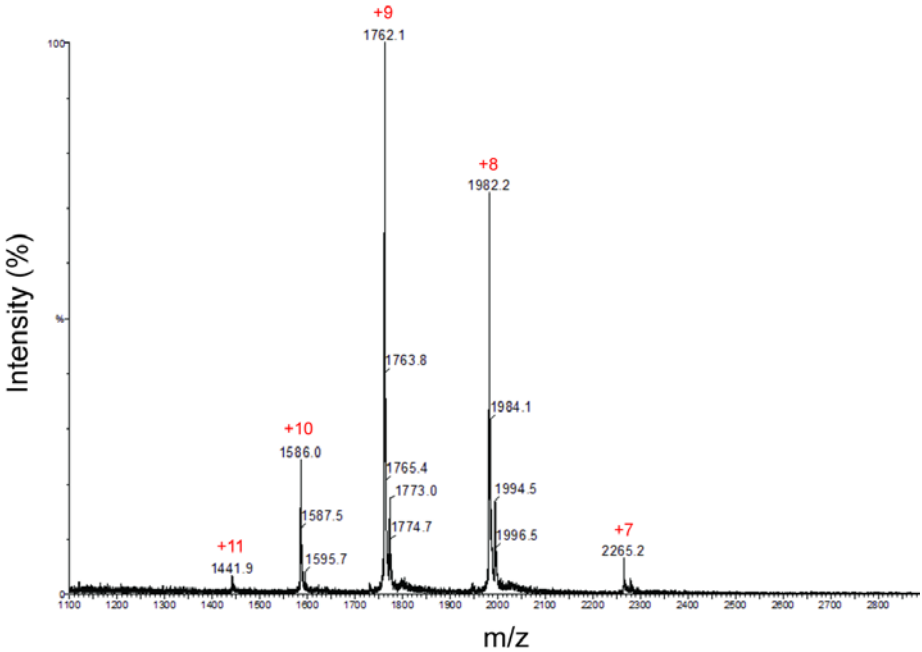

FIGURE 4. ESI-MS of refolded, purified rhFL.

The experimentally determined molecular weight of 15,849.92 ± 0.51 kDa agrees well with the theoretical molecular weight of 15,850.2 kDa. The number of charges (red) is indicated on each peak.

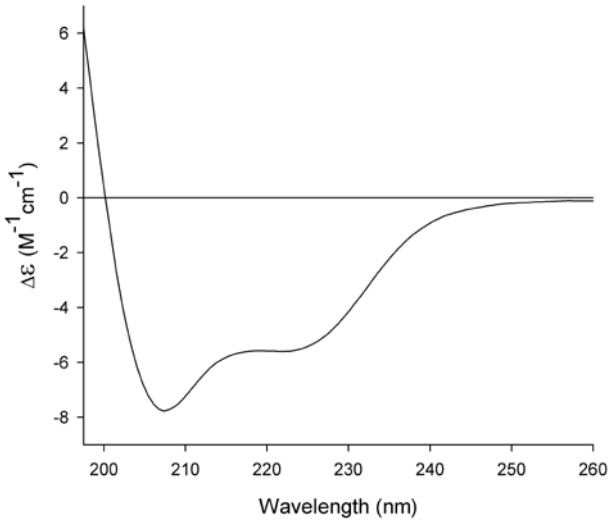

FIGURE 5. Far UV-CD spectrum of refolded, purified rhFL.
The two negative bands at 208 and 223 nm indicate a high α-helical content.

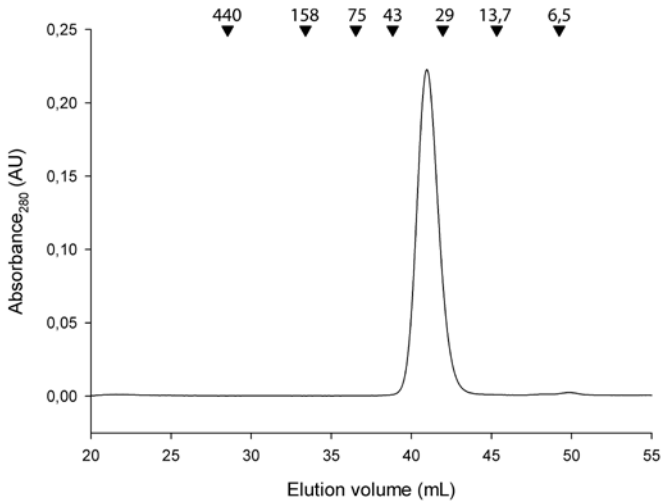

FIGURE 6. Analytical gel-filtration on refolded, purified rhFL.
The elution volume corresponds well to the molecular weight of dimeric rhFL (31,7 kDa), indicating that the refolded cytokine possesses the correct quaternary structure. The elution volumes and molecular weight of the protein standards used to calibrate the column are indicated.

The biological activity of the refolded cytokine was tested using the human leukemic cell lines OCI-AML3 (Wang *et al.*, 1989) and THP-1 (Tsuchiya *et al.*, 1980), which express the wild type Flt3 receptor (Quentmeier *et al.*, 2003) and proliferate in response to FL (Dehmel *et al.*, 1996; Drexler *et al.*, 1999). Our rhFL strongly stimulated the proliferation of both cell lines. rhFL-dependent phosphorylation of the Flt3 receptor and the downstream signaling molecule MEK, were monitored by Western blot analysis. Data for the OCI-AML3 cell line are shown in **Fig. 7**. Similar results were obtained with the THP-1 cell line (data not shown).

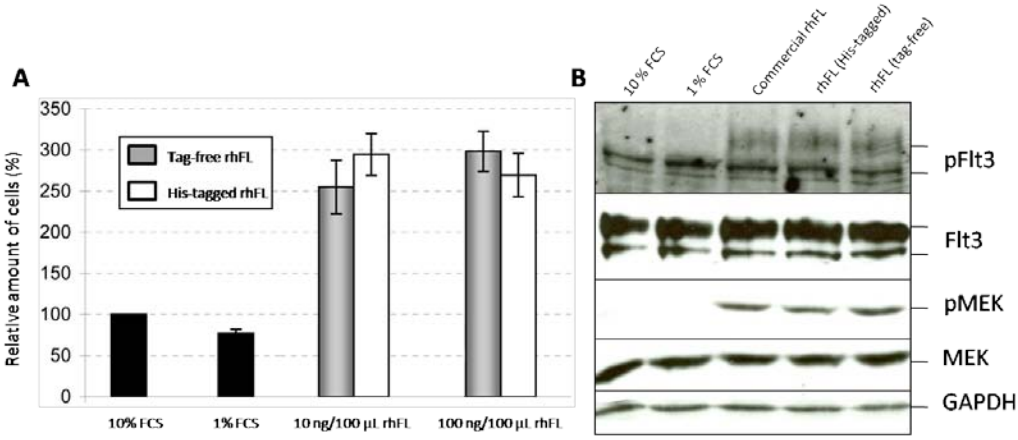

FIGURE 7. OCI-AML3 proliferation assay and Western blot analysis.

(A) rhFL stimulates the proliferation of the leukemic cell line, OCI-AML3 which expresses the wild type Flt3 receptor. Each experiment was performed in triplicate and three independent experiments were done**. (B)** rhFL induces phosphorylation of Flt3 and its downstream target, MEK. Commercially available rhFL, produced in insect cells, was used as a positive control. GAPDH shows equal loading of the cell lysates. His-tagged rhFL showed the same bioactivity as tag-free rhFL.

His-tagged rhFL exhibited the same bioactivity as tag-free rhFL. The two bands of the Flt3 receptor in the immunoblot represent two different Flt3 receptor species: (1) a faster migrating, mannose-rich, immature form; and a slower migrating, cell-surface expressed, complex sugar-type form (Lyman *et al.*, 1993a; Lyman *et al.*, 1993b; Maroc *et al.*, 1993). Notably, the anti-phosphoFLT3 antibody recognizes both FLT3 species: the high-mannose form of the protein is detected under every condition tested, whereas the complex glycosylated form is detected only after addition of exogenous rhFL. We propose that the intracellular high mannose form of FLT3 might be constitutively phosphorylated in a ligand independent manner, like in FLT3-ITD (Schmidt-Arras *et al.*, 2005), whereas the complex glycosylated form at the cell surface becomes phosphorylated only upon binding of exogenous rhFL.

DISCUSSION

A detailed method for the production of human glycosylated Flt3 ligand in the methylotrophic yeast *P. pastoris* system has been reported previously (Zhang *et al.*, 2005). Remarkably, however, the production of recombinant hFL via more conventional expression systems, such as *E. coli*, is inadequately described in the scientific literature. We have successfully overexpressed the extracellular domain of hFL (residues 1–134) capable of activating the Flt3 receptor (Escobar *et al.*, 1998), in the *E. coli* Rosetta-gami(DE3) strain. Interestingly, expression of rhFL could not be obtained in the BL21-CodonPlus(DE3)-RIL and BL21-CodonPlus(DE3)-RP strains, despite the fact that they all, like the Rosetta-gami(DE3) strain, contain plasmids that encode for extra tRNAs. This highlights the need for testing protein expression in a variety of cell strains, especially when one tries to express eukaryotic proteins in prokaryotic expressions systems. An initial exploration of expression conditions indicated that rhFL consistently ended up in the insoluble fraction which suggested the formation of inclusion bodies. We therefore focused our efforts on maximizing the yield of rhFL inclusion bodies and in developing efficient protocols for the *in vitro* refolding and ensuing purification of rhFL.

One of the greatest challenges underlying the *in vitro* refolding of proteins that contain disulfide-bridges in their native state, is the correct matching of the relevant cysteine residues during the folding process. In our construct of rhFL we expected three disulfide bridges per subunit (Cys4-Cys85, Cys44-Cys127, Cys93-Cys132). To facilitate disulfide-bridge formation we used the GSH:GSSG redox couple and maintained the refolding buffer at an alkaline pH (Singh and Panda, 2005). Importantly, we found that the inclusion of 1 M arginine in the refolding buffer dramatically improved the yields of refolded protein from about 1 mg per liter of culture to a final yield of 5 mg of pure rhFL. The role of arginine in protein refolding has been the subject of extensive investigation in recent years. It is currently accepted that arginine serves to suppress protein aggregation during refolding, rather than to facilitate the refolding process (Arakawa and Tsumoto, 2003; Singh and Panda, 2005). The established purification protocols for rhFL feature three standard chromatographic steps which can be readily adapted for the large scale purification of rhFL. Indeed, one of the advantages of expression systems based on *E. coli* is the relative ease with which protein production can be scaled up.

We have sought to confirm the bioactivity of rhFL using a cell-proliferation assay and the activation of the Flt3 receptor in the human leukemic cell lines OCI-AML3 and THP-1 which express the wild-type Flt3 receptor. This activity-benchmarking is essential before a recombinant protein can be used for cellular, physiological, and biophysical studies. We have shown that rhFL produced in *E. coli* is at least as active as commercially available rhFL produced as a glycoprotein in insect cells (**Fig. 7**). rhFL decorated with N- and O-linked glycans produced in yeast (*P. pastoris*) has also been shown to be sufficiently bioactive (Zhang *et al.*, 2005). The levels of bioactivity we

have observed for unglycosylated rhFL produced in a bacterial host, indicate that glycosylation is not important for receptor binding and activation, at least *in vitro*. Furthermore, the bioactivity of rhFL carrying an N-terminal His-tag exhibits proliferative and signaling activity that is for all practical purposes indistinguishable from tag-free rhFL. The availability of His-tagged bioactive rhFL may indeed prove an important tool in biochemical and cellular assays. For instance, one may use rhFL immobilized on a Ni-NTA matrix to trap FL-Flt3 complexes, or in SPR experiments to study ligand–receptor interactions.

In this report, we have described a comprehensive, cost-effective and efficient method leading to the production of milligram amounts of highly active recombinant hFL in *E. coli*. Our methods respond to a growing need for the efficient production of high-value recombinant human cytokines for biochemical, biophysical, physiological, and clinical studies.

ACKNOWLEDGMENTS

We are grateful to the Department of Ultrastructure at the Vrije Universiteit Brussel (Belgium) for access to CD-spectroscopy facilities. KV is a doctoral fellow of the Fund for Scientific Research-Flanders, Belgium (FWO). This work was supported by research grants from the FWO (G.0643.07) and Ghent University (BOF01Z01705) to SNS, and from the German Research Foundation (SFB 655 TP16) to CT.

AUTHORSHIP

KV designed and created the expression construct and performed expression tests. KV and SE purified and refolded FL. MA and GV carried out mass spectrometry analyses. IV performed N-terminal sequence analysis. SK and CT conducted bioactivity assays in the THP-1 and OCI-AML3 cell lines. KV and SNS wrote the manuscript.

Chapter 3

Inducible Production of Human FLT3 Ectodomain Variants in Mammalian Cells and Preliminary Crystallographic Analysis of FLT3 Ligand-Receptor complexes

Kenneth Verstraete[1], Bert Remmerie[1], Jonathan Elegheert[1], Beatrice Lintermans[2], Guy Haegeman[2], Peter Vanhoenaker[2], Kathleen Van Craenenbroeck[2], Savvas N. Savvides[1]

[1]Unit for Structural Biology, Laboratory for Protein Biochemistry and Biomolecular Engineering (L-ProBE), Ghent University, Belgium

[2]Laboratory of Eukaryotic Gene Expression and Signal Transduction (LEGEST), Ghent University, Belgium

Redrafted from: Acta Crystallographica Section F (2011) **67**: 325 – 331

ABSTRACT

The extracellular complex between the hematopoietic receptor Flt3 and its cytokine ligand (FL) is the cornerstone of signaling cascades central to early hematopoiesis and the immune system. Here we report efficient protocols for the production of two ectodomain variants of human Flt3 receptor, $Flt3_{D1-D5}$ and $Flt3_{D1-D4}$, for structural studies. We established tetracycline-inducible stable cell lines in HEK293S cells deficient in N-acetylglycosaminyltransferase I ($GnTI^{-/-}$) that can secrete the target proteins with limited and homogeneous N-linked glycosylation to milligram amounts. The ensuing preparative purification of Flt3 receptor-ligand complexes yielded monodisperse complex preparations that were amenable to crystallization. Crystals of $Flt3_{D1-D4}$:FL and $Flt3_{D1-D5}$:FL complexes diffracted to Bragg spacings of 4.3 Å and 7.8 Å, respectively, and exhibited variable diffraction quality even within the same crystal. The resulting data led to the successful structure determination of the two Flt3 receptor-ligand complexes via a combination of molecular replacement and density-modification protocols exploiting the non-crystallographic symmetry and high solvent content of the crystals.

INTRODUCTION

The Fms-like tyrosine kinase 3 (Flt3) receptor and its cognate cytokine, termed Flt3 ligand (FL), initiate signalling pathways in hematopoietic stem cells and early hematopoietic progenitors of myeloid and lymphoid origin to develop the pluripotent cellular population of the human hematopoietic and immune systems (Lyman *et al.*, 1993b; Hannum *et al.*, 1994; Stirewalt and Radich, 2003; Drexler and Quentmeier, 2004; Parcells *et al.*, 2006; Onai *et al.*, 2007; Kikushige *et al.*, 2008; Liu and Nussenzweig, 2010). Flt3 receptor is primarily expressed on early hematopoietic progenitors in the bone marrow environment and is crucially involved in the development and homeostasis of antigen-presenting dendritic cells (Onai *et al.*, 2007; Waskow *et al.*, 2008; Schmid *et al.*, 2010). Injection of exogenous FL leads to a massive expansion of dendritic cells and this has prompted its use in cancer immunotherapy (Fong *et al.*, 2001). On the other hand, overexpression of wild type or oncogenic forms of the Flt3 receptor and/or FL autocrine signaling loops are associated with various hematologic malignancies (Kiyoi *et al.*, 1998; Stirewalt and Radich, 2003; Griffith *et al.*, 2004; Zheng *et al.*, 2004b; Parcells *et al.*, 2006; Kiyoi and Naoe, 2006). Most notably, mutational fingerprints in Flt3 are the predominant prognostic factor in acute myeloid leukemia (AML) (Eklund, 2010) and have rationalized the targeting of Flt3 in a clinical setting (Kindler *et al.*, 2010).

Flt3 is together with platelet-derived growth factor receptors (PDGFRα/β), colony-stimulating factor 1 receptor (CSF-1R), and KIT, a member of the type III receptor tyrosine kinase (RTKIII) family (Grassot *et al.*, 2006). As such, Flt3 has been predicted to exhibit a modular structure featuring an extracellular segment with five immunoglobulin (Ig)-like domains (residues 27-543), a single transmembrane helix (TM, residues 544-563), a cytoplasmic juxtamembrane domain (JM, residues 572-603) and an intracellular kinase module (residues 604-958) (Lyman *et al.*, 1993b; Maroc *et al.*, 1993). A fully functional Flt3 isoform that lacks the fifth Ig-domain has been identified in mice (Lavagna *et al.*, 1995). FL is a non-covalently linked dimeric four-helical bundle cytokine that is structurally homologous to Stem Cell Factor (SCF) and Colony Stimulating Factor 1 (CSF-1), which are the ligands of KIT and CSF-1R, respectively (Lyman *et al.*, 1993a; Hannum *et al.*, 1994; Savvides *et al.*, 2000).

Several FL-splice variants have been identified (Lyman *et al.*, 1995a; McClanahan *et al.*, 1996) leading to biologically active membrane-bound or soluble forms of FL (Escobar *et al.*, 1998), which activate the receptor by ligand-induced dimerization (Kiyoi *et al.*, 2002). Despite the staggering body of biomedical literature on the physiological and clinical importance of the Flt3-FL complex, the structural basis of the Flt3 extracellular assembly has remained uncharacterized. Here we report protocols for the efficient production of Flt3 ectodomain variants and the crystallization of their complexes with FL for structural studies.

MATERIALS AND METHODS

Expression constructs

A cDNA clone (Image ID 5272266) encoding the full-length human Flt3 receptor was purchased from IMAGENES. PCR-fragments encoding residues 1 to 540, 27 to 540 and 27 to 437 were gel-purified (Qiagen, cat. No. 28704) and subcloned into the pCR2.1-TOPO vector (Invitrogen, Cat. No. KNM4500-01). Mammalian expression constructs were generated in the pHLsec (Aricescu *et al.*, 2006) and pcDNA4/TO (Invitrogen, cat. No. V1020-20) vectors, by restriction site-dependent cloning. Modified versions of these vectors contained the human cystatine S (Barash *et al.*, 2002) or chicken receptor protein tyrosine phosphatase σ (RPTPσ) (Aricescu *et al.*, 2006) secretion signal at their multicloning site. All expression constructs included a C-terminal hexahistine tag. Plasmid-DNA was propagated in *E. coli* TOP10-cells (Invitrogen, cat. No. C4040-50) and purified by chromatography (Qiagen, cat. No. 12145). PCR was performed using Easy-A polymerase (Stratagene, Cat. No. 600400). Restriction enzymes were purchased from New England Biolabs. Inserts were ligated into the expression vectors using the LigaFast ligation system (Promega, Cat. No. M8221). The final expression constructs were sequence verified (Cogenics, Meylan, France) and matched the human Flt3 reference sequence in the NCBI database (NP_004110.2).

Transient expression of Flt3 in HEK293 cells

The human embryonic kidney cell lines, HEK293T (ATCC no. CRL-1573) and HEK293S GnTI$^{-/-}$ TetR cells (Reeves *et al.*, 2002) were grown in DMEM/F12 medium (GIBCO/Invitrogen, cat. No. 32500-043) supplemented with 10% heat-inactivated foetal calf serum (FCS) (Sigma, Cat. No. F7524), 3 mM L-glutamine (Sigma, Cat. No. G3126), 10^6 units per liter of penicillin G (Sigma, Cat. No. P7794) and 1 g/L streptomycin (Sigma, Cat. No. S9137), in a 5% CO_2 atmosphere at 37°C. Small-scale transient expression tests were performed in 6-well tissue culture plates (Corning, Cat. No. 3506) as described (Aricescu *et al.*, 2006). The medium of confluently grown cells was replaced with serum-free medium containing 5 µM kifunensine (Toronto Research Chemicals, Cat. No. K450000) and purified plasmid-DNA mixed with 25-kDa branched polyethyleneimine (Sigma, Cat. No. 408727) was added. Transfected cells were allowed to express the recombinant protein for 5 days and samples were prepared by mixing the medium with half a volume of Laemmli-buffer containing β-mercaptoethanol. Recombinant proteins in the conditioned medium were separated by SDS-PAGE (15% gel), followed by Western blot analysis using a HRP-coupled antibody directed against the C-terminal His-tag (Invitrogen, cat. No. R931-25). Femto Luminol (Thermo Scientific, cat. No. 34095) was used as the chemiluminescent substrate. Large-scale expression experiments in HEK293T cells were performed in roller-bottles (GBO, cat. No. 681070).

Tetracycline-inducible stable HEK293S GnTI$^{-/-}$ TetR cell lines secreting recombinant Flt3

pcDNA4/TO expression contructs (containing the RPTPσ secretion signal) were linearized in a non-essential region using the SapI-restriction enzyme (New England Biolabs) and the DNA was repurified using Qiaquick-spin columns (Qiagen, cat. No. 28104). Four hours prior to transfection, the medium of 50% confluent HEK293S GnTI$^{-/-}$ TetR cells grown in a 75 cm^2 tissue culture flask (Corning, cat. No. 430725) was replaced with fresh medium. Cells were transfected according to the calcium phosphate method using 30 µg of linearized DNA per flask. Four hours post-transfection, the medium was replaced again with fresh medium. After 24 hours the transfected cells were detached with trypsin/EDTA and diluted in three 175 cm^2 flasks at different dilutions, under selective pressure (200 µg/mL Zeocin, Invivogen, Cat. No. ant-zn-1). Consequently, the medium was refreshed every 3-4 days until foci appeared (after 2-3 weeks). Ten foci were isolated using filter papers soaked with trypsin/EDTA and transferred to 24-well tissue culture plates, and subsequently expanded to 175 cm^2 flasks (Greiner Bio-One, cat. No. 660160). Concomitantly, the clones were tested for protein expression in 6-well format. To induce expression, the growth medium of confluently grown cells was replaced with serum-free medium supplemented with 2 µg/mL tetracycline (Duchefa, cat. No. T0150) and 5 mM sodium butyrate (Sigma, cat. No. 303410). The expression level of the clones was compared by Western blot analysis. The most strongly expressing clones were prepared for long-term storage at 193 K using a mixture of 50% cells in DMEM/F12 (supplemented with 10% FCS) and 50% freezing solution (80% FCS and 20% DMSO (Sigma, catalogue No. D2650)). For large-scale expression experiments, the medium of fifty 175 cm^2 tissue culture flasks was used. Five days post induction, the medium was collected and clarified from cell debris by centrifugation and, finally stored at -20° C until further use.

Selenomethionine labelling of recombinant Flt3$_{D1-D4}$

Stable transfected HEK293S GnTI$^{-/-}$ cells were grown to confluence in DMEM/F12 medium containing 10% FCS. Prior to induction, the cells were washed once with phosphate-buffered saline (PBS) in order to remove most of the residual methionine. Subsequently, serum-free DMEM medium, devoid of methionine (MP Biomedicals, cat. No. 091642254) but supplemented with 30 mg/L selenomethionine (Acros Organics, cat. No. 259960010), 2 µg/mL tetracycline and 5 mM sodium butyrate, was added to the cells. We observed a significant reduction in protein expression compared to our standard protocols, which we attribute to increased levels of cell death owing to the toxicity of selenomethione.

Protein purification

Defrosted medium (2.5 L) was filtered through a 0.22 µm bottle-top filter (Corning, cat. No. 431174) and, without further additions, was loaded overnight onto a Talon Superflow column (Clontech, cat. No. 635507) with a bed volume of 20 mL connected to an ÄKTApurifier (GE Healthcare) system and equilibrated with 300 mM NaCl, 50 mM NaH_2PO_4, pH 7.2 at a flow rate of 5 mL/min. After loading, the column was washed with equilibration buffer containing 5 mM imidazole and the protein was eluted with buffer containing 200 mM imidazole. EDTA (1 mM) and protease inhibitors (Roche, cat. No. 11873580001) were added to the protein solution (~ 30 mL). Next, the protein was concentrated to 1 mL using a Vivaspin concentrator with a molecular weight cutoff of 10 kDa (Sartorius, cat. No. VS15RH02).

Subsequently, the partially purified recombinant Flt3 was injected onto a Superdex 200 column (GE Healthcare, cat. No. 17-1069-01) with 150 mM NaCl, 10 mM HEPES, pH 7.2 as running buffer. The fractions corresponding to recombinant Flt3 were pooled and concentrated to 1 mL using a Vivaspin concentrator (Sartorius, cat. No. VS0404). As a final polishing step, the protein solution was diluted 5-fold with 20 mM Tris/HCl pH 7.0 and loaded onto a MonoQ-column (GE Healhcare, cat. No. 17-5166-01) equilibrated with 20 mM Tris/HCl, pH 7.0. The protein was eluted using a linear gradient from 0 to 1 M NaCl and collected in fractions of 200 µL, and was stored at - 80° C until further use.

Crystallization of Flt3 ligand-receptor complexes

Flt3 ligand-receptor complexes were formed by mixing excess molar amounts of purified FL (2 x 138 residues, 31.7 kDa) (Verstraete *et al.*, 2009) with the purified receptor ectodomains. Protein concentrations were determined by absorbance at 280 nm using a NanoDrop spectrophotometer and the calculated extinction coefficients of the recombinant proteins: $\varepsilon_{280}(Flt3_{D1-D5}) = 76205\ M^{-1}cm^{-1}$, $\varepsilon_{280}(Flt3_{D1-D4}) = 50850\ M^{-1}cm^{-1}$ and $\varepsilon_{280}(FL) = 39710\ M^{-1}cm^{-1}$. The complex was separated from excess FL by gel filtration using a Superdex 200 column equilibrated with 150 mM NaCl, 10 mM HEPES, pH 7.2. Fractions corresponding to the complex were pooled and concentrated using a Vivaspin concentrator (Sartorius, cat. No. VS0404) to a final concentration of 5 mg/mL. The concentrated protein solution was aliquoted and flash frozen into liquid nitrogen and subsequently stored at -80° C until further use.

Initial crystal screening was carried out using the ProPlex (Molecular Dimensions, cat. No. MD1-38), Crystal Lite (Hampton Research, cat. No. HR2-128) and PEG ION I (Hampton Research, cat. No. HR2-126) screens. Crystallization drops were set up manually at 293 K in 24-well sitting-drop crystallization plates (Hampton Research. Cat. No. HR3-160) by mixing 1 µL of reservoir solution (500 µL) with 1 µL of protein solution at a concentration of 5 mg/mL. Crystallization conditions were optimized using chemicals of the highest purity available.

Derivatization of Flt3$_{D1-D4}$:FL crystals with heavy-atoms for phasing

Flt3$_{D1-D4}$:FL crystals were incubated in stabilisation buffer (artificial mother liquor containing a 10% higher concentration of precipitant) containing 0.5-5 mM of candidate heavy-atom compounds. A variety of Pt^{2+}, Pb^{2+}, and Hg^{2+} salts as well as the tantalum cluster Ta_6Br_{12}, were tried under different incubation times ranging from 1 minute to several hours.

X-ray data collection and analysis

Single crystals were transferred to a drop of stabilisation buffer (artificial mother liquor containing a 10% higher concentration of precipitant) with the use of a nylon loop (Hampton Research) mounted onto SPINE standard cryocaps (Molecular Dimensions, cat. No. MD7-406). The concentration of cryoprotectant was gradually adjusted by adding increasing amounts of stabilizing buffer containing a higher concentration of cryoprotectant to the drop until the desired concentration of cryoprotectant was reached. A 3-minute equilibration time was allowed between subsequent additions. Subsequently, the crystals were flash-frozen into liquid nitrogen and loaded into SPINE/ESRF pucks for storage and transport. Diffraction experiments were conducted at beamlines X06SA (PXI) and X06DA (PXIII) of the Swiss Light Source (Paul Scherrer Institute, Villigen, Switzerland) and ID23-1 of the ESRF (Grenoble, France). All data were integrated and scaled using the XDS suite (Kabsch, 2010). Molecular replacement was performed using Phaser (McCoy *et al.*, 2007). MR-search models for individual Flt3 Ig-domains were prepared with Chainsaw (Stein, 2008) and the KIT structure (Yuzawa *et al.*, 2007) as template. Density modification was performed using PARROT (Cowtan, 2010) and rigid-body refinement was conducted in PHENIX (Adams *et al.*, 2010).

RESULTS AND DISCUSSION

Protein expression and purification

Obtaining sufficient amounts of the Flt3 ectodomain for structural studies proved to be challenging. Our initial strategy was to express the full-length His-tagged Flt3 ectodomain (Flt3$_{D1-D5}$) by transient expression in HEK293T cells in the presence of kifunensine (Aricescu *et al.*, 2006; Chang *et al.*, 2007) to ensure properly folded recombinant receptor carrying limited N-linked glycans that could be further reduced by treatment with deglycosylating enzymes such as endoglycosidase H (EndoH) for crystallization purposes. However, despite the high quality and stability of recombinant Flt3$_{D1-D5}$ obtained via this approach, Flt3$_{D1-D5}$ yields were very low (0.1 mg per liter of culture medium) which posed tremendous hurdles for extensive crystal screening and additional biophysical studies.

Inspired by the work of Barash *et al.*, we exchanged the native Flt3 secretion signal with the RPTPσ or cystatine S secretion signal (Barash *et al.*, 2002). Western blot analysis showed that the

introduced signal peptides resulted in a moderate increase in the expression level with the RPTPσ secretion signal showing the largest effect (**Fig. 1A**). After verification by N-terminal sequencing that the leader sequence was correctly processed, the RPTPσ secretion sequence was retained as a general approach to improve the yields of secreted recombinant Flt3. Additional comparisons investigating the expression efficiency of pHL- and pcDNA4/TO-expression constructs showed similar yields of Flt3 indicating that the presence of the SV40-ori (present on pcDNA4/TO), which allows episomal replication of the expression plasmid in HEK293T cells, had no obvious effect on expression levels (**Fig. 1A**).

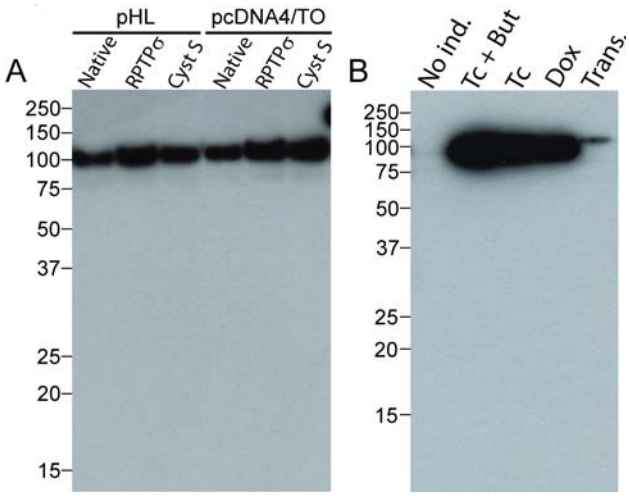

FIGURE 1

(A) Transient expression of Flt3$_{D1-D5}$ in HEK293T cells.

HEK293T cells, seeded in 6-well plates, were transiently transfected with pHL-Flt3$_{D1-D5}$ (lanes 1-3) and pcDNA4/TO-Flt3$_{D1-D5}$ (lanes 4-6): Five days post-transfection, the expression of Flt3$_{D1-D5}$-His in the medium was analyzed by Western blot immunodetection using anti-His-HRP. Lanes 1 and 4: native Flt3 secretion signal (Native), Lanes 2 and 5: chicken RPTPσ secretion signal (RPTPσ), Lanes 3 and 6: human cystatine S secretion signal (Cyst S).

(B) Inducible expression in stably tranfected HEK293S GnTI$^{-/-}$ cell lines.

A stable HEK293S GnTI$^{-/-}$ TetR Flt3$_{D1-D5}$ clone was analyzed for inducible expression. Cells were seeded in 6-well plates and induced for 5 days as indicated (Lane 1: serum-free medium (No ind.), lane 2: induction with 2 µg/mL tetracycline (Tc) and 5mM sodium butyrate (But), Lane 3: induction with 2 µg/mL tetracycline (Tc) alone, lane 4: induction with the tetracycline analogue doxycycline (Dox), 2 µg/mL). As a control a sample of transiently transfected HEK293T cells was loaded in lane 5. Immunodetection was performed as in (A).

In an effort to further improve our production of recombinant Flt3 (with the RPTPσ secretion signal), we decided to establish stable cell lines in HEK293S GnTI$^{-/-}$ TetR cells. The use of this HEK293 variant offers two major advantages. First, this cell line is devoid of N-acetylglucosaminyltransferase I (GnTI) activity and is thereby able to express target proteins with limited and homogeneous N-linked glycosylation that is very sensitive to EndoH-treatment (Chang *et al.*, 2007; Reeves *et al.*, 2002). Second, this cell line is stably transfected with the pcDNA6-TR

vector encoding the tetracycline-responsive repressor, which binds and blocks the promoter in the absence of tetracycline or an analogue such as doxycycline. This allows tetracycline-regulated expression (Yao *et al.*, 1998; Reeves *et al.*, 2002). Inducible expression systems allow growth of cell cultures under optimal conditions up until the moment of induction, which could have a beneficial effect on the protein yield as compared to constitutive expression.

Inducible HEK293S GnTI$^{-/-}$ cell lines were established as described and found to secrete $Flt3_{D1-D5}$ in high amounts upon treatment with tetracycline or doxycycline, when compared to transient expression experiments (**Fig. 1B**). The addition of sodium butyrate, a histone deacetylase inhibitor (Monneret, 2005), further boosted the expression levels. Using the same approach, a stable cell line that expressed an Flt3 ectodomain variant lacking the fifth Ig-domain ($Flt3_{D1-D4}$) was established. Our rationale for targeting this construct for structural studies was based on the existence of a fully active splice-variant of murine Flt3 lacking extracellular domain 5 (Lavagna *et al.*, 1995). Following large-scale expression experiments, the ectodomains were purified form the medium by a combination of metal-affinity chromatography, gel filtration and anion-exchange chromatography. The use of a Talon matrix employing immobilized Co^{2+} in the important first capture step via metal-affinity chromatography gave the best results in terms of overall yield and purity. We observed that Ni sepharose column matrices consistently suffered from depletion of Ni^{2+} upon passage of clarified culture medium containing the secreted target proteins. The final yields of purified $Flt3_{D1-D5}$ and $Flt3_{D1-D4}$ were ~ 2 mg per liter of medium. Flt3 ligand-receptor complexes were formed by the addition of recombinant FL produced in *E. coli* (Verstraete *et al.*, 2009) and were purified by gel-filtration chromatography (**Fig. 2**) for use in crystallization trials.

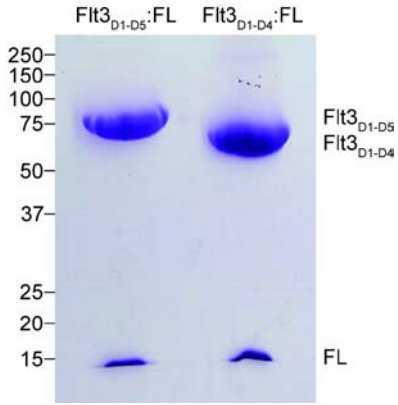

FIGURE 2. Coomassie-stained SDS-PAGE gel of the purified Flt3:FL complexes.

Lane 1: $Flt3_{D1-D5}$:FL and lane 2: $Flt3_{D1-D4}$:FL. The molecular weight of the processed His-tagged Flt3 ectodomains without glycosylation is calculated as 59.7 kDa for $Flt3_{D1-D5}$ (527 residues) and 48.0 kDa for $Flt3_{D1-D4}$ (423 residues). The band at 15 kDa represents denatured FL, which is a homodimer of 31.7 kDa under native conditions.

The strategy to develop inducible expression in stably transfected HEK293 GnTI$^{-/-}$ cells could be generally applicable for structural studies involving eukaryotic receptor ectodomains that are difficult to express. Moreover, the high costs associated with low-level transient expression - originating from large-scale plasmid-DNA preparation kits and kifunensine - can thereby be significantly reduced.

Crystallization of Flt3 complexes and data collection

Flt3$_{D1-D5}$:FL complex

Using commercially available sparse-matrix screens, a dozen of hits for the Flt3$_{D15}$:FL complex were identified. These conditions were characterized by the presence of medium molecular weight polyethylene glycols (PEG 3350 – PEG 8000) in the concentration range of 10 to 15 % and various salts (chlorides, citrates, phosphates, sulphates, acetates) at 0.1 – 0.2 M as co-precipitant. The pH-range varied from 6.5 to 8.5. Crystal optimization coupled to extensive screening via X-ray diffraction experiments identified 200 mM lithium citrate, 12 – 14% w/v PEG 3350 and 100 mM Tris/HCl/HCl pH 7.0 as the best condition. The crystals grew within one week and had a plate-like appearance with overall dimensions of 50 Å x 200 Å x 10 – 20 Å (**Fig. 3A,B**).

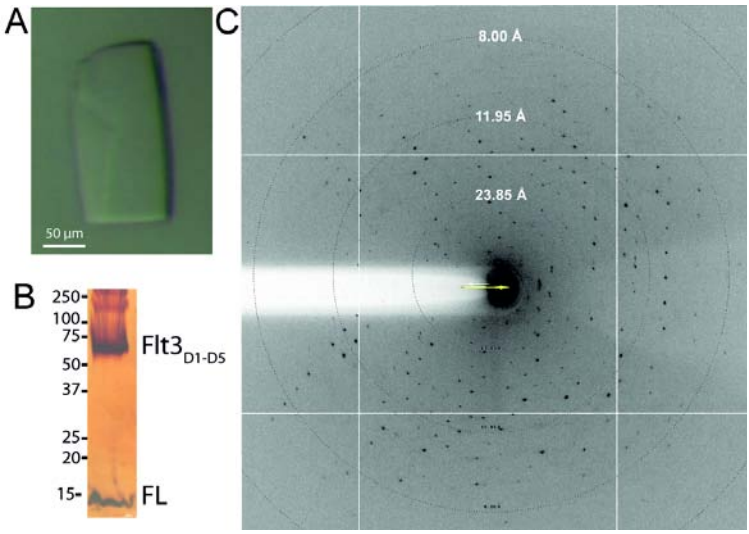

FIGURE 3. Crystallization and data collection for the Flt3$_{D1-D5}$:FL complex

(A) Plate-like crystals of the Flt3$_{D1-D5}$:FL complex.

(B) Silver-stained SDS-PAGE gel of dissolved crystals.

(C) X-ray diffraction image from the Flt3$_{D1-D5}$:FL crystal that led to a complete 7.8 Å dataset.

However, many crystals were not single or showed obvious physical defects. Flt3$_{D1-D5}$ crystals typically diffracted anisotropically to ~10 Å resolution using highly collimated synchrotron X-ray beams. Extensive efforts to improve crystal quality using a variety of approaches including

microseeding, crystallization additives, and crystal dehydration and annealing protocols (Heras and Martin, 2005), failed to provide consistent improvements in diffraction quality. Furthermore we were able to grow crystals of the complex after reduction of glycosylation using EndoH, albeit without obtaining the desired improvement in diffraction quality. Nonetheless we found that optimization of the cryoprotection protocol based on incremental adjustments of the cryoprotecting solution to a final 20% (v/v) glycerol consistently gave better results. We therefore embarked on a large-scale screening of crystals, which resulted in a complete dataset to 7.8 Å resolution (**Fig. 3C, Table I**).

$Flt3_{D1-D4}$:FL complex

Initial crystallization experiments identified numerous hits for the $Flt3_{D1-D4}$:FL complex. By analogy to the crystallization condition consensus for the $Flt3_{D1-D5}$:FL complex, these conditions were based on a medium molecular PEG, 0.1 – 0.2 M salt at pH 6-8.5. Based on crystal morphology arguments (overall crystal size, crystal thickness in the third dimension, singleness), a dozen conditions were selected for optimization. Diffraction experiments indicated 11-13 % w/v PEG 4000, 100 mM $MgCl_2$, 50 mM MES pH 6.0 as the most promising condition. Rod-like crystals appeared after 2-3 days and reached their final size within 10 days. They grew as single rods measuring 0.3 x 0.1 x 0.02-0.05 mm^3 (**Fig. 4A,B**) or as clusters that could easily be separated by manual intervention.

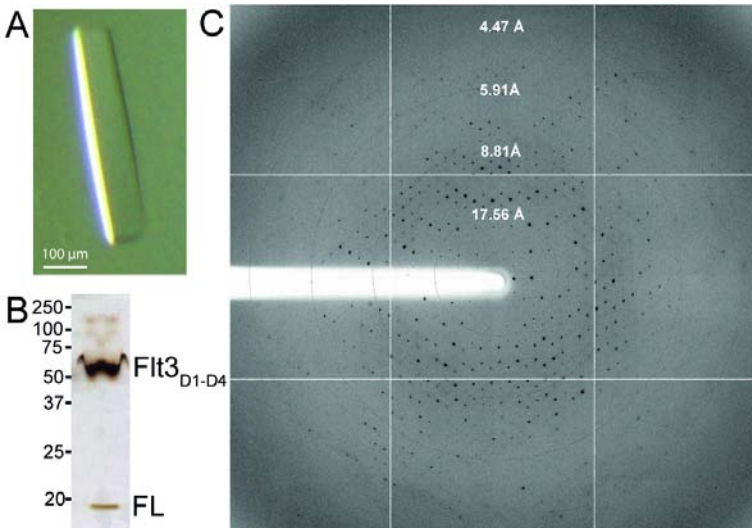

FIGURE 4. Crystallization and data collection for the $Flt3_{D1-D4}$:FL complex.

(A) Rod-like crystals of the $Flt3_{D1-D4}$:FL complex.

(B) Silver-stained SDS-PAGE gel of dissolved crystals.

(C) X-ray diffraction image from the $Flt3_{D1-D4}$:FL crystal that led to a complete 4.3 Å dataset

$Flt3_{D1-D4}$-FL crystals generally diffracted to Bragg spacings of 5 to 4.5 Å. In contrast to the broad crystallization propensity of the $GlcNac_2Man_5$-glycosylated complex, we were not able to obtain crystals of the complex after treatment with EndoH, consistent with the notion that the extent of glycosylation is often not a strong predictor of crystallization behaviour (Mesters and Hilgendfeld, 2007). A recurring phenomenon we observed during the course of crystal screening and characterization was often the dramatic variation in diffraction quality even within the same crystal. Thus, we were unable to successfully employ data collection strategies based on collecting partial datasets by systematically irradiating different parts of the crystal, followed by merging of the resulting data failed to deliver data of good quality. Cryoprotection of $Flt3_{D1-D4}$:FL crystals with 20% PEG 400 combined with a stochastic approach to crystal screening resulted in final dataset to 4.3 Å (**Fig. 4C, Table I**).

TABLE I. X-ray data collection statistics

	$Flt3_{D1-D4}$:FL	$Flt3_{D1-D5}$:FL
DATA COLLECTION		
Source	ESRF ID23-1	ESRF ID23-1
Wavelength (Å)	0.9714	1.0762
Detector	ADSC-Q315R	ADSC-Q315R
Resolution (Å)	40.00 - 4.30 (4.45 - 4.30)	40.00 - 7.80 (8.00 - 7.80)
Space group	$P2_1$	$P2_1$
Unit cell parameters	a=103.89 b=146.26 c=105.95 α=γ=90°, β=109.7°	a=124.74 b=153.51 c=133.85 α=γ=90°, β=94.6°
Wilson B ($Å^2$)	135	436
Unique reflections	20184 (1942)	5575 (374)
Redundancy	3.8 (3.8)	3.1 (3.0)
Completeness (%)	98.8 (98.9)	95.3 (90.8)
R_{meas} (%)[a]	10.8 (75.9)	12.5 (75.9)
Average $I/\sigma(I)$	12.04 (2.08)	8.8 (1.8)
Solvent content (%)[b], Matthews Coefficient ($Å^3$/Da)	59, 3.0	71, 4.2
No. complexes in asu	2	2

Values in parentheses correspond to the highest resolution shell as indicated.
[a] $R_{meas} = \sum_h \sqrt{n_h/(n_h-1)} \sum_h\sum_i |I(h,i)-\langle I(h)\rangle| / \sum_h\sum_i I(h,i)$, where n_h is the multiplicity, $I(h,i)$ is the intensity of the ith measurement of reflection h, and $\langle I(h)\rangle$ is the average value over multiple measurements. [b] Estimates of solvent content and Matthews coefficients were calculated via www.ruppweb.org/mattprob/ using the theoretical weight of the complexes without taking into account N-linked glycosylation (Matthews, 1968; Kantardjieff and Rupp, 2003).

Structure determination of the $Flt3_{D1-D4}$:FL complex

Due to the superior diffraction quality of $Flt3_{D1-D4}$:FL crystals we initially focused our efforts on the structure determination of the $Flt3_{D1-D4}$:FL complex. Phasing information for the crystal structure of $Flt3_{D1-D4}$:FL was initially determined at 4.3 Å resolution by maximum-likelihood

molecular replacement as implemented in PHASER (McCoy *et al.*, 2007), using the structure of human FL (PDB entry 1ETE) (Savvides *et al.*, 2000) and a homology model for $Flt3_{D3}$ based on the structure of human KIT_{D3} (PDB entry 2E9W) (Yuzawa *et al.*, 2007). This revealed the presence of two $Flt3_{D1-D4}$:FL complexes in the crystal asymmetric unit (asu) that packed against each other via a broad interface between the two FL ligands (**Fig. 5A**). This packing arrangement was consistent with all major peaks in the self-rotation function as calculated with MOLREP (Vagin and Teplyakov, 2010). Furthermore, the corresponding electron density map revealed a clear protein-solvent boundary for the two $Flt3_{D1-D4}$:FL complexes in the asu but was not of sufficient quality to allow model building. In our efforts to obtain additional experimental phase information we were confronted with the prohibitively poor diffracting capacity of $Flt3_{D1-D4}$:FL crystals derivatized with heavy-atoms or selenomethionine labelled $Flt3_{D1-D4}$.

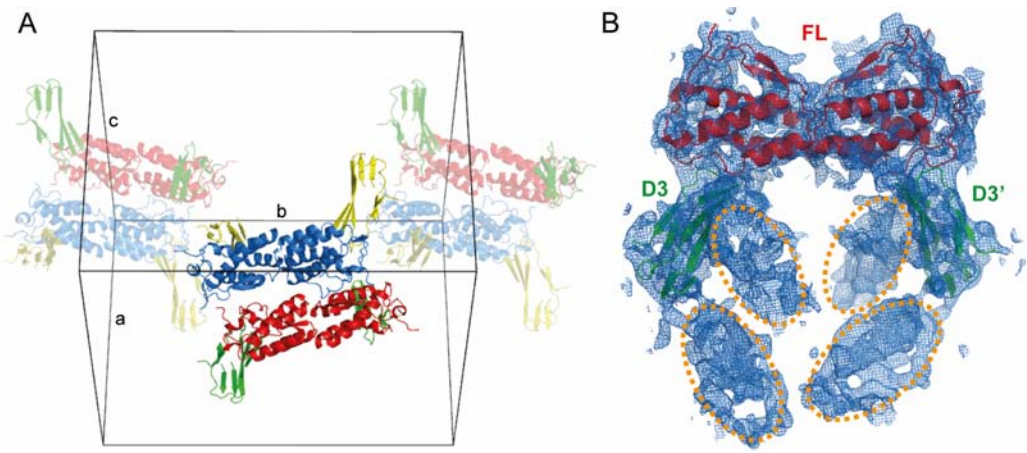

FIGURE 5

(A) Partial molecular replacement solution for the $Flt3_{D1-D4}$:FL complex showing the presence of two complexes in the crystal asymmetric unit. Two neighbouring symmetry mates along the b-axis are shown with appropriate depth cueing. FL (red and blue) and the MR-model for $Flt3_{D3}$ (green and yellow) are shown in ribbon representation.

(B) Density-modified electron density map (contoured at 1σ) showing clear and complete electron density for unmodelled Flt3 extracellular domains (dashed ellipses). The map (2mFo - DFc-like) is the result of phase-improvement protocols implemented in the program PARROT based on the partial model obtained by MR, using an NCS masking radius of 15 Å and 20 cycles of NCS-averaging and solvent flattening. FL (red) and the MR-model for $Flt3_{D3}$ (green) are shown in ribbon representation.

We therefore sought to improve phase quality via density modification approaches exploiting the presence of improper 4-fold non-crystallographic symmetry (NCS) and the high solvent content of the crystals (59%). Such approaches have been sparsely applied to structure determinations via molecular replacement due to possible limitations and phase bias imposed by the unimodal phase distribution inherent to calculated phases from protein models. However, when carefully applied, density modification based on initial phases calculated from partial molecular replacement models

can be very effective for both high and low resolution analyses (Keller *et al.*, 2006; Huyton *et al.*, 2007). Indeed, density modification protocols as implemented in the program PARROT (Cowtan, 2010) starting with Hendrickson-Lattman coefficients for the phase probability distribution calculated in PHASER based on our rigid-body refined molecular replacement solution (covering only about 40% of the scattering mass in the asymmetric unit), revealed contiguous density for several unmodelled Flt3 domains (**Fig. 5B**) including direct evidence for N-linked glycans. We note that extending the NCS-mask radius parameter in PARROT from its default value of 6 to 15-20 was crucial for maximizing the quality of the electron density maps and coverage of the asymmetric unit content. We subsequently used the dramatically improved electron density maps to select the correct MR solution for a homology model of $Flt3_{D4}$ based on KIT_{D4}, and to manually place a model for $Flt3_{D2}$ based on KIT_{D5}. Model (re)building and refinement, including modelling of the elusive $Flt3_{D1}$ into electron density, are under way and will be reported elsewhere. The crystallized $Flt3_{D1-D4}$:FL and $Flt3_{D1-D5}$:FL complexes undoubtedly constitute a major milestone towards elucidating the overall architecture and organization of the extracellular Flt3:FL assembly, as well as towards gaining insights into the main features of the interaction epitope. We are currently working to develop shorter receptor constructs in light of the structural insights obtained from the $Flt3_{D1-D4}$:FL and $Flt3_{D1-D5}$:FL complexes in an effort to obtain crystals that will allow a detailed dissection of the receptor–ligand interface to high resolution.

ACKNOWLEDGMENTS

KV, JE, and KVC have been supported by research fellowships from the Research Foundation Flanders, Belgium (FWO), and BR was supported by the IWT-Flanders, Belgium. SNS is supported by the FWO (Projects 3G064307 and G059710) and Ghent University (BOF instrument). We would like to thank Isabelle Vandenberghe (L-Probe, Unit for Mass Spectrometry and Proteomics) for N-terminal sequence analysis. We thank the European Synchrotron Radiation Facility (ESRF) and the Swiss Light Source (SLS) for synchrotron beam time allocation, and the staff of beamlines ID23-1 (ESRF), and X06SA/X06DA (SLS) for technical support. Access to these synchrotron facilities is supported by the European Commission under the 7th Framework Programme: Research Infrastructures, Grant Agreement Number 226716.

AUTHORSHIP

KVC, PV, BL and GH provided assistance in setting up a mammalian expression facility at the L-ProBE laboratory. KV designed and created Flt3 expression constructs, performed expression tests and Western blot analyses. KV and BR established stably transfected cell lines, performed large-scale expression experiments and purified recombinant Flt3 ectodomains. KV purified and crystallized Flt3:FL complexes. KV manipulated and cyroprotected the crystals. KV, JE, and SNS collected and analyzed data. KV and SNS performed crystallographic analysis of the data. KV and SNS wrote the manuscript. SNS directed the study.

Chapter **4**

Structural Insights into the Extracellular Assembly of the Hematopoietic FLT3 Signaling Complex

Kenneth Verstraete[1], Gonzalez Vandriessche[2], Mariska Januar[1], Jonathan Elegheert[1], Alexander Shkumatov[3], Ambroise Desfosses[4], Kathleen Van Craenenbroeck[5], Dmitri Svergun[3], Irina Gutsche[4], Bjorn Vergauwen[1], Savvas N. Savvides[1]

[1]Unit for Structural Biology, Laboratory for Protein Biochemistry and Biomolecular Engineering (L-ProBE), Ghent University, Belgium

[2]Unit for Mass Spectrometry and Proteomics, Laboratory for Protein Biochemistry and Biomolecular Engineering (L-ProBE), Ghent University, Belgium

[3]Biological Small Angle Scattering Group, EMBL, Hamburg, Germany

[4]Unit for Virus Host-Cell Interactions (UVHCI), Grenoble, France

[5]Laboratory of Eukaryotic Gene Expression and Signal Transduction (LEGEST), Ghent University, Belgium

Redrafted from: Blood (2011), *article in press*

ABSTRACT

The class-III receptor tyrosine kinase (RTKIII) Flt3 and its cytokine ligand (FL) play central roles in hematopoiesis and the immune system, by establishing signaling cascades crucial for the development and homeostasis of hematopoietic progenitors and antigen-presenting dendritic cells. However, Flt3 is also one of the most frequently mutated receptors in hematological malignancies and is currently a major prognostic factor and clinical target for acute myeloid leukemia (AML). Here, we report the structural basis for the Flt3 ligand-receptor complex and unveil an unanticipated extracellular assembly unlike any other RTKIII/V complex characterized to date. FL induces dimerization of Flt3 via a remarkably compact binding epitope localized at the tip of extracellular domain 3 of Flt3, and invokes a ternary complex devoid of homotypic receptor interactions. Comparisons of Flt3 with homologous receptors and available mutagenesis data for FL have allowed us to rationalize the unique features of the Flt3 extracellular assembly. Furthermore, thermodynamic dissection of complex formation points to a pronounced enthalpically-driven binding event coupled to an entropic penalty. Together, our data suggest that the high-affinity Flt3-FL complex is driven in part by a single preformed binding epitope on FL reminiscent of a 'lock-and-key' binding mode, thereby setting the stage for antagonist design.

INTRODUCTION

Hematopoiesis is a finely regulated process during which diverse cell types originating from a limited and self-renewing population of hematopoietic stem cells (HSC), are stimulated to proliferate and differentiate to create the cellular repertoire that sustains the mammalian hematopoietic and immune systems (Metcalf, 2008).

The Fms-like tyrosine kinase receptor 3 (Flt3) is the most recent addition to the diverse family of hematopoietic receptors. Flt3 is activated on HSC and early myeloid and lymphoid progenitors by its cognate ligand (FL), to initiate downstream signaling via the PI3K/AKT and the RAS/RAF/MEK/ERK pathways (Stirewalt and Radich, 2003; Parcells *et al.*, 2006). Consistent with the narrow expression profile of Flt3 in the bone marrow environment, signaling via the Flt3 ligand/receptor complex primarily impacts early hematopoiesis, particularly the proliferation and development of HSC and B-cell progenitors (Stirewalt and Radich, 2003; Kikushige *et al.*, 2008). In recent years Flt3 and FL emerged as potent regulators of dendritic cell (DC) development and homeostasis (Onai *et al.*, 2007; Waskow *et al.*, 2008; Liu *et al.*, 2009), and DC-mediated natural killer cell activation (Eidenschenk *et al.*, 2010), thereby gaining an important role at the interface of innate and acquired immunity and in cancer immunotherapy (Dong *et al.*, 2002; Wu and Liu, 2007). Notably, Flt3/FL-driven DC generation yields both classical- and plasmacytoid DC from bone-marrow progenitors regardless of myeloid or lymphoid commitment, a property that is currently unmatched by any other receptor/cytokine system relevant for DC physiology (Liu and Nussenzweig, 2010; Schmid *et al.*, 2010).

Flt3 is a class III receptor tyrosine kinase (RTKIII) together with the prototypic platelet-derived growth factor receptors (PDGFRα/β), colony-stimulating factor 1 receptor (CSF-1R), and KIT (Grassot *et al.*, 2006). Thus, Flt3 has been predicted to display a modular structure featuring an extracellular segment with 5 immunoglobulin (Ig)-like domains (residues 27-543), a single transmembrane (TM) helix (residues 544-563), a cytoplasmic juxtamembrane (JM) domain (residues 572-603) and a split intracellular kinase module (residues 604-958). The RTKIII family is closely related to the RTKV family of vascular endothelial growth factor receptors (VEGF-Rs), which have 7 extracellular Ig-like domains. The hallmark of RTKIII/V signaling lies in the activation of the extracellular receptor segments upon binding of the cognate cytokines, followed by intermolecular autophosphorylation and activation of the intracellular kinase domains (Lemmon and Schlessinger, 2010).

Besides the clear role of Flt3 signaling in hematopoiesis and immune system development, overexpression of wild type or oncogenic forms of Flt3 have been implicated in a number of hematopoietic malignancies (Stirewalt and Radich, 2003; Sanz *et al.*, 2009), and inflammatory disorders (Dehlin *et al.*, 2008). In particular, internal tandem duplication (ITD) in the JM-region or point mutations in the kinase activation loop occur in 35% of patients with acute myeloid leukemia (AML) resulting in constitutive activation of the receptor and uncontrolled proliferation of

hematopoietic precursors (Kiyoi *et al.*, 2002; Stirewalt and Radich, 2003; Parcells *et al.*, 2006; Reindl *et al.*, 2006; Fröhling *et al.*, 2007). Such mutational fingerprints have established Flt3 as the predominant prognostic factor in AML cases (Eklund, 2010), and have rationalized the targeting of Flt3 in a clinical setting (Stirewalt and Radich, 2003; Parcells *et al.*, 2006; Kindler *et al.*, 2010).

Although the cellular and physiological role of the Flt3 ligand-receptor interaction has been featured prominently in the biomedical literature over the last two decades, the Flt3 signaling complex has remained uncharacterized at the molecular and structural level. Such insights are the missing link to the structural and functional diversity of RTKIII/V extracellular complexes, and would help provide a nearly complete picture of the entire Flt3 signaling complex given the available structure of the Flt3 intracellular kinase domains (Griffith *et al.*, 2004). A recent flurry of studies of RTKIII/V extracellular complexes led to a structural paradigm for RTKIII/V activation, whereby the receptors bind via their N-terminal Ig-like domains to the activating dimeric cytokine and concomitantly make homotypic contacts between their membrane-proximal domains (Liu *et al.*, 2007; Ruch *et al.*, 2007; Yuzawa *et al.*, 2007; Chen *et al.*, 2008; Yang *et al.*, 2008; Yang *et al.*, 2010; Shim *et al.*, 2010; Leppänen *et al.*, 2010). A universal feature of all characterized RTKIII/V complexes thus far is that the cytokine-binding epitope is distributed equally between extracellular domains 2 and 3 covering ~2000 $Å^2$ of surface area, and that homotypic receptor-receptor interactions are mediated by well-conserved residues in the membrane-proximal domains (D4 in RTKIII and D7 in RTKV). Nonetheless, Flt3 appears to be an outlier among RTKIII/V receptors due to several unique features in its extracellular segment (Lyman *et al.*, 1993; Maroc *et al.*, 1993), thus raising the question whether the current structural paradigm could be extrapolated to Flt3. Notably, Flt3 exhibits intragenic homology relating extracellular domains 1 and 4, and domains 2 and 5, indicative of an ancient internal duplication event during evolution (**Appendix B**). Furthermore, Flt3 contains 12 additional cysteines that are not present in any of the homologous receptors, and has a unique N-terminal sequence of 50 amino acids preceding Ig-like domain 1 (**Appendix A**). Interestingly, a fully functional splice variant of murine Flt3 lacks extracellular domain 5 entirely, indicating that the domain most proximal to the cell-membrane is not critical for receptor activation (Lavagna *et al.*, 1995) contrary to other RTKIII/V receptors (Broudy *et al.*, 2001; Yang *et al.*, 2008; Yang *et al.*, 2010).

Here, we provide the structural basis of extracellular complex formation between Flt3 and its cognate cytokine. Our studies establish the uniqueness of Flt3 within the RTKIII/V family and provide a reference platform for further structure-function studies and antagonist design.

METHODS

Protein Expression and Isolation of Flt3:FL complexes

To support structural and biophysical studies of human Flt3 ectodomain complexes we designed a series of constructs for recombinant human Flt3 ectodomains ($Flt3_{D1}$ (residues 27-161), $Flt3_{D1-D2}$ (residues 27-244), $Flt3_{D1-D3}$ (residues 27-346), $Flt3_{D1-D4}$ (residues 27-434) and $Flt3_{D1-D5}$ (residues 27-541)), based on intron/exon boundaries and sequence alignments with homologous receptors (**Appendix A**). Faced with prohibitively poor protein yields (100-200 μg per liter of medium) we established tetracycline-inducible cell lines in HEK293S cells deficient in N-acetylglucosaminyl-transferase I (HEK293S $GnTI^{-/-}$) (Reeves *et al.*, 2002) that could secrete the target ectodomain variants with homogeneous glycosylation ($GlcNac_2Man_5$) to mg amounts as described in Verstraete *et al.* (2011). The yields and stability of $Flt3_{D1-D3}$ and $Flt3_{D1-D2}$ were much lower than for all other constructs. Ternary Flt3:FL complexes were prepared for structural studies by mixing purified Flt3 ectodomains with a molar excess of recombinant *E. coli*-derived human FL (Verstraete *et al.*, 2009) followed by preparative size-exclusion chromatography on a Superdex 200 column equilibrated with 150 mM NaCl, 10 mM HEPES, pH 7.2. The column was calibrated using thyroglobulin (669 kDa), ferritin (440 kDa), aldolase (158 kDa), conalbumin (75 kDa), ovalbumin (43 kDa), carbonic anhydrase (29 kDa) and ribonuclease (13.7 kDa) as molecular weight standards.

Isothermal Titration Calorimetry

Experiments were carried out using a VP-ITC MicroCalorimeter (MicroCal, MA) at 37° C, and data were analyzed using the Origin ITC analysis software package supplied by MicroCal. Purified recombinant Flt3 ectodomain constructs and FL were dialyzed overnight against 20 mM Hepes pH 7.4, 150 mM NaCl at 4° C. Protein concentrations were measured spectrophotometrically at 280 nm using calculated theoretical extinction coefficients and all solutions were extensively degassed prior to use. Titrations were always preceded by an initial injection of 3 μL, and were carried out using 10 μL injections applied 300 s apart. The sample was stirred at a speed of 400 rpm throughout. The thermal titration data were fit to the "one binding site model", and apparent molar reaction enthalpy ($\Delta H°$), apparent entropy ($\Delta S°$), dissociation constant (K_d) and stoichiometry of binding (N) were determined. Several titrations were performed to evaluate reproducibility.

Mapping of disulfide bridges and glycosylation sites by mass spectrometry

Gel slices containing EndoH-digested recombinant $Flt3_{D1-D5}$ obtained from Coomassie-stained polyacrylamide gels were digested with trypsin (Promega) as previously described (Vanrobaeys *et al.*, 2003). After digestion overnight at 37° C, the digestion mixture were dried and redissolved in 20 ml 0.1% formic acid. One microliter of the digestion mixture was mixed with an equal volume of 3 mg/ml α-cyano hydroxycinnamic acid (Sigma) in 50% acetronitrile/0.1% TFA and was

subsequently subjeted to mass spectrometric analyses on a 4800 plus TOF/TOF analyzer (Applied Biosystems).

About 75 pmoles of purified recombinant $Flt3_{D1-D5}$ were dissolved in 20 mM Tris-HCl, pH 8.0, and digested with trypsin (Promega), Glu-C and Asp-N endoproteinases (Sigma) at E/S = 1/35. After incubation at 37°C overnight, 1 mL of the digestion mixture were mixed with 5 ml of 3 mg/ml α-cyano hydroxycinnamic acid (Sigma) in 50% acetronitrile / 0.1% TFA prior to mass spectrometric analyses. The remaining volume of the digestion mixture was applied on a Spheri-5 PTC-C18 column (220 x 2.1 mm, Higgins Analytical) at a flow rate of 100 ml/min. Reversed phase chromatography of peptide mixture was performed on an Ettan LC (Amersham Biosciences) with on-line 96-well plate Frac-950 fractionator set at 20 mL/min. One microliter of the collected fractions was mixed with an equal volume of 3 mg/ml α-cyano hydroxycinnamic acid.

A table with the thereotical and measured masses of analyzed peptides is provided in **Appendix C**.

Crystallography of Flt3:FL complexes

The preparation and cryoprotection of $Flt3_{D1-D4}$:FL and $Flt3_{D1-D5}$:FL crystals is described in Verstraete *et al.*, 2011. Diffraction experiments were conducted under cryogenic conditions (100 K) on the X06SA (PXI) and X06DA (PXIII) beamlines at the Swiss Light Source (Paul Scherrer Institute, Villigen, Switzerland) and the ID23-1 beamline at the ESRF (Grenoble, France). All data were integrated and scaled using the XDS suite (Kabsch, 2010).

The structure of $Flt3_{D1-D4}$:FL was determined by maximum-likelihood molecular replacement (MR) as implemented in the program suite PHASER (McCoy *et al.*, 2007), using the structure of human FL (PDB entry 1ETE, Savvides *et al.*, 2000) and a homology model for $Flt3_{D3}$ based on the structure of human KIT_{D3} (PDB entry 2E9W, Yuzawa *et al.*, 2007). This showed the presence of two $Flt3_{D1-D4}$:FL complexes in the crystal asymmetric unit packing against each other via a broad interface between the two FL ligands (**Appendix D**). Electron density modification exploiting the presence of improper 4-fold non-crystallographic symmetry (NCS) and the high solvent content of the crystals (59%) via the program PARROT (Cowtan, 2010) revealed contiguous density for domains $Flt3_{D2}$ and $Flt3_{D4}$ (**Fig. 1A**), which allowed us to select the correct MR solution for a homology model of $Flt3_{D4}$ based on KIT_{D4}, and to manually place a model for $Flt3_{D2}$ based on KIT_{D5}. In the later stages of model building and refinement, we were able to model the core structure of $Flt3_{D1}$ for one of two receptor complexes starting with a homology model derived from $Flt3_{D4}$. Model (re)building was carried out manually in electron density maps after density modification, using the program COOT (Emsley *et al.*, 2010). Chain tracing was facilitated by mapping of the disulfide bridges and glycosylation sites in Flt3 by mass-spectrometry.

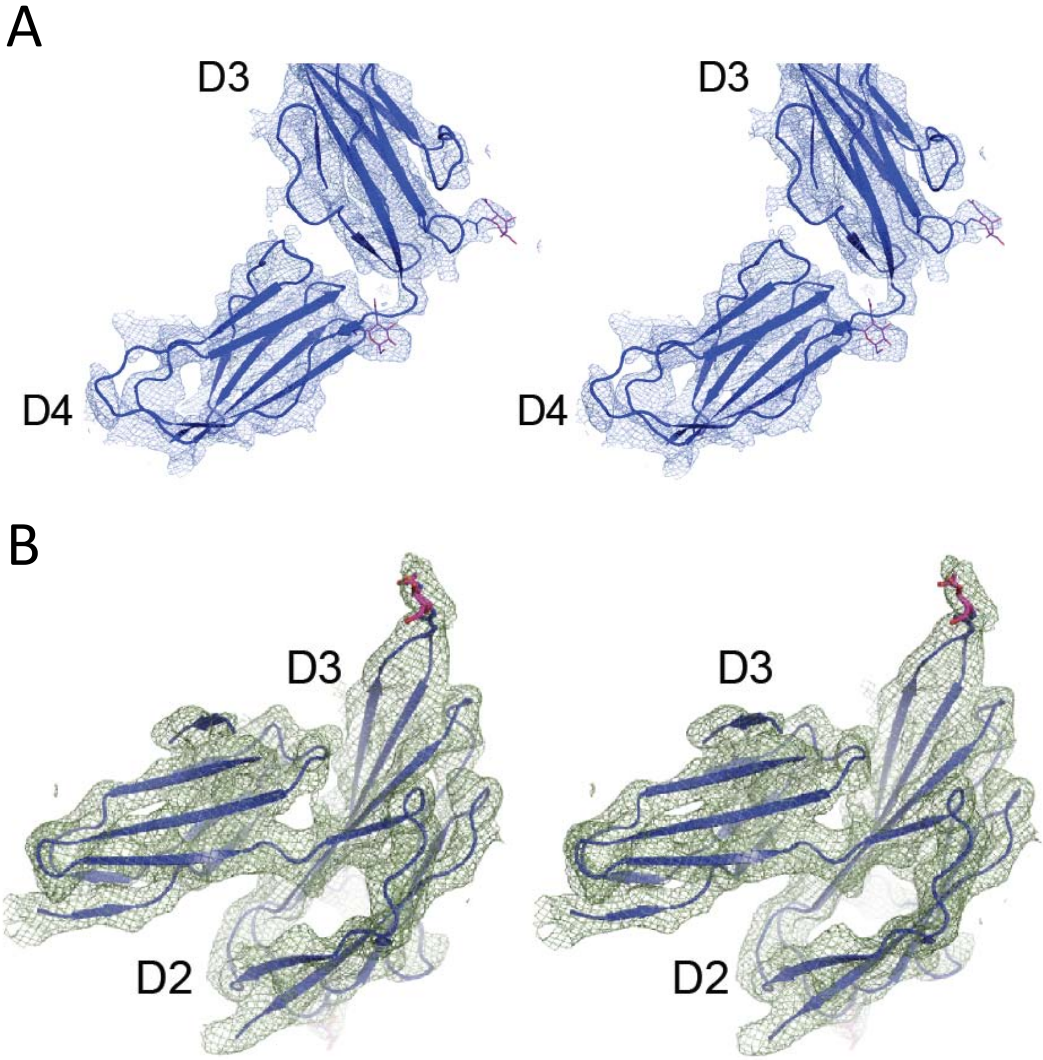

FIGURE 1. Quality of the electron density maps

(A) Unbiased electron density for $Flt3_{D4}$.

The electron density is contoured at 1σ and was obtained after implementation of phase improvement protocols based on a partial model of the complex consisting of only FL and $Flt3_{D3}$.The final model for domains 3 and 4 in one of the receptor chains in the $Flt3_{D1-D4}$-FL complex structure is shown in ribbon representation. N-linked glycans are shown in stick representation (magenta). This electron density map (2mFo - DFc-like) was obtained by applying NCS-averaging and solvent flattening protocols as implemented in PARROT, and proved to be crucial early in the structure determination process providing the complete electron density trace for $Flt3_{D4}$, including clear electron density for N-linked glycans.

(B) Quality of the electron density map to 4.3 Å resolution.

Stereo diagram illustrating the quality of the final 2mFo-DFc electron density map to 4.3 Å resolution (contoured at 1σ) for the $Flt3_{D1-D4}$:FL complex. The figure is centered on the $Flt3_{D2-D3}$ interface and junction, with the final model for $Flt3_{D2}$ (left) and $Flt3_{D3}$ (right) displayed in ribbon representation (blue). The N-linked NAG glycan residue modeled at Asn306 is shown in sticks (magenta).

Crystallographic refinement was carried out in PHENIX (Adams *et al.*, 2010) and, at at later stages, in autoBUSTER 2.8.0 (Blanc *et al.*, 2004). During refinement, tight RMSD-based NCS-restraints (4-fold non-proper NCS) were imposed. Several loop regions that did not obey the NCS were pruned out from the NCS-selection. Torsion angles of FL protomers were restrained to chain A (residues 3 - 132) of the previously determined 2.2 Å resolution structure of human FL (pdb 1ETE, Savvides *et al.*, 2000). Residues 7 – 13, which comprise the N-terminal loop that forms the major interaction site with $Flt3_{D3}$, were excluded from the FL reference model. Hydrogens bonding restraints for conserved secondary structure elements in the different Ig-like domains were manually defined using the ResDe tool (Hintze and Johnson, 2010), and subsequently converted to Buster distance restraints. During refinement, a low weight on the X-ray term (w = 24 in autoBuster) and a single B-factor per residue were applied. TLS parameterization, in which each domain was defined as a single TLS group, resulted in worse refinement statistics. The sterochemistry of the final model was validated using MolProbity (Chen *et al.*, 2010). A section of the final 2mFo-DFc electron density map is shown in **Fig. 1B**.

The structure of $Flt3_{D1-D5}$: FL was determined to 7.8 Å resolution by MR protocols implemented in PHASER (McCoy *et al.*, 2007), using the structure of the $Flt3_{D2-D3}$:FL subcomplex as determined in the $Flt3_{D1-D4}$:FL complex. The remaining domains were placed via additional rounds of molecular replacement and manual placement in electron density maps after density modification. Crystals of the $Flt3_{D1-D5}$:FL complex contained two complexes in the asymmetric unit interacting with each other in a fashion analogous to what we observed in the $Flt3_{D1-D5}$:FL complex (**Appendix D**). Due to the low resolution of the analysis we only applied rigid-body refinement (in autoBUSTER) using the FL protomer (residues 3-132), $Flt3_{D1}$ (residues 79 - 161), $Flt3_{D2-D3}$ (residues 167-345), $Flt3_{D4}$ (residues 348-434) and $Flt3_{D5}$ (residues 437-529) as rigid bodies. A single B-factor was used per domain.

Crystallographic data deposition

Coordinates and structure factors for the $Flt3_{D1-D4}$:FL and $Flt3_{D1-D5}$:FL complexes have been deposited in the Protein Data Bank (www.rcsb.org) and are accessible through accession numbers 3QS7 and 3QS9, respectively.

Small-angle X-ray Scattering

Small-angle X-ray scattering data were collected at beamline X33 at DESY, Hamburg. The measurements were carried out at 283 K, within a momentum transfer range of 0.01 $Å^{-1} < s < 0.45$ $Å^{-1}$ where $s = 4\pi\sin(\theta)/\lambda$ and 2θ is the scattering angle. All samples were measured at several solute concentrations ranging from 0.5 to 6 mg/ml in 50 mM $NaPO_4$ pH 7.40, 100 mM NaCl, with intermittent buffer solution (50 mM $NaPO_4$, pH 7.40, 100 mM NaCl). A standard data collection time of 2 min was used for all samples split into four 30-second time frames to assess and remove

effects from radiation damage to the samples. Time frames were processed to yield radially-averaged curves of normalized intensity versus the momentum transfer. Time frames are combined, excluding those that are affected by aggregation induced by radiation damage, to give the average scattering curve for each measurement. The data were processed using standard procedures, corrected for buffer contribution, and extrapolated to infinite dilution using the program PRIMUS (Konarev *et al.*, 2003). The radius of gyration R_g and forward scattering $I(0)$, the maximum particle dimension D_{max} and the distance distribution function $p(r)$ were evaluated using the program GNOM (Svergun, 1992). The molecular mass was calculated by comparison with a reference bovine serum albumin (BSA) sample. Constrained rigid-body refinement was carried out in SASREF7 (Petoukhov and Svergun, 2005) using a number of modeling scenarios. The best model was obtained in the case where a core structure of $Flt3_{D2-D4}$:FL was fixed and $Flt3_{D1}$ and $Flt3_{D5}$ allowed to move without imposing any symmetry constraints. The scattering patterns from the high-resolution models were calculated using the program CRYSOL (Svergun *et al.*, 1995).

Electron microscopy

For preparation of negatively stained $Flt3_{D1-D5}$:FL complex, purified complex at ~0.05 mg/mL in PBS buffer was applied to the clear side of carbon on a carbon-mica interface and stained with 2 % (w/v) uranyl acetate. Images were recorded under low-dose conditions with a JEOL 1200 EX II microscope at 100 kV and at nominal 40000x magnification. Selected negatives were then digitized on a Zeiss scanner (Photoscan TD) at a step size of 14 micrometer giving a pixel size of 3.5 Å at the specimen level. Using the boxer routine of the EMAN image processing software (Ludtke *et al.*, 1999), 25134 subframes of 96x96 pixels containing individual $Flt3_{D1-D5}$:FL complex particles were selected interactively, CTF-corrected with CTFFIND3 (Mindell and Grigorieff, 2003) and Bsoft (Heymann *et al.*, 2008), and low-path-filtered at 15 Å with Imagic-5. Subsequent data processing was performed with Imagic-5 software package (van Heel *et al.*, 1996). The translationally centered data set was subjected to multivariate statistical analysis and classification that provided a set of references for multi-reference alignment.

RESULTS

Isolation of recombinant Flt3 ectodomain complexes and thermodynamic binding profile of complex formation

High-affinity complexes of purified glycosylated $Flt3_{D1-D5}$, $Flt3_{D1-D4}$, and $Flt3_{D1-D3}$ with recombinant human FL produced in *E. coli* (Verstraete *et al.*, 2009), consistent with bivalent binding of FL to each of the ectodomain constructs, were initially established by analytical size-exclusion chromatography (SEC). Subsequent batches for structural studies were obtained via preparative SEC in the presence of excess molar amounts of purified FL (**Fig. 2A-C**). The elution profiles for all three ectodomain complexes were indicative of ligand-induced receptor dimerization. In constrast to $Flt3_{D1-D5}$ and $Flt3_{D1-D4}$, preparations of recombinant $Flt3_{D1-D3}$ consistently contained a significant portion of receptor that was incapable of binding the ligand even in the presence of excess molar amounts of FL (**Fig. 2A-C**). Conversely, excess molar amounts of $Flt3_{D1-D3}$ did result in a complete titration of FL towards complex formation. On the other hand, we were not able to observe complex formation for $Flt3_{D1}$ and $Flt3_{D1-D2}$ via SEC providing direct evidence that these ectodomain constructs do not carry a high-affinity ligand binding site.

Characterization of Flt3 extracellular complexes by isothermal titration calorimetry (ITC) led to a number of consensus observations **(Fig. 2D-F)**. Firstly, all three characterized complexes exhibit high-affinity binding characterized by a strongly exothermic enthalpic term coupled to an entropic penalty. Secondly, FL exhibits bivalent binding to both $Flt3_{D1-D5}$ and $Flt3_{D1-D4}$ (N=0.5, 2 molecules of Flt3 to 1 molecule FL). We note that the observed stoichiometry for the FL: $Flt3_{D1-D3}$ interaction (N=0.12) is likely due to the inability of recombinant $Flt3_{D1-D3}$ to engage completely in a ternary complex in the presence of a molar excess of FL (**Fig. 2C**). Nonetheless, the ITC data clearly show that $Flt3_{D1-D3}$ is capable of a high-affinity ternary complex just like the larger ectodomain constructs, and that only about 25% of recombinant $Flt3_{D1-D3}$ may adopt an active conformation. Notably, the sequential exclusion of the membrane-proximal domains $Flt3_{D4}$ and $Flt3_{D5}$ leads to a modest decrease in affinity (K_d [$Flt3_{D1-D5}$:FL] = 8.7 nM ; K_d [$Flt3_{D1-D4}$:FL] = 40 nM ; K_d [$Flt3_{D1-D3}$:FL] = 74.6 nM) while the thermodynamic profiles remain similar (**Fig. 2D-F**). Taken together, our data suggest that the membrane-proximal module $Flt3_{D4-D5}$ does not contribute significantly to the overall stability of the complex.

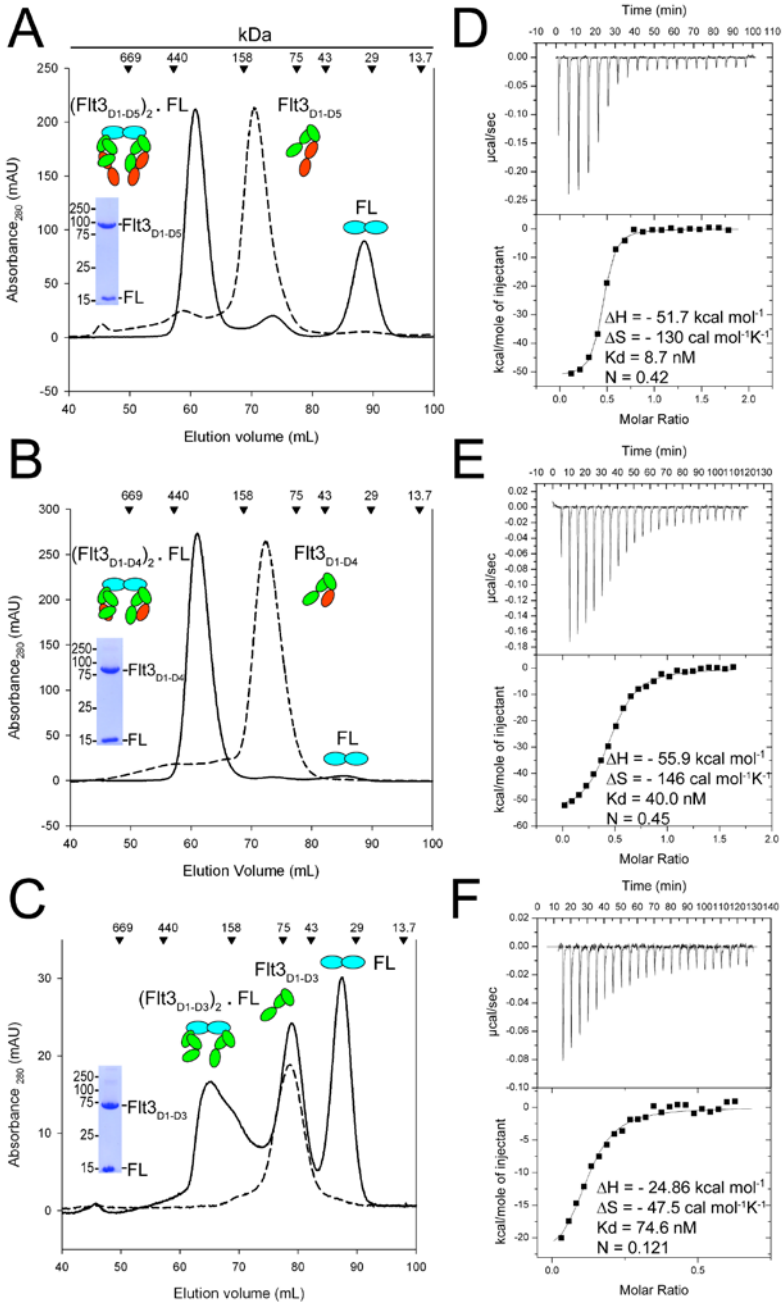

FIGURE 2. FL binds bivalently to Flt3 ectodomain variants to form high-affinity complexes. **(A-B)** Isolation of $Flt3_{D1-D5}$:FL and $Flt3_{D1-D4}$:FL by size-exclusion chromatography (SEC). Also shown, are Coomassie-stained SDS-PAGE strips corresponding to the peak fraction of the isolated complexes. (**C)** Size-exclusion chromatography on the $Flt3_{D1-D3}$:FL mixture at the end of an ITC experiment, showing that a large amount of $Flt3_{D1-D3}$ remains in the unbound form. Identical elution profiles were obtained in standard SEC experiments as well, in the presence of a large molar excess of FL. (**D-F)** Binding isotherms and thermodynamic parameters of FL binding to Flt3 ectodomains obtained by ITC. All ITC experiments were carried out by titrating recombinant human Flt3 extracellular domains with FL.

Overall structure of the Flt3 $_{D1-D4}$:FL complex

The crystal structure of the Flt3$_{D1-D4}$:FL complex was determined to 4.3 Å resolution based on data obtained from a large-scale screening of crystals (**Table I**).

TABLE I. X-ray data collection and refinement statistics.

	Flt3$_{D1-D4}$:FL	Flt3$_{D1-D5}$:FL
Data collection		
Source, Wavelength (Å)	ESRF ID23-1, 0.9762	ESRF ID23-1, 1.0762
Detector	ADSC-Q315R	ADSC-Q315R
Resolution (Å)	40.00 - 4.30 (4.45 - 4.30)	35.00 - 7.80 (8.00 - 7.80)
Space group	$P2_1$	$P2_1$
Unit cell parameters	a=103.89 b=146.26 c=105.95 α=γ=90°, β=109.7°	a=124.75 b=153.55 c=133.87 α=γ=90°, β=94.6°
Wilson B (Å^2)	135	401
Unique reflections	20184 (1942)	5656 (382)
Multiplicity	3.8 (3.8)	3.4 (3.2)
Completeness (%)	98.8 (98.9)	96.6 (92.9)
R_{meas} (%)[a]	10.8 (75.9)	12.8 (80.7)
Average $I/\sigma(I)$	12.04 (2.08)	9.1 (1.9)
Refinement		
Resolution (Å)	40.00 - 4.30 (4.53 - 4.30)	35.00 - 7.80 (8.72 - 7.80)
Reflections working set / test set	19172 / 1010 (2763 / 141)	5090 / 565 (1437 / 159)
R_{work} / R_{free}	0.260 / 0.281 (0.268 / 0.268)	0.337 / 0.346 (0.334 / 0.313)
R.m.s. deviations		
Bonds (Å)	0.010	n.a.
Angles (°)	1.12	n.a.
Average ADP (Å^2)	169	364
Ramachandran analysis (%)		
Favorable	89.8	n.a.
Outliers	2.0	n.a.
Protein Data Bank access code	3QS7	3QS9

The values in parentheses refer to the highest resolution shell. [a] $R_{meas} = \sum_h \sqrt{n_h/(n_h-1)} \sum_h \sum_i |I(h,i)-\langle I(h)\rangle| / \sum_h \sum_i I(h,i)$, where n_h is the multiplicity, $I(h,i)$ is the intensity of the ith measurement of reflection h, and $\langle I(h)\rangle$ is the average value over multiple measurements.

Confronted with the recurring poor diffraction quality of Flt3$_{D1-D4}$:FL crystals derivatized with heavy-atoms and selenomethionine-labeled Flt3$_{D1-D4}$, we successfully combined molecular replacement strategies relying on the high resolution structure of human FL (Savvides *et al.*, 2000) and a homology model for Flt3$_{D3}$ (Yuzawa *et al.*, 2007), with phase improvement protocols (Cowtan, 2010) exploiting the non-crystallographic symmetry and high solvent content of the crystals. Such approaches combined with crystallographic refinement employing information from high resolution structures have recently emerged as a powerful option in macromolecular structure determination at low resolution (Blanc *et al.*, 2004; Huyton *et al.*, 2007; Schroder *et al.*, 2010). The

ensuing electron density maps were exceptionally revealing and contained contiguous electron density for several unmodeled receptor domains, including direct crystallographic evidence for N-linked glycans (**Fig. 1A**). To facilitate chain tracing we determined the atypical disulfide-bond network of Flt3 as well as the actual number of N-linked glycosylation sites in extracellular Flt3 by mass-spectrometry. We could confirm that all nine N-linked glycosylation sites are at least partially occupied and that all cysteine residues present in $Flt3_{D1-D4}$ are engaged in disulfide-bonds (**Fig. 3A).**

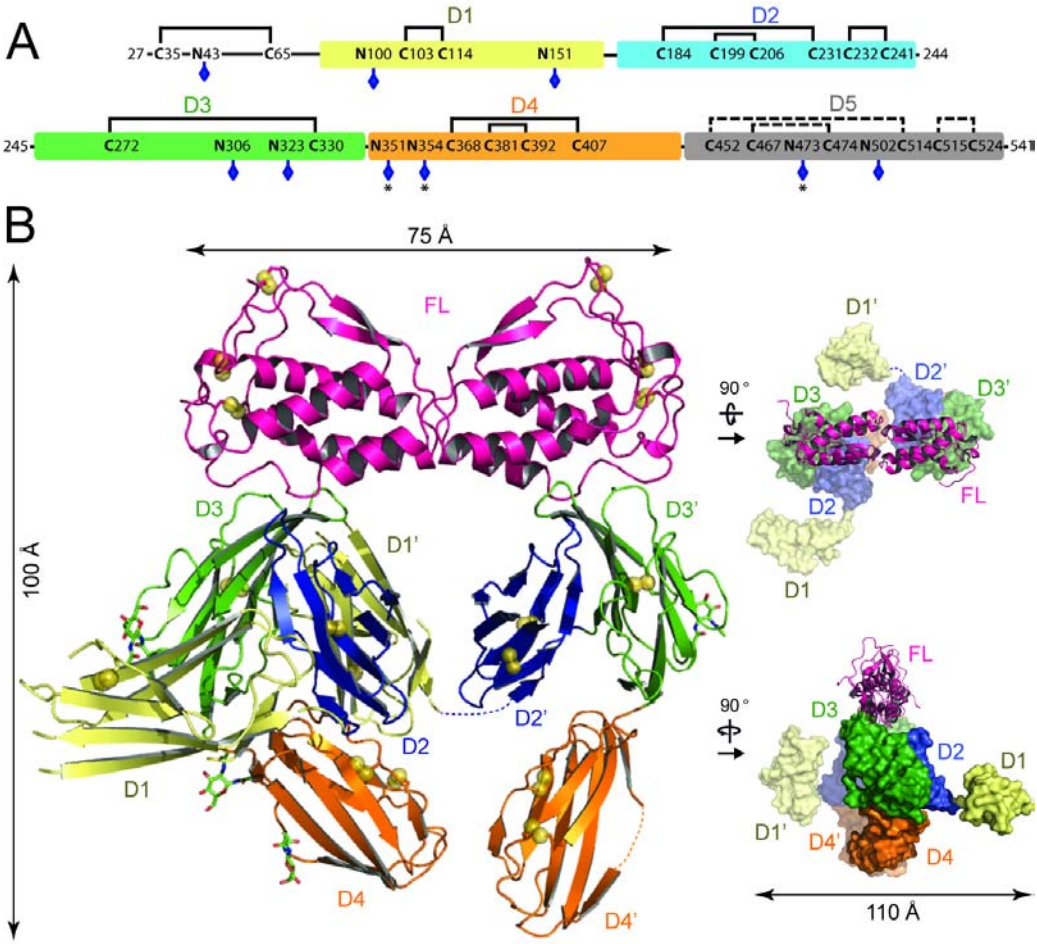

FIGURE 3. Crystal structure of the $Flt3_{D1-D4}$:FL complex. (A) Domain organization of the Flt3 extracellular segment. The five Ig-like domains of Flt3 (D1: residues 79-161, D2: residues 167-244, D3: residues 245-345, D4: residues 348-434 and D5: residues 435-533) are shown as colored boxes. N-linked glycosylation sites are indicated with blue diamonds. Partially occupied glycosylation sites are indicated with an asterisk. Also shown is the disulfide bond network in $Flt3_{D1-D4}$ as determined by mass-spectrometry. The putative disulfide bridges in $Flt3_{D5}$ are shown as dashed lines, based on homology with $Flt3_{D2}$ and KIT_{D5}. **(B)** Overall structure of the $Flt3_{D1-D4}$:FL complex. The crystal structure of the $Flt3_{D14}$:FL complex is shown in the vertical axis of the plane. Flt3 domains follow the coloring scheme in panel A. Disulfide bridges are shown as yellow spheres and N-linked glycans as green sticks. The structural panels to the right show two alternative views of the complex with FL in ribbon representation and the receptor in surface representation.

The structure of the $Flt3_{D1-D4}$:FL complex is unlike any of the structurally characterized RTKIII/V complexes to date and is characterized by a number of surprising features (**Fig. 3B**). The $Flt3_{D1-D4}$:FL assembly can be described as a moderately open horseshoe ring structure measuring 100 Å x 75 Å x 110 Å, comprising FL, $Flt3_{D2}$, $Flt3_{D3}$ and $Flt3_{D4}$. FL bivalently binds to two receptor molecules and is accommodated by a binding epitope at the membrane-distal tip of $Flt3_{D3}$, while $Flt3_{D2}$ leans against the concave side of $Flt3_{D3}$ and is stowed underneath FL in the ring opening (**Fig. 3B**). Intriguingly, the apparent two-fold symmetry of the complex about the FL dimer interface only holds for the FL:$Flt3_{D2-D3}$ subcomplex, as both $Flt3_{D1}$ and $Flt3_{D4}$ adopt asymmetric orientations compared to their tandem modules in the complex (**Fig. 3B**). Remarkably, $Flt3_{D4}$ does not engage in any obvious homotypic interactions as seen in the KIT structure (Yuzawa *et al.*, 2007). The N-terminal $Flt3_{D1}$ exhibits significant disorder and domain plasticity manifested by at least two different orientations about the D1-D2 linker region (residues 162-166), and protrudes perpendicularly away from the plane of the ring assembly at the level of $Flt3_{D2}$ without making any interactions with the rest of the complex (**Fig. 3B**). Our electron density maps allowed us to reliably model only the core of the $Flt3_{D1}$ structure (residues 79-161), but residual positive difference electron density extending away from the N-terminus of our model suggested that the atypical 50 amino acid module preceding $Flt3_{D1}$ is likely associated with the core domain structure.

Flt3 employs a remarkably compact cytokine-binding epitope

Perhaps the most unanticipated feature of the $Flt3_{D1-D4}$:FL complex is that the ligand-binding epitope is almost exclusively contributed by $Flt3_{D3}$ (**Fig. 4A**) for which electron density was exceptionally clear including information for some side-chains. This module is a member of the "I-set" Ig domains and is structurally homologous to extracellular domain 3 of KIT (Liu *et al.*, 2007; Yuzawa *et al.*, 2007) and CSF-1R (Chen *et al.*, 2008), featuring 8 β-strands making up the *ABED* and *A'FGC* β-sheets. However, the topology of $Flt3_{D3}$ is unusual such that the polypeptide chain extending from $Flt3_{D2}$ forms the N-terminal *A* strand in $Flt3_{D3}$ (residues 246 - 249) by complementing strand *B* in a parallel fashion, while the *AA'* loop of $Flt3_{D3}$ (residues 250 - 258) adopts an extended conformation (**Fig. 1B**). $Flt3_{D2}$, which in all other RTKIII/V complexes contributes roughly half of the ligand-binding epitope, packs against the hydrophobic patch projected by the *ABED*-face of $Flt3_{D3}$ centered around Trp269 burying ~1000 $Å^2$ (**Fig. 4B**). $Flt3_{D2}$ is homologous to KIT_{D5} and is a member of the C2 subset of the Ig-family (*ABED/CFG* topology), but contains an additional solvent-exposed disulfide (Cys232-Cys241) bridging strands *F* and *G*. Although the *AB* and *EF* loops of $Flt3_{D2}$ point in the direction of the ligand they remain too far to engage in any interactions. The only point on $Flt3_{D2}$ approaching FL within a distance that could mediate any form of interaction is centered on Asp180 on the AB loop of $Flt3_{D2}$. However, it is not clear whether this interaction actually occurs because we were not able to model the side-chain of Asp180 (**Fig. 4A**).

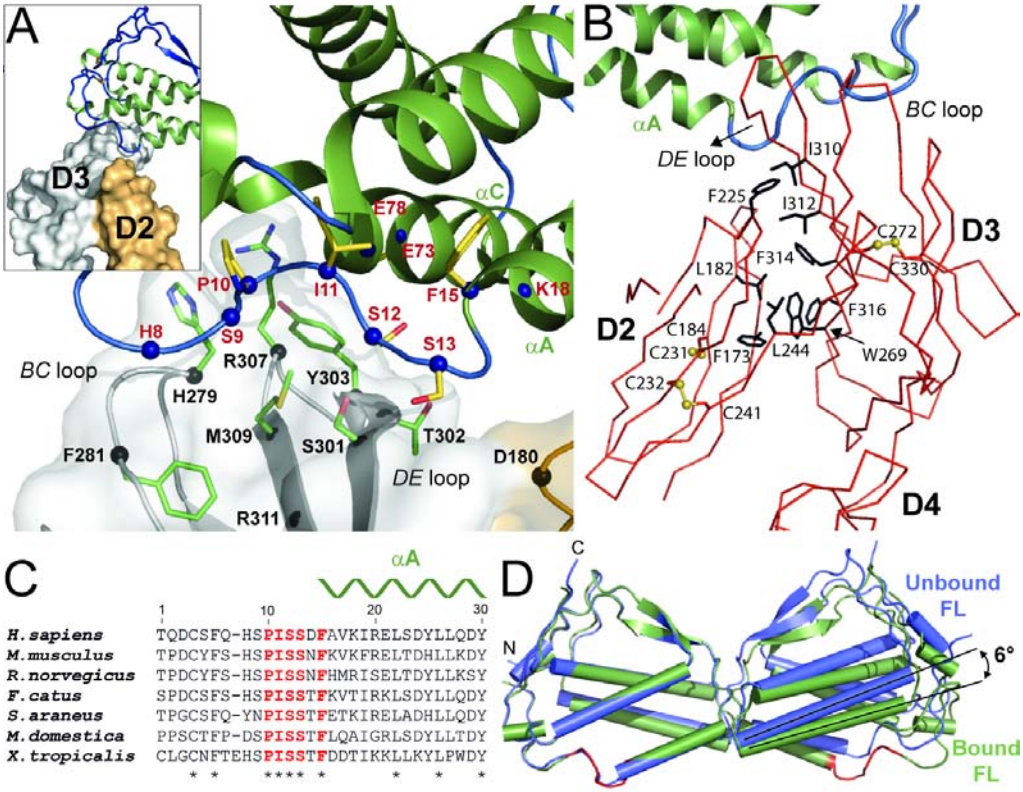

FIGURE 4. **The Flt3-FL binding interface.** (**A)** Close-up view of the Flt3-FL binding interface. FL is colored in green, $Flt3_{D3}$ in grey and $Flt3_{D2}$ in orange. Residues that constitute the cytokine-receptor interface are shown as sticks protruding from spheres centered at their Cα positions. FL residues are colored in yellow and Flt3 residues are colored in green. (**B)** The unusual $Flt3_{D2}$-$Flt3_{D3}$ interface**.** $Flt3_{D2\text{-}D4}$ (Cα trace in red) is shown together with FL in ribbon representation (green). Residues at the hydrophobic interface are shown as black sticks. Disulfide bonds in $Flt3_{D2\text{-}D3}$ are shown as ball and sticks (yellow). (**C)** Structure-based alignment of diverse FL sequences revealing strict conservation of the PISSXF-segment (residues 10 - 15) within the N-terminal loop (coloured in red). A complete alignment can be found in Appendix E. (**D)** Structural comparison of bound versus the unbound FL.

The FL binding epitope on $Flt3_{D3}$ engages in extensive interactions with the N-terminal loop (residues 8-13) of FL leading to αA and Lys18 on αA, and is mainly contributed by the *BC* loop of $Flt3_{D3}$ (residues 279-280) and strand *D* (residues 301-303). Additional interactions are mediated by the *DE* loop of $Flt3_{D3}$ (residue 307) which contacts a small patch on the C-terminal region of helix αC of FL defined by residues 73 and 78. Therefore, the Flt3 ligand-receptor interaction results in a single contact site covering merely ~900 $Å^2$ of buried surface area. Structure-based alignments using diverse FL sequences revealed a remarkably strict conservation of the PISSxF cassette as well as Phe81 and Leu115, which help to lock the N-terminal loop in its observed conformation (**Fig. 4C, Appendix E**).

Plasticity of FL upon binding to Flt3

Comparison of FL in its unbound (Savvides *et al.*, 2000) and now in its receptor-bound form reveals that the cytokine ligand does not undergo any significant local structural changes at its receptor binding epitope (**Fig. 4D**). This is contrary to what has been observed in Stem Cell Factor (SCF) in complex with KIT, whereby the cytokine ligand undergoes a cascade of structural rearrangements (Liu *et al.*, 2007; Yuzawa *et al.*, 2007). However, the two FL subunits display a hinge-like rigid-body rearrangement about the dimer interface, which increases the tilt angle between the two protomers by 5-6° (**Fig. 4D**). A similar motion was previously observed in the SCF-KIT$_{D1-D5}$ complex although SCF, unlike FL, already appears to have significant variability in the receptor-free form as shown by the range of its intersubunit tilt angles (2° to 6°) (Yuzawa *et al.*, 2007).

The Flt3$_{D3}$-Flt3$_{D4}$ domain elbow and the absence of homotypic receptor interactions

A second striking feature of the Flt3$_{D1-D4}$:FL complex is the absence of any obvious specific homotypic receptor interactions. Based on the current paradigm of RTKIII activation such interactions would be mediated by extracellular domain D4. While Flt3$_{D4}$ does point to its tandem Flt3$_{D4}$, in the complex, the two receptor domains stay clearly away from each other and deviate from the two-fold symmetry of the complex. The inability of Flt3$_{D4}$ to engage in homotypic interactions may also explain the observed disorder for this part of the structure, as we could only reliably model and refine a complete Flt3$_{D4}$-Flt3$_{D4'}$ tandem in only one of the two complexes in the asymmetric unit of the crystal, whereas for the second we could only place one of the two domains.

Closer inspection of the Flt3$_{D4}$ topology and sequence reveals that Flt3$_{D4}$ does not possess the conserved structure-sequence fingerprints seen in all other RTKIII/V homologues for this domain. For instance, Flt3$_{D4}$ has two additional disulfide bridges, a solvent exposed cross-strand disulfide bridge (Cys368-Cys407) connecting strands *B* and *E*, and a second (Cys381-Cys392) connecting its unusual *C'E* loop with strand *C*. Most importantly, Flt3$_{D4}$ displays an *EF*-loop that drastically differs both in structure and sequence from all homologues (**Fig. 5A-C**). The *EF*-loop constitutes the otherwise conserved 'tyrosine corner' motif in I-set Ig-domains (Harpaz and Chothia, 1994), and has been shown to mediate homotypic interactions in the case of KIT$_{D4}$ (Yuzawa *et al.*, 2007) and VEGFR$_{D7}$ (Yang *et al.*, 2010) (**Fig. 5B**).

Structural comparisons of the two independent Flt3$_{D1-D4}$:FL complexes in the crystal asymmetric unit revealed slight orientational plasticity of Flt3$_{D4}$ about the Flt3$_{D3}$-Flt3$_{D4}$ linker region. This stretch of residues and strand *A* of Flt3$_{D4}$ are well conserved in Flt3 and KIT and other RTKIII suggesting a common functional role (**Fig. 5D**). A comparison of KIT in the cytokine-bound and -unbound forms, showed that the KIT$_{D3}$-KIT$_{D4}$ linker region acts as a hinge to reorient KIT$_{D4}$ for homotypic interactions upon ligand binding. Despite the absence of such homotypic contacts in

Flt3, the domain elbow defined by $Flt3_{D3}$ and $Flt3_{D4}$ is similar to KIT, suggesting preservation of this interdomain relationship in both forms of the receptor. Thus, the orientation of $Flt3_{D4}$ appears to be restricted by a core of well-defined hydrophobic interactions mediated by Phe261 (*A'* strand of $Flt3_{D3}$), Val345 ($Flt3_{D3}$-$Flt3_{D4}$ linker), Phe349 (*A* strand of $Flt3_{D4}$) and Tyr376 (*BC* loop of $Flt3_{D4}$), as well as additional interactions between the *AA'* loop of $Flt3_{D3}$ and the *C'E* loop of $Flt3_{D4}$ (**Fig. 5A**).

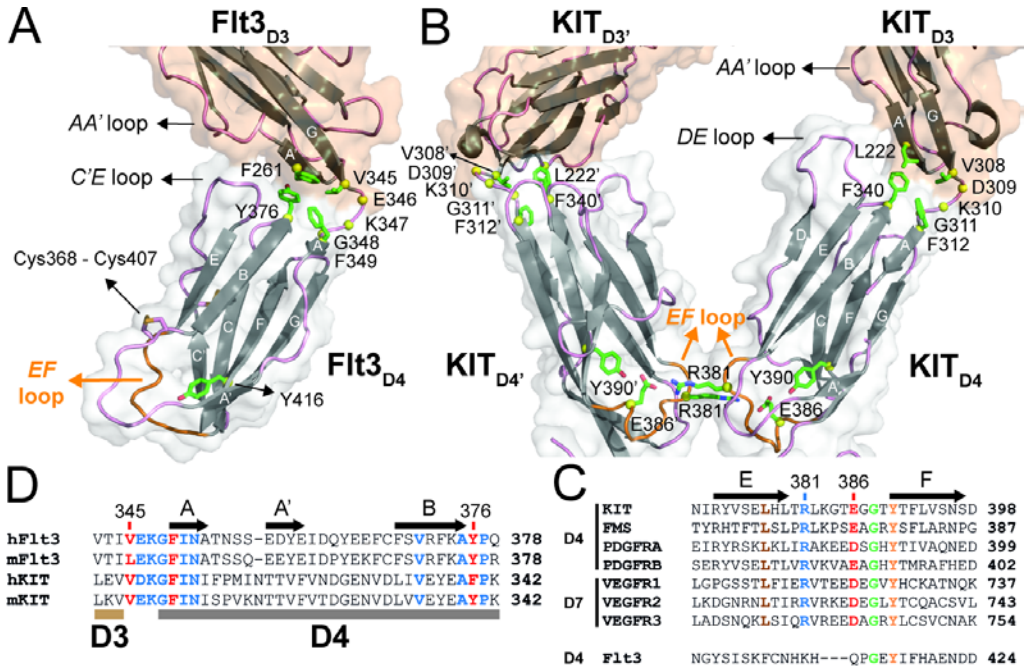

FIGURE 5. The $Flt3_{D3}$-$Flt3_{D4}$ elbow and the absence of homotypic receptor contacts in the Flt3:FL complex.

(A) The $Flt3_{D3}$-$Flt3_{D4}$ elbow. $Flt3_{D3}$ (partially shown) and $Flt3_{D4}$ are shown in ribbon representation. For clarity purposes only the laThe locations of the atypical disulfide bridges in $Flt3_{D4}$ (Cys368-Cys407 and Cys381-Cys391) are indicated. Residues mediating hydrophobic interactions between $Flt3_{D3}$ and $Flt3_{D4}$ are shown as green sticks. Residues in the $Flt3_{D3}$-$Flt3_{D4}$ linker (346-348) are shown as yellow spheres centered at their Cα positions. The side-chains of residues mediating contacts between the *AA'* loop of $Flt3_{D3}$ and the *C'E* loop of $Flt3_{D4}$ could not be modelled due to the low resolution of our analysis. The *EF*-loop of $Flt3_{D4}$ constituting the 'tyrosine corner' around Y416 (green sticks) is shown in orange. **(B)** Sequence conservation of residues involved at the D3-D4 interface in KIT and Flt3 based on comparisons between human and murine Flt3 and KIT sequences. **(C)** KIT_{D3}-KIT_{D4} orientation in the KIT:SCF complex. Homotypic receptor contacts between tandem ectodomain 4 modules in the KIT-SCF complex are mediated by salt-bridges via residues R381 and E386 residing on the *EF* loops (orange) (PDB entry 2E9W). Residues at the hydrophobic KIT_{D3}-KIT_{D4} interface are shown as green sticks. Residues in the KIT_{D3}-KIT_{D4} linker region (D309-G311) are shown as yellow spheres. **(D)** $Flt3_{D4}$ displays an atypical *EF*-loop within the RTKIII/V family. The pair of residues mediating the homotypic contacts in KIT_{D4} and VEGFR-2_{D7} is well conserved in the corresponding domains of all RTKIII/V members but not in $Flt3_{D4}$.

Architecture of the complete extracellular assembly of the Flt3 signaling complex

Crystals of $Flt3_{D1-D5}$:FL grew reproducibly from a number of crystallization conditions but proved to be of low diffraction quality despite repeated attempts to improve crystal quality by various methods including glycan shaving. Nonetheless, a robust dataset to 7.8 Å resolution proved sufficient to elucidate the architecture of the complete extracellular Flt3 complex by molecular replacement based on the $Flt3_{D2-D3}$: FL subcomplex as refined in the $Flt3_{D1-D4}$:FL crystal structure (**Table I**). We could subsequently place into electron density and optimize by rigid-body refinement protocols $Flt3_{D1}$ and $Flt3_{D4}$, extracted from the crystal structure of the $Flt3_{D1-D4}$:FL complex, as well as a conservative homology model of $Flt3_{D5}$ derived from the structure of human KIT_{D5} (Yuzawa *et al.*, 2007). While the low resolution of the $Flt3_{D1-D5}$:FL structure does not allow discussion of structural details, it does provide a reliable and valuable depiction of the organization features of the complete extracellular Flt3 complex.

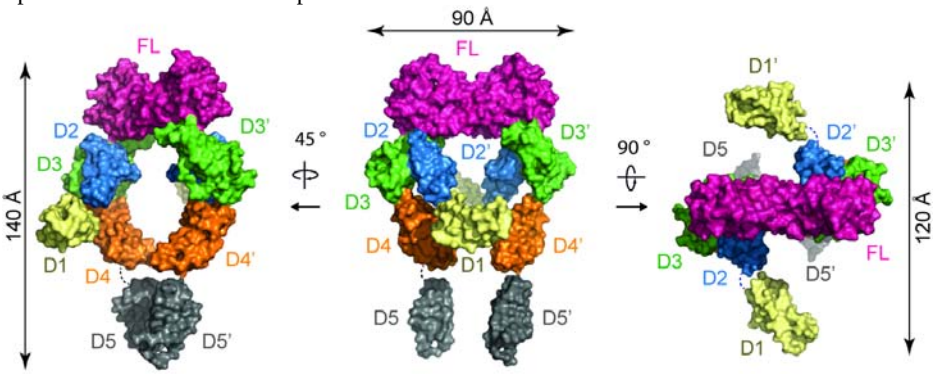

FIGURE 6. Assembly of the complete Flt3 ectodomain complex. Surface representations of the full-length Flt3 ectodomain complex. The central view shows the complex with the two-fold symmetry axis of FL oriented vertically in the plane of the paper.

In the full-length ectodomain complex, the core structure observed in $Flt3_{D1-D4}$:FL is mounted onto two membrane-proximal $Flt3_{D5}$ facing each other to form an assembly resembling a hollow tennis racket (140x75x110 Å) (**Fig. 6)**. Remarkably, the asymmetry exhibited by the tandem $Flt3_{D4}$ modules in $Flt3_{D1-D4}$:FL is not present in the complete extracellular complex. Instead, the two $Flt3_{D4}$ segments face each other nearly symmetrically according to the 2-fold symmetry of the $Flt3_{D2-D3}$:FL core structure and approach to about 20 Å from each other. While this inter-receptor separation is maintained at the ensuing $Flt3_{D5}$ modules, the apparent two-fold symmetry breaks down. Furthermore, the asymmetric projection of the N-terminal $Flt3_{D1}$ domains perpendicularly out of the plane of the racket head occurs in a manner analogous to what we observed in the $Flt3_{D1-D4}$:FL complex. Complementary studies of the full-length ectodomain complex by negative-stain negative-stain electron microscopy (EM), and small-angle X-ray scattering (SAXS) in solution corroborated the overall structural features revealed by the crystal structure (**Fig. 7A,B**).

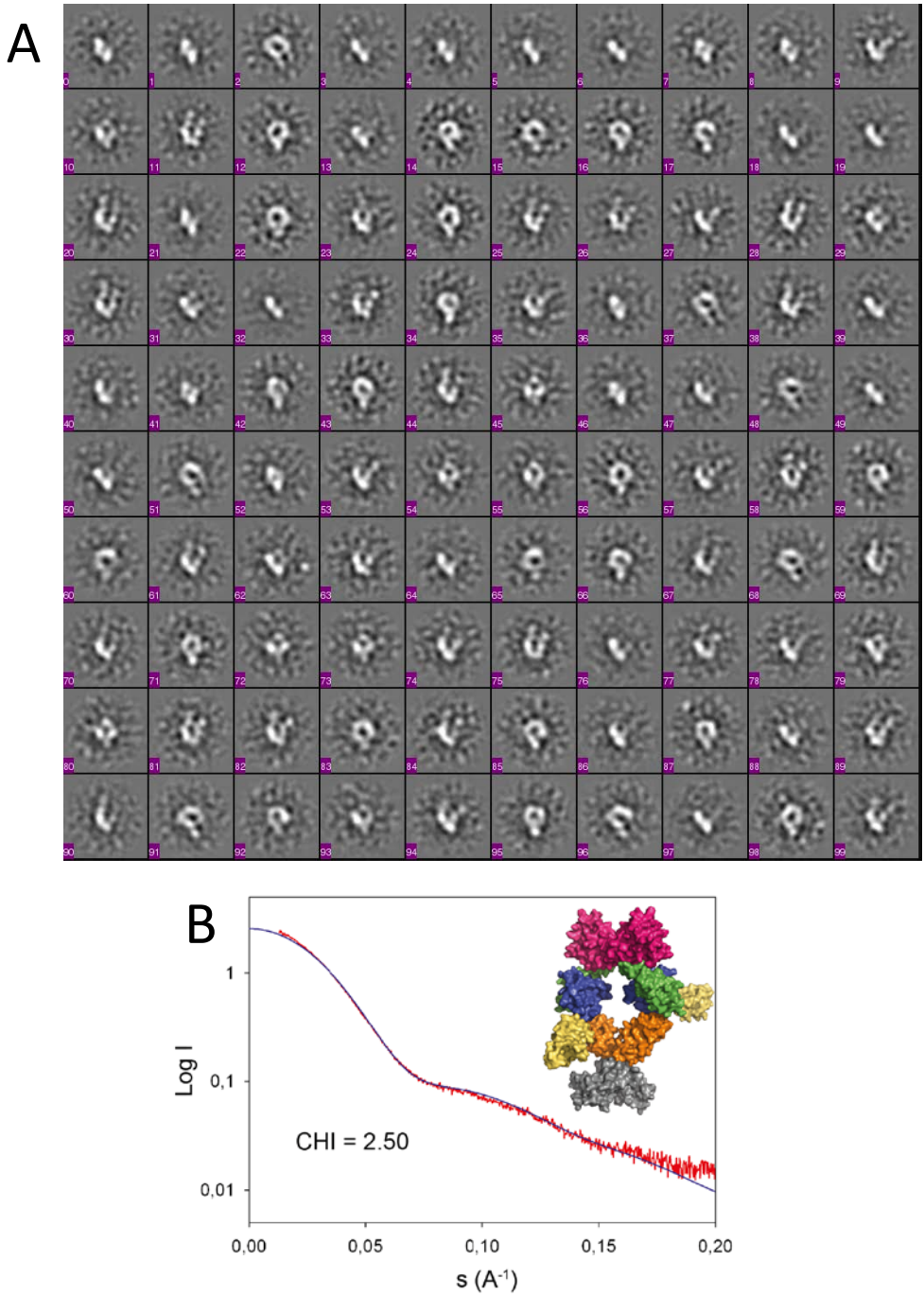

FIGURE 7. Negative-stain electron microscopy and SAXS analysis of the Flt3$_{D1-D5}$-FL complex. **A.** The displayed gallery of 100 class averages of the Flt3$_{D1-D5}$:FL complex allows to recognize features corresponding to projections of the crystal structure at different orientations, notably the slightly open horseshoe ring structure with well-defined individual extracellular domains. **B**. The crystal structure of the Flt3$_{D1-5}$-FL complex was refined as a rigid-body model against the experimental scattering curve obtained by SAXS. Fitting of the theoretical scattering curve calculated from the refined model (inset) to the experimental scattering curve shows a good agreement (χ^2=2.5).

DISCUSSION

Cytokine-mediated activation of hematopoietic cell-surface receptors is central to developing and sustaining hematopoiesis and the immune system. The RTKIII receptor Flt3 and its cognate cytokine ligand FL are arguably the most exciting new addition to the repertoire of hematopoietic factors, due to their activity on hematopoietic progenitors and pronounced impact on the development and homeostasis of antigen-presenting DC. As the importance of Flt3 signaling in early and late hematopoiesis continues to mount, we sought to elucidate the structural basis of the extracellular Flt3 receptor-ligand complex. The structural studies we report here complemented by a thermodynamic dissection of complex formation show that the Flt3-FL interaction is characterized by high-affinity bivalent binding of FL to Flt3 that does not invoke homotypic receptor interactions. The assembly showcases several unexpected features, which now establish Flt3 as a structural outlier within the RTKIII/V family (**Fig. 8**).

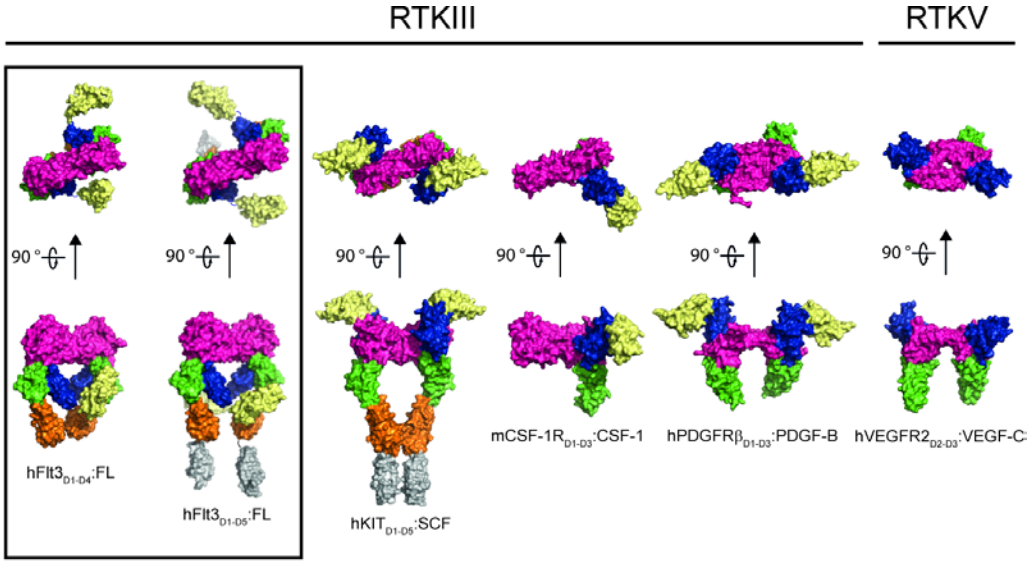

Figure 8. Comparison of representative RTKIII/V extracellular complexes.
The structures shown represent the architecture of receptor-cytokine complexes for the different members of the RTKIII/V family: From left to right: human Flt3:FL (this study), human KIT:SCF (pdb 2E9W), mouse CSF-1R:CSF-1 (pdb 3EJJ), human PDGF-Rβ:PDGF-B (pdb 3MJG) and human VEGF-R2:VEGF-C (PDB 2X1X). The dimeric ligands are colored in magenta. Receptor ectodomains are colored as follows: D1 in pale yellow, D2 in blue, D3 in green, D4 in orange and D5 in grey.

The Flt3:FL interaction epitope is surprisingly a fraction of typical helical cytokine-receptor interaction, and is dominated by contacts between a preformed N-terminal segment of FL and $Flt3_{D3}$. Consistent with the polar receptor-cytokine interface, the thermodynamic blueprint of the interaction calls for an enthalpically-driven binding event. The interaction carries a concomitant

significant entropic cost, which we now can rationalize in terms of the absence of a hydrophobic effect and the intrinsic entropy loss associated with bringing interaction partners together.

The Flt3-FL interaction interface covers a compact ~900 $Å^2$, which is at least 2 times less extensive than the buried surface area at the receptor-cytokine epitopes of all other RTKIII/V complexes, whereby the activating cytokine is harbored by a broad grapple defined by extracellular domains 2 and 3 (Liu *et al.*, 2007; Yuzawa *et al.*, 2007; Chen *et al.*, 2008; Leppanen *et al.*, 2010; Shim *et al.*, 2010) (**Fig. 8**). Comparison with diverse helical cytokine-receptor interactions (Stroud and Wells, 2004; Wang *et al.*, 2009) shows that Flt3 is the only receptor for a helical cytokine that uses a single interaction site to bind its cognate ligand. Heterodimeric protein-protein interactions bury on average ~1300 $Å^2$ of surface area, which is strongly correlated with high-affinity binding (Janin *et al.*, 2008). Flt3 and FL are clearly able to establish a tight interaction via a much more compact binding interface. A plausible explanation could be drawn from the rigidity of the receptor epitope on FL as a preformed binding platform, reminiscent of a classical 'lock-and-key' binding mode observed in affinity-matured antibody-antigen interactions (Sundberg and Mariuzza, 2002). Furthermore, a series of single amino acid substitutions (H8R, S9G, P10S, S13P/F, F15L) within the segment contributing almost the entire receptor binding epitope on FL, abolish receptor activation completely (Graddis *et al.*, 1998). This illustrates not only the possible individual contribution of each residue in this segment to binding but also the likely conformational stringency of the region. Indeed, a comparison of diverse FL sequences showed that not only the receptor-binding epitope is exquisitely conserved but also residues that help to lock the N-terminal loop both in its observed receptor-bound and receptor-free forms (**Fig. 4C, Appendix E**).

Comparison of the Flt3-FL interaction and representative receptor-cytokine epitopes for all other RTKIII/V, shows that engagement of Ig-like domain 3 (*BC* loop; *DE* loop and flanking residues) is the only common epitope feature of ligand binding (**Fig. 8**). It thus appears that binding of D3 of RTKIII/V to the activating cytokine satisfies a geometric requirement that allows receptor molecules to approach to a critical distance of ~60 Å from one another. This notion reinforces a fascinating aspect of RTKIII/V activation in that the cognate protein ligands are all dimeric with similar dimensions despite their grouping into two fundamentally different folds (4-helix bundles versus all-β cystine-knot scaffolds) (Savvides *et al.*, 2000; Yuzawa *et al.*, 2007; Chen *et al.*, 2008; Leppanen *et al.*, 2010; Shim *et al.*, 2010). Recently, interleukin-34 (IL-34) was identified as a second ligand to CSF-1R (Lin *et al.*, 2008), thus adding a perplexing dimension to RTKIII signaling as IL-34 bears no sequence similarity to the currently known cytokine ligands for RTKIII/V or other proteins.

The uniqueness of the Flt3 extracellular complex is further highlighted by the absence of homotypic receptor interactions. Such interactions have recently emerged as an important aspect of RTKIII/V activation and are mediated by conserved structure-sequence fingerprints in the membrane-proximal domains (Yuzawa *et al.*, 2007; Ruch *et al.*, 2007; Chen *et al.*, 2008; Yang *et al.*, 2008; Yang *et al.*, 2010). In both of our Flt3-FL complexes, the membrane-proximal modules

remain separated by ~20 Å at the D4-D5 junction, consistent with our comparative ITC data showing no significant contribution by the D4-D5 module. Flt3 is the only RTKIII/V family member that lacks the conserved set of residues involved in homotypic interactions in the homologous receptors, which now offers a strong rationale for the absence of such interactions in the extracellular Flt3 complex. Additional support comes from the existence of a fully active murine Flt3 isoform that lacks $Flt3_{D5}$ demonstrating the dispensability of the membrane-proximal domain for receptor activation (Lavagna *et al.*, 1995), contrary to the apparent importance of KIT_{D5} in signaling (Broudy *et al.*, 2001). However, it is possible that homotypic interactions could be enhanced within the two-dimensional spatial confinement of the cell membrane, and as a result of additional interactions between TM and/or cytosolic segments of Flt3. In fact, the difference in the affinity for the complete ectodomain complex versus previously reported values for native Flt3 based on cell-assays (Turner *et al.*, 1996; Graddis *et al.*, 1998) may reflect a combination of such factors. To this end, recent studies have highlighted the importance of homotypic interactions between TM and JM regions in RTKIII/V activation and pathology profiles (Finger *et al.*, 2009; Oates *et al.*, 2010). Interestingly, oncogenic variants of Flt3 carrying ITD in the JM segment are constitutively active as homodimers or as heterodimers with wild-type receptor, indicating that enhanced intracellular receptor interactions can drive activation (Kiyoi *et al.*, 2002). Recently, a number of mutations in the extracellular segment of Flt3 were identified in AML patients (Schnittger *et al.*, 2006; Fröhling *et al.*, 2007), which we now can map onto the Flt3 ectodomain (**Fig. 9**). However, the clinical relevance of these mutations will have to await further study.

In the absence of structural information for unbound Flt3 we are left to wonder about any possible domain rearrangements in Flt3 upon FL binding. Structural studies of KIT in the bound and unbound forms showed that KIT undergoes a large conformational switch at the KIT_{D3-D4} junction leading to homotypic receptor interactions (Yuzawa *et al.*, 2007). However, the extensive and unique hydrophobic interface observed between $Flt3_{D2}$ and $Flt3_{D3}$ (1000 $Å^2$), the hydrophobic interface between $Flt3_{D3}$ and $Flt3_{D4,}$ and additional contacts between loops thereof, provide evidence that the $Flt3_{D2-D4}$ ectodomain segment would be too rigid to undergo significant domain rearrangements. This is further supported by our structural studies of the complete extracellular complex, which showed that the relative orientation of $Flt3_{D3}$ and $Flt3_{D4}$ only differs slightly from that observed in the $Flt3_{D1-D4}$:FL complex. Nonetheless, Flt3 does exhibit significant domain plasticity at the two extremities of the extracellular assembly. This is most pronounced for $Flt3_{D1}$, which emanates from the core of the assembly without making contacts with other complex components. We note that the stacking of $Flt3_{D2}$ against $Flt3_{D3}$ provides a fixed angle for projecting $Flt3_{D1}$ from a point approximately halfway down the height of the complex. $Flt3_{D1}$ is the largest and most atypical domain in Flt3 and the entire RTKIII/V family, but its role in Flt3 signaling is currently unknown. We are thus tempted to propose that $Flt3_{D1}$ could mediate intermolecular contacts at the cell surface and/or stabilize the unbound receptor.

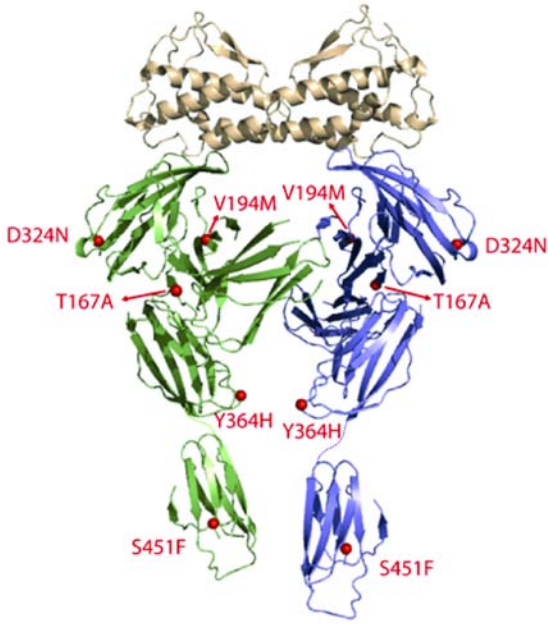

FIGURE 9. Mapping of non-synonymous sequence variants identified in the Flt3 ectodomain of AML patients. While the majority of oncogenic alterations in the *Flt3* gene are located in the JM and TKD regions, several mutations in the extracellular domains have recently been identified in AML patients. Expression of Flt3 carrying a mutation at position 451 (S451F) in BaF3 cells resulted in cytokine-independent proliferation and constitutive Flt3 autophosphorylation, demonstrating the oncogenic potential of this sequence variant. S451 is located at the solvent exposed site of strand *B* in the membrane proximal domain 5. Although the D324N variant did not result in ligand-independent activation it is associated with a higher risk of myeloid leukemias. D324 is located in the EF-loop of domain 3. A possible role in leukemogenesis has not been demonstrated yet for the other sequence variants (T167A, V194M, Y364H).

The availability of structures for the complete extracellular Flt3 receptor-ligand complex including a delineation of the receptor-cytokine interface, will likely have a significant impact on renewed efforts to antagonize Flt3 activity in a clinical setting. This is because wild type and mutated forms of Flt3 as well as autocrine secretion of FL have been implicated in the development of myeloid leukemias (Kindler *et al.*, 2010; Sanz *et al.*, 2009; Stirewalt and Radich, 2003; Zheng *et al.*, 2004). Current strategies focus on inhibition of the intracellular kinase domains of Flt3, but are faced with drug specificity issues and the emergence of primary and secondary resistance to treatment (Kindler *et al.*, 2010). More recently, an alternative therapeutic approach based on monoclonal antibodies directed against the extracellular domain of Flt3 (Piloto *et al.*, 2006) indicated a possible momentum shift towards combined strategies in clinical targeting of Flt3. A daunting challenge in inhibiting protein-protein interactions is the extent of the interaction epitope which often covers >1500 $Å^2$ and the lack of prior knowledge of functional hotspots (Wells and

McClendon, 2007). In this regard, the compactness of the Flt3 ligand-receptor interface provides favorable perspectives for the druggability of the extracellular Flt3 binding epitope.

ACKNOWLEDGEMENTS

KV, JE, BV, and KVC are research fellows of the Research Foundation Flanders, Belgium (FWO). This research project was supported by grants from the FWO (3G064307 and G059710) and Ghent University (BOF instrument) to SNS. AVS and DIS were supported by HFSP Research Grant Ref. RGP 55/2006. We thank the European Synchrotron Radiation Facility (ESRF) and the Swiss Light Source (SLS) for synchrotron beam time allocation, and the staff of beamlines ID-23 (ESRF), and X06SA/X06DA (SLS) for technical support. Access to these synchrotron facilities is supported by the European Commission under the 7th Framework Programme: Research Infrastructures, Grant Agreement Number 226716.

AUTHORSHIP

Contribution: KV and MJ expressed and purified recombinant proteins, and performed ITC measurements and data analysis. KV crystallized Flt3:FL complexes. KV manipulated and cyroprotected the crystals. KV, JE, and SNS carried out crystallographic experiments and analyzed data. KV and SNS determined and refined crystal structures. BV assisted in the design and analysis of ITC data. KVC assisted in tissue-culture and mammalian protein expression. IG carried out electron microscopy imaging, AD and IG analyzed the electron microscopy data. GVD collected and analyzed mass-spectrometry data. DIS, AVS, KV, and SNS contributed to SAXS data collection and analysis. KV, BV, and SNS wrote the manuscript. KV and SNS designed the study. SNS directed the study.

Chapter 5

Summary & Perspectives

SUMMARY

Flt3 is a type III tyrosine kinase receptor (RTKIII) expressed at the cell surface of early hematopoietic progenitors and, upon activation by its cognate ligand FL, initiates signaling pathways crucial for the development of the human hematopoietic and immune systems. Flt3 signaling is especially important during the early stages of hematopoiesis and for the development of antigen-presenting dendritic cells. In this work, the first structural insights into the Flt3 ligand-receptor interaction are presented.

Recombinant production of human FL and Flt3 ectodomains and isolation of Flt3:FL complexes

In the first stage of the project efficient protocols for the recombinant production of FL and Flt3 ectodomains needed to be established. A 'soluble form' of FL could be refolded from inclusion bodies produced in *E. coli*. Optimization of the refolding protocol resulted in yields that approached 5 mg per liter of culture. The bioactivity of our recombinant human FL was demonstrated by cell-based phosphorylation and proliferation assays.

Flt3 ectodomain variants were produced in stably transfected HEK293S GnTI$^{-/-}$ TetR cells. These cells allow for tetracycline-regulated expression and secrete proteins with limited and homogeneous N-linked glycosylation which can be minimized by treatment with EndoH. Contrary to the ectodomains of homologous receptors expressed in our laboratory, the yields for Flt3 in transient expression experiments were prohibitively low. The strategy to develop inducible stable cell lines in HEK293 GnTI$^{-/-}$ cells could therefore be generally applicable for structural studies involving eukaryotic receptor ectodomains that are difficult to express. It is further hypothesized that the low expression yields we observed in our transient expression experiments might explain why the Flt3 ligand-receptor interaction has remained so ill-characterized when compared to its homologues.

The Flt3 ectodomain (Flt3$_{D1-D5}$, residues 1 to 542) contains five immunoglobulin (Ig)-like domains. To delineate the ligand-binding epitope and to obtain various ligand-receptor complexes for structural studies by X-ray crystallography, five Flt3 ectodomain variants that were serially truncated at the C-terminus (Flt3$_{D1-D5}$, Flt$_{D1-D4}$, Flt3$_{D1-D3}$, Flt3$_{D1-D2}$ and Flt3$_{D1}$) were produced in stably transfected HEK293S GnTI$^{-/-}$ cell lines. Their ability to interact with recombinant *E. coli*-derived FL was evaluated by size exclusion chromatography (SEC) and isothermal titration calorimetry (ITC). It was found that FL and receptor fragments Flt3$_{D1-D5}$, Flt3$_{D1-D4}$ and Flt3$_{D1-D3}$ form high-affinity ternary complexes in which the dimeric ligand bivalently binds two receptor fragments. For the Flt3$_{D1-D2}$ and Flt3$_{D1}$ fragments, no complex formation was observed.

Crystallization of Flt3:FL complexes

Subsequently, highly pure preparations of $Flt3_{D1-D5}$:FL, $Flt3_{D1-D4}$:FL and $Flt3_{D1-D3}$:FL ternary complexes, which were isolated by SEC in the presence of an excess molar amount of FL, were subjected to an extensive crystallization screening. No crystals were obtained for the $Flt3_{D1-D3}$:FL complex, even when the receptor was glycan-minimized with EndoH. On the contrary, homogeneously glycosylated $Flt3_{D1-D5}$:FL and $Flt3_{D1-D4}$:FL complexes resulted in a large number of hits. For both complexes, crystallization conditions were characterized by the presence of 10 - 15 % medium molecular weight PEGs, 0.1 - 0.2 M of various salts and a pH value of 6.5 - 8.5. Crystal optimization and ensuing diffraction experiments showed that these crystals had an inherently low diffraction capacity. $Flt3_{D1-D5}$:FL crystals generally diffracted only to a resolution of 10 Å, while $Flt3_{D1-D4}$:FL diffracted to 4.5 to 5 Å. $Flt3_{D1-D5}$:FL crystals that were formed with a glycan-shaved receptor also diffracted poorly, and for the $Flt3_{D1-D4}$:FL complex, no crystals could be formed after the receptor had been treated with EndoH. For structural analysis of the Flt3:FL complex, we were therefore dependent on these weakly diffracting crystals. Screening hundreds of crystals and an extensive optimization of the cryoprotection protocol finally resulted in a dataset to 4.3 Å for the $Flt3_{D1-D4}$:FL complex and a dataset to 7.8 Å for the $Flt3_{D1-D5}$:FL complex.

Structure solution of the $Flt3_{D1-D4}$:FL complex

The 4.3 Å dataset for the $Flt3_{D1-D4}$:FL complex could be phased by a combination of molecular replacement (MR) and density modification. Initially, two copies of FL, for which the high-resolution structure was determined previously (pdb 1ETE), were easily located. This indicated the presence of two $Flt3_{D1-D4}$:FL complexes in the asymmetric unit. Subsequently, an MR-search with a structural model for $Flt3_{D3}$, based on the homologous KIT_{D3} structure (pdb 2E9W), located three copies for Ig-domain D3, with each copy identically packed against one FL protomer. After manual placement of a fourth copy of D3, the partial solution was rigid-body refined. Ensuing density modification protocols, employing the four-fold non-crystallographic symmetry, generated maps that contained well defined contiguous density for some of the missing domains of $Flt3_{D1-4}$. These maps allowed us to select the correct MR-solution for one $Flt3_{D4}$ copy, and to manually place two additional copies of $Flt3_{D4}$ and four copies of $Flt3_{D2}$. In the later stages of the structure solution process it was possible to locate two copies of $Flt3_{D1}$. The structure was refined in autoBuster with tight NCS-restraints and a low weight on the X-ray term. To facilitate the chain chasing process the atypical disulfide bond network in the Flt3 ectodomain as well as the actual number of glycosylation sites were determined by mass spectrometry. Coordinates and structure factors were deposited to the Protein Databank with accession code 3QS7.

Flt3 is a structural and functional outlier in the RTKIII/V family

The determined structure of the $Flt3_{D1-D4}$:FL ternary complex showed that the Flt3:FL interaction is unlike any of the other structurally characterized RTKIII/V complexes to date. While all other RTKIII/V receptors bind their ligand in the groove presented by D2 and D3, the interaction of Flt3 with FL is solely mediated by $Flt3_{D3}$, while $Flt3_{D2}$ is tightly packed against $Flt3_{D3}$ through a hydrophobic interface. Furthermore, the two copies of $Flt3_{D1}$ that could be located emerge asymmetrically from the plane of the complex without making any interactions with the ligand or other domains of the receptor. A third remarkable feature of the $Flt3_{D1-D4}$:FL complex is the absence of homotypic contacts between the adjacent $Flt3_{D4}$ domains. According to the current paradigm of RTKIII activation, D4-mediated homotypic receptor-receptor contacts are formed upon ligand binding and are crucial to activate the intracellular tyrosine kinase domains.

Flt3 ligand-receptor interface

Similar to KIT_{D3} and CSF-$1R_{D3}$, $Flt3_{D3}$ uses it *BC* and *DE* loops to accommodate the ligand. The receptor-binding epitope on FL is almost entirely contained in the N-terminal segment preceding the first α-helix. This segment was previously identified as the region most crucial for receptor binding by a random mutagenesis screen. Furthermore, the residues in this segment (PISSXF) and surrounding residues that stabilize its conformation are strictly conserved among a wide variety of species, suggesting that the Flt3 ligand-receptor interaction mode is conserved as well. Indeed, unlike the homologous KIT:SCF and CSF-1R:CSF-1 ligand-receptor pairs, Flt3 has been shown to have a wide species cross-reactivity.

Although our low-resolution structural analysis does not provide information about specific ligand-receptor interactions, the residues present at the interface clearly indicate that FL and $Flt3_{D3}$ engage through a polar interaction. This is in agreement with our thermodynamic data that had shown that Flt3:FL complex formation is driven by a large exothermic enthalpy.

Absence of homotypic contacts and structural analysis of the $Flt3_{D1-D5}$:FL complex

For the other RTKIII receptors it has been shown that D4 couples ligand-binding to receptor activation by mediating homotypic receptor-receptor contacts through a pair of well conserved salt bridges located in the *EF* loop of D4. Point mutations that target these salt bridges allow ligand binding but severely compromise signaling. It is thought that these specific contacts between adjacent receptors orient the intracellular tyrosine kinase domains in a signaling competent state. Flt3 is the only member of the RTKIII-family that lacks these salt bridges. The absence of these residues is in agreement with the observation that adjacent $Flt3_{D4}$ do not interact. Since homotypic contacts are crucially important in the activation process of the other RTKIII members and, given

the conserved mechanism of autoinhibition of the tyrosine kinase domains, it is difficult to rationalize how the Flt3 receptor is activated then.

It was hypothesized that the lack of homotypic receptor contacts in the $Flt3_{D1-D4}$:FL structure was due to the absence of the membrane-proximal domain $Flt3_{D5}$. We therefore determined the architecture of the complete Flt3:FL extracellular assembly by rigid-body refinement against the obtained 7.8 Å X-ray dataset. The resulting structure (pdb 3QS9) showed that the $Flt3_{D1-D5}$:FL complex also adopts an open conformation, thereby demonstrating that also $Flt3_{D5}$ does not mediate homotypic receptor-receptor interactions. In this regard, it is interesting to note that a murine Flt3 isoform, which lacks the fifth Ig-like domain, was reported to be equally active as the full length receptor.

In conclusion, our study shows that Flt3, in contrast to KIT and CSF-1R, does not form receptor-receptor interactions in ternary complexes formed between its ectodomain and ligand. It is however possible that homotypic Flt3 receptor interactions are enhanced within the two-dimensional spatial confinement of the cell membrane, and as a result of additional interactions between the TM and/or cytosolic segments of Flt3. In fact, the difference in the affinity for the complete ectodomain complex versus previously reported values for native Flt3 based on cell-assays may reflect a combination of such factors.

PERSPECTIVES

Does receptor binding occurs in a cooperative way?

Several lines of evidence suggest the existence of communication mechanisms between the receptor-binding epitopes of dimeric helical bundle cytokines. For example, in SEC experiments, the KIT_{D1-D3}:SCF complex does not dissociate in the presence of a high excess of ligand. This suggests a positively cooperative binding mode for KIT (Lemmon *et al.*, 1997). In the determined structure of the murine CSF-$1R_{D1-D3}$:CSF-1 complex, only one copy of CSF-$1R_{D1-D3}$ was bound to the ligand, although the crystallization mixture contained more than a twofold molar excess of CSF-$1R_{D1-D3}$. Here the authors suggested that the binding of one CSF-$1R_{D1-D3}$ fragment lowers the affinity for the second (Chen *et al.*, 2008). For all Flt3 constructs that formed a complex with the ligand, no dissociation in the excess of ligand was observed in SEC experiments. This suggests that Flt3 receptor binding is cooperative. Therefore, it would be interesting to investigate if a heterofunctional form of FL, in which one protomer has a mutated receptor-binding epitope, still displays high-affinity receptor binding. Such a ligand can be produced by co-refolding differentially tagged wild-type and mutated forms of FL.

Probing the role of the different Ig-like domains in ligand-binding and receptor activation by cell-based assays

On the basis of our determined structures there is no clear function for D1. Possible roles for this domain include stabilizing/autoinhibiting unbound Flt3, clustering ligand-receptor complexes at the cell surface or mediating interactions with other players at the cell surface. Also the role of D5 in human Flt3 remains unclear. Although there exists an active murine isoform that lacks D5, such an isoform has not been reported in human.

The importance of these domains in ligand-binding and receptor activation could be investigated by expressing domain-deletion variants of the full length Flt3 receptor in an appropriate mammalian cell system. Ensuing binding assays with radiolabeled FL, and phosphorylation and proliferation assays could then provide valuable insights into the function of these domains.

Development of small-molecule Flt3 antagonists that inhibit ligand binding

It has been proposed that FL is involved in leukemogenesis by autocrine signaling loops since it is expressed in the majority of AML blasts. Furthermore, the dramatically increased serum levels of FL, following chemotherapy mitigate the inhibition and cytotoxicity of Flt3 tyrosine kinase inhibitors. These findings suggest a rationale for targeting FL-Flt3 interaction as a therapeutic strategy. The structure of the Flt3 ligand-receptor complex shows that the compact receptor-binding epitope of FL is almost exclusively contained in the N-terminal peptide segment preceding the first α-helix. Furthermore, this segment likely does not undergo conformational changes upon receptor binding. This finding could stimulate the development of small-molecule or peptide-based receptor antagonists.

Obtaining a high-resolution structure of the Flt3 ligand-receptor complex

In retrospect, the relatively weak diffraction capacity of the obtained crystals for the Flt3 ligand-receptor complexes is likely related to the apparently inherent flexibility of the terminal Ig-domains. Furthermore, $Flt3_{D1-D5}$ contains 9 N-linked glycosylation sites. Based upon the acquired structural insights, a mininal $Flt3_{D2-D3}$:FL complex is an interesting target to crystallize. The compactness of this complex could allow the formation of crystals with higher internal order. Furthermore, $Flt3_{D2-D3}$ only contains two glycosylation sites, which could be targeted by site-directed mutagenesis. The expression of receptor constructs without D1 has yet to be explored. A possibly strategy also includes co-expression with FL in mammalian cells.

Crystallization of Flt3 receptor fragments

In the absence of structural information for unbound Flt3 we are left to wonder about any possible domain rearrangements in Flt3 upon FL binding. To this end, $GlcNac_2Man_5$ and EndoH-treated $Flt3_{D1-D5}$, $Flt3_{D1-D4}$ and $Flt3_{D1-D3}$ receptor fragments have been subjected to an extensive crystallization screening using an automated robotic system. However, for none of these fragments crystals were obtained. The crystallization of $Flt3_{D1-D2}$ was not attempted because of its low expression yields. However, for $Flt3_{D1}$ (residues 27-161) crystals could be obtained. These crystals currently diffract anisotropically to a resolution of 4.7 Å. $Flt3_{D1}$ contains 3 N-linked glycosylation sites. EndoH treated $Flt3_{D1}$ failed to crystallize. Strategies to improve the crystal quality could focus on eliminating one or more glycosylation sites by site-directed mutagenesis, and/or on isolating differently glycosylated species by high-resolution ion exchange chromatography.

It would also be interesting to see if isolated $Flt3_{D4}$ or $Flt3_{D5}$ domains can be crystallized. The expression of these domains has not been tempted yet.

SAMENVATTING

Flt3 is een type III tyrosine kinase receptor (RTKIII) die geëxpresseerd wordt aan het celoppervlak van primitieve hematopoietische progenitoren. Na activatie door zijn cognaat cytokine, Flt3 ligand (FL), initieert Flt3 signaaltransductiecascades die cruciaal zijn voor de ontwikkeling van het humane hematopoïetische stelsel en immuunsysteem. De door Flt3 gemediëerde signalisatie is in het bijzonder belangrijk voor de ontwikkeling van antigen-presenterende dendritische cellen. In dit werk werden de eerste structurele inzichten voor de Flt3 ligand-receptor interactie bekomen.

Recombinante productie van de humane FL en Flt3 ectodomeinen en isolatie van Flt3:FL complexen

In het eerste stadium van het project dienden er efficiënte protocols voor de recombinante aanmaak van de FL en Flt3 ectodomeinen ontwikkeld te worden. Een 'oplosbare' vorm van FL kon bekomen worden door het *in vitro* heropvouwen van in *E. coli* geproduceerde inclusielichamen. Optimalizatie van het heropvouwingsprotocol resulteerde in een opbrengst tot 5 mg recombinant FL per liter *E. coli* cultuur. De bioactiviteit van deze vorm van humaan recombinant FL werd aangetoond via cel-gebaseerde fosforylatie- en proliferatie assays.

Flt3 ectodomeinen varianten werden geproduceerd in stabiel getransfecteerde HEK293S GnTI$^{-/-}$ TetR cellen. Deze cellen laten tetracycline gereguleerde expressie toe en zij secreteren eiwitten met een beperkte N-gelinkte glycosylatie die bovendien zeer gevoelig is voor behandeling met EndoH. In tegenstelling tot de ectodomeinen van homologe receptoren die ook in het laboratorium geëxpresseerd werden, waren de opbrengsten via transiente expressie-experimenten in HEK293T cellen zeer laag voor Flt3. De strategie die wij gevolgd hebben om induceerbare stabiele cellijnen in HEK293S GnTI$^{-/-}$ cellen te ontwikkelen kan mogelijks algemeen toepasbaar zijn voor structurele studies met eukaryote ectodomeinen die moeilijk te expresseren zijn. De lage opbrengsten voor Flt3 die wij waarnamen in transiënte expressie-experimenten verklaren mogelijks waarom de Flt3 ligand-receptor interactie tot heden zo slecht gekarakteriseerd was.

De extracellulaire regio van Flt3 ($Flt3_{D1-D5}$) bevat 5 immunoglobuline (Ig) domeinen. Om de ligand-bindende epitoop af te lijnen, en om verscheidene ligand-receptor complexen te verkrijgen voor structurele studies, werden er 5 Flt3 ectodomein varianten die sequentieel getrunceerd waren aan de C-terminus ($Flt3_{D1-D5}$, $Flt3_{D1-D4}$, $Flt3_{D1-D3}$, $Flt3_{D1-D2}$ en $Flt3_{D1}$) geproduceerd in stabiel getransfecteerde HEK293S GnTI$^{-/-}$ cellijnen. Het vermogen van deze receptorfragmenten om met recombinant FL te interageren werd geëvalueerd via 'gelfiltratie-chromatografie' en 'isothermale titratie calorimetrie (ITC)'. Er werd vastgesteld dat FL en de $Flt3_{D1-D5}$, $Flt3_{D1-D4}$ en $Flt3_{D1-D3}$

ectodomain varianten ternaire complexen kunnen vormen met een hoge affiniteit, waarin het dimere ligand bivalent bindt aan twee receptoren. Voor de $Flt3_{D1-D2}$ en $Flt3_{D1}$ fragmenten kon geen complex met FL aangetoond worden.

Kristallisatie van Flt3:FL complexen

Heel sterk opgezuiverde preparaties van $Flt3_{D1-D5}$:FL, $Flt3_{D1-D4}$:FL en $Flt3_{D1-D3}$:FL ternaire complexen werden onderworpen aan een extensieve kristallisatiescreening. Voor het $Flt3_{D1-D3}$:FL complex werden geen kristallen bekomen, ook niet wanneer de receptor behandeld was met EndoH. Voor de homogeen geglycosyleerde $Flt3_{D1-D5}$:FL en $Flt3_{D1-D4}$:FL complexen echter, werden talrijke kristallisatiehits bekomen. Na kristaloptimalisatie werden diffractie-experimenten uitgevoerd. Deze toonden aan dat de kristallen een inherent lage diffractiecapaciteit hadden. $Flt3_{D1-D5}$:FL kristallen diffracteerden slechts tot een resolutie van 10 Å, terwijl kristallen voor het $Flt3_{D1-D4}$:FL complex diffracteerden tot 4.5 Å. Door middel van het testen van honderden kristallen, in combinatie met een uitvoerige optimalisatie van het cryoprotectieprotocol werden uiteindelijk een dataset tot 4.3 Å voor het $Flt3_{D1-D4}$:FL complex en een dataset tot 7.8 Å voor het $Flt3_{D1-D5}$:FL complex bekomen.

Structuuroplossing van het $Flt3_{D1-D4}$:FL complex

De 4.3 Å dataset voor het $Flt3_{D1-D4}$:FL complex kon gefaseerd worden via een combinatie van ‘molecular replacement (MR)’ en ‘density modification’. Gebruikmakend van de gekende structuur van FL (pdb 1ETE) konden initieel twee kopijen van FL gelokaliseerd worden. Dit duidde op de aanwezigheid van twee $Flt3_{D1-D4}$:FL complexen in de asymmetrische eenheid. Vervolgens werd een zoekmodel voor $Flt3_{D3}$, gebaseerd op D3 van de homologe KIT receptor, ook via MR gelokaliseerd.

Na ‘rigid-body’ verfijning van de partiële oplossing, werden via ‘density modification’ protocollen elektronendensiteitsmappen bekomen die continue densiteit bevatten voor sommige van de niet gemodelleerde Ig-domeinen van $Flt3_{D1-D4}$. Zo konden modellen voor $Flt3_{D2}$ en $Flt3_{D4}$ geplaatst worden, en in latere stadia ook modellen voor $Flt3_{D1}$. De structuur werd verfijnd in autoBuster. Ter ondersteuning van een correcte bepaling van het sequentieregister werden het atypische disulfidebrugnetwerk en de glycosylatieplaatsen in het Flt3 ectodomein bepaald via massaspectrometrie. De coördinaten en structuurfactoren van de finale structuur voor het $Flt3_{D1-D4}$:FL complex werden gedeponeerd in de ‘Protein Data Bank’ onder de toegangscode 3QS7.

De Flt3:FL interactie is een uitzondering in de RTKIII/V familie

De bepaalde structuur voor het ternaire $Flt3_{D1-D4}$:FL complex toonde aan dat de Flt3:FL interactie sterk afwijkt van de andere gekarakteriseerde complexen in de RTKIII/V-familie. Terwijl de andere receptoren van deze familie hun ligand binden in de groef gepresenteerd door Ig-domeinen D2 en D3, interageert Flt3 met FL enkel door middel van D3. In de Flt3 receptor pakt D2 tegen D3 via een breed en hydrofoob interactie-oppervlak. Het is ook opmerkelijk dat D1 van de

Flt3 receptor niet interageert met het ligand of met andere domeinen van de receptor. Een derde merkwaardig punt in het $Flt3_{D1-D4}$:FL complex is de afwezigheid van receptor-receptor interacties. Volgens het huidige model voor RTKIII-activatie zijn deze homotypische receptor interacties nodig om de intracellulaire tyrosine kinase domeinen te activeren.

De Flt3 ligand-receptor interactie

Net zoals KIT_{D3} en $CSF\text{-}1R_{D3}$, gebruik $Flt3_{D3}$ zijn *BC* en *EF* loops om contact te maken met FL. De receptor-bindende epitoop van FL is bijna volledig gelokaliseerd in het N-terminale segment dat de eerste α-helix voorafgaat. Deze regio werd voorheen reeds geïdentificeerd als zeer cruciaal voor receptor binding via een random-mutagenese screen. Bovendien is dit segment strikt geconserveerd in een wijde variëteit aan soorten.

Hoewel onze lage resolutie studie geen informatie verschaft over directe interacties, is het duidelijk dat FL en Flt3 elkaar binden via een polaire interactie. Dit is in overeenstemming met onze ITC-metingen die voorheen aangetoond hadden dat de Flt3:FL complexvorming gedreven is door een sterk exotherme enthalpie.

De afwezigheid van homotypische contacten en de structurele analyse van het $Flt3_{D1-D5}$:FL complex

Voor de andere RTKIII-receptoren is het aangetoond dat D4 ligand-binding koppelt aan receptor-activatie door homotypische receptor-receptor interacties te mediëren. Deze contacten worden gevormd door een paar sterk geconserveerde zoutbruggen. Wanneer deze zoutbruggen gedeleteerd worden via plaatsgerichte mutagenese wordt de mogelijkheid tot signalisatie in deze receptoren ernstig gecompromitteerd. Men veronderstelt dat deze specifieke receptor-receptor interacties vereist zijn om de intracellulaire tyrosine kinase domeinen te oriënteren in een staat die activatie toelaat.

Flt3 is het enige lid van de RTKIII-familie waarbij deze zoutbruggen afwezig zijn. Het ontbreken van deze residuen is dan ook in overeenstemming met de observatie dat er geen homotypische interacties gevormd worden tussen de $Flt3_{D4}$ protomeren. Echter, omdat homotypische contacten cruciaal zijn voor de activatie van de andere RTKIII receptoren, en omdat het mechanisme van autoinhibitie van het tyrosine kinase domein wel geconserveerd is, is het moeilijk te rationalizeren hoe de Flt3 receptor geactiveerd wordt.

Om na te gaan of homotypische interacties misschien door $Flt3_{D5}$ gemediëerd worden werd de architectuur van het $Flt3_{D1-D5}$:FL complex bepaald via ‘rigid-body’ verfijning tegen de opgemeten 7.8 Å dataset. De resulterende structuur (pdb 3QS9) vertoonde net zoals het $Flt3_{D1-D4}$:FL complex geen receptor-receptor interacties. Daarmee werd aangetoond dat ook $Flt3_{D5}$ geen homotypische interacties mediëert. Hierbij is het interessant op te merken dat er in de muis een actieve isoform voor Flt3 bestaat waarbij domein 5 ontbreekt.

Onze studie toont dus aan dat Flt3, in tegenstelling tot zijn dichtste homologen, KIT en CSF-1R, geen receptor-receptor interacties vormt in ternaire complexen tussen zijn ectodomein en ligand. Het is echter mogelijk dat, wanneer de receptor geëxpresseerd wordt aan het celoppervlak, zwakke homotypische extracellulaire interacties versterkt worden door de dimensionaliteit van het celmembraan en als het gevolg van additionele interacties tussen de transmembranaire helices en/of cytosolische segmenten.

APPENDICES

Appendix A

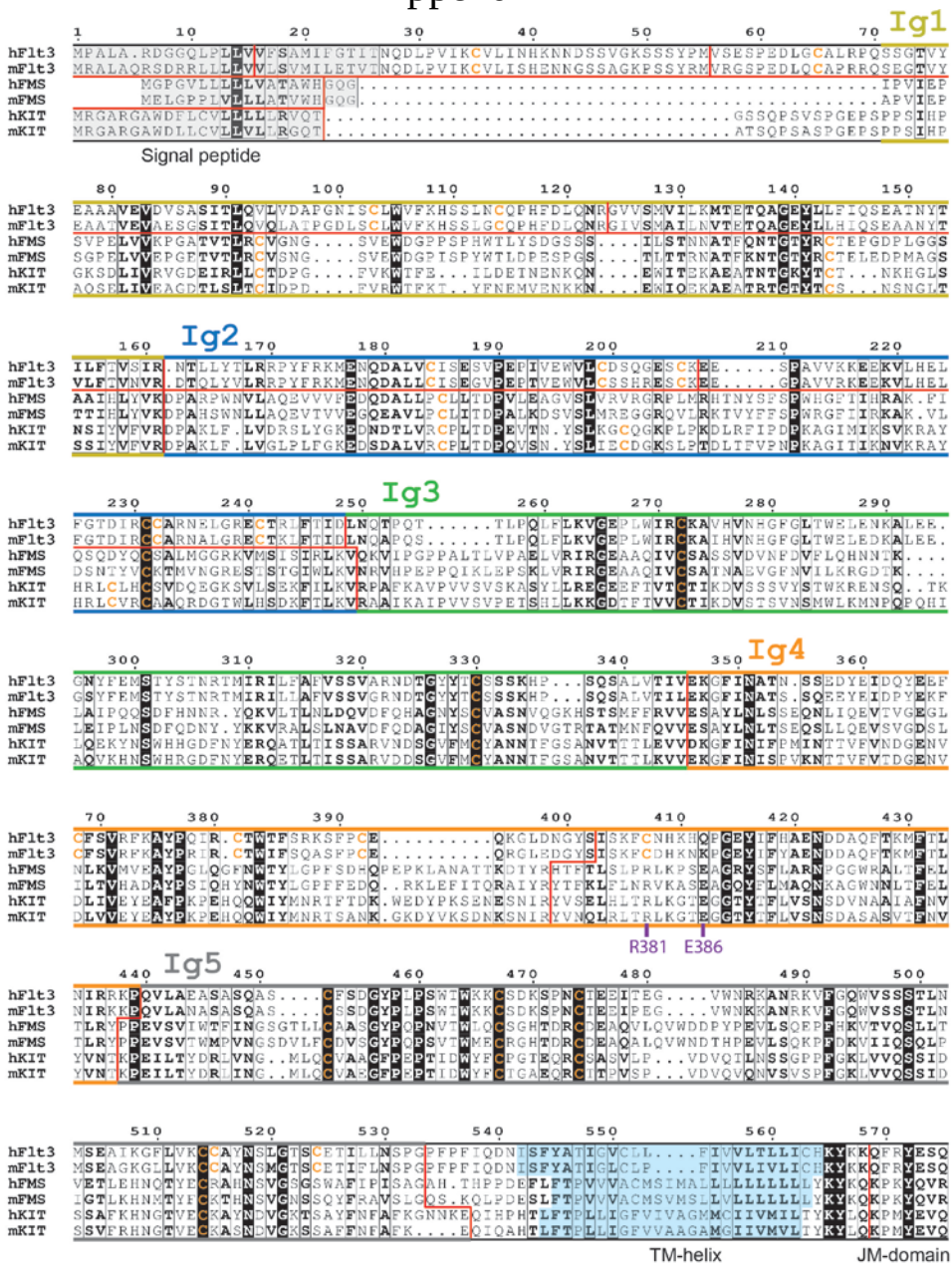

Sequence comparison of the extracellular region of Flt3, FMS (CSF-1R) and KIT.

The NCBI-reference sequences for the human (h) and murine (m) Flt3, FMS and KIT receptors were aligned using ClustalW (Larkin *et al.*, 2007). Strictly conserved residues are colored white on a black background and semi-conserved residues are shown in black bold. The signal peptides (grey) and predicted transmembrane (TM) helices (blue) are highlighted. Cysteine residues in the ectodomains are colored orange. Exons borders (red) were retrieved from www.ensembl.org. They correspond well to the boundaries of the Ig-like domains as seen in the KIT_{D1-D5} and $CSF1-R_{D1-D3}$ structures (Yuzawa *et al.*, 2007, Chen *et al.*, 2008). Note that Flt3 contains an extra exon preceding D1. Furthermore, Flt3 has a unique genomic structure in D1 and D2. Resdiues R381 and E386 of human KIT are indicated in purple. These residues are not conserved in Flt3. TM-helices were predicted using TMHMM (Krogh *et al.*, 2001).

Appendix B

```
                                 D1
hFlt3D1-D2    56 VSESPEDLGCALRPQSSGTVYEAAAVEVDVSASITLQVLVDAPGNISCLWVFKHSSLNCQ 115
mFlt3D1-D2    57 VRGSPEDLQCAPRRQSEGTVYEAATVEVAESGSITLQVQLATPGDLSCLWVFKHSSLGCQ 116
hFlt3D4-D5   347 -------------KGFINATNSSEDYEIDQYEEFCFSVRFKAYPQIRCTWTFSRKSFPCE 393
mFlt3D4-D5   348 -------------KGFINATSSQEEYEIDPYEKFCFSVRFKAYPRIRCTWIFSQASFPCE 394
                                 D4

                                                                D1        D2
hFlt3D1-D2   116 PHFDLQNRGVVSMVILKMTETQAGEYLLFIQSEATNYTILFTVSIRNTLLYTLRRPYFRK 175
mFlt3D1-D2   117 PHFDLQNRGIVSMAILNVTETQAGEYLLHIQSEAANYTVLFTVNVRDTQLYVLRRPYFRK 176
hFlt3D4-D5   394 -QKGLDNG--YSISKFCNHKHQPGEYIFHAENDDAQFTKMFTLNIR-------RKPQVLA 443
mFlt3D4-D5   395 -QRGLEDG--YSISKFCDHKNKPGEYIFYAENDDAQFTKMFTLNIR-------KKPQVLA 444
                                                            D4        D5

hFlt3D1-D2   176 MENQDALVCISESVPEPIVEWVLCDSQGESCKEESPAVVK---KEEKVLHELFGTD---- 228
mFlt3D1-D2   177 MENQDALLCISEGVPEPTVEWVLCSSHRESCKEEGPAVVR---KEEKVLHELFGTD---- 229
hFlt3D4-D5   444 EASASQASCFSDGYPLPSWTWKKCSDKSPNCTEEITEGVWNRKANRKVFGQWVSSSTLNM 503
mFlt3D4-D5   445 NASASQASCSSDGYPLPSWTWKKCSDKSPNCTEEIPEGVWNKKANRKVFGQWVSSSTLNM 504

                                                 D2
hFlt3D1-D2   229 --------IRCCARNELGRECTRLFTID-- 248
mFlt3D1-D2   230 --------IRCCARNALGRECTKLFTID-- 249
hFlt3D4-D5   504 SEAIKGFLVKCCAYNSLGTSCETILLNSPG 533
mFlt3D4-D5   505 SEAGKGLLVKCCAYNSMGTSCETIFLNSPG 534
                                                 D5
```

Sequence comparion of $Flt3_{D1-D2}$ and $Flt3_{D4-D5}$

The regions corresponding to human and murine Flt3 Ig-like domains D1 and D2 (residues 56 - 248 of hFlt3) were aligned with the regions corresponding to domains D4 and D5 (residues 347- 533 of hFlt3). Strictly conserved residues are colored white on a black background and semi-conserved residues are shown in black bold. Cysteine residues are colored orange. Human $Flt3_{D1-D2}$ and $Flt3_{D1-D5}$ share 26% sequence identity. Sequences were aligned using ClustalW (Larkin *et al.*, 2007).

Appendix C

Asp-N peptides

measured mass	calculated mass	sequence positions	remarks
2013.30	2013.09	248 – 265*	No glycosylation at #250
2081.56	2081.28	96 – 118	Glycosylation at #100, disulfide bridge between #103 and #114
3486.61	3486.78	29 – 43 62 – 76*	Glycosylation at #43, disulfide bridge between #35 and #65
4156.83	4156.11	29 – 43 62 – 83	Glycosylation at #43, disulfide bridge between #35 and #65

Glu-C peptides

measured mass	calculated mass	sequence positions	remarks
1499.56	1499.61	196 – 204 205 – 208	Disulfide bridge between #199 and #206
1628.60	1628.65	196 – 204 205 – 209*	Disulfide bridge between #199 and #206
1573.53	1573.72	347 – 357	Glycosylation at #351 and #354
1777.52	1777.78	347 – 360*	Glycosylation at #351 <u>or</u> #354
1980.58	1980.86	347 – 360*	Glycosylation at #351 and #354
4018.67	4018.32**	25 – 44* 63 – 77*	Glycosylation at #43, disulfide bridge between #35 and #65
(4134.96)	4133.35**	25 – 44* 62 – 77	Glycosylation at #43, disulfide bridge between #35 and #65
(4263.21)	4262.39**	24 – 44* 62 – 77	Glycosylation at #43, disulfide bridge between #35 and #65
5559.91	5560.18**	25 – 58 62 - 77	Glycosylation at #43, disulfide bridge between #35 and #65

Tryptic peptides

measured mass	calculated mass	sequence positions	remarks
1735.62	1735.76	381 – 387 389 – 395	Disulfide bridge between #381 and #392
1775.74	1775.71	323 – 334 272 - 273	Glycosylation at #323, disulfide bridge between #330 and #272
2187,03	1983,98	491 – 508	Glycosylation at #502
2214.78	2214.95	317 – 307	Glycosylation at #306 ***
2485,03	2281,98	467 – 485	Glycosylation at #473
3542.46	3542.78	133 – 161	Glycosylation at #151
3811.30	3811.62	348 – 372 406 – 410	Glycosylation at #351 <u>or</u> #354, disulfide bridge between #368 and #407
4014.43	4014.70	348 – 372 406 – 410	Glycosylation at #351 and #354, disulfide bridge between #368 and #407
(5332.29)	5333.06**	176 – 215* 231 – 234 240 – 243	Disulfide bridges between #184 – #231 and #232 – #241 (from X-ray data)
6614.06	6614.55**	176 – 215* 220 – 234* 240 – 243	Disulfide bridges between #184 – #231 and #232 – #241 (from X-ray data)
8998.44	8998.13**	35 – 41 50 – 108 109 – 123	Glycosylation at 100 ***, disulfide bridges between #35 - #65 and #103 – #114

* Peptide containing in-complete or on-specific cleavage
** Averaged values
*** Contains also very small amount of fucose (+ 146 Da)

Appendix D

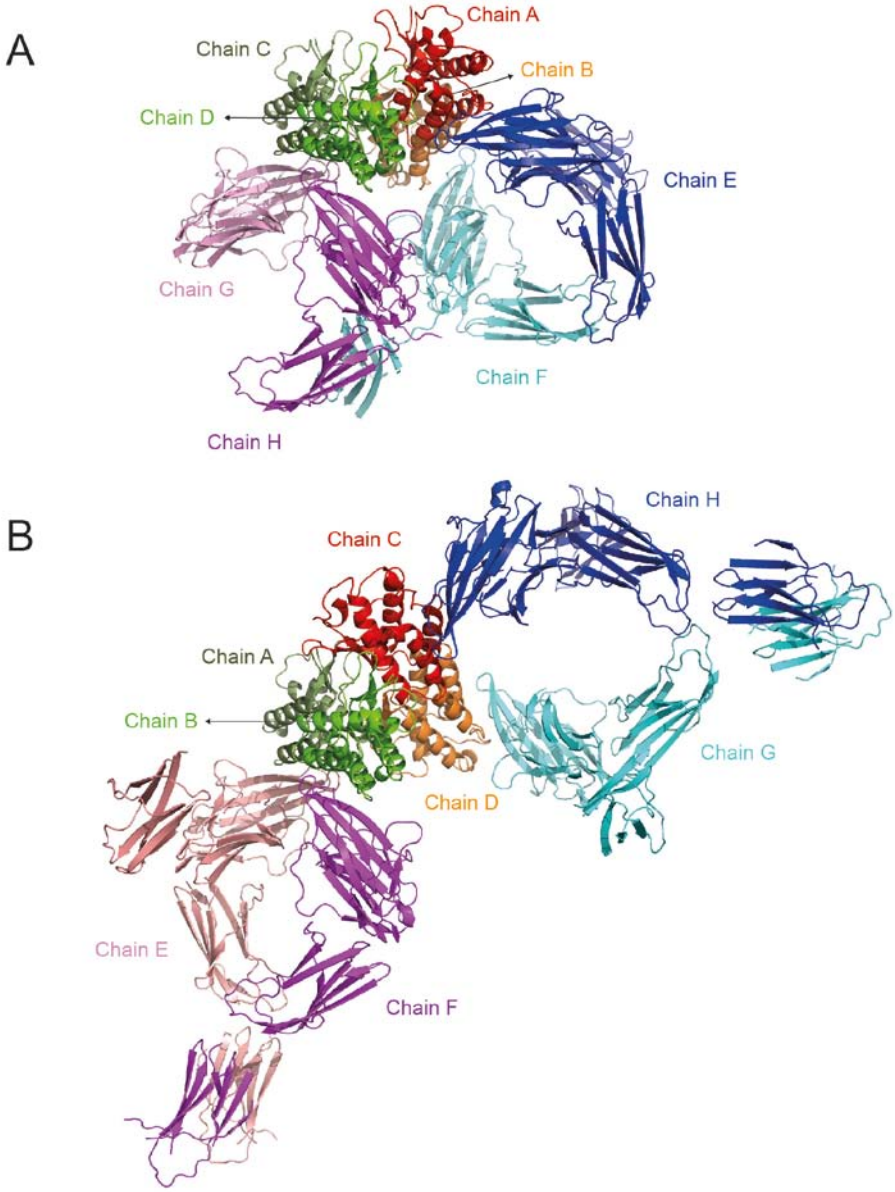

(A) The asymmetric unit of Flt3$_{D1-D4}$:FL complex crystals. The Flt3$_{D1-D4}$:FL complex crystallized in spacegroup P2$_1$ with two complexes in the asymmetric unit (asu). The two helical ligands in the different complexes (chains A-B and chains C-D) make extensive interactions in the asu. The receptor chains are labeled E, F, H and G. No density was visible for domains D1 of receptor chains G and H. D4 of chain G was also not modelled because of its weak density. **(B) The asymmetric unit of Flt3$_{D1-D5}$:FL complex crystals.** Similar to the Flt3$_{D1-D4}$:FL complex, the Flt3$_{D1-D5}$:FL complex crystallized in spacegroup P2$_1$ with two complexes in the assymetric unit (asu). The contacts between the two complexes are entirely mediated by the two ligands (chains A-B and chains C-D). The Flt3 receptor chains are labeled E, F, H and G. The structure was refined by rigid-body refinement in autoBuster 2.8.0 D1 of chain F could not be modelled.

Appendix E

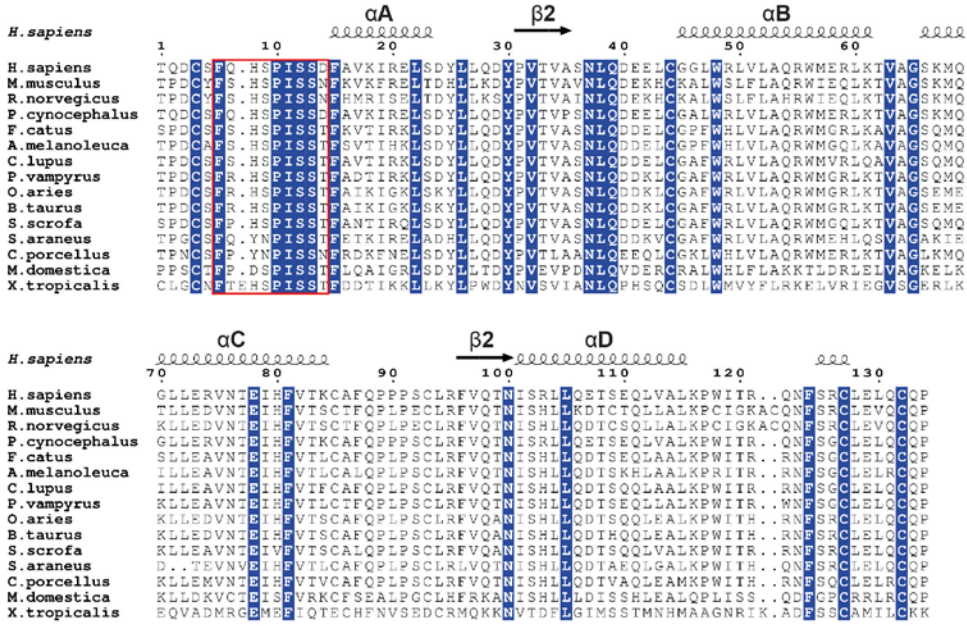

Interspecies comparison of FL sequences.

Sequence numbering and secondary structure assignment are according to the crystal structure of human Flt3 ligand (pdb 1ETE, Savvides *et al.*, 2000). Strictly conserved residues in the included FL sequences are colored white on a blue background. The highly conserved N-terminal receptor-binding loop (residues 6-14) is highlighted in a red box. Other strictly conserved residues include the cysteines involved in disulfide bridge formation, residues Glu78 and Phe81, which stabilize the N-terminal loop, and residues Leu27 and Tyr30 at the dimer interface. The sequences were retrieved from the NCBI and Ensembl databases: *Homo sapiens* (NP_001450.2), *Mus musculus* (NP_038548.3), *Rattus norvegicus* (XP_002725623.1), *Papio cynocephalus* (AAO72538.1), *Felis catus* (NP_001009842.1), *Ailuropoda melanoleuca* (XP_002917887.1), *Canis lupus familiaris* (NP_001003350.1), *Pteropus vampyrus* (ENSPVAT00000010957), *Ovis aries* (NP_001072128.1), *Bos taurus* (NP_851373.1), *Sus scrofa* (ACZ63257.1), *Sorex araneus* (ENSSARP00000002887), *Cavia porcellus* (ENSCPOP00000020385), *Monodelphis domestica* (XP_001379894), *Xenopus tropicalis* (XP_002938571.1). Sequences were aligned using ClustalW (Larkin *et al.*, 2007). Secondary structure information was extracted and rendered with ESPript (Gouet *et al.*, 2003).

REFERENCES

Abu-Duhier, F.M., Goodeve, A.C., Wilson, G.A., Care, R.S., Peake, I.R., and Reilly, J.T. (2001). Genomic structure of human FLT3: implications for mutational analysis. Br J Haematol *113*, 1076-1077.

Adams, P.D., Afonine, P.V., Bunkoczi, G., Chen, V.B., Davis, I.W., Echols, N., Headd, J.J., Hung, L.W., Kapral, G.J., Grosse-Kunstleve, R.W., *et al.* (2010). PHENIX: a comprehensive Python-based system for macromolecular structure solution. Acta Crystallogr D Biol Crystallogr *66*, 213-221.

Adolfsson, J., Borge, O.J., Bryder, D., Theilgaard-Monch, K., Astrand-Grundstrom, I., Sitnicka, E., Sasaki, Y., and Jacobsen, S.E. (2001). Upregulation of Flt3 expression within the bone marrow Lin(-)Sca1(+)c-kit(+) stem cell compartment is accompanied by loss of self-renewal capacity. Immunity *15*, 659-669.

Agnes, F., Shamoon, B., Dina, C., Rosnet, O., Birnbaum, D., and Galibert, F. (1994). Genomic structure of the downstream part of the human FLT3 gene: exon/intron structure conservation among genes encoding receptor tyrosine kinases (RTK) of subclass III. Gene *145*, 283-288.

Antonysamy, M.A., and Thomson, A.W. (2000). Flt3 ligand (FL) and its influence on immune reactivity. Cytokine *12*, 87-100.

Arakawa, T., and Tsumoto, K. (2003). The effects of arginine on refolding of aggregated proteins: not facilitate refolding, but suppress aggregation. Biochem Biophys Res Commun *304*, 148-152.

Arbach, H., Viglasky, V., Lefeu, F., Guinebretiere, J.M., Ramirez, V., Bride, N., Boualaga, N., Bauchet, T., Peyrat, J.P., Mathieu, M.C., *et al.* (2006). Epstein-Barr virus (EBV) genome and expression in breast cancer tissue: effect of EBV infection of breast cancer cells on resistance to paclitaxel (Taxol). J Virol *80*, 845-853.

Aricescu, A.R., Lu, W., and Jones, E.Y. (2006). A time- and cost-efficient system for high-level protein production in mammalian cells. Acta Crystallogr D Biol Crystallogr *62*, 1243-1250.

Auerbach, R., Huang, H., and Lu, L. (1996). Hematopoietic stem cells in the mouse embryonic yolk sac. Stem Cells *14*, 269-280.

Bae, J.H., and Schlessinger, J. (2010) Asymmetric tyrosine kinase arrangements in activation or autophosphorylation of receptor tyrosine kinases. Mol Cells *29*, 443-448.

Ball, S.G., Shuttleworth, C.A., and Kielty, C.M. (2007). Vascular endothelial growth factor can signal through platelet-derived growth factor receptors. J Cell Biol *177*, 489-500.

Barash, S., Wang, W., and Shi, Y. (2002). Human secretory signal peptide description by hidden Markov model and generation of a strong artificial signal peptide for secreted protein expression. Biochem Biophys Res Commun *294*, 835-842.

Barleon, B., Totzke, F., Herzog, C., Blanke, S., Kremmer, E., Siemeister, G., Marme, D., and Martiny-Baron, G. (1997). Mapping of the sites for ligand binding and receptor dimerization at the extracellular domain of the vascular endothelial growth factor receptor FLT-1. J Biol Chem *272*, 10382-10388.

Bell, C.A., Tynan, J.A., Hart, K.C., Meyer, A.N., Robertson, S.C., and Donoghue, D.J. (2000). Rotational coupling of the transmembrane and kinase domains of the Neu receptor tyrosine kinase. Mol Biol Cell *11*, 3589-3599.

Bennasroune, A., Fickova, M., Gardin, A., Dirrig-Grosch, S., Aunis, D., Cremel, G., and Hubert, P. (2004). Transmembrane peptides as inhibitors of ErbB receptor signaling. Mol Biol Cell *15*, 3464-3474.

Besmer, P., Murphy, J.E., George, P.C., Qiu, F.H., Bergold, P.J., Lederman, L., Snyder, H.W., Jr., Brodeur, D., Zuckerman, E.E., and Hardy, W.D. (1986). A new acute transforming feline retrovirus and relationship of its oncogene v-kit with the protein kinase gene family. Nature *320*, 415-421.

Birg, F., Courcoul, M., Rosnet, O., Bardin, F., Pebusque, M.J., Marchetto, S., Tabilio, A., Mannoni, P., and Birnbaum, D. (1992). Expression of the FMS/KIT-like gene FLT3 in human acute leukemias of the myeloid and lymphoid lineages. Blood *80*, 2584-2593.

Blanc, E., Roversi, P., Vonrhein, C., Flensburg, C., Lea, S.M., and Bricogne, G. (2004). Refinement of severely incomplete structures with maximum likelihood in BUSTER-TNT. Acta Crystallogr D Biol Crystallogr *60*, 2210-2221.

Blechman, J.M., Lev, S., Brizzi, M.F., Leitner, O., Pegoraro, L., Givol, D., and Yarden, Y. (1993a). Soluble c-kit proteins and antireceptor monoclonal antibodies confine the binding site of the stem cell factor. J Biol Chem *268*, 4399-4406.

Blechman, J.M., Lev, S., Givol, D., and Yarden, Y. (1993b). Structure-function analyses of the kit receptor for the steel factor. Stem Cells *11 Suppl 2*, 12-21.

Blechman, J.M., Lev, S., Barg, J., Eisenstein, M., Vaks, B., Vogel, Z., Givol, D., and Yarden, Y. (1995). The fourth immunoglobulin domain of the stem cell factor receptor couples ligand binding to signal transduction. Cell *80*, 103-113.

Bocharov, E.V., Mayzel, M.L., Volynsky, P.E., Goncharuk, M.V., Ermolyuk, Y.S., Schulga, A.A., Artemenko, E.O., Efremov, R.G., and Arseniev, A.S. (2008a). Spatial structure and pH-dependent conformational diversity of dimeric transmembrane domain of the receptor tyrosine kinase EphA1. J Biol Chem *283*, 29385-29395.

Bocharov, E.V., Mineev, K.S., Volynsky, P.E., Ermolyuk, Y.S., Tkach, E.N., Sobol, A.G., Chupin, V.V., Kirpichnikov, M.P., Efremov, R.G., and Arseniev, A.S. (2008b). Spatial structure of the dimeric transmembrane domain of the growth factor receptor ErbB2 presumably corresponding to the receptor active state. J Biol Chem *283*, 6950-6956.

Bocharov, E.V., Mayzel, M.L., Volynsky, P.E., Mineev, K.S., Tkach, E.N., Ermolyuk, Y.S., Schulga, A.A., Efremov, R.G., and Arseniev, A.S. (2010) Left-handed dimer of EphA2 transmembrane domain: Helix packing diversity among receptor tyrosine kinases. Biophys J *98*, 881-889.

Brasel, K., McKenna, H.J., Morrissey, P.J., Charrier, K., Morris, A.E., Lee, C.C., Williams, D.E., and Lyman, S.D. (1996). Hematologic effects of flt3 ligand *in vivo* in mice. Blood *88*, 2004-2012.

Brigogne, G., Blanc, E., Brandl, M., Flensburg, C., Keller, P., Paciorek, W., Roversi, P., Smart, O.S., Vorhein, C., and Womack, T.O. (2009). BUSTER, version 2.8.0. Cambridge, United Kingdom: Global Phasing Ltd.

Broudy, V.C., Lin, N.L., Buhring, H.J., Komatsu, N., and Kavanagh, T.J. (1998). Analysis of c-kit receptor dimerization by fluorescence resonance energy transfer. Blood *91*, 898-906.

Broudy, V.C., Lin, N.L., and Sabath, D.F. (2001). The fifth immunoglobulin-like domain of the Kit receptor is required for proteolytic cleavage from the cell surface. Cytokine *15*, 188-195.

Bryder, D., Rossi, D.J., and Weissman, I.L. (2006). Hematopoietic stem cells: the paradigmatic tissue-specific stem cell. Am J Pathol *169*, 338-346.

Buza-Vidas, N., Cheng, M., Duarte, S., Nozad, H., Jacobsen, S.E., and Sitnicka, E. (2007). Crucial role of FLT3 ligand in immune reconstitution after bone marrow transplantation and high-dose chemotherapy. Blood *110*, 424-432.

Camargo, F.D., Chambers, S.M., Drew, E., McNagny, K.M., and Goodell, M.A. (2006). Hematopoietic stem cells do not engraft with absolute efficiencies. Blood *107*, 501-507.

Carlberg, K., and Rohrschneider, L. (1994). The effect of activating mutations on dimerization, tyrosine phosphorylation and internalization of the macrophage colony stimulating factor receptor. Mol Biol Cell *5*, 81-95.

Carow, C.E., Kim, E., Hawkins, A.L., Webb, H.D., Griffin, C.A., Jabs, E.W., Civin, C.I., and Small, D. (1995). Localization of the human stem cell tyrosine kinase-1 gene (FLT3) to 13q12-->q13. Cytogenet Cell Genet *70*, 255-257.

Chabot, B., Stephenson, D.A., Chapman, V.M., Besmer, P., and Bernstein, A. (1988). The proto-oncogene c-kit encoding a transmembrane tyrosine kinase receptor maps to the mouse W locus. Nature *335*, 88-89.

Chan, P.M. (2011). Differential signaling of Flt3 activating mutations in acute myeloid leukemia: a working model. Protein Cell.

Chang, V.T., Crispin, M., Aricescu, A.R., Harvey, D.J., Nettleship, J.E., Fennelly, J.A., Yu, C., Boles, K.S., Evans, E.J., Stuart, D.I., *et al.* (2007). Glycoprotein structural genomics: solving the glycosylation problem. Structure *15*, 267-273.

Chen, L., Placone, J., Novicky, L., and Hristova, K. (2010). The extracellular domain of fibroblast growth factor receptor 3 inhibits ligand-independent dimerization. Sci Signal *3*, ra86.

Chen, V.B., Arendall, W.B., 3rd, Headd, J.J., Keedy, D.A., Immormino, R.M., Kapral, G.J., Murray, L.W., Richardson, J.S., and Richardson, D.C. (2010). MolProbity: all-atom structure validation for macromolecular crystallography. Acta Crystallogr D Biol Crystallogr *66*, 12-21.

Chen, X., Liu, H., Focia, P.J., Shim, A.H., and He, X. (2008). Structure of macrophage colony stimulating factor bound to FMS: diverse signaling assemblies of class III receptor tyrosine kinases. Proc Natl Acad Sci U S A *105*, 18267-18272.

Chillon, M.C., Fernandez, C., Garcia-Sanz, R., Balanzategui, A., Ramos, F., Fernandez-Calvo, J., Gonzalez, M., and Miguel, J.F. (2004). FLT3-activating mutations are associated with poor prognostic features in AML at diagnosis but they are not an independent prognostic factor. Hematol J *5*, 239-246.

Chklovskaia, E., Jansen, W., Nissen, C., Lyman, S.D., Rahner, C., Landmann, L., and Wodnar-Filipowicz, A. (1999). Mechanism of flt3 ligand expression in bone marrow failure: translocation from intracellular stores to the surface of T lymphocytes after chemotherapy-induced suppression of hematopoiesis. Blood *93*, 2595-2604.

Chklovskaia, E., Nowbakht, P., Nissen, C., Gratwohl, A., Bargetzi, M., and Wodnar-Filipowicz, A. (2004). Reconstitution of dendritic and natural killer-cell subsets after allogeneic stem cell transplantation: effects of endogenous flt3 ligand. Blood *103*, 3860-3868.

Choudhary, C., Brandts, C., Schwable, J., Tickenbrock, L., Sargin, B., Ueker, A., Bohmer, F.D., Berdel, W.E., Muller-Tidow, C., and Serve, H. (2007). Activation mechanisms of STAT5 by oncogenic Flt3-ITD. Blood *110*, 370-374.

Christensen, J.L., and Weissman, I.L. (2001). Flk-2 is a marker in hematopoietic stem cell differentiation: a simple method to isolate long-term stem cells. Proc Natl Acad Sci U S A *98*, 14541-14546.

Christinger, H.W., Fuh, G., de Vos, A.M., and Wiesmann, C. (2004). The crystal structure of placental growth factor in complex with domain 2 of vascular endothelial growth factor receptor-1. J Biol Chem *279*, 10382-10388.

Chung, I., Akita, R., Vandlen, R., Toomre, D., Schlessinger, J., and Mellman, I. (2010). Spatial control of EGF receptor activation by reversible dimerization on living cells. Nature *464*, 783-787.

Constantinescu, S.N., Keren, T., Socolovsky, M., Nam, H., Henis, Y.I., and Lodish, H.F. (2001). Ligand-independent oligomerization of cell-surface erythropoietin receptor is mediated by the transmembrane domain. Proc Natl Acad Sci U S A *98*, 4379-4384.

Cowtan, K. (2006). The Buccaneer software for automated model building. 1. Tracing protein chains. Acta Crystallogr D Biol Crystallogr *62*, 1002-1011.

Cowtan, K. (2010). Recent developments in classical density modification. Acta Crystallogr D Biol Crystallogr *66*, 470-478.

Davis-Smyth, T., Chen, H., Park, J., Presta, L.G., and Ferrara, N. (1996). The second immunoglobulin-like domain of the VEGF tyrosine kinase receptor Flt-1 determines ligand binding and may initiate a signal transduction cascade. EMBO J *15*, 4919-4927.

Dehlin, M., Bokarewa, M., Rottapel, R., Foster, S.J., Magnusson, M., Dahlberg, L.E., and Tarkowski, A. (2008). Intra-articular fms-like tyrosine kinase 3 ligand expression is a driving force in induction and progression of arthritis. PLoS ONE *3*, e3633.

Dehmel, U., Zaborski, M., Meierhoff, G., Rosnet, O., Birnbaum, D., Ludwig, W.D., Quentmeier, H., and Drexler, H.G. (1996). Effects of FLT3 ligand on human leukemia cells. I. Proliferative response of myeloid leukemia cells. Leukemia *10*, 261-270.

DiNitto, J.P., Deshmukh, G.D., Zhang, Y., Jacques, S.L., Coli, R., Worrall, J.W., Diehl, W., English, J.M., and Wu, J.C. (2010). Function of activation loop tyrosine phosphorylation in the mechanism of c-Kit auto-activation and its implication in sunitinib resistance. J Biochem *147*, 601-609.

Dong, J., McPherson, C.M., and Stambrook, P.J. (2002). Flt-3 ligand: a potent dendritic cell stimulator and novel antitumor agent. Cancer Biol Ther *1*, 486-489.

Dosch, D.D., and Ballmer-Hofer, K. (2010) Transmembrane domain-mediated orientation of receptor monomers in active VEGFR-2 dimers. FASEB J *24*, 32-38.

Drexler, H.G., Meyer, C., and Quentmeier, H. (1999). Effects of FLT3 ligand on proliferation and survival of myeloid leukemia cells. Leuk Lymphoma *33*, 83-91.

Drexler, H.G., and Quentmeier, H. (2004). FLT3: receptor and ligand. Growth Factors *22*, 71-73.

Dykstra, B., Kent, D., Bowie, M., McCaffrey, L., Hamilton, M., Lyons, K., Lee, S.J., Brinkman, R., and Eaves, C. (2007). Long-term propagation of distinct hematopoietic differentiation programs *in vivo*. Cell Stem Cell *1*, 218-229.

Ebihara, Y., Wada, M., Ueda, T., Xu, M.J., Manabe, A., Tanaka, R., Ito, M., Mugishima, H., Asano, S., Nakahata, T., *et al.* (2002). Reconstitution of human haematopoiesis in non-obese diabetic/severe combined immunodeficient mice by clonal cells expanded from single CD34+CD38- cells expressing Flk2/Flt3. Br J Haematol *119*, 525-534.

Eidenschenk, C., Crozat, K., Krebs, P., Arens, R., Popkin, D., Arnold, C.N., Blasius, A.L., Benedict, C.A., Moresco, E.M., Xia, Y., *et al.* (2010). Flt3 permits survival during infection by rendering dendritic cells competent to activate NK cells. Proc Natl Acad Sci U S A *107*, 9759-9764.

Eklund, E.A. (2010). Genomic analysis of acute myeloid leukemia: potential for new prognostic indicators. Curr Opin Hematol *17*, 75-78.

Elegheert J., Desfosses A., Shkumatov A., Wu X., Bracke N., Verstraete K., Van Craenenbroeck K., Brooks B.R., Svergun D., Vergauwen B., Gutsche I., Savvides S.N. (*in preparation).* Architecture and plasticity of human Colony-Stimulating Factor 1 Receptor revealed by its complete extracellular signaling complex.

Emsley, P., Lohkamp, B., Scott, W.G., and Cowtan, K. (2010). Features and development of Coot. Acta Crystallogr D Biol Crystallogr *66*, 486-501.

Escobar, S., brasel, K., Anderberg, R., and Lyman, S. (1998). Structure function studies of human Flt3 ligand. Blood *86*, 21a.

Finger, C., Escher, C., and Schneider, D. (2009). The single transmembrane domains of human receptor tyrosine kinases encode self-interactions. Sci Signal *2*, ra56.

Fleishman, S.J., Schlessinger, J., and Ben-Tal, N. (2002). A putative molecular-activation switch in the transmembrane domain of erbB2. Proc Natl Acad Sci U S A *99*, 15937-15940

Fong, L., Hou, Y., Rivas, A., Benike, C., Yuen, A., Fisher, G.A., Davis, M.M., and Engleman, E.G. (2001). Altered peptide ligand vaccination with Flt3 ligand expanded dendritic cells for tumor immunotherapy. Proc Natl Acad Sci U S A *98*, 8809-8814.

Fröhling, S., Scholl, C., Levine, R.L., Loriaux, M., Boggon, T.J., Bernard, O.A., Berger, R., Dohner, H., Dohner, K., Ebert, B.L., *et al.* (2007). Identification of driver and passenger mutations of FLT3 by high-throughput DNA sequence analysis and functional assessment of candidate alleles. Cancer Cell *12*, 501-513.

Fuh, G., Li, B., Crowley, C., Cunningham, B., and Wells, J.A. (1998). Requirements for binding and signaling of the kinase domain receptor for vascular endothelial growth factor. J Biol Chem *273*, 11197-11204.

Garceau, V., Smith, J., Paton, I.R., Davey, M., Fares, M.A., Sester, D.P., Burt, D.W., and Hume, D.A. (2010). Pivotal Advance: Avian colony-stimulating factor 1 (CSF-1), interleukin-34 (IL-34), and CSF-1 receptor genes and gene products. J Leukoc Biol *87*, 753-764.

Garrett, T.P., McKern, N.M., Lou, M., Elleman, T.C., Adams, T.E., Lovrecz, G.O., Zhu, H.J., Walker, F., Frenkel, M.J., Hoyne, P.A., *et al.* (2002). Crystal structure of a truncated

epidermal growth factor receptor extracellular domain bound to transforming growth factor alpha. Cell *110*, 763-773.

Gilliland, D.G., and Griffin, J.D. (2002). The roles of FLT3 in hematopoiesis and leukemia. Blood *100*, 1532-1542.

Gouet, P., Robert, X., and Courcelle, E. (2003). ESPript/ENDscript: Extracting and rendering sequence and 3D information from atomic structures of proteins. Nucleic Acids Res *31*, 3320-3323.

Graddis, T.J., Brasel, K., Friend, D., Srinivasan, S., Wee, S., Lyman, S.D., March, C.J., and McGrew, J.T. (1998). Structure-function analysis of FLT3 ligand-FLT3 receptor interactions using a rapid functional screen. J Biol Chem *273*, 17626-17633.

Grassot, J., Gouy, M., Perriere, G., and Mouchiroud, G. (2006). Origin and molecular evolution of receptor tyrosine kinases with immunoglobulin-like domains. Mol Biol Evol *23*, 1232-1241.

Gratwohl, A., John, L., Baldomero, H., Roth, J., Tichelli, A., Nissen, C., Lyman, S.D., and Wodnar-Filipowicz, A. (1998). FLT-3 ligand provides hematopoietic protection from total body irradiation in rabbits. Blood *92*, 765-769.

Griffith, J., Black, J., Faerman, C., Swenson, L., Wynn, M., Lu, F., Lippke, J., and Saxena, K. (2004). The structural basis for autoinhibition of FLT3 by the juxtamembrane domain. Mol Cell *13*, 169-178.

Halaby, D.M., Poupon, A., and Mornon, J. (1999). The immunoglobulin fold family: sequence analysis and 3D structure comparisons. Protein Eng *12*, 563-571.

Hannum, C., Culpepper, J., Campbell, D., McClanahan, T., Zurawski, S., Bazan, J.F., Kastelein, R., Hudak, S., Wagner, J., Mattson, J., *et al.* (1994). Ligand for FLT3/FLK2 receptor tyrosine kinase regulates growth of haematopoietic stem cells and is encoded by variant RNAs. Nature *368*, 643-648.

Harpaz, Y., and Chothia, C. (1994). Many of the immunoglobulin superfamily domains in cell adhesion molecules and surface receptors belong to a new structural set which is close to that containing variable domains. J Mol Biol *238*, 528-539.

Heinrich, M.C., Corless, C.L., Duensing, A., McGreevey, L., Chen, C.J., Joseph, N., Singer, S., Griffith, D.J., Haley, A., Town, A., *et al.* (2003). PDGFRA activating mutations in gastrointestinal stromal tumors. Science *299*, 708-710.

Heldin, C.H., Ostman, A., and Ronnstrand, L. (1998). Signal transduction via platelet-derived growth factor receptors. Biochim Biophys Acta *1378*, F79-113.

Heras, B., and Martin, J.L. (2005). Post-crystallization treatments for improving diffraction quality of protein crystals. Acta Crystallogr D Biol Crystallogr *61*, 1173-1180.

Heymann, J.B., Cardone, G., Winkler, D.C., and Steven, A.C. (2008). Computational resources for cryo-electron tomography in Bsoft. J Struct Biol *161*, 232-242.

Hicklin, D.J., and Ellis, L.M. (2005). Role of the vascular endothelial growth factor pathway in tumor growth and angiogenesis. J Clin Oncol *23*, 1011-1027.

Hintze, B.J. and Johnson, S.J. (2010). ResDe: a new tool for visual definition of distance restraints for crystallographic refinement. J Appl Cryst *43*, 1540-1542

Hirota, S., Isozaki, K., Moriyama, Y., Hashimoto, K., Nishida, T., Ishiguro, S., Kawano, K., Hanada, M., Kurata, A., Takeda, M., *et al.* (1998). Gain-of-function mutations of c-kit in human gastrointestinal stromal tumors. Science *279*, 577-580.

Horiuchi, K., Morioka, H., Takaishi, H., Akiyama, H., Blobel, C.P., and Toyama, Y. (2009). Ectodomain shedding of FLT3 ligand is mediated by TNF-alpha converting enzyme. J Immunol *182*, 7408-7414.

Hsu, Y.R., Wu, G.M., Mendiaz, E.A., Syed, R., Wypych, J., Toso, R., Mann, M.B., Boone, T.C., Narhi, L.O., Lu, H.S., *et al.* (1997). The majority of stem cell factor exists as monomer under physiological conditions. Implications for dimerization mediating biological activity. J Biol Chem *272*, 6406-6415.

Huang, E., Nocka, K., Beier, D.R., Chu, T.Y., Buck, J., Lahm, H.W., Wellner, D., Leder, P., and Besmer, P. (1990). The hematopoietic growth factor KL is encoded by the Sl locus and is the ligand of the c-kit receptor, the gene product of the W locus. Cell *63*, 225-233.

Hubbard, S.R., and Till, J.H. (2000). Protein tyrosine kinase structure and function. Annu Rev Biochem *69*, 373-398.

Hubbard, S.R. (2004). Juxtamembrane autoinhibition in receptor tyrosine kinases. Nat Rev Mol Cell Biol *5*, 464-471.

Hubbard, S.R., and Miller, W.T. (2007). Receptor tyrosine kinases: mechanisms of activation and signaling. Curr Opin Cell Biol *19*, 117-123.

Hudak, S., Hunte, B., Culpepper, J., Menon, S., Hannum, C., Thompson-Snipes, L., and Rennick, D. (1995). FLT3/FLK2 ligand promotes the growth of murine stem cells and the expansion of colony-forming cells and spleen colony-forming units. Blood *85*, 2747-2755.

Huse, M., and Kuriyan, J. (2002). The conformational plasticity of protein kinases. Cell *109*, 275-282.

Huyton, T., Zhang, J.G., Luo, C.S., Lou, M.Z., Hilton, D.J., Nicola, N.A., and Garrett, T.P. (2007). An unusual cytokine:Ig-domain interaction revealed in the crystal structure of leukemia inhibitory factor (LIF) in complex with the LIF receptor. Proc Natl Acad Sci U S A *104*, 12737-12742.

Irusta, P.M., Luo, Y., Bakht, O., Lai, C.C., Smith, S.O., and DiMaio, D. (2002). Definition of an inhibitory juxtamembrane WW-like domain in the platelet-derived growth factor beta receptor. J Biol Chem *277*, 38627-38634.

Janin, J., Bahadur, R.P., and Chakrabarti, P. (2008). Protein-protein interaction and quaternary structure. Q Rev Biophys *41*, 133-180.

Jemal, A., Siegel, R., Xu, J., and Ward, E. (2010). Cancer statistics, 2010. CA Cancer J Clin *60*, 277-300.

Jiang, X., Gurel, O., Mendiaz, E.A., Stearns, G.W., Clogston, C.L., Lu, H.S., Osslund, T.D., Syed, R.S., Langley, K.E., and Hendrickson, W.A. (2000). Structure of the active core of human stem cell factor and analysis of binding to its receptor kit. EMBO J *19*, 3192-3203.

Kabsch, W. (2010). Xds. Acta Crystallogr D Biol Crystallogr *66*, 125-132.

Kancha, R.K., Grundler, R., Peschel, C., and Duyster, J. (2007). Sensitivity toward sorafenib and sunitinib varies between different activating and drug-resistant FLT3-ITD mutations. Exp Hematol *35*, 1522-1526.

Kantardjieff, K.A., and Rupp, B. (2003). Matthews coefficient probabilities: Improved estimates for unit cell contents of proteins, DNA, and protein-nucleic acid complex crystals. Protein Sci *12*, 1865-1871.

Karsunky, H., Merad, M., Cozzio, A., Weissman, I.L., and Manz, M.G. (2003). Flt3 ligand regulates dendritic cell development from Flt3+ lymphoid and myeloid-committed progenitors to Flt3+ dendritic cells *in vivo*. J Exp Med *198*, 305-313.

Keller, S., Pojer, F., Heide, L., and Lawson, D.M. (2006). Molecular replacement in the 'twilight zone': structure determination of the non-haem iron oxygenase NovR from Streptomyces spheroides through repeated density modification of a poor molecular-replacement solution. Acta Crystallogr D Biol Crystallogr *62*, 1564-1570.

Kikushige, Y., Yoshimoto, G., Miyamoto, T., Iino, T., Mori, Y., Iwasaki, H., Niiro, H., Takenaka, K., Nagafuji, K., Harada, M., *et al.* (2008). Human Flt3 is expressed at the hematopoietic stem cell and the granulocyte/macrophage progenitor stages to maintain cell survival. J Immunol *180*, 7358-7367.

Kindler, T., Lipka, D.B., and Fischer, T. (2010). FLT3 as a therapeutic target in AML: still challenging after all these years. Blood.

Kiyoi, H., Towatari, M., Yokota, S., Hamaguchi, M., Ohno, R., Saito, H., and Naoe, T. (1998). Internal tandem duplication of the FLT3 gene is a novel modality of elongation mutation which causes constitutive activation of the product. Leukemia *12*, 1333-1337.

Kiyoi, H., Ohno, R., Ueda, R., Saito, H., and Naoe, T. (2002). Mechanism of constitutive activation of FLT3 with internal tandem duplication in the juxtamembrane domain. Oncogene *21*, 2555-2563.

Kiyoi, H., Yanada, M., and Ozekia, K. (2005). Clinical significance of FLT3 in leukemia. Int J Hematol *82*, 85-92.

Kiyoi, H., and Naoe, T. (2006). Biology, clinical relevance, and molecularly targeted therapy in acute leukemia with FLT3 mutation. Int J Hematol *83*, 301-308.

Konarev, P.V., Volkov, V.V., Sokolova, A.V., Koch, M.H.J., and Svergun, D.I. (2003). PRIMUS: a Windows PC-based system for small-angle scattering data analysis. Journal of Applied Crystallography *36*, 1277-1282.

Koths, K. (1997). Structure-function studies on human macrophage colony-stimulating factor (M-CSF). Mol Reprod Dev *46*, 31-37; discussion 37-38.

Krogh, A., Larsson, B., von Heijne, G., and Sonnhammer, E.L. (2001). Predicting transmembrane protein topology with a hidden Markov model: application to complete genomes. J Mol Biol *305*, 567-580.

Laemmli, U.K. (1970). Cleavage of structural proteins during the assembly of the head of bacteriophage T4. Nature *227*, 680-685.

Larkin, M.A., Blackshields, G., Brown, N.P., Chenna, R., McGettigan, P.A., McWilliam, H., Valentin, F., Wallace, I.M., Wilm, A., Lopez, R., *et al.* (2007). Clustal W and Clustal X version 2.0. Bioinformatics *23*, 2947-2948.

Lavagna, C., Marchetto, S., Birnbaum, D., and Rosnet, O. (1995). Identification and characterization of a functional murine FLT3 isoform produced by exon skipping. J Biol Chem *270*, 3165-3171.

Lemmon, M.A., Pinchasi, D., Zhou, M., Lax, I., and Schlessinger, J. (1997). Kit receptor dimerization is driven by bivalent binding of stem cell factor. J Biol Chem *272*, 6311-6317.

Lemmon, M.A., and Ferguson, K.M. (2007). A new twist in the transmembrane signaling tool-kit. Cell *130*, 213-215.

Lemmon, M.A., and Schlessinger, J. (2010). Cell signaling by receptor tyrosine kinases. Cell *141*, 1117-1134.

Leppänen, V.M., Prota, A.E., Jeltsch, M., Anisimov, A., Kalkkinen, N., Strandin, T., Lankinen, H., Goldman, A., Ballmer-Hofer, K., and Alitalo, K. (2010). Structural determinants of growth factor binding and specificity by VEGF receptor 2. Proc Natl Acad Sci U S A *107*, 2425-2430.

Lev, S., Yarden, Y., and Givol, D. (1992a). Dimerization and activation of the kit receptor by monovalent and bivalent binding of the stem cell factor. J Biol Chem *267*, 15970-15977.

Lev, S., Yarden, Y., and Givol, D. (1992b). A recombinant ectodomain of the receptor for the stem cell factor (SCF) retains ligand-induced receptor dimerization and antagonizes SCF-stimulated cellular responses. J Biol Chem *267*, 10866-10873.

Lev, S., Blechman, J., Nishikawa, S., Givol, D., and Yarden, Y. (1993). Interspecies molecular chimeras of kit help define the binding site of the stem cell factor. Mol Cell Biol *13*, 2224-2234.

Li, E., You, M., and Hristova, K. (2005). Sodium dodecyl sulfate-polyacrylamide gel electrophoresis and forster resonance energy transfer suggest weak interactions between fibroblast growth factor receptor 3 (FGFR3) transmembrane domains in the absence of extracellular domains and ligands. Biochemistry *44*, 352-360.

Li, E., and Hristova, K. (2006). Role of receptor tyrosine kinase transmembrane domains in cell signaling and human pathologies. Biochemistry *45*, 6241-6251.

Li, E., You, M., and Hristova, K. (2006). FGFR3 dimer stabilization due to a single amino acid pathogenic mutation. J Mol Biol *356*, 600-612.

Li, W., and Stanley, E.R. (1991). Role of dimerization and modification of the CSF-1 receptor in its activation and internalization during the CSF-1 response. EMBO J *10*, 277-288.

Li, Y., Li, H., Wang, M.N., Lu, D., Bassi, R., Wu, Y., Zhang, H., Balderes, P., Ludwig, D.L., Pytowski, B., *et al.* (2004). Suppression of leukemia expressing wild-type or ITD-mutant FLT3 receptor by a fully human anti-FLT3 neutralizing antibody. Blood *104*, 1137-1144.

Li, Z., and Li, L. (2006). Understanding hematopoietic stem-cell microenvironments. Trends Biochem Sci *31*, 589-595.

Liu, H., Chen, X., Focia, P.J., and He, X. (2007). Structural basis for stem cell factor-KIT signaling and activation of class III receptor tyrosine kinases. EMBO J *26*, 891-901.

Lin, H., Lee, E., Hestir, K., Leo, C., Huang, M., Bosch, E., Halenbeck, R., Wu, G., Zhou, A., Behrens, D., *et al.* (2008). Discovery of a cytokine and its receptor by functional screening of the extracellular proteome. Science *320*, 807-811.

Liu, K., Victora, G.D., Schwickert, T.A., Guermonprez, P., Meredith, M.M., Yao, K., Chu, F.F., Randolph, G.J., Rudensky, A.Y., and Nussenzweig, M. (2009). *In vivo* analysis of dendritic cell development and homeostasis. Science *324*, 392-397.

Liu, K., and Nussenzweig, M.C. (2010). Origin and development of dendritic cells. Immunol Rev *234*, 45-54.

Lokker, N.A., O'Hare, J.P., Barsoumian, A., Tomlinson, J.E., Ramakrishnan, V., Fretto, L.J., and Giese, N.A. (1997). Functional importance of platelet-derived growth factor (PDGF) receptor extracellular immunoglobulin-like domains. Identification of PDGF binding site and neutralizing monoclonal antibodies. J Biol Chem *272*, 33037-33044.

Lu, C.M., Yu, J.F., Huang, W.D., Zhou, X., Zhang, W.Y., Xi, H., and Zhang, X.G. (2002). Increasing bioactivity of Flt3 ligand by fusing two identical soluble domains. Sheng Wu Hua Xue Yu Sheng Wu Wu Li Xue Bao (Shanghai) *34*, 697-702.

Lu, H.S., Clogston, C.L., Wypych, J., Parker, V.P., Lee, T.D., Swiderek, K., Baltera, R.F., Jr., Patel, A.C., Chang, D.C., Brankow, D.W., *et al.* (1992). Post-translational processing of membrane-associated recombinant human stem cell factor expressed in Chinese hamster ovary cells. Arch Biochem Biophys *298*, 150-158.

Lu, H.S., Chang, W.C., Mendiaz, E.A., Mann, M.B., Langley, K.E., and Hsu, Y.R. (1995). Spontaneous dissociation-association of monomers of the human-stem-cell-factor dimer. Biochem J *305 (Pt 2)*, 563-568.

Lu, H.S., Jones, M.D., Shieh, J.H., Mendiaz, E.A., Feng, D., Watler, P., Narhi, L.O., and Langley, K.E. (1996). Isolation and characterization of a disulfide-linked human stem cell factor dimer. Biochemical, biophysical, and biological comparison to the noncovalently held dimer. J Biol Chem *271*, 11309-11316.

Ludtke, S.J., Baldwin, P.R., and Chiu, W. (1999). EMAN: semiautomated software for high-resolution single-particle reconstructions. J Struct Biol *128*, 82-97.

Lyman, S.D., James, L., Vanden Bos, T., de Vries, P., Brasel, K., Gliniak, B., Hollingsworth, L.T., Picha, K.S., McKenna, H.J., Splett, R.R., *et al.* (1993a). Molecular cloning of a ligand for the flt3/flk-2 tyrosine kinase receptor: a proliferative factor for primitive hematopoietic cells. Cell *75*, 1157-1167.

Lyman, S.D., James, L., Zappone, J., Sleath, P.R., Beckmann, M.P., and Bird, T. (1993b). Characterization of the protein encoded by the flt3 (flk2) receptor-like tyrosine kinase gene. Oncogene *8*, 815-822.

Lyman, S.D., James, L., Johnson, L., Brasel, K., de Vries, P., Escobar, S.S., Downey, H., Splett, R.R., Beckmann, M.P., and McKenna, H.J. (1994). Cloning of the human homologue of the murine flt3 ligand: a growth factor for early hematopoietic progenitor cells. Blood *83*, 2795-2801.

Lyman, S.D. (1995). Biology of flt3 ligand and receptor. Int J Hematol *62*, 63-73.

Lyman, S.D., James, L., Escobar, S., Downey, H., de Vries, P., Brasel, K., Stocking, K., Beckmann, M.P., Copeland, N.G., Cleveland, L.S., *et al.* (1995a). Identification of soluble and membrane-bound isoforms of the murine flt3 ligand generated by alternative splicing of mRNAs. Oncogene *10*, 149-157.

Lyman, S.D., Seaberg, M., Hanna, R., Zappone, J., Brasel, K., Abkowitz, J.L., Prchal, J.T., Schultz, J.C., and Shahidi, N.T. (1995b). Plasma/serum levels of flt3 ligand are low in

normal individuals and highly elevated in patients with Fanconi anemia and acquired aplastic anemia. Blood *86*, 4091-4096.

Lyman, S.D., Stocking, K., Davison, B., Fletcher, F., Johnson, L., and Escobar, S. (1995c). Structural analysis of human and murine flt3 ligand genomic loci. Oncogene *11*, 1165-1172.

Lyman, S.D. (1998). Biologic effects and potential clinical applications of Flt3 ligand. Curr Opin Hematol *5*, 192-196.

Lyman, S.D., and Jacobsen, S.E. (1998). c-kit ligand and Flt3 ligand: stem/progenitor cell factors with overlapping yet distinct activities. Blood *91*, 1101-1134.

Mackarehtschian, K., Hardin, J.D., Moore, K.A., Boast, S., Goff, S.P., and Lemischka, I.R. (1995). Targeted disruption of the flk2/flt3 gene leads to deficiencies in primitive hematopoietic progenitors. Immunity *3*, 147-161.

MacKenzie, K.R., Prestegard, J.H., and Engelman, D.M. (1997). A transmembrane helix dimer: structure and implications. Science *276*, 131-133.

Manning, G., Whyte, D.B., Martinez, R., Hunter, T., and Sudarsanam, S. (2002). The protein kinase complement of the human genome. Science *298*, 1912-1934.

Maraskovsky, E., Daro, E., Roux, E., Teepe, M., Maliszewski, C.R., Hoek, J., Caron, D., Lebsack, M.E., and McKenna, H.J. (2000). *In vivo* generation of human dendritic cell subsets by Flt3 ligand. Blood *96*, 878-884.

Maroc, N., Rottapel, R., Rosnet, O., Marchetto, S., Lavezzi, C., Mannoni, P., Birnbaum, D., and Dubreuil, P. (1993). Biochemical characterization and analysis of the transforming potential of the FLT3/FLK2 receptor tyrosine kinase. Oncogene *8*, 909-918.

Martin, F.H., Suggs, S.V., Langley, K.E., Lu, H.S., Ting, J., Okino, K.H., Morris, C.F., McNiece, I.K., Jacobsen, F.W., Mendiaz, E.A., *et al.* (1990). Primary structure and functional expression of rat and human stem cell factor DNAs. Cell *63*, 203-211.

Matthews, B.W. (1968). Solvent content of protein crystals. J Mol Biol *33*, 491-497.

Matthews, W., Jordan, C.T., Wiegand, G.W., Pardoll, D., and Lemischka, I.R. (1991). A receptor tyrosine kinase specific to hematopoietic stem and progenitor cell-enriched populations. Cell *65*, 1143-1152.

Moriki, T., Maruyama, H., and Maruyama, I.N. (2001). Activation of preformed EGF receptor dimers by ligand-induced rotation of the transmembrane domain. J Mol Biol *311*, 1011-1026.

McClanahan, T., Culpepper, J., Campbell, D., Wagner, J., Franz-Bacon, K., Mattson, J., Tsai, S., Luh, J., Guimaraes, M.J., Mattei, M.G., *et al.* (1996). Biochemical and genetic characterization of multiple splice variants of the Flt3 ligand. Blood *88*, 3371-3382.

McCoy, A.J., Grosse-Kunstleve, R.W., Adams, P.D., Winn, M.D., Storoni, L.C., and Read, R.J. (2007). Phaser crystallographic software. J Appl Crystallogr *40*, 658-674.

McDonough, S.K., Larsen, S., Brodey, R.S., Stock, N.D., and Hardy, W.D., Jr. (1971). A transmissible feline fibrosarcoma of viral origin. Cancer Res *31*, 953-956.

McKenna, H.J., Stocking, K.L., Miller, R.E., Brasel, K., De Smedt, T., Maraskovsky, E., Maliszewski, C.R., Lynch, D.H., Smith, J., Pulendran, B., *et al.* (2000). Mice lacking flt3 ligand have deficient hematopoiesis affecting hematopoietic progenitor cells, dendritic cells, and natural killer cells. Blood *95*, 3489-3497.

Merzlyakov, M., and Hristova, K. (2008). Forster resonance energy transfer measurements of transmembrane helix dimerization energetics. Methods Enzymol *450*, 107-127.

Mesters, J.R., and Hilgendfeld, R. (2007). Protein glycosylation, sweet to crystal growth? Crystal Growth & Design *7*, 2251-2253.

Metcalf, D. (2007). On hematopoietic stem cell fate. Immunity *26*, 669-673.

Metcalf, D. (2008). Hematopoietic cytokines. Blood *111*, 485-491.

Mikkola, H.K., and Orkin, S.H. (2006). The journey of developing hematopoietic stem cells. Development *133*, 3733-3744.

Mindell, J.A., and Grigorieff, N. (2003). Accurate determination of local defocus and specimen tilt in electron microscopy. J Struct Biol *142*, 334-347.

Mol, C.D., Dougan, D.R., Schneider, T.R., Skene, R.J., Kraus, M.L., Scheibe, D.N., Snell, G.P., Zou, H., Sang, B.C., and Wilson, K.P. (2004). Structural basis for the autoinhibition and STI-571 inhibition of c-Kit tyrosine kinase. J Biol Chem *279*, 31655-31663.

Molineux, G., McCrea, C., Yan, X.Q., Kerzic, P., and McNiece, I. (1997). Flt-3 ligand synergizes with granulocyte colony-stimulating factor to increase neutrophil numbers and to mobilize peripheral blood stem cells with long-term repopulating potential. Blood *89*, 3998-4004.

Monneret, C. (2005). Histone deacetylase inhibitors. European Journal of Medicinal Chemistry *40*, 1-13.

Moriki, T., Maruyama, H., and Maruyama, I.N. (2001). Activation of preformed EGF receptor dimers by ligand-induced rotation of the transmembrane domain. J Mol Biol *311*, 1011-1026.

Morrison, S.J., and Weissman, I.L. (1994). The long-term repopulating subset of hematopoietic stem cells is deterministic and isolatable by phenotype. Immunity *1*, 661-673.

Muller, Y.A., Li, B., Christinger, H.W., Wells, J.A., Cunningham, B.C., and de Vos, A.M. (1997). Vascular endothelial growth factor: crystal structure and functional mapping of the kinase domain receptor binding site. Proc Natl Acad Sci U S A *94*, 7192-7197.

Nakao, M., Yokota, S., Iwai, T., Kaneko, H., Horiike, S., Kashima, K., Sonoda, Y., Fujimoto, T., and Misawa, S. (1996). Internal tandem duplication of the flt3 gene found in acute myeloid leukemia. Leukemia *10*, 1911-1918.

Noordeen, N.A., Carafoli, F., Hohenester, E., Horton, M.A., and Leitinger, B. (2006). A transmembrane leucine zipper is required for activation of the dimeric receptor tyrosine kinase DDR1. J Biol Chem *281*, 22744-22751.

Oates, J., King, G., and Dixon, A.M. (2009). Strong oligomerization behavior of PDGFbeta receptor transmembrane domain and its regulation by the juxtamembrane regions. Biochim Biophys Acta *1798*, 605-615.

Oefner, C., D'Arcy, A., Winkler, F.K., Eggimann, B., and Hosang, M. (1992). Crystal structure of human platelet-derived growth factor BB. EMBO J *11*, 3921-3926.

Ogiso, H., Ishitani, R., Nureki, O., Fukai, S., Yamanaka, M., Kim, J.H., Saito, K., Sakamoto, A., Inoue, M., Shirouzu, M., *et al.* (2002). Crystal structure of the complex of human epidermal growth factor and receptor extracellular domains. Cell *110*, 775-787.

Omura, T., Heldin, C.H., and Ostman, A. (1997). Immunoglobulin-like domain 4-mediated receptor-receptor interactions contribute to platelet-derived growth factor-induced receptor dimerization. J Biol Chem *272*, 12676-12682.

Onai, N., Obata-Onai, A., Schmid, M.A., Ohteki, T., Jarrossay, D., and Manz, M.G. (2007). Identification of clonogenic common Flt3+M-CSFR+ plasmacytoid and conventional dendritic cell progenitors in mouse bone marrow. Nat Immunol *8*, 1207-1216.

Pandit, J., Bohm, A., Jancarik, J., Halenbeck, R., Koths, K., and Kim, S.H. (1992). Three-dimensional structure of dimeric human recombinant macrophage colony-stimulating factor. Science *258*, 1358-1362.

Papayannopoulou, T., Nakamoto, B., Andrews, R.G., Lyman, S.D., and Lee, M.Y. (1997). *In vivo* effects of Flt3/Flk2 ligand on mobilization of hematopoietic progenitors in primates and potent synergistic enhancement with granulocyte colony-stimulating factor. Blood *90*, 620-629.

Parcells, B.W., Ikeda, A.K., Simms-Waldrip, T., Moore, T.B., and Sakamoto, K.M. (2006). FMS-like tyrosine kinase 3 in normal hematopoiesis and acute myeloid leukemia. Stem Cells *24*, 1174-1184.

Passegue, E., Jamieson, C.H., Ailles, L.E., and Weissman, I.L. (2003). Normal and leukemic hematopoiesis: are leukemias a stem cell disorder or a reacquisition of stem cell characteristics? Proc Natl Acad Sci U S A *100 Suppl 1*, 11842-11849.

Pemmaraju, N., Kantarjian, H., Ravandi, F., and Cortes, J. (2011). FLT3 inhibitors in the treatment of acute myeloid leukemia: The start of an era? Cancer. [Epub ahead of print]

Peng, H.L., Zhang, G.S., Gong, F.J., Shen, J.K., Zhang, Y., Xu, Y.X., Zheng, W.L., Dai, C.W., Pei, M.F., and Yang, J.J. (2008). Fms-like tyrosine kinase (FLT) 3 and FLT3 internal tandem duplication in different types of adult leukemia: analysis of 147 patients. Croat Med J *49*, 650-669.

Petoukhov, M.V., and Svergun, D.I. (2005). Global rigid body modeling of macromolecular complexes against small-angle scattering data. Biophysical Journal *89*, 1237-1250.

Philo, J.S., Wen, J., Wypych, J., Schwartz, M.G., Mendiaz, E.A., and Langley, K.E. (1996). Human stem cell factor dimer forms a complex with two molecules of the extracellular domain of its receptor, Kit. J Biol Chem *271*, 6895-6902.

Piloto, O., Nguyen, B., Huso, D., Kim, K.T., Li, Y., Witte, L., Hicklin, D.J., Brown, P., and Small, D. (2006). IMC-EB10, an anti-FLT3 monoclonal antibody, prolongs survival and reduces nonobese diabetic/severe combined immunodeficient engraftment of some acute lymphoblastic leukemia cell lines and primary leukemic samples. Cancer Res *66*, 4843-4851.

Pretlow, T.G., 2nd, Williams, E.E., Davis, M.L., and Zettergren, J.G. (1973). Separation of spleen colony forming units (CEU-S) from mouse bone marrow cells using velocity sedimentation in an isokinetic gradient of Ficoll in tissue culture medium. Am J Pathol *72*, 201-220.

Quentmeier, H., Reinhardt, J., Zaborski, M., and Drexler, H.G. (2003). FLT3 mutations in acute myeloid leukemia cell lines. Leukemia *17*, 120-124.

Rajakumar, A., Powers, R.W., Hubel, C.A., Shibata, E., von Versen-Hoynck, F., Plymire, D., and Jeyabalan, A. (2009). Novel soluble Flt-1 isoforms in plasma and cultured placental explants from normotensive pregnant and preeclamptic women. Placenta *30*, 25-34.

Ralph, P., Warren, M.K., Ladner, M.B., Kawasaki, E.S., Boosman, A., and White, T.J. (1986). Molecular and biological properties of human macrophage growth factor, CSF-1. Cold Spring Harb Symp Quant Biol *51 Pt 1*, 679-683.

Razumovskaya, E., Masson, K., Khan, R., Bengtsson, S., and Ronnstrand, L. (2009). Oncogenic Flt3 receptors display different specificity and kinetics of autophosphorylation. Exp Hematol *37*, 979-989.

Reeves, P.J., Callewaert, N., Contreras, R., and Khorana, H.G. (2002). Structure and function in rhodopsin: high-level expression of rhodopsin with restricted and homogeneous N-glycosylation by a tetracycline-inducible N-acetylglucosaminyltransferase I-negative HEK293S stable mammalian cell line. Proc Natl Acad Sci U S A *99*, 13419-13424.

Reindl, C., Bagrintseva, K., Vempati, S., Schnittger, S., Ellwart, J.W., Wenig, K., Hopfner, K.P., Hiddemann, W., and Spiekermann, K. (2006). Point mutations in the juxtamembrane domain of FLT3 define a new class of activating mutations in AML. Blood *107*, 3700-3707.

Robb, L. (2007). Cytokine receptors and hematopoietic differentiation. Oncogene *26*, 6715-6723.

Robinson, D.R., Wu, Y.M., and Lin, S.F. (2000). The protein tyrosine kinase family of the human genome. Oncogene *19*, 5548-5557.

Rocnik, J.L., Okabe, R., Yu, J.C., Lee, B.H., Giese, N., Schenkein, D.P., and Gilliland, D.G. (2006). Roles of tyrosine 589 and 591 in STAT5 activation and transformation mediated by FLT3-ITD. Blood *108*, 1339-1345.

Ronnstrand, L. (2004). Signal transduction via the stem cell factor receptor/c-Kit. Cell Mol Life Sci *61*, 2535-2548.

Rosnet, O., Marchetto, S., deLapeyriere, O., and Birnbaum, D. (1991). Murine Flt3, a gene encoding a novel tyrosine kinase receptor of the PDGFR/CSF1R family. Oncogene *6*, 1641-1650.

Rosnet, O., Schiff, C., Pebusque, M.J., Marchetto, S., Tonnelle, C., Toiron, Y., Birg, F., and Birnbaum, D. (1993). Human FLT3/FLK2 gene: cDNA cloning and expression in hematopoietic cells. Blood *82*, 1110-1119.

Ross, J., and Li, L. (2006). Recent advances in understanding extrinsic control of hematopoietic stem cell fate. Curr Opin Hematol *13*, 237-242.

Ruch, C., Skiniotis, G., Steinmetz, M.O., Walz, T., and Ballmer-Hofer, K. (2007). Structure of a VEGF-VEGF receptor complex determined by electron microscopy. Nat Struct Mol Biol *14*, 249-250.

Russ, W.P., and Engelman, D.M. (1999). TOXCAT: a measure of transmembrane helix association in a biological membrane. Proc Natl Acad Sci U S A *96*, 863-868.

Sacca, R., Stanley, E.R., Sherr, C.J., and Rettenmier, C.W. (1986). Specific binding of the mononuclear phagocyte colony-stimulating factor CSF-1 to the product of the v-fms oncogene. Proc Natl Acad Sci U S A *83*, 3331-3335.

Sanz, M., Burnett, A., Lo-Coco, F., and Lowenberg, B. (2009). FLT3 inhibition as a targeted therapy for acute myeloid leukemia. Curr Opin Oncol *21*, 594-600.

Sato, T., Yang, X., Knapper, S., White, P., Smith, B.D., Galkin, S., Small, D., Burnett, A., and Levis, M. (2011). FLT3 ligand impedes the efficacy of FLT3 inhibitors *in vitro* and *in vivo*. Blood.

Savvides, S.N., Boone, T., and Andrew Karplus, P. (2000). Flt3 ligand structure and unexpected commonalities of helical bundles and cystine knots. Nat Struct Biol *7*, 486-491.

Schlessinger, J., Plotnikov, A.N., Ibrahimi, O.A., Eliseenkova, A.V., Yeh, B.K., Yayon, A., Linhardt, R.J., and Mohammadi, M. (2000). Crystal structure of a ternary FGF-FGFR-heparin complex reveals a dual role for heparin in FGFR binding and dimerization. Mol Cell *6*, 743-750.

Schlessinger, J., and Lemmon, M.A. (2003). SH2 and PTB domains in tyrosine kinase signaling. Sci STKE *2003*, RE12.

Schmid, M.A., Kingston, D., Boddupalli, S., and Manz, M.G. (2010). Instructive cytokine signals in dendritic cell lineage commitment. Immunol Rev *234*, 32-44.

Schmidt-Arras, D., Schwable, J., Bohmer, F.D., and Serve, H. (2004). Flt3 receptor tyrosine kinase as a drug target in leukemia. Curr Pharm Des *10*, 1867-1883.

Schmidt-Arras, D.E., Bohmer, A., Markova, B., Choudhary, C., Serve, H., and Bohmer, F.D. (2005). Tyrosine phosphorylation regulates maturation of receptor tyrosine kinases. Mol Cell Biol *25*, 3690-3703.

Schnittger, S., Schoch, C., Dugas, M., Kern, W., Staib, P., Wuchter, C., Loffler, H., Sauerland, C.M., Serve, H., Buchner, T., *et al.* (2002). Analysis of FLT3 length mutations in 1003 patients with acute myeloid leukemia: correlation to cytogenetics, FAB subtype, and prognosis in the AMLCG study and usefulness as a marker for the detection of minimal residual disease. Blood *100*, 59-66.

Schnittger, S., Kohl, T.M., Leopold, N., Schoch, C., Wichmann, H.E., Kern, W., Lohse, P., Hiddemann, W., Haferlach, T., and Spiekermann, K. (2006). D324N single-nucleotide polymorphism in the FLT3 gene is associated with higher risk of myeloid leukemias. Genes Chromosomes Cancer *45*, 332-337.

Schroder, G.F., Levitt, M., and Brunger, A.T. (2010). Super-resolution biomolecular crystallography with low-resolution data. Nature *464*, 1218-1222.

Shah, A.J., Smogorzewska, E.M., Hannum, C., and Crooks, G.M. (1996). Flt3 ligand induces proliferation of quiescent human bone marrow CD34+CD38- cells and maintains progenitor cells *in vitro*. Blood *87*, 3563-3570.

Shaw, S.G., Maung, A.A., Steptoe, R.J., Thomson, A.W., and Vujanovic, N.L. (1998). Expansion of functional NK cells in multiple tissue compartments of mice treated with Flt3-ligand: implications for anti-cancer and anti-viral therapy. J Immunol *161*, 2817-2824.

Shen, J., and Maruyama, I.N. (2011). Nerve growth factor receptor TrkA exists as a preformed, yet inactive, dimer in living cells. FEBS Lett *585*, 295-299.

Shim, A.H., Liu, H., Focia, P.J., Chen, X., Lin, P.C., and He, X. (2010). Structures of a platelet-derived growth factor/propeptide complex and a platelet-derived growth factor/receptor complex. Proc Natl Acad Sci U S A *107*, 11307-11312.

Shulman, T., Sauer, F.G., Jackman, R.M., Chang, C.N., and Landolfi, N.F. (1997). An antibody reactive with domain 4 of the platelet-derived growth factor beta receptor allows BB binding

while inhibiting proliferation by impairing receptor dimerization. J Biol Chem *272*, 17400-17404.

Singh, S.M., and Panda, A.K. (2005). Solubilization and refolding of bacterial inclusion body proteins. J Biosci Bioeng *99*, 303-310.

Sitnicka, E., Buza-Vidas, N., Larsson, S., Nygren, J.M., Liuba, K., and Jacobsen, S.E. (2003). Human CD34+ hematopoietic stem cells capable of multilineage engrafting NOD/SCID mice express flt3: distinct flt3 and c-kit expression and response patterns on mouse and candidate human hematopoietic stem cells. Blood *102*, 881-886.

Small, D., Levenstein, M., Kim, E., Carow, C., Amin, S., Rockwell, P., Witte, L., Burrow, C., Ratajczak, M.Z., Gewirtz, A.M., *et al.* (1994). STK-1, the human homolog of Flk-2/Flt-3, is selectively expressed in CD34+ human bone marrow cells and is involved in the proliferation of early progenitor/stem cells. Proc Natl Acad Sci U S A *91*, 459-463.

Stein, J., Borzillo, G.V., and Rettenmier, C.W. (1990). Direct stimulation of cells expressing receptors for macrophage colony-stimulating factor (CSF-1) by a plasma membrane-bound precursor of human CSF-1. Blood *76*, 1308-1314.

Stein, N. (2008). CHAINSAW: a program for mutating pdb files used as templates in molecular replacement. Journal of Applied Crystallography *41*, 641-643.

Sternberg, D.W., and Licht, J.D. (2005). Therapeutic intervention in leukemias that express the activated fms-like tyrosine kinase 3 (FLT3): opportunities and challenges. Curr Opin Hematol *12*, 7-13.

Sternberg, M.J., and Gullick, W.J. (1990). A sequence motif in the transmembrane region of growth factor receptors with tyrosine kinase activity mediates dimerization. Protein Eng *3*, 245-248.

Stirewalt, D.L., and Radich, J.P. (2003). The role of FLT3 in haematopoietic malignancies. Nat Rev Cancer *3*, 650-665.

Stirewalt, D.L., Appelbaum, F.R., Willman, C.L., Zager, R.A., and Banker, D.E. (2003a). Mevastatin can increase toxicity in primary AMLs exposed to standard therapeutic agents, but statin efficacy is not simply associated with ras hotspot mutations or overexpression. Leuk Res *27*, 133-145.

Stirewalt, D.L., Guthrie, K.A., Beppu, L., Bryant, E.M., Doney, K., Gooley, T., Appelbaum, F.R., and Radich, J.P. (2003b). Predictors of relapse and overall survival in Philadelphia chromosome-positive acute lymphoblastic leukemia after transplantation. Biol Blood Marrow Transplant *9*, 206-212.

Streeter, P.R., Minster, N.I., Kahn, L.E., Hood, W.F., Vickery, L.E., Thurman, T.L., Monahan, J.B., Welply, J.K., McKearn, J.P., and Woulfe, S.L. (2001). Progenipoietins: biological characterization of a family of dual agonists of fetal liver tyrosine kinase-3 and the granulocyte colony-stimulating factor receptor. Exp Hematol *29*, 41-50.

Stroud, R.M., and Wells, J.A. (2004). Mechanistic diversity of cytokine receptor signaling across cell membranes. Sci STKE *2004*, re7.

Stuttfeld, E., and Ballmer-Hofer, K. (2009). Structure and function of VEGF receptors. IUBMB Life *61*, 915-922.

Sudo, Y., Shimazaki, C., Ashihara, E., Kikuta, T., Hirai, H., Sumikuma, T., Yamagata, N., Goto, H., Inaba, T., Fujita, N., *et al.* (1997). Synergistic effect of FLT-3 ligand on the granulocyte colony-stimulating factor-induced mobilization of hematopoietic stem cells and progenitor cells into blood in mice. Blood *89*, 3186-3191.

Sun, P.D., Foster, C.E., and Boyington, J.C. (2004). Overview of protein structural and functional folds. Curr Protoc Protein Sci *Chapter 17*, Unit 17 11.

Sundberg, E.J., and Mariuzza, R.A. (2002). Molecular recognition in antibody-antigen complexes. Adv Protein Chem *61*, 119-160.

Svergun, D.I. (1992). Determination of the Regularization Parameter in Indirect-Transform Methods Using Perceptual Criteria. Journal of Applied Crystallography *25*, 495-503.

Svergun, D., Barberato, C., and Koch, M.H.J. (1995). CRYSOL - A program to evaluate x-ray solution scattering of biological macromolecules from atomic coordinates. Journal of Applied Crystallography *28*, 768-773.

Tao, Q., Backer, M.V., Backer, J.M., and Terman, B.I. (2001). Kinase insert domain receptor (KDR) extracellular immunoglobulin-like domains 4-7 contain structural features that block receptor dimerization and vascular endothelial growth factor-induced signaling. J Biol Chem *276*, 21916-21923.

Thiede, C., Steudel, C., Mohr, B., Schaich, M., Schakel, U., Platzbecker, U., Wermke, M., Bornhauser, M., Ritter, M., Neubauer, A., *et al.* (2002). Analysis of FLT3-activating mutations in 979 patients with acute myelogenous leukemia: association with FAB subtypes and identification of subgroups with poor prognosis. Blood *99*, 4326-4335.

Tiesman, J., and Hart, C.E. (1993). Identification of a soluble receptor for platelet-derived growth factor in cell-conditioned medium and human plasma. J Biol Chem *268*, 9621-9628.

Toffalini, F., and Demoulin, J.B. (2010). New insights into the mechanisms of hematopoietic cell transformation by activated receptor tyrosine kinases. Blood *116*, 2429-2437.

Tsuchiya, S., Yamabe, M., Yamaguchi, Y., Kobayashi, Y., Konno, T., and Tada, K. (1980). Establishment and characterization of a human acute monocytic leukemia cell line (THP-1). Int J Cancer *26*, 171-176.

Turner, A.M., Lin, N.L., Issarachai, S., Lyman, S.D., and Broudy, V.C. (1996). FLT3 receptor expression on the surface of normal and malignant human hematopoietic cells. Blood *88*, 3383-3390.

Vagin, A., and Teplyakov, A. (2010). Molecular replacement with MOLREP. Acta Crystallogr D Biol Crystallogr *66*, 22-25.

van Heel, M., Harauz, G., Orlova, E.V., Schmidt, R., and Schatz, M. (1996). A new generation of the IMAGIC image processing system. J Struct Biol *116*, 17-24.

Vanrobaeys, F., Devreese, B., Lecocq, E., Rychlewski, L., De Smet, L., and Van Beeumen, J. (2003). Proteomics of the dissimilatory iron-reducing bacterium Shewanella oneidensis MR-1, using a matrix-assisted laser desorption/ionization-tandem-time of flight mass spectrometer. Proteomics *3*, 2249-2257.

Verstraete, K., Koch, S., Ertugrul, S., Vandenberghe, I., Aerts, M., Vandriessche, G., Thiede, C., and Savvides, S.N. (2009). Efficient production of bioactive recombinant human Flt3 ligand in *E. coli*. Protein J *28*, 57-65.

Verstraete, K., Remmerie B., Elegheert J., Lintermans, B., Haegeman, G., Vanhoenacker, P., Van Craenenbroeck, K. and Savvides, S.N. (2011). Inducible production of recombinant human Flt3 ectodomain variants in mammalian cells and preliminary crystallographic analysis of Flt3 ligand-receptor complexes. Acta Crystallogr Sect F Struct Biol Cryst Commun *67*, 325-331.

Wagers, A.J., Sherwood, R.I., Christensen, J.L., and Weissman, I.L. (2002). Little evidence for developmental plasticity of adult hematopoietic stem cells. Science *297*, 2256-2259.

Walter, M., Lucet, I.S., Patel, O., Broughton, S.E., Bamert, R., Williams, N.K., Fantino, E., Wilks, A.F., and Rossjohn, J. (2007). The 2.7 A crystal structure of the autoinhibited human c-Fms kinase domain. J Mol Biol *367*, 839-847.

Wang, C., Curtis, J.E., Minden, M.D., and McCulloch, E.A. (1989). Expression of a retinoic acid receptor gene in myeloid leukemia cells. Leukemia *3*, 264-269.

Wang, X., Lupardus, P., Laporte, S.L., and Garcia, K.C. (2009). Structural biology of shared cytokine receptors. Annu Rev Immunol *27*, 29-60.

Wang, Z.E., Myles, G.M., Brandt, C.S., Lioubin, M.N., and Rohrschneider, L. (1993). Identification of the ligand-binding regions in the macrophage colony-stimulating factor receptor extracellular domain. Mol Cell Biol *13*, 5348-5359.

Waskow, C., Liu, K., Darrasse-Jeze, G., Guermonprez, P., Ginhoux, F., Merad, M., Shengelia, T., Yao, K., and Nussenzweig, M. (2008). The receptor tyrosine kinase Flt3 is required for dendritic cell development in peripheral lymphoid tissues. Nat Immunol *9*, 676-683.

Wehrman, T., He, X., Raab, B., Dukipatti, A., Blau, H., and Garcia, K.C. (2007). Structural and mechanistic insights into nerve growth factor interactions with the TrkA and p75 receptors. Neuron *53*, 25-38.

Wells, J.A., and McClendon, C.L. (2007). Reaching for high-hanging fruit in drug discovery at protein-protein interfaces. Nature *450*, 1001-1009.

Wiesmann, C., Fuh, G., Christinger, H.W., Eigenbrot, C., Wells, J.A., and de Vos, A.M. (1997). Crystal structure at 1.7 A resolution of VEGF in complex with domain 2 of the Flt-1 receptor. Cell *91*, 695-704.

Wilks, A.F., and Kurban, R.R. (1988). Isolation and structural analysis of murine c-fes cDNA clones. Oncogene *3*, 289-294.

Wilson, A., Oser, G.M., Jaworski, M., Blanco-Bose, W.E., Laurenti, E., Adolphe, C., Essers, M.A., Macdonald, H.R., and Trumpp, A. (2007). Dormant and self-renewing hematopoietic stem cells and their niches. Ann N Y Acad Sci *1106*, 64-75.

Wodnar-Filipowicz, A., Lyman, S.D., Gratwohl, A., Tichelli, A., Speck, B., and Nissen, C. (1996). Flt3 ligand level reflects hematopoietic progenitor cell function in aplastic anemia and chemotherapy-induced bone marrow aplasia. Blood *88*, 4493-4499.

Wodnar-Filipowicz, A. (2003). Flt3 ligand: role in control of hematopoietic and immune functions of the bone marrow. News Physiol Sci *18*, 247-251.

Wu, L., and Liu, Y.J. (2007). Development of dendritic-cell lineages. Immunity *26*, 741-750.

Wypych, J., Bennett, L.G., Schwartz, M.G., Clogston, C.L., Lu, H.S., Broudy, V.C., Bartley, T.D., Parker, V.P., and Langley, K.E. (1995). Soluble kit receptor in human serum. Blood *85*, 66-73.

Yang, Y., Yuzawa, S., and Schlessinger, J. (2008). Contacts between membrane proximal regions of the PDGF receptor ectodomain are required for receptor activation but not for receptor dimerization. Proc Natl Acad Sci U S A *105*, 7681-7686.

Yang, Y., Xie, P., Opatowsky, Y., and Schlessinger, J. (2010). Direct contacts between extracellular membrane-proximal domains are required for VEGF receptor activation and cell signaling. Proc Natl Acad Sci U S A *107*, 1906-1911.

Yao, F., Svensjo, T., Winkler, T., Lu, M., Eriksson, C., and Eriksson, E. (1998). Tetracycline repressor, tetR, rather than the tetR-mammalian cell transcription factor fusion derivatives, regulates inducible gene expression in mammalian cells. Hum Gene Ther *9*, 1939-1950.

You, M., Li, E., Wimley, W.C., and Hristova, K. (2005). Forster resonance energy transfer in liposomes: measurements of transmembrane helix dimerization in the native bilayer environment. Anal Biochem *340*, 154-164.

Youssoufian, H., Rowinsky, E.K., Tonra, J., and Li, Y. (2010). Targeting FMS-related tyrosine kinase receptor 3 with the human immunoglobulin G1 monoclonal antibody IMC-EB10. Cancer *116*, 1013-1017.

Yuzawa, S., Opatowsky, Y., Zhang, Z., Mandiyan, V., Lax, I., and Schlessinger, J. (2007). Structural basis for activation of the receptor tyrosine kinase KIT by stem cell factor. Cell *130*, 323-334.

Zhang, S., and Broxmeyer, H.E. (1999). p85 subunit of PI3 kinase does not bind to human Flt3 receptor, but associates with SHP2, SHIP, and a tyrosine-phosphorylated 100-kDa protein in Flt3 ligand-stimulated hematopoietic cells. Biochem Biophys Res Commun *254*, 440-445.

Zhang, S., and Broxmeyer, H.E. (2000). Flt3 ligand induces tyrosine phosphorylation of gab1 and gab2 and their association with shp-2, grb2, and PI3 kinase. Biochem Biophys Res Commun *277*, 195-199.

Zhang, Y.L., Chen, S.S., Yang, K.G., Su, L., Deng, Y.C., and Liu, C.Z. (2005). Functional expression, purification, and characterization of human Flt3 ligand in the Pichia pastoris system. In Protein Expr Purif, pp. 246-254.

Zhang, Z., Zhang, R., Joachimiak, A., Schlessinger, J., and Kong, X.P. (2000). Crystal structure of human stem cell factor: implication for stem cell factor receptor dimerization and activation. Proc Natl Acad Sci U S A *97*, 7732-7737.

Zheng, R., Klang, K., Gorin, N.C., and Small, D. (2004a). Lack of KIT or FMS internal tandem duplications but co-expression with ligands in AML. Leuk Res *28*, 121-126.

Zheng, R., Levis, M., Piloto, O., Brown, P., Baldwin, B.R., Gorin, N.C., Beran, M., Zhu, Z., Ludwig, D., Hicklin, D., *et al.* (2004b). FLT3 ligand causes autocrine signaling in acute myeloid leukemia cells. Blood *103*, 267-274.

Zsebo, K.M., Williams, D.A., Geissler, E.N., Broudy, V.C., Martin, F.H., Atkins, H.L., Hsu, R.Y., Birkett, N.C., Okino, K.H., Murdock, D.C., *et al.* (1990). Stem cell factor is encoded at the Sl locus of the mouse and is the ligand for the c-kit tyrosine kinase receptor. Cell *63*, 213-224.

DANKWOORD

Eerst en vooral had ik graag mijn promotor, Prof. Savvas Savvides bedankt voor zijn ondersteunende rol en voor het vertrouwen dat hij in mij heeft gesteld gedurende mijn vijfjarige doctoraatsperiode. Ik wens zijn ondernemingszin en openheid te prijzen, alsook zijn immer aanwezige enthousiasme. Hartelijk bedankt, Savvas!

Ik wens ook mijn co-promotor, Prof. Em. Jozef Van Beeumen, en de andere leden van de examencommissie uitdrukkelijk te bedanken voor het uitvoerig nalezen van mijn thesis en voor de vele suggesties ter verbetering van de tekst.

Verder wil ik Dr. Bjorn Vergauwen bedanken voor zijn waardevol advies bij de interpretatie van wetenschappelijke resultaten en voor de vele interessante discussies.

Een bijzondere dank gaat uit naar Jonathan Elegheert voor het delen van zijn uitstekende technische kennis, in het bijzonder aangaande X-stralenkristallografie.

Ik wens ook Bert Remmerie te bedanken voor de goede samenwerking en voor de vele interessante gesprekken onder de middagpauzes en tijdens de talrijke lange avonden op het laboratorium.

Ook Dr. Kathleen Van Craenenbroeck, Beatrice Lintermans en Dr. Peter Vanhoenaker wil ik uitdrukkelijk bedanken voor de leuke samenwerking en voor de ondersteuning bij het opzetten van een weefselkweekinfstrastructuur. Hun inbreng was cruciaal voor het verloop van mijn doctoraatsproject.

Ik wens ook Dr. Gonzalez Van Driessche te bedanken voor zijn uitvoerige massaspectrometrische analyse van de Flt3 receptor. Ik had graag ook Ann Dansercoer bedankt voor het uitvoeren van grootschalige expressie-experimenten.

In het bijzonder wil ik ook mijn twee fantastische thesisstudenten, Sevgi en Mariska, danken voor hun grote enthousiasme en de werklust die zij ten toon spreidden.

Verder wil ik ook de vele andere (ex)-collega's in het L-ProBE laboratorium bedanken die mij altijd met raad en daad hebben bijgestaan: Géraldine, Ester, Jan S., Lina, Jimmy, Isabel, Ingrid, Freddy, Kedar, Ruben, Nathalie, Jan F., ... Zij die nog moeten doctoreren wens ik dan ook veel succes toe met de verderzetting van hun doctoraat.

Graag zou ik ook het FWO-Vlaanderen bedanken voor hun financiële steun.

Tenslotte wens ik mijn vriendin Kasia, mijn ouders Goedele en Patrick, en mijn broer Jens te bedanken voor hun onmisbare steun.

Kenneth

CURRICULUM VITAE

PERSONAL INFORMATION

Name:	Kenneth F.A. Verstraete	**Birth:**	March 23th, 1983, Deinze
Nationality:	Belgium	**Familial status:**	Cohabitation
Adress:	Monterreystraat 58, Ghent	**Languages:**	Dutch (native)
Phone:	+32 473 21 04 24		English (fluent)
Email:	kenneth.verstraete@ugent.be		French (intermediate)
Work Adress:	L-ProBE		Polish (basics)
	K.L. Ledeganckstraat 35		
	9000 Ghent		
	+32 9 264 51 26		

EDUCATION

Oct 2009 – Mar 2011	PhD student - Ghent University Laboratory for Protein Biochemistry and Biomolecular Engineering, Faculty of Sciences – Ghent University
Oct 2005 – Sept 2009	PhD student - FWO Laboratory for Protein Biochemistry and Biomolecular Engineering, Faculty of Sciences – Ghent University
Oct 2003 – Jul 2005	Master in Biochemistry, Ghent University (*great distinction*)
Oct 2001 – Jul 2003	Bachelor in Chemistry, Ghent University (*great distinction*)

AWARDS & HONORS

Participation in EMBO-Workshop (competitive selection):
"Structural Characterization of Macromolecular Complexes",
2 – 7 June 2008, ESRF, Grenoble, France

FWO doctoral scholarship
"Structural and thermodynamic characterization of the hematopoietic Flt3 ligand-receptor complex"
Laboratory for Protein Biochemistry and Biomolecular Engineering, Faculty of Sciences, Department of Biochemistry and Microbiology, Ghent University
Promotor: Prof. Dr. S.N. Savvides; Co-promotor: Prof. Dr. J. Van Beeumen

Innogenetics-award for 'best' Masters Thesis

"Structure-function studies on human ATP citrate lyase, a potential drug target in metabolic disorders such as obesity' Academic year 2004 – 2005, Laboratory for Protein Biochemistry and Biomolecular Engineering, Faculty of Sciences, Department of Biochemistry and Microbiology, Ghent University. Promotor: Prof. Dr. J. Van Beeumen, Mentor: D. Devos

RESEARCH PUBLICATIONS (peer-reviewed in journals of the ISI Citation Index-SCI)

5. "Structural insights into the extracellular assembly of the hematopoietic Flt3 signaling complex."

Verstraete K, Vandriessche G, Januar M, Elegheert J, Shkumatov A, Desfosses A, Van Craenenbroeck K, Svergun D, Gutsche I, Vergauwen B, Savvides SN.

Blood, 2011, *in press*

4. "Inducible production of recombinant human Flt3 ectodomain variants in mammalian cells and preliminary crystallographic analysis of Flt3 ligand-receptor complexes."

Verstraete K, Remmerie B , Elegheert J, Lintermans B, Van Craenenbroeck K, Savvides SN.

Acta Crystallographica Section F (2011) 67: 325 – 331

3. "The viral oncoprotein BARF1 sequesters and inactivates the human cytokine CSF-1 using a distinct binding mode. "

Elegheert J, Bracke N, Pouliot P, Shkumatov A, Tarbouriech N, Burmeister W, **Verstraete K**, Gutsche I, Svergun D, Lambrecht B, Vergauwen B, Savvides SN. *In preparation*

2. "Architecture and plasticity of human Colony-Stimulating Factor 1 Receptor revealed by its complete extracellular signaling complex."

Elegheert J, Desfosses A, Shkumatov A, Wu X, Bracke N, **Verstraete K**, Van Craenenbroeck K, Brooks BR, Svergun D, Vergauwen B, Gutsche I, Savvides SN. *In preparation*

1. "Efficient production of bioactive recombinant human Flt3 ligand in *E. coli*. "

Verstraete K, Koch S, Ertugrul S, Vandenberghe I, Aerts M, Vandriessche G, Thiede C, Savvides SN. Protein J. 2009 Feb;28(2):57-65.

CONFERENCES AND COURSES

9. NWO-study group meeting: "Protein Research, Nucleic acids and Lipids & Biomembranes "

6 – 7 December 2010, congress centre "Koningshof", Veldhoven, The Netherlands

8. **Introduction to 'negative-stain' elektron microscopy: data collection and image analysis.** Collaboration with dr. Irina Gutsche (UVHCI, Grenoble), 13 – 21 November 2008, ESRF, Grenoble, France

7. **EMBO Workshop: "Structural Characterization of Macromolecular Complexes "**
2 – 7 June 2008, ESRF, Grenoble, France

6. **CCP4 Study Weekend: "Low Resolution Structure Determination and Validation "**
3 – 5 January 2008, University of Leeds, Leeds, UK

5. **NWO-study group meeting: "Protein Research "**
11 – 12 December 2006, congress centre "De Werelt ", Lunteren, The Netherlands

4. **Biacore T100 Training**, SPR-training course organised by Biacore
10 – 11 October 2006, Faculty of Veterinary Medicine – Ghent University, Merelbeke

3. **MicroCal Conference: "Applications of Biocalorimetry 5"**
4 – 7 July 2006, Hotel Melia, Zaragoza, Spain

2. **"Course on Biomolecular Structure Determination"**, organised by the "Belgian Biophysical Society" and the "FWO-interest group: Protein Structure and Dynamics"
7 – 9 June 2006, KUL, Leuven

1. **"Life, a Nobel Story"**, "Molecular and Cellular Biology" – symposium organised by the **"**Royal Flemish Chemical Society",
28 April 2004, Brussels Expo (Heizel), Brussels

ORAL PRESENTATIONS

1."The hematopoietic receptor Flt3 is a structural and functional outlier within the receptor tyrosine kinase III family."
NWO-study group meeting: Protein Research, Nucleic acids and Lipids & Biomembranes,
6 - 7 December, 2010, Veldhoven, The Netherlands

POSTER PRESENTATIONS (* presenting author)

7. "Structural insights into the extracellular assembly of the hematopoietic Flt3 signaling complex" Verstraete K*****, Vandriessche G, Januar M, Elegheert J, Shkumatov A, Desfosses A, Van Craenenbroeck K, Svergun D, Gutsche I, Vergauwen B, Savvides SN

NWO-study group meeting: Protein Research, Nucleic acids and Lipids & Biomembranes,
6 - 7 December, 2010, Veldhoven, The Netherlands

6. "Structure function studies between the Epstein-barr viroreceptor BARF1 and its ligand CSF-1" Bracke N*****, Elegheert J, Pouilot P, Tarbouriech N, Verstraete K, Gutsche I, Burmeister W, Vergauwen B, Lambrecht B, Savvides SN
NWO-study group meeting: Protein Research, Nucleic acids and Lipids & Biomembranes,
6 - 7 December, 2010, Veldhoven, The Netherlands

5. "The viral oncoprotein BARF1 sequesters and inactivates the human cytokine CSF-1 using a distinct binding mode"
Elegheert J*****, Bracke N, Pouliot P, Shkumatov A, Tarbouriech N, Gutsche I, Burmeister W, Verstraete K, Svergun D, Lambrecht B, Vergauwen B and Savvides SN
NWO-study group meeting: Protein Research, Nucleic acids and Lipids & Biomembranes,
6 - 7 December, 2010, Veldhoven, The Netherlands

4. "A combined approach towards elucidating the human Flt3 ligand-receptor complex"
Verstraete K, Remmerie B, Elegheert J, Van Craenenbroeck K, Desfosses A, Svergun D, Gutsche I, Savvides SN***** *NWO-study group meeting: Protein Research, Lunteren, The Netherlands,*
April 2009

3. "Towards the structural and thermodynamic characterization of the Flt3 ligand-receptor interaction." Verstraete K*****, Gutsche I, Koch S, Van Craenenbroeck K, Tiede C, Svergun D, Savvides SN PhD *symposium Faculty of Sciences, Ghent University,*
April 28th, 2009, ICC, Ghent

2. "Towards a better understanding of extracellular cytokine receptor biology: the initial characterization of a lectin/R complex."
Remmerie B*****, Verstraete K, Elegheert J, Vergauwen B, Savvides SN
33rd FEBS Congres, Athens, Greece, 28 Juni– 3 Juli, 2008.
Abstract: FEBS Journal ***275:*** *228-228, 2008*

1. "Towards the structural and thermodynamic characterization of the Flt3 ligand-receptor interaction" Verstraete K***,** Koch S, Ertugrul S, Van Craenenbroeck K, Haegeman G, Tiede C, Savvides SN *EMBO Workshop: Structural Characterization of Macromolecular Complexes,*
2 – 7 June 2008, Grenoble, France

GUIDANCE of MASTER's THESIS STUDENTS

Oct 2010 – Jun 2011	**Structural analysis of human ATP citrate lyase by small angle X-ray scattering.** Yehudi Bloch, Master in Biochemistry, Ghent University
Oct 2009 – Jun 2010	**Dissection of the interaction between Flt3 ligand and the extracellular domains of its receptor.** Mariska Januar, Master in Biochemistry, Ghent University
Aug 2006 – Jun 2007	**Structural and thermodynamic characterization of the complex between the hematopoietic cytokine, Flt3L and its receptor, Flt3** Sevgi Ertugrul, Erasmus student - 'Ankara University', Turkey
Feb 2005 – Jun 2006	**Expression and purification of adenylate kinase from *P. falciparum*.** Magalie Boedt, Master in Biochemistry, Ghent University